ELECTROCHEMICAL REDUCTION OF CARBON DIOXIDE USING GOLD CATHODES

A thesis submitted in fulfilment

of the requirements for the

degree of Doctor of Philosophy

in Chemical and Process Engineering

University of Canterbury

New Zealand

Hani Taleshi Ahangari

August 2019

ABSTRACT

Electrochemical reduction of carbon dioxide (CO_2) is a promising means of storing energy from intermittent electrical resources (like solar and wind) in chemical forms. To be able to make this process feasible, selective catalysts with low overpotential are needed. The present study is concerned with the electrochemical CO_2 reduction at ambient conditions in an aqueous electrolyte.

The majority of this study focuses on electrochemical CO_2 reduction on gold cathodes (polycrystalline gold, gold on carbon paper and gold clusters). The thesis begins with the electrochemical CO_2 conversion to CO using a custom electrolysis H-cell, which is coupled to a Gas Chromatography (GC) for the gaseous product detection. The gaseous products analysis confirmed that H_2 and CO were the major products of the reaction. Then, the general aspects of electrochemical CO_2 reduction experiment were investigated. The next step was designing the electrochemical flow cell that significantly increases Faradaic efficiency of the reaction toward CO (15-45%). During these attempts, we aimed to study different polycrystalline gold surfaces as catalyst for CO_2 electroreduction. This enabled us to investigate the effect of surface morphology on the gold catalytic activity and selectivity. Our results suggest that the rougher gold surface favours CO production over unwanted hydrogen evolution reaction.

The next step was performing prolong galvanostatic CO_2 reduction experiment with stable activity and selectivity by using periodic cyclic voltammetry, open circuit potential or short anodic pulses . In contrast with the previous literature, our results suggest that no gold oxide would form by these cleaning steps and a constant catalytic activity and selectivity can be maintained over long-term electrolysis by removing the impurities like Fe, Zn and Cu sources from the electrolyte. The results obtained in this part, cover an important gap in the literature and provide useful information for many researchers who are trying to understand the mechanism of electrochemical CO_2 reduction during deactivation.

The sensitivity of CO_2 reduction reaction on cell hydrodynamics at various electrolyte solutions has been investigated using a flow cell set-up. Our observations show that the Faradaic efficiency for CO production is around 90% regardless of the electrolyte concentration whereas in the custom H-cell, the Faradaic efficiency for CO decreases from 75% to 35% when the electrolyte concentration is increased from 0.1 mol L^{-1} to 0.5 mol L^{-1}.

Lastly, the electrocatalytic CO_2 reduction was performed on different gold clusters (Au_6, Au_9, Au_{13} and Au_{101}) adsorbed onto carbon paper substrates. These clusters showed very high Faradaic efficiency toward CO (around 90%) at -1.5 V vs Ag|AgCl using relatively low gold loadings (90 µg cm^{-2}). Also, Au_{13} was found to show the highest selectivity for CO production amongst other clusters. The understanding of the gold clusters behaviour studied experimentally in this thesis, could help to augment the activity and selectivity of the electrochemical CO_2 reduction.

ACKNOWLEDGMENTS

I would like to express my gratitude to my supervisor, Associate Professor Aaron Marshall, for his invaluable guidance, enthusiasm, generous support, and most importantly to develop and encourage me as a researcher in the best possible way. I am very thankful for your warm supervision throughout the journey. I would also like to thank my co-supervisor, Dr. Alex Yip for all of his support during my PhD. I am really grateful to a number of people who have helped me during my research:

- Dr. Vladimir Golovko who gave me additional ideas, viewpoints and resources during my research.
- CAPE technical staff, especially Leigh Richardson, Glen Wilson, Stephen Beuzenberg, Michael Sandridge, Rayleen Fredericks, and Graham Furniss for their technical help and being so approachable.
- CAPE administrative staff, Ranee Hearst and Joanne Pollard for their kindness and help.
- My research peers, especially Dr. Calvin Lim in heaven and Dr. Steven Jared for their problem solving sessions.
- PhD student Shailendra Sharma from the Chemistry, not only for synthesise the gold nanoparticles, but also for assistance during the running of experiments.
- The intern student Thibault Portail from Institut National des Science de Lyon, for his assistance and ideas during the experimentation.
- Technical staff outside of CAPE, Mike Flaws at Mechanical Engineering and Rob McGregor at Chemistry for sharing their unique expertise and experience and Dr. Colin Doyle from the University of Auckland for his help with XPS.
- Mr and Mrs Stanbury, my landlords. I really appreciate you because of being so kind and considerate. The words cannot describe my feelings to you. You are angels.
- My parents and my family in laws for their unconditional support and kindness. I could have never done my PhD without your love to pursue this path.

Lastly, Pariya, my wife and my best friend. Thank you for your love, kindness, and patience. I love you.

UNIVERSITY OF CANTERBURY
Te Whare Wānanga o Waitaha
CHRISTCHURCH NEW ZEALAND

Co-Authorship Form

This form is to accompany the submission of any thesis that contains research reported in co-authored work that has been published, accepted for publication, or submitted for publication. A copy of this form should be included for each co-authored work that is included in the thesis. Completed forms should be included at the front (after the thesis abstract) of each copy of the thesis submitted for examination and library deposit.

Please indicate the chapter/section/pages of this thesis that are extracted from co-authored work and provide details of the publication or submission from the extract comes:

The results for chapter 5 submitted to the "Electrocatalysis" as a full paper entitled "Preventing the deactivation of gold cathodes during electrocatalytic CO_2 reduction while avoiding gold dissolution".

Please detail the nature and extent (%) of contribution by the candidate:
The candidate is the first author of the paper and performed 100% of the experiments and wrote most of the text.

Certification by Co-authors:

If there is more than one co-author then a single co-author can sign on behalf of all

The undersigned certifies that:

- The above statement correctly reflects the nature and extent of the PhD candidate's contribution to this co-authored work
- In cases where the candidate was the lead author of the co-authored work he or she wrote the text

Name: *Aaron Marshall* Signature:  Date: *20/5/2019*

UNIVERSITY OF CANTERBURY
Te Whare Wānanga o Waitaha
CHRISTCHURCH NEW ZEALAND

Co-Authorship Form

This form is to accompany the submission of any thesis that contains research reported in co-authored work that has been published, accepted for publication, or submitted for publication. A copy of this form should be included for each co-authored work that is included in the thesis. Completed forms should be included at the front (after the thesis abstract) of each copy of the thesis submitted for examination and library deposit.

Please indicate the chapter/section/pages of this thesis that are extracted from co-authored work and provide details of the publication or submission from the extract comes:

Chapter 6 is a reproduction of the publication:
Taleshi Ahangari, H; Portail, T; Marshal, A.T. Comparing the electrocatalytic reduction of CO_2 to CO on gold cathodes in batch and continuous flow electrochemical cells. Electrochemistry Communications. 2019, 101, 78-81.

Please detail the nature and extent (%) of contribution by the candidate:
The candidate is the first author of the paper and performed 90% of the experiments and wrote most part of the text.

Certification by Co-authors:

If there is more than one co-author then a single co-author can sign on behalf of all

The undersigned certifies that:

- The above statement correctly reflects the nature and extent of the PhD candidate's contribution to this co-authored work
- In cases where the candidate was the lead author of the co-authored work he or she wrote the text

Name: *Aaron Marshall* Signature:  Date: *20/5/2019*

UNIVERSITY OF CANTERBURY
Te Whare Wānanga o Waitaha
CHRISTCHURCH NEW ZEALAND

Co-Authorship Form

This form is to accompany the submission of any thesis that contains research reported in co-authored work that has been published, accepted for publication, or submitted for publication. A copy of this form should be included for each co-authored work that is included in the thesis. Completed forms should be included at the front (after the thesis abstract) of each copy of the thesis submitted for examination and library deposit.

Please indicate the chapter/section/pages of this thesis that are extracted from co-authored work and provide details of the publication or submission from the extract comes:
Chapter 7 is a collaborative work between Hani Taleshi Ahangari and Shailendra Sharma under the supervision of A.T Marshall and V. Golovko, and the results will be submitted to the "ACS Catalysis" shortly.

Please detail the nature and extent (%) of contribution by the candidate:
Gold clusters were synthesised by Shailendra Sharma (PhD student).
I performed CO_2 reduction reaction experiments
Written by myself (50%) and Shailendra Sharma (50%)

Certification by Co-authors:

If there is more than one co-author then a single co-author can sign on behalf of all

The undersigned certifies that:

- The above statement correctly reflects the nature and extent of the PhD candidate's contribution to this co-authored work
- In cases where the candidate was the lead author of the co-authored work he or she wrote the text

Name: *Aaron Marshall* Signature:  Date: *20/5/2019*

Table of Contents

ABSTRACT I
ACKNOWLEDGMENTS III
ABBREVIATIONS X
1 Introduction 12
1.1 Overview 12
1.2 Electrochemical CO_2 reduction 13
1.3 Thesis scope and structure 15
1.4 Publications and conference contributions 16
2 Literature Review 18
2.1 Introduction 18
2.2 The nature of the electrode 19
2.3 CO_2 reduction on gold metal 21
2.3.1 The effect of pressure in CO_2 electroreduction 24
2.3.2 The effect of temperature in CO_2 electroreduction 25
2.3.3 The effect of electrolyte in CO_2 electroreduction 26
2.3.4 The effect of electrode crystalline structure in CO_2 electroreduction 29
2.3.5 Reaction mechanism 32
2.3.6 pH and mass transport effect in CO_2 electroreduction 35
2.3.7 The effect of electrochemical reactor configuration in CO_2 electroreduction 38
2.4 Deactivation during electrochemical CO_2 reduction 40
2.5 Brief summary of the literature review 42
3 Experimental Methods 44
3.1 Introduction 44
3.2 Electrochemical reactor configuration 44
3.3 Electrode preparation 46
3.4 Materials and chemicals 47
3.5 Electrochemical techniques 50
3.5.1 Cyclic voltammetry 50

3.5.2 Electrochemical Impedance Spectroscopy 51
3.5.3 Galvanostatic vs potentiostatic CO_2 reduction 52
3.6 CO_2 reduction product quantification 54
3.6.1 Gas chromatography 54
3.6.2 High Performance Liquid Chromatography (HPLC) 56
3.7 Conclusions 57
4 Electrochemical CO_2 Conversion on Polycrystalline Gold 58
4.1 Introduction 58
4.2 Results and discussion 58
4.2.1 CO oxidation on gold electrode 58
4.2.2 The effect of scan rate on CV 60
4.2.3 Galvanostatic CO_2 reduction 62
4.2.4 Potentiostatic CO_2 reduction 65
4.2.5 Formate formation on gold electrode 66
4.2.5.1 CV changes during formate formation 68
4.2.6 The effect of different electrolyte in IR-drop 70
4.3 Conclusions 73
5 Preventing the Deactivation on Gold Electrodes 74
5.1 Introduction 74
5.2 Experimental 76
5.3 Results and discussion 77
5.3.1 Continuous galvanostatic CO_2 reduction on gold 77
5.3.2 Preventing the deactivation by using periodic anodic treatments 81
5.3.3 Preventing deactivation without gold dissolution 82
5.3.4 Using periodic open circuit or anodic treatments to prevent deactivation 85
5.4 Conclusion 87
5.5 Additional material 88
6 Electrocatalytic CO_2 Reduction in a Continuous Flow Electrochemical Cell 92
6.1 Introduction 92
6.2 Experimental 94

6.2.1 Electrochemical cell configuration 94
6.2.2 Electrolysis measurements 94
6.2.3 Product Quantification 95
6.3 Results 95
6.3.1 The Effect of Electrolyte Concentration 95
6.3.2 The Effect of Electrolyte Flow Rate 97
6.4 Conclusion 98
6.5 Additional material 98
7 Electrochemical CO_2 Reduction Using Atomically Precise Gold Clusters 104
7.1 Introduction 104
7.2 Experimental 107
7.3 Results and discussions 108
7.3.1 Deposition of clusters 108
7.3.2 Electrocatalytic reduction of CO_2 on gold clusters 111
8 Conclusions and Recommendations 117
Appendix 1: The thermodynamic potentials 120
Appendix 2: Making reference electrodes 122
Appendix 3: Gas Chromatography 123
Appendix 4: High Performance Liquid Chromatography 130
Appendix 5: Gold cluster synthesis 132
Appendix 6: Copyright permissions 144
References 148

ABBREVIATIONS

AC	Alternating current
AES	Auger electron spectroscopy
CE	Current efficiency
CSTR	Continuous stirred tank reactor
CV	Cyclic voltammetry
DAD	Diode array detector
DC	Direct Current
DFT	Density functional theory
DI	De-ionised
EASA	Electrochemically active surface area
EDS	Energy dispersive X-ray spectroscopy
EDTA	Ethylenediaminetetraacetic acid
EIS	Electrochemical impedance spectroscopy
ESI	Electrospray ionisation
FE	Faradaic efficiency
FID	Flame ionisation detector
FWHM	Full width at half maximum
GC	Gas chromatography
GDE	Gas diffusion electrode
GDL	Gas diffusion layer
HER	Hydrogen evolution reaction
HNMR	Proton nuclear magnetic resonance
HPLC	High performance liquid chromatography
HSGC	Head-space gas chromatography
IC	Ion chromatography
ICP-MS	Inductively coupled plasma mass spectrometry
IPA	Isopropyl alcohol
MS	Mass spectrometry
OCP	Open circuit potential
OER	Oxygen evolution reaction
PEEK	Polyether ether ketone

PEM	Proton exchange membrane
PPB	Part per billion
PPM	Part per million
PTFE	Polytetrafluoroethylene
RDE	Rotating disc electrode
RHE	Reversible hydrogen electrode
RID	Refractive index detectore
RMS	Root mean square
Sat.	Saturated
SCCM	Standard cubic centimetres per minute
SCE	Standard calomel electrode
SEM	Scanning electron microscopy
SHE	Standard hydrogen electrode
TCD	Thermal conductivity detector
UV-Vis	Ultraviolet-visible
XPS	X-ray photoelectron spectroscopy

1 Introduction

1.1 Overview

The global carbon dioxide (CO_2) concentration in the atmosphere has increased drastically over the last few decades. The CO_2 accumulation in the atmosphere can potentially lead to a global catastrophe such as global climate changes [1, 2]. The increase in the average temperature influences the sea levels which subsequently can lead to extreme weather events. Additionally, higher atmospheric CO_2 concentration affects the H^+ concentration in the ocean surface water (as the primary source of CO_2 dissolution). Thus, marine ecosystems can be affected by high atmospheric CO_2 level [3, 4].

The current primary energy sources in the earth for heat and electricity production are based on fossil fuels which result in raising the CO_2 level in the atmosphere [5]. Furthermore, it is believed that non-sustainable fuels are finite resources and are depleting [6]. Table 1.1 shows that fossil fuels will be eventually run out, although the numbers are a rough estimate as new resources will be discovered. Thus, the development of a new carbon cycle which can solve the energy demanding seems to be challenging. Different studies have been conducted to address CO_2 storage [7] and reuse [8] including using renewable resources with higher energy density or using liquid fuels with minimum carbon contents. Furthermore, one of the advantages of liquid fuels is more accessible storage, transport and distribution with no property changes. However, the knowledge for an industrial conversion of CO_2 to fuels is not developed yet due to low production rate and the process cost [9], but it provides an alternative way to produce clean, renewable and sustainable energy. While direct CO_2 capture from the atmosphere is not feasible at the moment, concentrated CO_2 can be sourced from natural gas fields, soda ash plants or cement manufactures [10].

Table 1.1 The global non-sustainable energy reserves and estimation of finishing time by the current consumption rate (adapted from [11]).

Fossil Fuel	Proven Reserves (kW hr)	Years Remaining
Oil	2.75×10^{15}	97
Natural gas	1.91×10^{15}	55
Coal	5.04×10^{16}	116

1.2 Electrochemical CO_2 reduction

There are different pathways for CO_2 conversion into carbon-based chemicals including thermochemical, biochemical, photochemical and electrochemical reduction. While the first three approaches suffer from high energy requirements and low efficiency, electrochemical reduction of CO_2 can produce a wide range of products including CO, alcohols, formic acid and higher hydrocarbons under atmospheric pressure and temperature [12]. This process can be driven utilising obtained electricity through any source of renewable energies such as solar or wind and can easily be coupled with them [13-15]. Another interesting aspect is that water can be used as the proton source which is needed for the reaction. For example, the below reaction in equation 1.1 is not spontaneous:

$$2CO_2 \leftrightarrow 2CO + O_2 \qquad \Delta G = 514.46 \text{ kJ mol}^{-1} \qquad (1.1)$$

If the above reaction splits into two half-cell reactions (equation 1.2 and 1.3), then it can be driven by applying a voltage (more than $-\Delta G/nF$) between the anode and the cathode in which n is taken from table 1.2 and F is Faraday number (equivalent to 96485 C per mol e^-). General cathodic and anodic reactions are [16]:

$$2CO_2 + 4H^+ + 4e^- \leftrightarrow 2CO + 2H_2O \qquad \text{(cathode)} \qquad (1.2)$$

$$2H_2O \leftrightarrow O_2 + 4e^- + 4H^+ \qquad \text{(anode)} \qquad (1.3)$$

Electrochemical devices show notably higher efficiencies over traditional chemical reactors. Also, the reaction thermodynamic can easily be set precisely through the applied potential. Last but not least, an indirect reaction between precursors and intermediates through redox process on the catalyst surface may take place which means unique products might be formed during electrochemical CO_2 reduction. By far the most widely used CO_2 conversion method is electrochemical CO_2 reduction as it has all the advantages as mentioned earlier [17].

Low-temperature electrolysis in an aqueous media utilises the electrical driving force to split water and reduce CO_2 at room pressure and temperature [14]. By applying a potential (voltage) difference between the anode (where water splitting takes place) and the cathode (where CO_2 reduction takes place), the formed protons at the anode can pass through the membrane (a proton conductive membrane) and reaches to the cathode surface. Depending on the used catalyst and the process conditions, a variety of reaction may take place. Some of

the main possible reactions together with their thermodynamic potentials are shown in Table 1.2. The equilibrium potential changes by pH is constructed based on the thermodynamic data and can be seen in Appendix 1.

Based on the data presented in Table 1.2 (by using the coefficients in equation 1.4), the energy requirements for CO_2 reduction to CO is quite close to that of hydrogen evolution reaction (HER) (100 mV higher than HER). Interestingly, HER will be dominant in acidic media and most of the CO_2 reduction studies have been performed at neutral pH. Yet, one of the main challenges in electrochemical CO_2 reduction is that the actual potential is much more negative than the equilibrium potentials and sometimes it reaches to around -2.1 V vs Ag|AgCl [18-21]. This is most likely due to high energy requirements for the activated CO_2^{*-} formation through CO_2 electron reduction [22-24]. A well-designed electrocatalyst can play a key role to minimise the overpotential on one hand and improve the process efficiency on the other hand by an easier adsorbed intermediates reaction.

$$kCO_2 + n\,(H^+ + e^-) \leftrightarrow \text{Product} + mH_2O \qquad (1.4)$$

Table 1.2 Main products of the electrochemical reduction of CO_2 and the thermodynamic potentials in an aqueous solution at pH 0 and pH 7 [25].

Product formula	k	n	m	ΔG° (kJ mol^{-1})	E (V vs SHE) pH=0	E (V vs SHE) pH=7
CO	1	2	1	20.06	-0.103	-0.52
HCOOH	1	2	0	38.4	-0.20	-0.614
HCHO	1	4	1	27.5	-0.07	-0.484
CH_3OH	1	6	1	-17.9	0.03	-0.38
CH_4	1	8	2	-130.8	0.168	-0.245
C_2H_5OH	2	12	3	-49.21	0.09	-0.324
C_2H_4	2	12	4	-40.52	0.08	-0.334
H_2	0	2	0	0	0	-0.414

Electrochemical CO_2 reduction is generally conducted in an electrochemical cell, most of which have a similar structure containing electrodes (anode and cathode), electrolyte and a membrane as can be seen in Figure 1.1. Briefly, CO_2 reduction takes place at the electrode surface when the CO_2 gas passes through the cathode and reacts with the electrons generated at the anode.

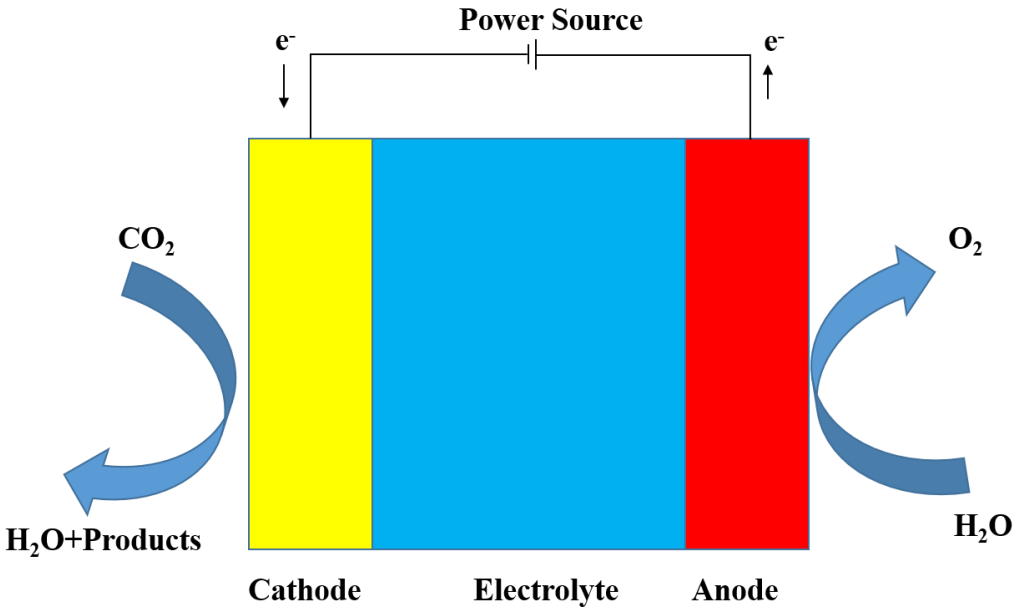

Figure 1.1: A basic schematic of CO_2 electrochemical devices.

1.3 Thesis scope and structure

Electrochemical CO_2 reduction is finding a balance between the proper electrode material and the solution pH. The electrode should be active and selective for electrochemical CO_2 reduction on one hand and be inactive for HER, on the other hand. The solution pH (in an aqueous media) is another critical concern as it directly affects CO_2 solubility and HER. A fundamental understanding of electrochemical CO_2 reduction is highly recommended before commercialising the process. Despite the significant process development since its early days, there are still many issues that should be solved before starting the process commercially.

The present PhD project aims to do a fundamental study to understand the electrochemical CO_2 reduction on gold electrodes. Most of the work in this thesis is focused on gold for discovering new and efficient electrocatalyst for CO_2 electroreduction. The used experimental method in this project is simple and well established. Although, several new findings helped us to expand our knowledge on gold electrodes. Within this thesis, the following steps are taken to achieve the thesis objectives:

- Chapter 3 represents an overview of the experimental method used in this thesis.
- Chapter 4 presents results on galvanostatic CO_2 reduction and investigates the effect of different parameters in a traditional H-cell electrochemical cell.

- Chapter 5 gives an overview of the deactivation on polycrystalline gold electrodes and how the deactivation can be prevented by cyclic voltammetry or gentle anodic pulse without gold dissolution.
- Chapter 6 presents results on galvanostatic and potentiostatic CO_2 reduction on a flow cell. During this chapter, the effect of applied potential together with the electrolyte concentration has been investigated. The results show how cell configuration / electrolyte hydrodynamics can have a significant impact on product distribution. Additionally, a high interfacial pH (electrode / electrolyte interface) created within the porous carbon paper plays a key role in the high CO production.
- Chapter 7 describes the selective electrocatalytic CO_2 reduction to CO on different gold nanoparticles using the flow cell. In this chapter, different nanoparticles have been examined.
- Chapter 8 is a summary and draws the conclusion and outlook based on the results in this thesis.

1.4 Publications and conference contributions

Results shown herein have been published or accepted for publication in peer-reviewed journals:

- H.Taleshi Ahangari, T.Portail, A.T.Marshall, Comparing the electrocatalytic reduction of CO_2 to CO on gold cathodes in batch and continuous flow electrochemical cells, Electrochemistry Communications, 101 78-81 (2019).
- A.T.Marshall, C.F.C.Lim, H.Taleshi Ahangari, D.A.Harrington, Experimental consideration for electrocatalytic CO_2 reduction, ECS Transactions, 80 (10) 1191-1201 (2017).

Results in this thesis were also presented at different conferences as oral or poster presentation. The presenting author is underlined:

- <u>H. Taleshi Ahangari</u>, S. Kumar Sharma, V. Golovko, A.T.Marshall, Electrocatalytic Au nanoparticles performance during electrochemical reduction of CO_2 on gold cathodes, Materials @ UC, University of Canterbury, Christchurch, New Zealand, December 2018.

- H.Taleshi Ahangari, A.T.Marshall, An investigation on the experimental parameters affecting electrochemical reduction of CO_2 on gold cathodes, 47th Chemeca conference, Queenstown, New Zealand, September 2018.
- H.Taleshi Ahangari, A.T.Marshall, Electrocatalytic reduction of CO_2 to CO at Au cathodes in a continuous flow-cell: Effect of process parameters, 69th ISE meeting, Bologna, Italy, September 2018.
- H.Taleshi Ahangari, A.T.Marshall, Maintaining gold catalytic activity during CO_2 electrochemical reduction, Asia-Pacific Conference on Energy Storage and Conversion, Singapore, July 2018.
- H.Taleshi Ahangari, A.T.Marshall, Electrochemical reduction of carbon dioxide on gold cathodes, 100th Raci Centenary Congress, Melbourne, Australia, 2017.

2 Literature Review

2.1 Introduction

The electrochemical CO_2 reduction is CO_2 conversion into reduced products by using electrical sources. Comprehensive studies have been conducted over the last few decades on factors which influence electrochemical conversion of CO_2. It has been illustrated that the activity and selectivity depend on many factors such as electrode material, working electrode potential, electrolyte type and its composition, pressure, temperature and pH [16, 26, 27]. Owing to increasing attention to CO_2 electroreduction over the last few years, significant improvements have been made in this field; however, it is a complicated topic and many features are still unknown. For instance, Table 2.1 shows gaseous products' current efficiencies in a potentiostatic CO_2 reduction at -1.6 V vs Ag|AgCl in 0.1 mol L^{-1} $KHCO_3$ on a Cu electrode. Despite similar conditions for all of these experiments, the product distribution differs remarkably from one to another, showing the fact that there are many unknown parameters present in an electrochemical CO_2 reduction.

Table 2.1 Current efficiencies for different products in potentiostatic CO_2 electroreduction on Cu electrodes at -1.6 V vs Ag|AgCl in 0.1 mol L^{-1} $KHCO_3$ saturated with CO_2.

Current efficiency (%)				Reference
CH_4	H_2	CO	C_2H_4	
25	10	4	38	[28]
40	20	5	22	[29]
15	25	5	16	[30]
5	73	7	15	[31]
6	40	5	4	[32]
5	67	3	9	[33]
40	30	4	22	[34]

Hence, the literature review is presented using a collaborative mixture of old and recent work, to discuss the role of each factor affecting the electrochemical conversion of CO_2 to useful products, and to give the reader an idea of where the issue has come from and where it is going.

2.2 The nature of the electrode

The early systematic studies on the electrocatalytic activity of heterogeneous metal electrodes for the electrochemical reduction of CO_2 have been performed in the 1980s [35-37]. From this point, many researchers have gone on to publish their investigations on various polycrystalline and monocrystalline metal electrodes for CO_2 conversion [27, 30, 35, 38-42]. Azuma *et al.* [36] have worked on the electrochemical reduction of CO_2 using 32 metal electrodes (mainly transition metals) in potassium bicarbonate ($KHCO_3$) electrolyte at various temperatures. They proposed a systematic rule for CO_2 electroreduction on different metallic electrodes, as their experiments showed that HCOOH formation is notably higher on In, Cd, Sn, Pb, Tl and Hg while CO is mainly formed on metals such as Ag and Au cathodes. Similarly, Noda *et al.* [43] have conducted CO_2 electroreduction on various metal surfaces in aqueous $KHCO_3$ at room temperature. They classified the metallic electrodes into four groups given that each electrode is active for a particular product. The first group includes Pb, Hg, In, Sn, Cd, Tl and Bi, and produces $HCOO^-$ / HCOOH as the main product. This group exhibits high hydrogen overpotential and is more selective to formate (or formic acid) as the CO_2 electroreduction reaction products. These metals do not have the ability to break the carbon-oxygen bond, and also, these metals have negligible CO adsorption properties showing the fact that the formation of CO_{ads} from CO_2^{*-} radical is not preferred. But, the radical anions are protonated at the carbon atom, producing $HCOO^-$ as the main product. Therefore, hydrogen production is not favoured using this group of metals.

The second group (*e.g.* Ag, Au, Zn and Pd) consists of metals that produce CO as the main CO_2 electroreduction reaction product. These metals are commonly known for their intermediate hydrogen overpotential as well as weak CO adsorption properties. The first C-O bond breaking of the CO_2^{*-} radical is favoured on these metals as CO (g) is the main product. Indeed, further reduction of CO_{ads} is prevented due to the weak adsorption of CO; thus, CO would be released as a gaseous product.

Relatively high current efficiencies of CH_4 and C_2H_4 can be obtained using the third group (Cu) as they are capable of reducing CO_{ads}. Cu has intermediate hydrogen overpotential but having an intermediate adsorption property at ambient conditions makes it feasible for the further reduction of CO_{ads} to hydrocarbons.

The fourth group (*e.g.* Pt, Ni, Fe and Ti) are not capable of reducing CO_2. Hence, H_2 is the main product. These metals provide low hydrogen overpotential and are widely used for water electrolysis. The strong CO adsorption properties on these metals can cause electrode poisoning through the blockage of the active sites. In other words, the formation of tightly adsorbed CO_{ads} monolayer on the electrode surface prevents further reduction of CO_{ads} to hydrocarbons; thus, instead of CO protonation, the protons are generally reduced to H_2.

A perceptive view of CO_2 reduction reaction can be obtained by Hori's pioneer work [20, 27, 29, 35]. They performed galvanostatic (at -5 mA cm^{-2}) CO_2 reduction using various metals and measured current efficiencies as shown in Table 2.2. They also defined the catalyst activity by the value of the stable potential needed for this current density (less overpotential for highly active electrodes). The selectivity which was reported as current efficiency enables us to classify the metallic electrodes into several groups (like what Noda *et al.* did).

Table 2.2 Current efficiencies for electrochemical CO_2 reduction at various metallic electrodes (adapted from [27]).

Metal	Potential	j	Current efficiency (%)					
	V vs. RHE	mA cm^{-2}	CH_4	C_2H_4	CO	$HCOO^-$	H_2	Total
Ni	-1.18	-5	1.8	0	0	1	89	92
Fe	-0.57	-5	0	0.1	0	0	95	95
Pt	-0.67	-5	0	0	0	0	96	96
Ti	-1.20	-5	0	0	0	0	100	100
Pb	-1.23	-5	0	0	0	97	5	102
Hg	-1.11	-0.5	0	0	0	99	0	100
Tl	-1.20	-5	0	0	0	95	6	101
In	-1.15	-5	0	0	2	95	5	100
Sn	-1.08	-5	0	0	7	88	5	100
Cd	-1.23	-5	1.3	0	14	78	9	103
Au	-0.75	-5	0	0	87	1	10	98
Ag	-0.97	-5	0	0	81	1	12	95
Zn	-1.14	-5	0	0	79	6	10	95
Pd	-0.80	-5	2.9	0	28	3	26	60
Ga	-0.84	-5	0	0	23	0	79	102
Cu	-1.04	-5	33.3	25.5	1.3	9	20	103

It should be noted that the presented results in Table 2.2 are primarily based on the current efficiencies obtained at ambient conditions in aqueous solutions. The product distribution strongly depends on process condition like pressure, temperature and other factors which will be discussed in detail in section 2.3.

2.3 CO_2 reduction on gold metal

The gold catalytic activity for CO oxidation was firstly investigated by Roberts *et al.* [44] in an electrochemical cell. After two papers were published in 1985 and 1987 by Hutchings [45] and Haruta [46], the next 18 years have experienced a remarkable increase in papers about gold catalysis properties, from around 40 in 1987 to over 800 in 2005 [47] and more than 5000 in 2019.

Table 2.3 CO current efficiencies and activity of gold electrocatalyst at 298 K.

Cathode	Potential V vs SHE	CO current efficiency / %	Current density / mA cm^{-2}	Electrolyte	Reference
Bulk Au	-1.91	33	100	0.5 M $KHCO_3$	[48]
Bulk Au	-1.15	50	20	0.5 M $KHCO_3$	[49]
Bulk Au	-1.38	1.3	8	0.1 M $KHCO_3$	[50]
Bulk Au	-1.83	23.6	5	0.2 M $KHCO_3$	[51]
Bulk Au	-1.1	80	7	0.1 M $KHCO_3$	[52]
Au film	-0.71	28		0.5 M $KHCO_3$	[53]
Au film	-0.91	70	1	0.5 M $KHCO_3$	[53]
Au film	-1.06	62		0.5 M $KHCO_3$	[53]
Au film	-1.76	70	25	0.2 M $KHCO_3$	[54]
Au nanowire	-0.76	94	2	0.5 M $KHCO_3$	[55]
Au NPS	-1.4	21.3	5	0.2 M $KHCO_3$	[51]
Au/C	-2.22	64	200	0.5 M $KHCO_3$	[48]
Au/CNT*	-0.96	70	10	0.5 M $NaHCO_3$	[56]
Au NPS/C	-0.67	78	1	0.5 M $KHCO_3$	[57]
Au NPS	-1.38	88%	36	0.1 M $KHCO_3$	[50]
Au NPS/C	-1.08	90	3	0.5 M $KHCO_3$	[58]
Au NPS/C	-0.82	98	16	0.5 M $KHCO_3$	[57]

* Carbon nano tube

Among all the polycrystalline metal electrodes, gold is well known as the most active and selective electrocatalyst to convert CO_2 to CO [38, 49, 55, 58, 59]. However, while the gold price is the main drawback for industrial application, it is still a popular catalyst for fundamental studies because of its activity and selectivity [58, 60]. Although, recent advances in gold nanoparticles synthesis did cause a cost reduction and also a significant increase in the activity by enhanced surface area. Table 2.3 shows a summary of the production rate and current efficiencies obtained by various research groups on gold electrodes. However, the experimental parameter is different from one experiment to another one, but it can be concluded that at a fixed electrolyte concentration, the CO current efficiency is decreased by increasing the potential.

In an early study, Hori *et al.* [49] conducted electrochemical CO_2 reduction using a gold electrode in 0.5 mol L^{-1} aqueous $KHCO_3$ concentration. Unlike those metals producing formate requiring high overpotentials, Hori *et al.* showed high catalytic activity toward CO production on gold (current efficiency was 91% at -1.3 V vs Ag|AgCl with a partial current density of -3.7 mA cm^{-2}) could be achieved at low overpotentials. Seven years later, he [38] again reported 87% CO current efficiency with a trace amount of formate (<1%) under galvanostatic CO_2 reduction (at -5 mA cm^{-2}) in 0.1 mol L^{-1} $KHCO_3$. However, this high current efficiency would drop if the applied potential is not in an appropriate range. The potential importance has been highlighted by Azuma *et al.* [36, 37] who conducted the CO_2 electrolysis on gold cathodes with a low CO current efficiency (17% at -2.2 V vs SCE in 0.05 mol L^{-1} $KHCO_3$) at low temperatures. The effect of potential was also elucidated by Noda *et al.* [43] who obtained a current efficiency of 82% for CO with the current density of -4 mA cm^{-2} at -1.2 V vs Ag|AgCl in 0.1 mol L^{-1} $KHCO_3$ as illustrated in Figure 2.1. They observed a significant decrease in the CO current efficiency (16%) while the potential was increased to -1.5 V vs Ag|AgCl. Figure 2.1 illustrates a typical example of the product selectivity dependency on the electrode potential. It is clear that at lower overpotentials (more positive), CO is the main CO_2 electroreduction product reaching to the maximum amount of around -1.3 V vs Ag|AgCl. The hydrogen current efficiency seems to be following the opposite trend to that of CO. As the overpotential increases, the selectivity toward CO decreases while that for H_2 increases. Formate has been reported to be negligible over electrolysis, so the trend has been ignored.

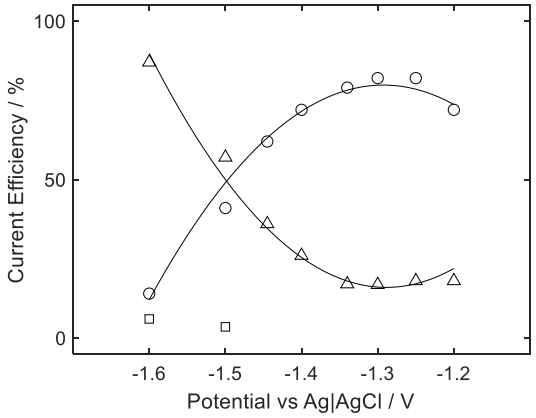

Figure 2.1: The product distribution at different potentials using the gold electrode at 298 K in 0.1 mol L^{-1} $KHCO_3$. CO(circle), H_2 (triangle) and formate (square). Adapted from [43].

Rodriguez *et al*. [61] reported on the kinetics of CO oxidation using gold electrodes in a solution with $HClO_4$ and NaOH. They proposed that the rate-determining step is the first electron transfer; so, CO adsorption promotes the adsorption of its oxidant. They have found that catalytic activity in alkaline solution is notably higher because CO and OH enhance each other's bonding on the gold surface in alkaline electrolyte. They have also focused on CO electrooxidation on gold in an alkaline media by using electrochemical spectroscopic analysis and Density Functional Theory (DFT) study [62]. They concluded that by using a more negative (higher) adsorption potential, more CO would be adsorbed. Increasing the pH did cause a potential reduction; hence, in alkaline solution more CO would be achieved. Cuesta and co-worker [63] carried out a study on the adsorption of CO on silver and gold electrodes. They suggested that CO chemisorbed (strong adsorption) in alkaline media and had weak adsorption (physisorption) in acidic media. Blizanac [64] studied the electrooxidation of CO on a gold crystal. They observed that the C-O stretching frequency is highly dependent on the geometry of the adsorption site. Also, the rate of CO oxidation is changing by crystal phase which means the morphology of CO spectra depends on the surface construction. Koper *et al*. [65] reported an unusual adsorption state of CO on a gold electrode at different overpotentials due to the surface structure. They applied more negative potentials in an alkaline electrolyte to get CO adsorption reversibly. Recently, Jaramillo *et al.* [66] observed methanol formation on gold cathodes for the first time. They proposed that by either strengthening the CO adsorption or increasing the overpotential on gold, proton transfer would be faster than CO desorption from the electrode. In this circumstance, hydrocarbon or alcohol formation may occur. Their DFT calculations showed less energy requirement for methanol formation compared with methane formation on gold.

Electrochemical CO_2 reduction on gold is also of great importance for syngas (a mixture of CO and H_2) production. The formed syngas via competitive CO_2 electroreduction and HER would make it feasible for the downstream processing for ammonia, alcohols or other hydrocarbons generation utilising heterogeneous Fisher-Tropsch catalysis [67, 68]. The main advantage of syngas production, rather than direct CO production, is further application depending on the mixture composition (H_2/CO ratio). The syngas could also be used as either feed or intermediate for bulk chemicals production [9].

2.3.1 The effect of pressure in CO_2 electroreduction

One of the main issues in the electrochemical CO_2 reduction in aqueous media is the limited CO_2 solubility in the liquid phase under atmospheric conditions [69, 70]. The CO_2 solubility in an aqueous solution is 0.034 mol L^{-1} under standard condition [68, 71]. One simple way to resolve this limited solubility is to increase the CO_2 pressure which results in an enhanced CO_2 concentration in the electrolyte according to Henry's law. Investigations into CO_2 electrolysis at high pressures have been explored by many researchers on metallic electrodes such as Pt [72], Cu [72], Hg [73], In [73], Sn [72], Pb [72, 73], Bi [72], Ag [74], Pd [74] and Rh [72]. It is also expected that high pressures will not increase the current density due to higher CO_2 concentration in the electrolyte, while the product distribution is altered at higher pressures [72, 75, 76]. Hara *et al.* [72] are one of the pioneers who performed CO_2 electroreduction at high pressures. They investigated the effect of high pressures (30 atm) on galvanostatic CO_2 reduction (-163 mA cm^{-2}) using a gold cathode. They reported that at a fixed potential of -1.3 V vs Ag|AgCl, a current efficiency of 76% and 15% for CO and H_2 could be obtained, respectively. They proposed that increasing the pressure does not affect CO formation but did cause an increase in the formate formation. Dufek et al. [77] reported 80% current efficiency for CO in a pressurised electrolysis (18.5 atm) on Ag cathodes. The reported current density (-225 mA cm^{-2}) was five times higher than that of ambient pressure. A summary of a high-pressure CO_2 electroreduction experiment using different electrodes is given in Table 2.4. Interestingly, the product distribution easily changes by pressure [78]. Nevertheless, high-pressure CO_2 electroreduction is still considered as the most feasible method for a commercial electrochemical CO_2 reduction [68].

Table 2.4 The electrochemical CO_2 reduction at high pressures using different metallic electrodes.

Cathode	Pressure / atm	Potential V vs SHE	Current density / mA cm^{-2}	Main product	current efficiency / %	Reference
Ag	20	-1.02	-300	CO	86	[79]
Ag	18.5	Not reported	-225	CO	80	[77]
Au	30	-1.1	-163	CO	76	[72]
Pd	20	-1.13	-300	CO	57.5	[79]
Rh	30	-1.21	-163	CO	61	[72]
Pt	30	-1.28	-163	$HCOO^-$	50.4	[72]
Cu	30	-1.44	-163	$HCOO^-$	53.7	[72]
Sn	30	-1.19	-163	$HCOO^-$	92.3	[72]
Pb	30	-1.37	-163	$HCOO^-$	95.5	[72]
Pb	60	Not reported	-200	$HCOO^-$	100.4	[73]
Bi	30	-1.22	-82.7	$HCOO^-$	82.7	[72]
Hg	20	Not reported	-200	$HCOO^-$	100.9	[73]
In	60	Not reported	-200	$HCOO^-$	107	[73]

2.3.2 The effect of temperature in CO_2 electroreduction

In the literature, most of the experiments were performed at ambient temperature and pressure while industrial electrolysis is generally conducted at 80-150 ˚C due to heat generation during exothermic reactions [9]. Thus, the temperature is a parameter that should be considered during electrochemical CO_2 conversion.

The gold catalytic activity has been examined at different temperatures. In contrast to Azuma *et al.* [37] who concluded that HER could be suppressed by lowering the temperature on gold, Kaneco *et al.* [80] pointed out the temperature does not necessarily affect the product distribution as different trends have been observed in a range of potentials (Figure 2.2). One possibility could be less active sites on the electrode surface for protons in the methanol-based electrolyte at low temperatures. They also investigated the effect of temperature on current densities. The maximum CO partial current density was obtained at 0 ˚C while hydrogen production decreased remarkably at lower temperatures. Hence, the CO selectivity at a lower temperature was higher. It is worth noting that the same trend was observed at higher

potentials. The Tafel plots based on this study revealed that CO and HCOOH formation is not limited by CO_2 diffusion.

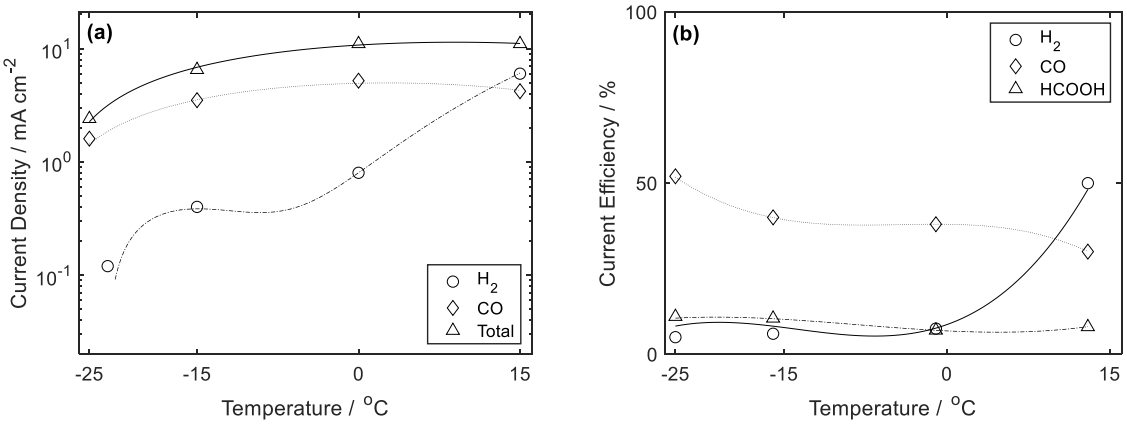

Figure 2.2: The effect of temperature on (a) current density and (b) current efficiency of CO_2 reduction reaction using gold electrode at -2 V vs SCE in 100 mM KOH+CH_3OH at 1 atm. Adapted from [80].

In another attempt to find out how temperature affects CO_2 electroreduction performance, Dufek *et al.* [81] investigated syngas production on Ag catalysts using a Gas Diffusion Electrode (GDE) system in different experimental conditions. They found a reduction in cathodic overpotential (0.32 V) can occur by increasing the temperature from 18 ˚C to 75 ˚C. This effect can be attributed to either HER and CO_2 reduction reaction at the cathode surface which can be affected by thermodynamics and kinetics or less CO_2 solubility at higher temperatures that can limit mass transport which subsequently increasing HER. However, they observed that the produced H_2/CO ratio could be controlled by either current density or CO_2 flow rate.

2.3.3 The effect of electrolyte in CO_2 electroreduction

The nature of the electrolyte, which conducts the charge transfer between two electrodes during chemical reactions, plays a significant role in electrochemical CO_2 reduction and introduces complexity to the process [27, 68, 70, 82]. Different electrolytes can give different product distribution even if the metal electrode is the same [16]. Many solutions, ranging from basic to acidic, were examined as electrolytes, including aqueous electrolytes and non-aqueous electrolytes [83, 84].

An aqueous electrolyte is obtained by ion dissolution in a hydro-solvent substance. The main advantage of this method is the process simplicity as well as stable electroconductivity,

enabling us to perform control experiments using different catalysts [16]. Using this type of electrolyte promotes HER which is normally competing with CO_2 reduction reaction. Additionally, in an aqueous electrolyte, low CO_2 solubility is another important issue [85]. Yet, they are still being used by many groups. The most commonly used aqueous media is $KHCO_3$ which was regularly used by early studies [19, 28, 35, 37, 86, 87]. One explanation could be the traditional application of KOH as a CO_2 absorbent which is used for CO_2 capture in industry. The KOH eventually converts to $KHCO_3$ through $CO_2/HCO_3^-/CO_3^{2-}$ equilibria [13, 88-90]. Thus, in a $KHCO_3$ solution saturated with CO_2, some species like HCO_3^- and CO_3^{2-} can be presented which would be beneficial for CO_2 capture.

On the other hand, there are many advantages of using non-aqueous electrolytes including easier investigation of the reaction mechanism by direct control on water concentration as well as higher CO_2 solubility in non-aqueous media. For instance, the CO_2 solubility in CH_3OH is five times that of water and is still being used in industry as a CO_2 absorber [91, 92]. Moreover, it is reported that HER in non-aqueous solutions is less than that of aqueous electrolytes due to lack of water, which is also beneficial to perform a CO_2 reduction experiment at low temperatures [27]. Regardless of the cathode material, CO is the major product, and the selectivity is totally different from aqueous electrolytes [9]. Additionally, some inert electrodes in aqueous media are active in non-aqueous electrolytes, and higher activities have been reported [16, 27, 68, 70]. However, it should be noted that using volatile and toxic organic solvents would make the product separation and solvent recovery more expensive [93].

Ionic liquid (salt in a liquid phase rather than dissolved neutral molecules in a solvent) electrolytes are another alternative which has been investigated recently and they usually promote CO_2 reduction (although they are not very common due to their price and sensitivity) reaction rate most likely due to a lower CO_2^{*-} intermediate energy [94]. It is well known that the energy needed to convert the stable CO_2 molecule into CO_2^{*-} is relatively high (see section 2.3.5). In the presence of ionic liquids, complexation can take place via interaction between CO_2 and the anion species in the ionic liquid (like BF_4^- or PF_6^-) which subsequently results in lower activation energy [95]. Gold nanoparticles in an ionic liquid system exhibit good selectivity (97% of current efficiency) while the current density is relatively low (-3 mA cm^{-2}) [58]. For a selective CO production (98% of current efficiency), Asadi *et al.* [96] used the ionic liquid in an acidic media (pH=4) with molybdenum bisulphate as the cathode. A high

current density of -65 mA cm^{-2} at -0.764 V vs RHE was reported by them. In another study, Deng *et al.* [97] investigated the effect of pH (by changing water concentration) on the selectivity in an aqueous ionic liquid electrolyte with Ag as the cathode. They observed a higher CO selectivity (current efficiency of 99%) at less water concentration (20 wt.%). Additionally, HER was remarkably enhanced with higher proton concentration.

The nature of used cations and anions in the electrolyte is of great importance. Different solutions such as $KHCO_3$, Na_2SO_4, K_2SO_4, K_2CO_3, H_3PO_4 or $NaHCO_3$ can be used as the electrolyte in the electrochemical conversion of CO_2 [26, 57, 98-100]. But, only limited studies have focused on the effects of anions (like HCO_3^-) or cations on CO_2 electroreduction. However, it has been frequently proposed that the electrolyte type affects the activity and selectivity. Additionally, the product distribution can be altered by changing the cationic electrolyte species, even if all other parameters are kept constant [26, 27].

While many studies highlighted that the larger cations promote CO production over HER on various electrodes [27, 101], Paik *et al.* [102] in an early study noted an increase in the reduction potential by increasing the cation size (Li^+, Na^+, $K^+$and Cs^+) when the current was kept constant on Hg electrode. These observations were confirmed by Hori [103] 13 years later for which the overpotentials were found to decrease by increasing the electrolyte concentration (for Na^+, Li^+ and K^+). Augustynski *et al*. [104] observed that the cathodic current peak's magnitude on a Pd electrode increases by the cation size. The cation size could also affect the CO_2 electroreduction product distribution at Cu electrodes wherein the unwanted HER decreased by increasing the cation size, while C_2H_4 production increased. Also, the reduction potential was the lowest when Cs^+ was used as the cationic species [105-107]. These features indicate that the electrolyte cations affect the CO_2 electroreduction activity and selectivity, and are likely related to the cations adsorption and reaction kinetics of the outer Helmholtz plane. Among those cations (Li^+, Na^+, $K^+$and Cs^+), Li^+ exhibits the highest hydration number and adsorbs to the electrode with difficulty. Hence, HER on Li^+ is the highest due to less stability of the molecule on the electrode surface [27]. Kenis *et al.* [101] conducted electrochemical CO_2 conversion to CO at a silver electrode and different large cations to be able to improve the process performance. The authors reported that the larger cations (like Cs^+) could cause an increase in the processing activity and selectivity toward CO production. They proposed that this behaviour is associated with the cation hydration and adsorption on the electrode. In another interesting study on an Ag electrode

done by Verma *et al*. [108], a high current density (-440 mA cm^{-2}) was achieved by using concentrated alkaline electrolyte (3 mol L^{-1} KOH). This effect is because of more stable CO_2^{*-} intermediate formation by a higher K^+ concentration, which can create a denser double layer (shorter Debye length) at the electrode / electrolyte interface. They [108] also showed that OH^- production was higher than usual when the electrolyte used was KOH. Hence, using an anion exchange membrane was beneficial as OH^- species can be transferred to the anolyte for oxygen evolution reaction (OER) which subsequently enhances CO_2 reduction.

Interestingly, the product distribution in a CO_2 electroreduction reaction is profoundly affected by anion species. Hori *et al.* [29] investigated the effect of anion species (like HCO_3^-, Cl^-, SO_4^-, ClO_4^- and $H_2PO_4^-$) on CO_2 electroreduction on a Cu electrode. They proposed that the local pH is affected by anion and the reaction pathway subsequently would be governed. For example, using $H_2PO_4^-$ electrolyte did cause an increase in HER at higher potentials (more negative). Such a reduction in CO_2 reduction reaction is attributed to a lower local pH which leads to a higher HER. A detailed description of the effect of local pH is presented in section 2.3.6.

Another interesting feature is that changing the electrolyte concentration can also promote CO_2 reduction reaction products. This is attributed to the pH value changes at the electrode/electrolyte interface which is changing by altering the buffer capacity. Hori [29] conducted galvanostatic CO_2 reduction on Cu electrodes at the current density of -5 mA cm^{-2} using a different concentration of $KHCO_3$. He achieved the highest current efficiency at relatively low $KHCO_3$ concentration. In another research, Zhong *et al.* [109] investigated the effects of $KHCO_3$ concentration on Cu cathodes using potentiostatic methods as the applied potential was found to play a key role in the product distribution. Their results suggest that not only dissolved CO_2 in $KHCO_3$ but also potassium cation (K^+) influence the product selectivity.

2.3.4 The effect of electrode crystalline structure in CO_2 electroreduction

The composition and structure of the electrode surface are also of importance in governing CO_2 electroreduction. The early CO_2 electroreduction studies reported a higher overpotential ($\geq$ 500 mV) to get a moderate activity and selectivity on a smooth polycrystalline cathode [38, 110]. This effect was further supported by Jaramillo *et al.* [111] observations who reported the gold electrode surface modification could alter the activity and selectivity. They claimed

that the roughened gold shows a higher current density than the normal gold electrode in a variety of potential ranges, but they were not sure whether this improvement in the activity was due to the increase of the HER or CO production.

The catalytic activity could be improved by changing the surface morphology (*e.g.* defects, steps, grain boundaries) through creating regions of enhanced strains. This is an important issue given that grain boundaries and crystal defects are said to be the most active sites [112, 113]. Not only chemical, but also electrochemical catalysis could be affected by nanostructured grain boundaries [114-117]. The grain boundary surface density on the oxide-derived gold is relatively high as the nanocrystals are interconnected by grain boundaries; however, the surface density cannot be measured precisely due to the complex morphology [57, 98, 118, 119]. Kanan *et al.* [113] quantitatively showed that the grain boundaries and crystal defects are the most active sites for CO_2 electroreduction on vapour deposited gold nanoparticles/carbon nanotube. This is not surprising given that oxide-derived gold has higher activity and selectivity for CO_2 electroreduction to CO compared with the bulk gold because of the grain boundaries. One explanation could be altering the intermediates' binding energy resulting the overall barriers reduction by lattice strain [120, 121]. Another possible reason for the enhanced CO_2 reduction activity is the active high-step densities which was created by dislocation surface termination [122, 123]. Nevertheless, those electrodes deserve on-going development and investigation as many aspects are still unknown.

Recent studies have mainly focused on using nanostructured catalysts as they show higher efficiency and stability (which is attributed to the impurities adaption by the electrocatalyst) during CO_2 electrolysis [57, 60, 98, 124-130]. Additionally, nanostructured surfaces contain more active or low-coordinated sites (*e.g.* edge sites) which favour CO_2 reduction reaction compared with a planar metallic surface [60, 98, 128, 131-133]. Hence, a nanostructured catalyst has also been used in this thesis. The highest current density ever reported on gold cathodes was 200 mA cm^{-2} (see table 2.3) by Delacour *et al.* [134] who dispersed gold nanoparticles on carbon-based supports with the aqueous electrolyte placed between the electrode and proton exchange membrane (PEM).

The clusters (ultra-small nanoparticles with atomically precise chemical composition) are promising materials for electrochemical CO_2 reduction. The geometrical, electronic, magnetic and optical properties of clusters are strongly dependent on their size. Chen *et al.* [135] used a range of ligand-protected gold clusters (from Au_{11} to Au_{140}) for electrochemical reduction

of oxygen. The smaller gold clusters were observed to be more active for electron transfer reaction. This effect was again confirmed for oxygen reduction reaction on silver electrodes [136]. Kwak *et al.* [137] reported the use of $PtAu_{24}(SC_6H_{13})_{18}$ (by doping Pt atom into a stable molecule-like gold nanocluster) for HER. The activity of this catalyst was found to be significantly higher than any other molecular catalyst for H_2 production. In another study, Zhao *et al.* [138] reported an improvement in HER (59.3 mA cm^{-2} at -0.4 V vs RHE) of MoS_2 because of favourable charge transfer and electronic interaction between cluster and support. Also, the interface between Au_{25} core and the ligands was proposed to affect the catalytic performance. Min *et al.* [139] deposited different types of gold nanoparticles (vary from small nanoparticles to aggregated clusters) on carbon paper. They found an increase in CO activity and selectivity with the gold amount reaching to a saturation point at 4 nm gold thickness (typically 40-80% current efficiency for CO). There has been some computational and experimental studies for catalytic and electrocatalytic reduction of CO_2 using metal clusters [140, 141]. Kauffman *et al.* [50] explored thiol-protected Au_{25} clusters interactions with weakly bound adsorbates. They showed that Au_{25} is selective for CO_2 reduction reaction and occurs within an overpotential of 90 mV which is less than the potential needed (200-300 mV reduction in potential) for bulk gold and gold nanoparticles. Recently, they [142] used density functional theory (DFT) to investigate electrochemical CO_2 reduction on gold cathodes and other nanoparticles. They predicted an increase in the *COOH and *CO intermediates stabilisation by decreasing the size. Also, they proposed that the product distribution would be affected by H adsorption. In another work, Mistry *et al.* [143] performed CO_2 reduction on different gold nanoparticles (1.1 nm to 7.7 nm in diameter) in a weak buffer $KHCO_3$ solution. They reported a drastic increase in the current density by smaller gold nanoparticles which is accompanied by lower current efficiencies for CO. This could partly be explained by the content of low-coordinated sites. They also demonstrated high current densities could be achieved by ligand-free micellar gold nanoparticles. This effect was previously highlighted by Sun *et al.* [58] who proposed that the edge sites are active for CO formation while the corner sites are active for HER as the edge sites result in a more stable COOH* intermediate. They found that 8nm gold nanoparticles have minimum corner sites, which favour HER, while the edge sites in this gold nanoparticle are particularly active for CO production.

One interesting approach to enhance electrocatalytic CO_2 reduction efficiency with great success is utilising metal oxide as an electrocatalyst in which the bulk metal is oxidised electrochemically, and the formed oxide layer (in CO_2 saturated media) acts as an

electrocatalyst. This method enables us to modify the catalyst surface by creating more active sites, by forming a nanocatalyst. This process has also been studied using bulk gold by applying periodic pulsed potentials where the oxide layer formed during pulsed anodisation as proposed by Chen *et al.* [57]. They concluded that the rate controlling step is forming the adsorbed CO_2^{*-} radicals while more active sites on gold-oxide catalysts make the initial electron transfer easier (lower Tafel slope). The proposed mechanism for CO production on normal gold and oxide-derived gold is shown in Figure 2.3. It is worth noting that the potential required for CO_2 electroreduction is quite a negative value and the gold would not exist in its oxide form.

For an active and selective CO_2 electroreduction, surface heterogeneity is beneficial by providing adjacent active sites for the reaction intermediate stabilisation. Metal nanoparticles can be used for this purpose by providing highly active sites (the interface between the nanoparticles and the support). High catalytic activity was achieved in various electrocatalytic processes via metal nanoparticles supported on oxide phases [144, 145]. Oxide supported gold nanoparticles such as Au/TiO_2 [146], Au/ITO [147], Au/SiO_2 [148] have been investigated for electrocatalytic process. An enhancement of the catalytic efficiency was observed toward methanol oxidation because of the interface between gold and the oxide phase lowering the reaction barriers [149, 150].

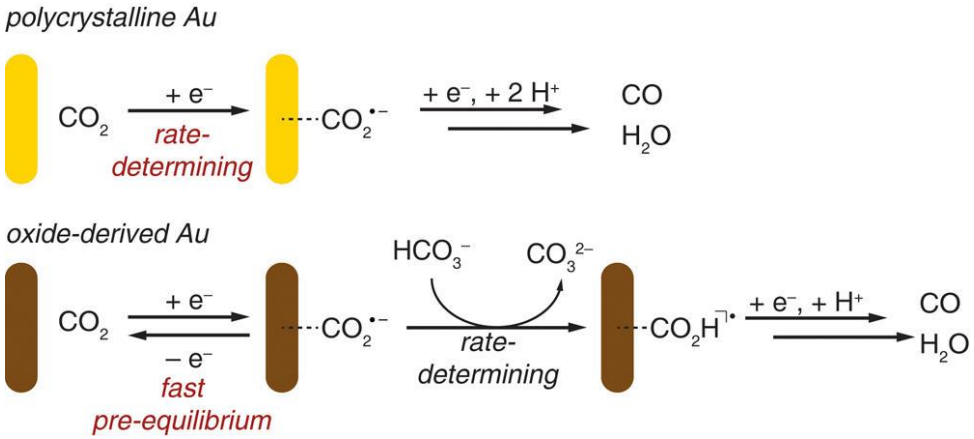

Figure 2.3: The proposed mechanism for electrochemical CO_2 reduction on polycrystalline and oxide-derived gold electrocatalysts. Figure taken from [57] with permission.

2.3.5 Reaction mechanism

Not surprisingly, understanding the reaction mechanism enables us to optimise the electrochemical reduction of CO_2 process by prediction of the product selectivity on a certain

electrode under a given set of conditions [110]. The reaction pathway for electrochemical conversion of CO_2 has been focused for many years on understanding why different metals form different products [151, 152]. CO_2 can be electrochemically reduced to a wide range of products and a commonly accepted mechanism for this reaction is illustrated in Figure 2.4. The type of metallic electrode is the most important parameter affecting the mechanism and subsequently product distribution. The molecular CO_2 geometry changes (from stable CO_2 to CO_2^{*-}) can also determine the mechanism and the overpotential required for the reaction [25].

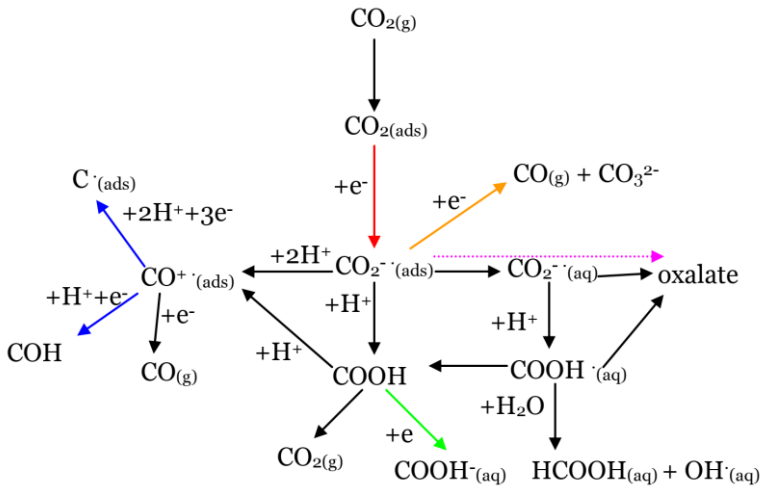

Figure 2.4: The proposed pathway for CO_2 electroreduction reaction in an acidic system. Figure taken from [153] with permission.

The main illustrated pathways are:

→ The CO_2 adsorption onto the electrode surface

→ CO production by CO_2^{-*} disproportionation (CO_2 reacts with CO_2^{-*} to form CO and CO_3^{2-})

→ Formate production by $COOH^*$ reduction

→ Adsorbed intermediate formation which is reduced to form alcohols and hydrocarbons

→ Oxalate formation

Many pathways have been proposed for the electrochemical CO_2 reduction to CO and $HCOO^-$. While early studies proposed formate formation via two electron transfer (the first one is to

form CO_2^{*-} radical anions accepting the proton from water for $HCOO^*$ generation and the second electron transfer is to form $HCOO^-$) [102, 154, 155], recent investigations suggest a proton-coupled electron transfer for $HCOO^-$ formation in which both *COOH and *OCHO intermediates eventually result in formate production [18, 156].

Consistent with Cahplin [153], the following steps have been proposed for CO_2 electroreduction to CO in an aqueous electrolyte [18, 123, 157]:

$$CO_2 + H^+ (aq) + e^- + * \rightarrow COOH^* \quad (2.1)$$

$$COOH^* + H^+ (aq) + e^- \rightarrow CO^* + H_2O \quad (2.2)$$

$$CO^* \rightarrow CO + * \quad (2.3)$$

$$H^+ (aq) + e^- + * \rightarrow H^* \quad (2.4)$$

$$H^* + H^+ (aq) + e^- \rightarrow H_2 + * \quad (2.5)$$

$$H^* + H^* \rightarrow H_2 + 2* \quad (2.6)$$

Where * indicates either a surface-bound species or a vacant active site. The CO_2^{*-} intermediate formation is an essential step in CO or formate production because it is the rate-limiting step [134].

Sun *et al.* [58] stated that a right balance in the first three steps (with high overpotential for $COOH^*$ formation) results in higher CO production on gold electrode; provided that equations 2.4, 2.5 and 2.6 slow down HER. However, these observations were previously highlighted on Ag electrode [60]. Briefly, it is proposed that the CO_2^{*-} radical adsorption on the electrode surface through C-coordination (stable CO_2^{*-}radical) favours CO formation. In this case, protonation is more accessible at the O atom and carboxyl intermediate forms ($COOH^*$). This is followed by carboxyl reduction to CO^* which can be desorbed as CO (g). On the other hand, formate formation takes place when CO_2^{*-} radical is weakly adsorbed on the electrode surface through O-coordination. In this way, the C atom is more accessible to get one proton from the electrolyte which subsequently forms $HCOO^-$ through one electron transfer [158, 159]. It is worth to note that formate is considered as a "dead-end'' product because it cannot be reduced to any other substance, while CO is a primary precursor for syngas or

hydrocarbons generation [29, 160]. Figure 2.5 clearly illustrates the pathways that can lead to either CO or $HCOO^-$ formation.

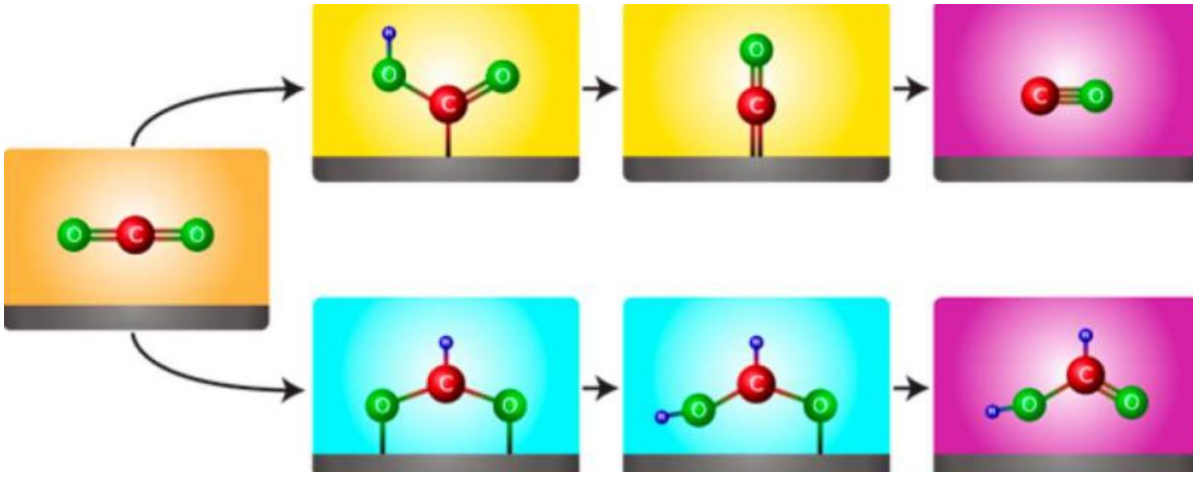

Figure 2.5: The proposed mechanism for CO and $HCOO^-$ production. Figure taken from [161] with permission.

2.3.6 pH and mass transport effect in CO_2 electroreduction

The solution pH is a key concern altering kinetics and molecular transport which should be considered in an electroreduction process since that reaction involves proton transfer (Table 1.2). Not only the CO_2 solubility, but also the CO_2 reduction reaction's thermodynamics (according to Nernst equation) is affected by pH values [162]. Electrochemical reduction of CO_2 in an aqueous electrolyte forms hydroxide ions (OH^-) which eventually changes the pH very close to the electrode/electrolyte interface. As discussed earlier in section 2.3.3, the buffer capacity of the electrolyte defines the product selectivity by changing the pH at the electrode / electrolyte interface.

The Pourbaix diagram is an electrochemical phase diagram showing the stable regions, corrosion regions (where metals dissolved into the solution in the form of ions) and passivity regions (where metal oxide is thermodynamically stable) of metals. Indeed, they represent the species existence based on their potentials and pH [163]. Figure 2.6 depicts the pH effect on CO_2 stable regions, where CO_2 cannot be presented in pH values higher than 8 due to CO_2 depletion via HCO_3^- production (CO_2 reaction with OH^-). Thus, CO_2 electroreduction occurs

at neutral pH while HCOOH formation occurs in acidic pH and $HCOO^-$ is formed over a broader pH range.

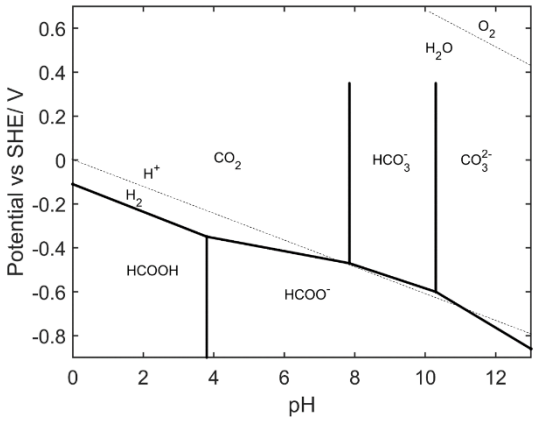

Figure 2.6: The Pourbaix diagram for CO_2 and related substances. Adapted from [154].

For an efficient CO_2 electroreduction, the unwanted HER needs to be minimised. The HER is well known to be highly dependent on the pH, and its equilibrium potential becomes more negative with higher pH [164]. The produced OH^- by CO_2 reduction reaction, on the other hand, is not affected by the pH compared with the HER. Thus, acidic pH is favoured for the HER by considering the fact that less overpotential is needed in comparison to the CO_2 reduction reaction.

Carbon dioxide introduction into the water or other aqueous solution involves a complex series of reversible reactions as can be seen in equations 2.7 and 2.8. The pH can adjust these compounds concentration. The dissolved carbonate concentration in the solution can easily be increased by higher pH values. However, it is well accepted that the carbonate species are not capable of being reduced on metallic electrodes, and the only species which can be reduced is dissolved CO_2 ($CO_{2(aq)}$) [27, 102, 152]. Although, Innocent *et al.* [165] proposed that hydrogen carbonate can be reduced on lead electrodes which is not consistent with the proposed mechanism in Figure 2.4. Infrared analysis in their studies showed no dissolved CO_2 during electrochemical formate formation.

$$CO_2(g) \overset{H_2O}{\longleftrightarrow} CO_2(aq) \overset{H_2O}{\longleftrightarrow} H_2CO_3(aq) \overset{H_2O}{\longleftrightarrow} HCO_3^-(aq) + H_3O^+ \quad (2.7)$$

$$HCO_3^-(aq) \overset{H_2O}{\longleftrightarrow} CO_3^{2-}(aq) + H_3O^+ \quad (2.8)$$

It has been proven that mass transport plays a key role in CO_2 electroreduction reactions [27, 29]. Current efficiencies toward carbon-based products at higher current densities decline due to lack of supplied CO_2 molecules at the electrode surface due to its limited solubility and diffusivity in the electrolyte; consequently, the HER will be dominated [164]. Generally, high local pH (pH close to the electrode surface) affects the product selectivity in two different ways. On one hand, during the electrolysis, the local pH is usually higher than that of the electrolyte pH because of the consumption of protons and also HER. This pH shifts the CO_2 toward HCO_3^- and CO_3^{2-} equilibria reaction causes decreasing CO_2 concentration on the electrode (Figure 2.6). Thus, the selectivity toward carbon-based electroreduction products would be reduced which is accompanied by an increase in HER [166, 167]. On the other hand, an increase in the local pH changes the surface coverage of adsorbing intermediates and a mass transport limitation for the protons is defined; hence, the selectivity toward carbon-based products would be enhanced [29, 168, 169].

The pH value was shown to affect the selectivity on copper electrodes. While low pH values mainly favour methane formation, longer carbon-based products (such as ethylene, ethanol and n-propanol) would be formed at higher pH values [29]. Interestingly, the rate limiting step for longer carbon-based products is independent of pH values, whereas the rate limiting step for methane formation is pH dependant [168, 170]. Because of the detrimental effect of pH in CO_2 electroreduction, Raciti *et al.* [171] have advocated strongly the importance of pH by developing a mass transport model for the electroreduction of CO_2 on copper nanowire as a working electrode. In his model, it has been found that the optimal pH for the carbon-based products is a value between 9 and 10. In another study, they [172] highlighted the same effect of pH and suggested more selectivity for higher hydrocarbons at higher pH on Cu electrodes. It is consistent with Billy *et al.* [173] results who proposed that acidic surfaces favour the formation of HCOOH and CH_4 on polycrystalline Cu electrodes while more basic surfaces enhance C_2H_4 production [173]. Similarly, Lim *et al.* [174] decreased the interfacial pH by increasing the rotational speed on a rotational Cu disc electrode and observed higher H_2 and CH_4 (over C_2H_4) production. Other studies have shown that the cations and anions concentration in the electrolyte can control the product distribution by affecting the local pH at the electrode / electrolyte interface [105, 170] (as discussed in section 2.3.3).

The rise in the interfacial pH is less extreme for the electrolytes such as phosphate and $KHCO_3$ compared with the electrolytes without buffering capacities (KCl or K_2SO_4). Phosphate

electrolytes have a stronger buffer ability compared with similar concentration of $KHCO_3$ (at neutral pH) because of closer pK_a to 7 (pK_a=7.21 for H_2PO_4 and pK_a=10.33 for HCO_3^-) [175]. Thus, the pH at the electrode surface would be higher for non-buffering electrolytes compared with $KHCO_3$ or phosphate buffers at the same experimental conditions [164]. On the other hand, the buffer ability increases with concentration; so, the pH at the electrode surface would be less for higher concentration buffer electrolytes. This rises in the pH by the buffer ability, can explain different selectivity between various electrolytes. Also, increasing the buffer electrolyte ($KHCO_3$) concentration could influence the selective K^+ transfer to the catholyte altering $CO_2/HCO_3^-/CO_3^{2-}$ equilibria. In this circumstance, the product distribution changes by the large cation (K^+) adsorption [176]. Furthermore, CO_2 solubility would be decreased by higher salt content (salting-out effect) introducing mass transport limitations [177-180]. Hence, most of the current efficiency goes for unwanted HER rather than CO_2 reduction reaction. The contribution of these limitations should be accounted during electrochemical CO_2 reduction reaction.

2.3.7 The effect of electrochemical reactor configuration in CO_2 electroreduction

In addition to the factors mentioned earlier, the reactor design has a profound effect on electrochemical CO_2 reduction. However, it is challenging to compare different experiments' results because there is no standard protocol for the process.

One of the most frequently used reactors in electrochemical CO_2 reduction is a H-cell reactor [36, 181-184] which employs cation exchange membrane (like selective proton conductive Nafion membrane) to separate anolyte from the catholyte to avoid electrolyte mixing (Figure 3.1). In this circumstance, the produced proton formed by the OER does not diffuse from the anolyte chamber to the cathodic chamber. Instead, the charge is carried by K^+ (when $KHCO_3$ is used as the electrolyte) and the pH in the anolyte chamber decreases. The used electrode in the anolyte should be active for OER with low overpotentials [185]. Cation exchange membrane can also be replaced by anion exchange membrane. In this case, OH^-, HCO_3^- and CO_3^{2-} will diffuse (when the electrolyte is bicarbonate) [186] causing a decrease in anodic performance, and some of the products (like formate) might be found in the anolyte [187]. Hori *et al.* [186] proposed that OH^- is formed during CO_2 electroreduction at the cathode surface in an aqueous electrolyte (equation 2.9), in which forms HCO_3^- or CO_3^{2-} through the reaction with dissolved CO_2:

$$CO_2 + H_2O + 2e^- \rightarrow CO + 2OH^- \quad (2.9)$$

The main drawbacks for H-cell reactors are limited electrode surface area, a large distance between the electrodes and low cell efficiency. The flow cell has been emerged to increase the surface area in a small cell volume. For an industrial electrochemical CO_2 reduction, it is vital to scale-up an electrochemical flow cell instead of a laboratory batch cell [188]. There has been some efforts on electrochemical cell design for CO_2 electroreduction such as microfluidic reactors [189, 190], polymer electrolyte membrane electrolysers [191] and solid-oxide electrolysers [192], with considerable differences in operational principles and working conditions. Several groups have performed CO_2 electroreduction using a flow cell with a different design but the same principle of using a buffer layer to achieve satisfactory product distribution [67, 193-196]. It has also been suggested that the electrolyte flow rate and electrochemical cell configuration affects the local pH by manipulating the mass transport properties of the reaction [164]. Some papers reported CO_2 bubbling as the main source of convection [30, 98, 197] and some papers investigated the effects of cell configuration on mass transport [173]. The CO_2 consumption increases with the electrolyte flow rate which enhances $HCOO^-$ formation from 10 to 20% [173] while the gas-bubbling tube position profoundly affects the hydrocarbon production [198].

Another important type of electrochemical flow reactor recently investigated is equipped with gas diffusion electrodes (GDE) and effectively enhances the CO_2 transfer rate and subsequently cell performance (Figure 2.7). The catalyst layer in a GDE includes carbon black as the support and gas diffusion layer (GDL) which is actually a hydrophobic porous material [67, 69]. There are many advantages of using GDE. Firstly, the porous medium in GDE facilitates CO_2 diffusion into the catalyst layer. Secondly, the catalyst mechanical support provision would be maintained and thirdly; it provides an enhanced electron and proton transfer [16].

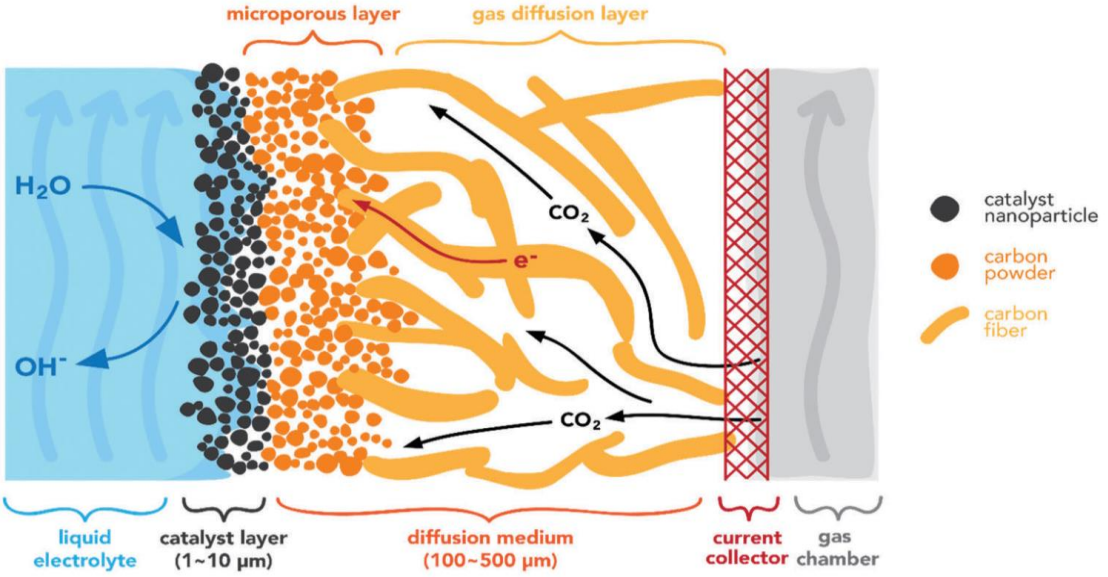

Figure 2.7: A schematic view of the gas diffusion electrode. Figure taken from [199] with permission.

The electrochemical reduction of CO_2 in a flow cell has been explored extensively by researchers [188, 200], but the enhanced performance obtained by the improvement in mass transport or other phenomena has not been clarified to date [68], and it is well known that the hydrodynamic effects due to the cell design and the electrolyte flow play a significant role in electrochemical CO_2 reduction. Thus, this topic needs to be explored more as it is likely the most efficient way for electrolysis.

2.4 Deactivation during electrochemical CO_2 reduction

One of the main challenges in the electrochemical CO_2 reduction is deactivation in which CO_2 reduction reaction decreases with time, and HER will be dominant. Although high selectivity for CO production has been reported in the literature [57, 94, 96, 97, 108, 201, 202], they are not necessarily active or stable over electrolysis. The deactivation has not been unique for gold [203, 204] but also has been widely observed on various metal electrodes such as Ag [205, 206] and Cu [86, 207]. Figure 2.8 illustrates the durability of the electrochemical conversion of CO_2 to CO based on literature. It can be observed that only 4% of reported electrocatalysis are active for more than 10 hours.

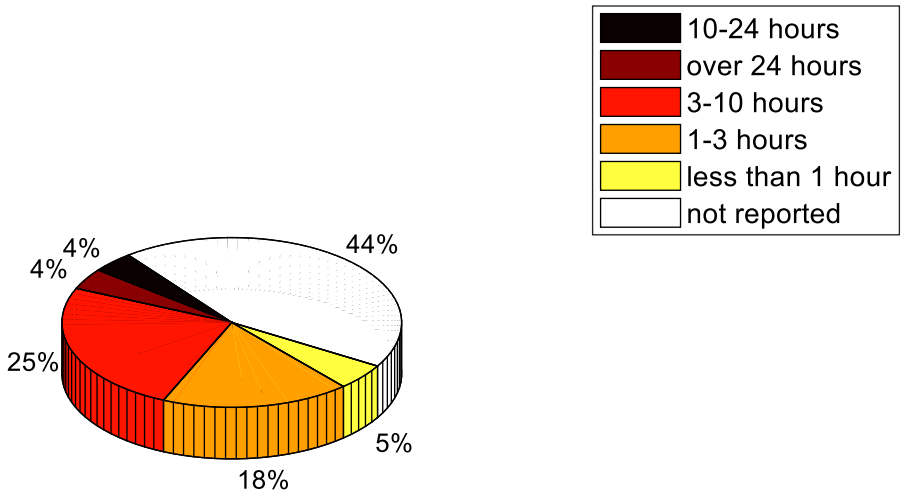

Figure 2.8: The stability of electrochemical CO_2 reduction based on the literature. Adapted from [9]

Many factors can cause an unstable CO_2 reduction reaction and this aspect of electrochemistry poorly understood. One possible explanation for the observed deactivation is metal oxide formation on the cathode surface which can decrease the CO_2 adsorption [208]. Also, organic impurities coming from the water or CO_2 gas can poison the cathode surface [209, 210]. In this case, using a modified electrode which is not oxidised under the electrolysis condition could partially solve the problem. Many proposed that the temperature can strongly influence the electrode deactivation [86, 211] and the electrode thermal treatment affects their adsorption properties [212].

Another well-known hypothesis for the deactivation is the CO_2 reduction reaction intermediates' accumulation. This phenomenon has been widely supported by performing surface analysis such as XPS [86, 213], EDS [181, 184, 214], Raman spectroscopy [215] and AES [86, 216] after CO_2 electroreduction, showing the presence of carbon on the surface, which is a good catalyst for HER [36, 217-219].

Metallic impurities sourced from the electrolyte can also poison the electrode surface. Hori *et al.* [210] proposed that trace amounts of contaminations such as Fe^{2+} and Zn^{2+} can decrease CO_2 reduction reaction and enhance HER. To support this idea, they have purposely added small quantities of Fe^{2+} and Zn^{2+} to the electrolyte and observed the rapid deactivation toward CO_2 reduction reaction. They also highlighted the role of pre-electrolysis in prolonged CO_2 electroreduction. However, pre-electrolysis was found to be ineffective, irreproducible and costly by other studies [131, 205, 207, 220-222]. Wuttig *et al.* [222] showed the

electrodeposition of metallic impurities at the electrode surface. Their studies suggested the presence of Zn and Pb on the copper electrode and Zn and Cu at Ag and Au electrodes. However, they could successfully remove the trace impurities by adding ethylenediaminetetraacetic acid (EDTA) into the electrolyte that can cause ion complexation formation.

Based on these hypotheses, several strategies have been proposed for prolonged CO_2 electrolysis, but the most practical one is applying anodic pulses or stripping cycling voltammetry during electrolysis [181, 203, 210, 213, 220, 223-225] that can strip off the poisonous species from the electrode surface. The main challenge for this method is changing the electrode surface structure by either significant electrode dissolution at relatively high potentials [203, 220, 226-230] or surface coverage changes by adsorbed intermediates [184, 231].

2.5 Brief summary of the literature review

Electrochemistry is a powerful technique to probe electron / proton transfer in a reaction which correlates the electron flows to the chemical changes. The main objectives of electrochemical CO_2 reduction reaction are finding a relationship between the catalyst property, and it's activity and using this information to enhance the catalyst activity and selectivity. As mentioned, a mixture of CO and H_2 is considered as syngas which is the main product in electrochemical CO_2 reduction on gold cathodes. The electrode material and process conditions are two important parameters for H_2/CO ratio. While several electrode materials such as Ag and Zn can electrochemically reduce CO_2 to CO in a CO_2 saturated aqueous electrolyte at ambient conditions, gold electrode shows the highest current efficiency towards CO evolution (87% at -0.75 V vs RHE at a fixed current density of -5 mA cm^{-2}) [27, 39]. Some of the recurring issues reported by many researchers on gold cathodes are low current density and rapid deactivation by increasing H_2 production rate [27, 57]. The main challenge for electrochemical reduction of CO_2 on gold cathodes is to develop an efficient and selective electrocatalyst for a long-term CO_2 electroreduction.

Interestingly, pH is another key factor that can influence the reaction mechanism and the product distribution by the specific intermediate formation and coverage on metal electrodes during CO_2 electroreduction [168]. The local pH can be increased at the electrode / electrolyte interface due to hydroxide formation in the cathodic reactions (as mentioned in equations 2.9).

Such knowledge is believed to be insightful for more active and selective electrocatalyst design for a commercial CO_2 electroreduction.

3.1 Introduction

This chapter addresses the experimental challenges related to CO_2 reduction reaction in this thesis. This chapter aims to introduce the overall experimental set-up, used materials, electrolysis methods and also the products quantification. The main advantage of the presented method is to identify the minor products of CO_2 reduction reaction to give a better understanding of the catalyst activity. Additionally, some experimental considerations, which are written for a particular chapter, are shown separately in that chapter.

3.2 Electrochemical reactor configuration

No standard cell has been designed so far to perform CO_2 reduction reaction. Hence, designing a custom cell seems to be necessary. Three different electrochemical cells set-up were used during the attempt to obtain accurate, repeatable and reproducible measurements. The first two reactors were made for the polycrystalline gold electrode experiments (Figure 3.1), while the third set-up was created for a flow cell configuration (Figure 3.2).

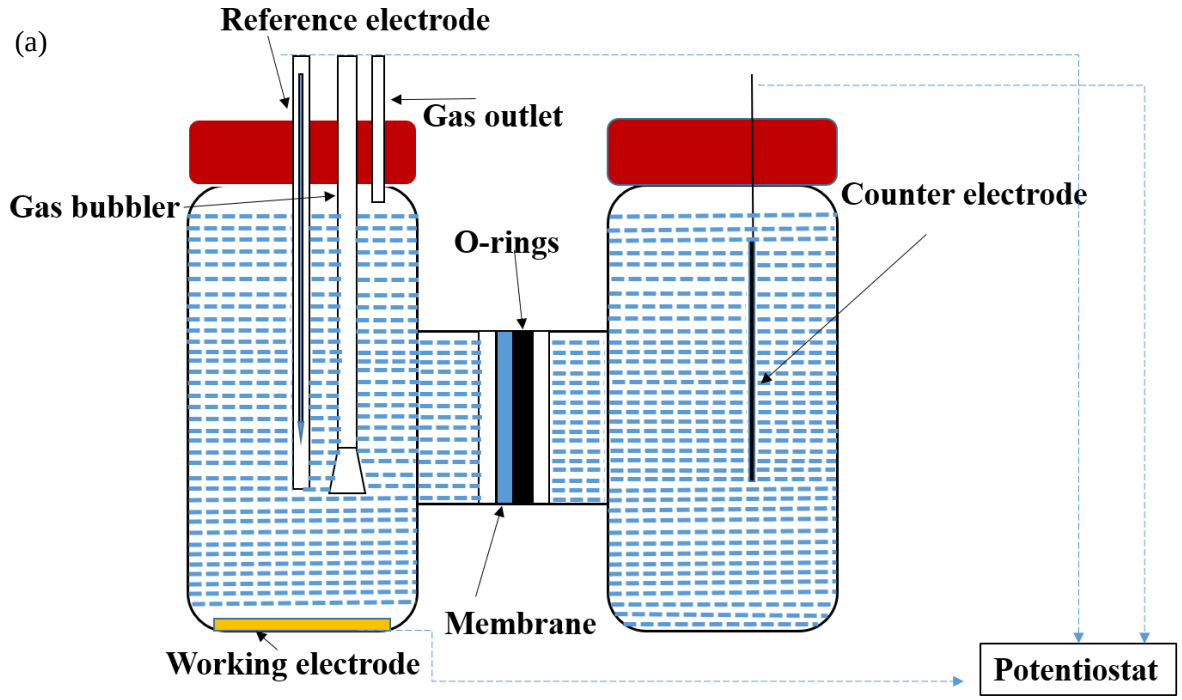

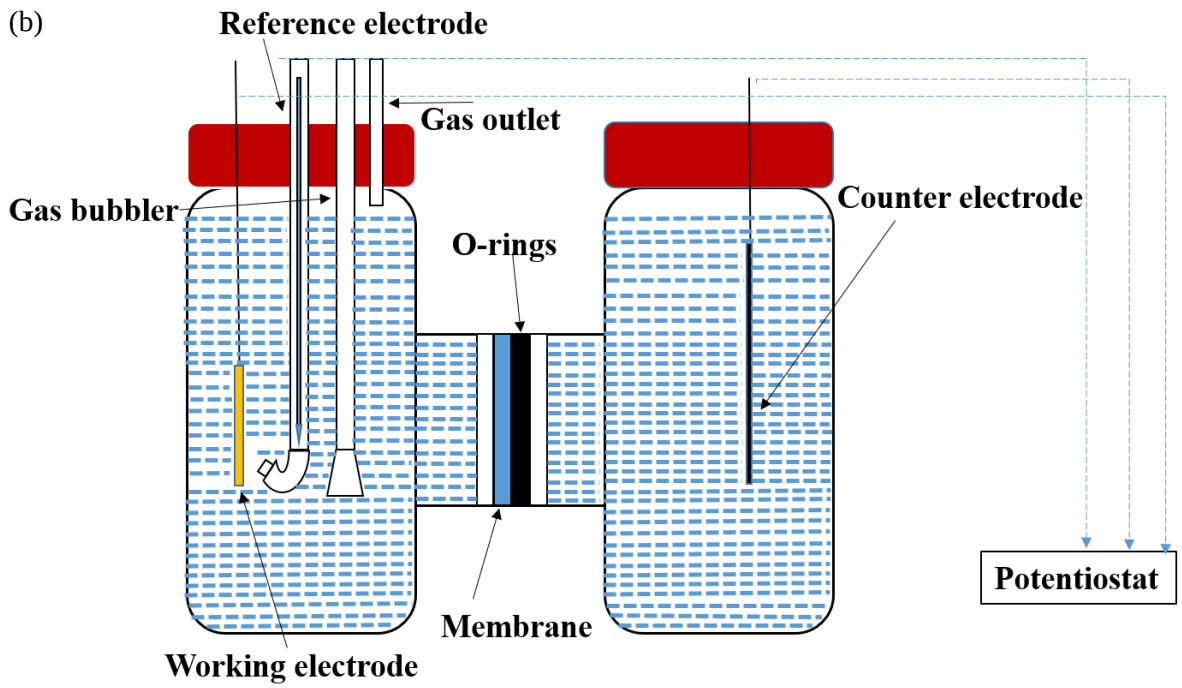

Figure 3.1: The electrochemical cell (H-type cell) design for polycrystalline disc electrodes: (a) The batch cell design with the polycrystalline gold electrode at the bottom, (b) The batch cell design using luggin capillary as the reference electrode holder.

The working electrode in the H-type cell design is connected to an electrical wire and placed inside a glass tube for the sake of being a conductive element to the potentiostat. The luggin capillary in Figure 3.1.b is filled with the used electrolyte, and its tiny tip is open to the solution which allows sensing the electrolyte potential close to the working electrode. The membrane separates the anolyte chamber from the catholyte and is secured in place with a nitrile O-ring. Also at the H-junction, a clamp is used to prevent leaks and air contamination. In this cell, CO_2 is continuously bubbled into the electrolyte during the experiments. The CO_2 flow rate was 20 mL min^{-1} for enough CO_2 transport to the electrode surface without gas bubbles interference. On the top of the catholyte chamber, there is a gas-tight cap which allows the placement of a gas bubbler to purge the gas bubbles through a glass frit. In order to prevent the leakage of the contamination from the reference electrode, a reference junction is used. Also, a gas outlet at the cap enables gas to be collected for further analysis. In this case, 50 mL of the electrolyte in the catholyte and 50 mL in the anolyte is used; however, to easier detection of liquid products in the electrolyte, some researchers prefer to use of smaller electrolyte volume [30].

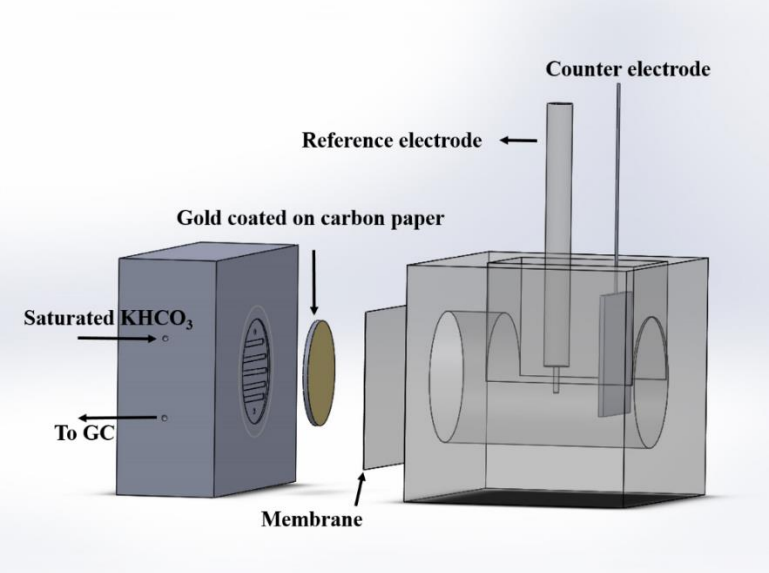

Figure 3.2: The design of used electrochemical flow cell in this study.

Another approach is using a flow cell design in which the reference electrode is placed in the anolyte compartment. The electrochemical cell set-up for the flow cell is different from that of the planar disc electrode as can be observed in Figure 3.2. The cell made from Polytetrafluoroethylene (PTFE), graphite and stainless steel and fitted with silicon O-rings. The working electrode is coated on a carbon paper which is electrically coupled to the graphite with a geometric area of 3.141 cm^2. It is well known that for a bulk electrolysis experiment, anode and cathode should be separated to avoid formed products oxidation at the anode, although some anionic products (like formate) can be detected in the counter electrode compartment as they do pass through the membrane. Also, formed species at the anode do not affect the cathodic reaction if they are separated [30, 196, 232]. The saturated electrolyte with the CO_2 is continuously pumped into the catholyte compartment from another glass container, which can hold approximately 100 mL of the electrolyte. The outlet electrolyte from the cell is collected to the same container. This container is designed to be gas-tight to be able to detect gas products during electrolysis. It should be noted that even small leaks in the electrochemical cell can result in significant errors in the product measurement.

3.3 Electrode preparation

Any electrode can be considered a working electrode as long as a net current flows through the cell [233]. This term is frequently used to mean inert material like platinum, gold or any other electrode that is used in the system. Polycrystalline gold plate (99.999%) sources from

Advent Research Materials Ltd, with the various geometric area, have been used in this study. In the current work, the gold electrode is mechanically polished using SiC papers (starts from 400 down to 2000 grit) followed by alumina slurries (1.0, 0.3 and 0.005 µm) to obtain a mirror finish for electrochemical measurements. In between polishing steps, the electrodes were rinsed with deionised (DI) water and then ultra-sonicated with isopropyl alcohol (IPA)/ DI water in a 1:2 (v/v) mixture to remove particles [234]. The electrodes were rinsed with DI water afterwards following by drying in atmospheric condition (Figure 3.3a). For the flow cell experiments, the gold was coated on carbon paper (SIGRACET GDL 10 AA, Ion Power) using the Sputtering method at a current of I= 20mA and different coating times (Figure 3.3b).

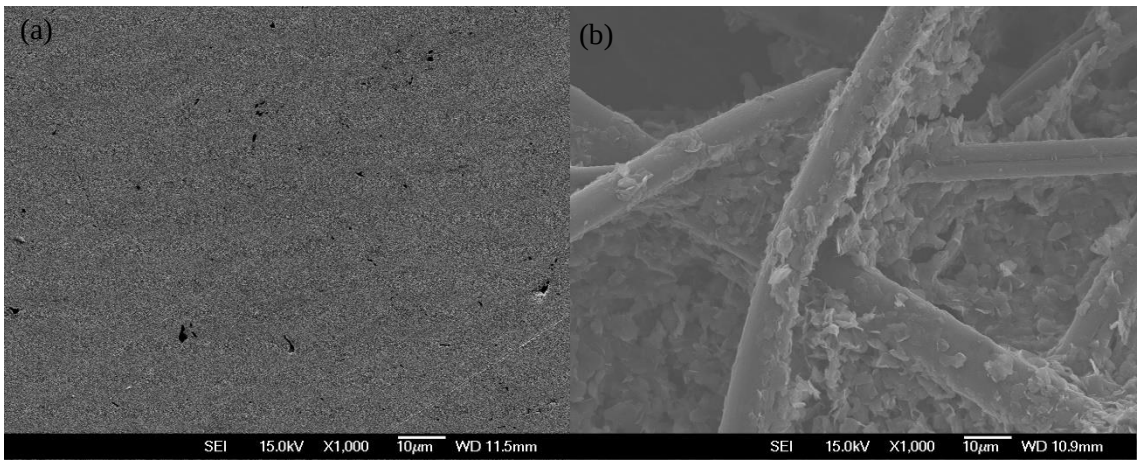

Figure 3.3: SEM images (1000× magnification) of gold samples before electrolysis experiment: (a) polycrystalline gold polished mechanically to a mirror finish, (b) gold sputtered on a carbon paper.

3.4 Materials and chemicals

The CO_2 gas (99.98% purity, instrument grade) in this thesis sources from BOC Ltd without further purification. Although, some works have done some additional steps by passing the CO_2 gas through a mixture of H_2SO_4 + H_2CrO followed by an activated Cu column [29] or addition of some water to the CO_2 gas to prevent liquid products evaporation [30]. To see a sizeable Faradaic efficiency for the electrolysis products, CO_2 was bubbled into the electrolyte because the reaction is mass transport limited [30]. Generally speaking, the CO_2 bubbling into the electrolyte serves several purposes. Firstly, it is the carbon source required for CO_2 electroreduction. Secondly, the CO_2 concentration in the electrolyte is increased by bubbling as it affects CO_2 partial pressure. Also, the electrolyte bubbling by CO_2 results in a pH reduction affecting the carbonate equilibrium in the electrolyte [235]. In most of the

experiments in this study, the CO_2 flow rate of 20 mL min^{-1} was chosen to transport sufficient CO_2 to the electrode surface on one hand and avoid gas bubble interference on the other hand.

For the majority of CO_2 reduction experiments, the used electrolyte was $KHCO_3$ sourced from Sigma Aldrich (99.7%, ACS reagent). The solutions prepared by adding high-purity DI water with a resistivity of 18.2 MΩ cm to make a 0.2 mol L^{-1} stock solution which is usually the working concentration. Table 3.1 shows the purity and supplier of the used materials in this work.

For the electrolysis experiments, the electrolyte was saturated with the CO_2 gas for 30 minutes. The electrolyte bubbling with CO_2 causes the pH reaches to the equilibrium value (the pH is around 7 for saturated 0.2 mol L^{-1} $KHCO_3$).

A Nafion 115 cation exchange membrane was used to separate the anolyte from the catholyte which was prepared by the established procedure in the literature [236-238]. Before using the membranes, we soaked them in DI water for 10 minutes. Then, to oxidise the organic impurities, we put them in 2% H_2O_2 solution heated to the boiling point followed by washing with DI water to remove any H_2O_2. A dilute solution of H_2SO_4 (0.05 mol L^{-1} at 80 ˚C) was used to strip off any metallic impurities followed by washing with DI water again to remove H_2SO_4. The next step was storing the membranes in 0.1 mol L^{-1} KOH overnight to give it sufficient time to exchange H^+ with K^+, and the final step was storing in 0.2 mol L^{-1} $KHCO_3$. The membranes were prepared in the K^+ form which is larger than that the protons at the pH ranges in this study. Hence, the primary charge carrier would be K^+ which is selectively transferred from the anolyte to the catholyte during the electrolysis. This effect is highlighted for long-term electrolysis at high currents or small anolyte volume which can cause charge depletion in the anolyte. On the other hand, $HCOO^-$ is one of the leading CO_2 reduction products which can be transported to the anolyte to be re-oxidised (that affects charge balance calculations). To prevent this effect, the cation exchange membrane is used in our CO_2 reduction experiments.

The counter electrode allows the current to flow between the working and counter electrode, avoiding the reference electrode. In other words, the counter electrode supports the current flow, so that no current passes through the reference electrode (keep the potential at the working electrode constant). So, the surface area ratio of the counter electrode to the working one should be high. To facilitate this, meshes or porous material by using inert substances is

often employed. In this work, porous carbon (for the batch cell set-up) and titanium mesh (25 × 25 mm for the flow cell set-up) coated by 6 µm Mixed Metal Oxide (MMO) were used as the counter electrode. In an electrochemical cell, it is essential to place the counter electrode in a reasonable distance from the working electrode as the counter electrode might experience massive changes, even at potentiostatic conditions [239].

A stable and reliable reference electrode is one of the most important factors that should be considered for CO_2 reduction experiment. The reference electrode is chosen based on the pH of the electrolyte, and the measured potential can be converted between references by knowing the used reference electrode and the electrolyte pH [240]. In this work, a self-made Ag|AgCl reference electrode (see Appendix 2) was used because of its simplicity and application. It's the best option for neutral pH conditions which is the same pH ranges in this study.

Table 3.1 The purity and supplier of substances used in this work.

Substance	Purity	Supplier
Argon, Ar	≥99.999%	BOC
IPA, $(CH_3)_2CHOH$	Analytical grade	Thermo Fisher Scientific
Nitric acid, 70% HNO_3	Analytical grade	Thermo Fisher Scientific
Potassium chloride, 99.8% KCl	Analytical grade	Thermo Fisher Scientific
Silver, Ag	≥99.9%	Sigma Aldrich
Sulphuric acid,98% H_2SO_4	Analytical grade	Thermo Fisher Scientific
Hydrochloric acid, 37% HCl	Analytical grade	Thermo Fisher Scientific
Potassium hydrogen carbonate, $KHCO_3$	≥ 99.7%	ACS reagent
Gold, Au	≥ 99.999%	Advent Research Material
Carbon paper, C	Ultra-high	SIGRSCET GDL 10 AA, Ion Power
Nafion 115	Ultra-high	Ion Power
Hydrogen	≥99.995%	BOC
Titanium	≥99.9%	Sigma Aldrich

3.5 Electrochemical techniques

Electrochemistry is a technique to probe electron transfer in the reactions which relates electron flows to the chemical changes. The chemical variations are often described as the oxide-redox reaction of the metal complex [241]. The electrochemical experiments in this thesis were performed using a Gamry potentiostat (Reference 3000) at room temperature. The most common experiments conducted by the Gamry potentiostat were cyclic voltammetry (CV), electrochemical impedance spectroscopy (EIS), potentiostatic (constant potential) and galvanostatic (constant current) reduction.

3.5.1 Cyclic voltammetry

The electrode characterisation before and after electrolysis is a crucial step in catalytic results analysis. Cyclic voltammetry (CV) is an electroanalytical technique commonly used for electrode characterisation (oxidation and reduction process of the molecular species). The CV is also beneficial for electron transfer probe in a catalytic chemical reaction. The voltammograms can be obtained by sweeping the potential using a specific scan rate while measuring the current response [242]. Oxidation reaction takes place during anodic sweep where the voltage is going to positive potentials and positive current is obtained. In contrast, a reduction process occurs by sweeping the potential to negative values and negative current would be achieved. In the latter case, the reaction would be at the working electrode surface by obtaining the electrons. That makes CV a potent tool not only for discovering the electrode surface oxidation or reduction or catalyst activity [243], but also all the processes involving electron transfer such as electrolyte adsorption, surface reconstructions, double layer capacitance as well as gas or organic impurities in the system [244-248].

As an initial experiment, we have performed CV on polycrystalline gold to study redox behaviour on one hand and remove any adsorbed species (sourced from polishing step) on the other hand. In this case, the potential swept between -0.75 V and 1.2 V vs Ag|AgCl (saturated KCl) in 0.2 mol L^{-1} $KHCO_3$ with CO_2 bubbling flow rate of 20 mL min^{-1} (Figure 3.4). The anodic sweep (going to positive potentials) represents an oxidation reaction resulting in a positive current, while the reduction process is obtained by going to the negative potentials (results in negative currents). Performing CV runs prior to any experiment is repeated, until a uniform and overlapped scan results (we usually perform 10 CV scans before each experiment as pre-treatment). The voltammogram clearly exhibits the gold oxidation and reduction peak

which is consistent with the literature [66, 227, 249-251]. It is worth to note that the CV shape is defined by the electrode nature and electrolyte composition. Hence, it can be considered as a fingerprint of each electrode material. For this reason, it is a great way to determine the cleanliness of the electrode surface.

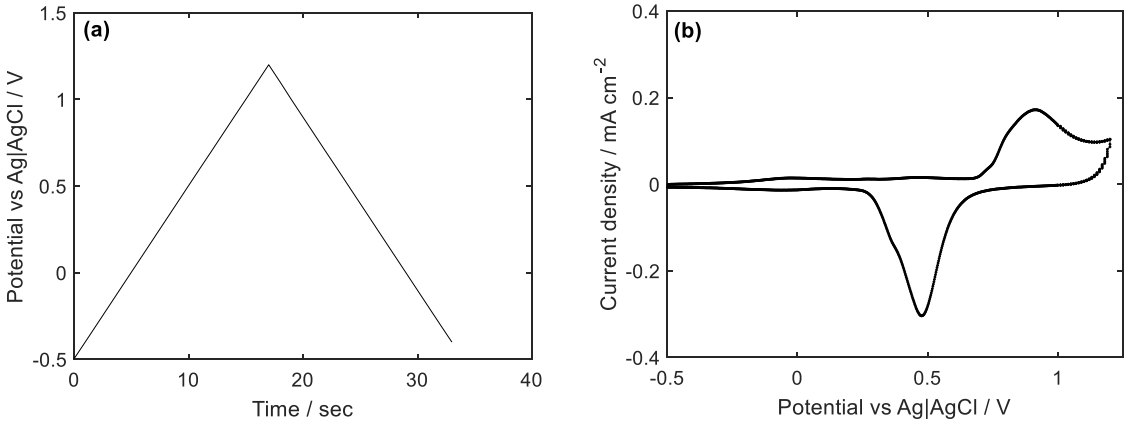

Figure 3.4: Cyclic voltammetry of a polycrystalline gold electrodes in 0.2 mol L^{-1} $KHCO_3$ (pH 6.8) with continuous CO_2 bubbling at 20 mL min^{-1} and scan rate of 100 mV s^{-1} : (a) potential as a function of time (scan rate is defined by line slope), (b) potential vs current.

3.5.2 Electrochemical Impedance Spectroscopy

Electrochemical Impedance Spectroscopy (EIS) is a powerful electrochemical technique which applies a sine wave current or small amplitude to the electrochemical cell and records the obtained current or potential response at different frequencies [252]. The main EIS application in this work is to measure the electrolyte resistance between the working and the reference electrodes. This application should take into account the working electrode's potential correction. The solution resistance depends on many factors including solution concentration, the distance between the working electrode and the reference one as well as the operating temperature (solution conductivity changes by the temperature which eventually affects the solution resistance) [30, 232].

Here, we measure the solution resistance every 15 minutes over a wide frequency range (100 kHz to 10 Hz) at 5 root mean squared (rms) AC potential signal on top of an applied DC current (hybrid EIS) or an applied DC voltage (potentiostatic EIS) for constant current and potential electrolysis, respectively. The solution resistance can be assumed easily by reading the real impedance value at zero phase angle (high frequencies) as can be seen in Figure 3.5 [176]. In most cases in this study, the resistance at 10 kHz could be read as the solution

resistance. In this case, the data shows a high-frequency inductive loop that can be fitted by an equivalent electrical circuit model given in Figure 3.5c. Herein, Rp denotes polarisation (charge transfer) resistance which is in parallel with the double-layer capacitance (Cf) while Rs represent the solution resistance. Besides, the inductance and resistance Lc and Rc, associated with the high-frequency electrochemical cell behaviour originated from cables position in a reactor [253]. The resistance in the proposed model was 1.986 ohm which was almost identical (1.996 ohm) with the amount obtained directly by reading the resistance directly from Bode or Nyquist plot.

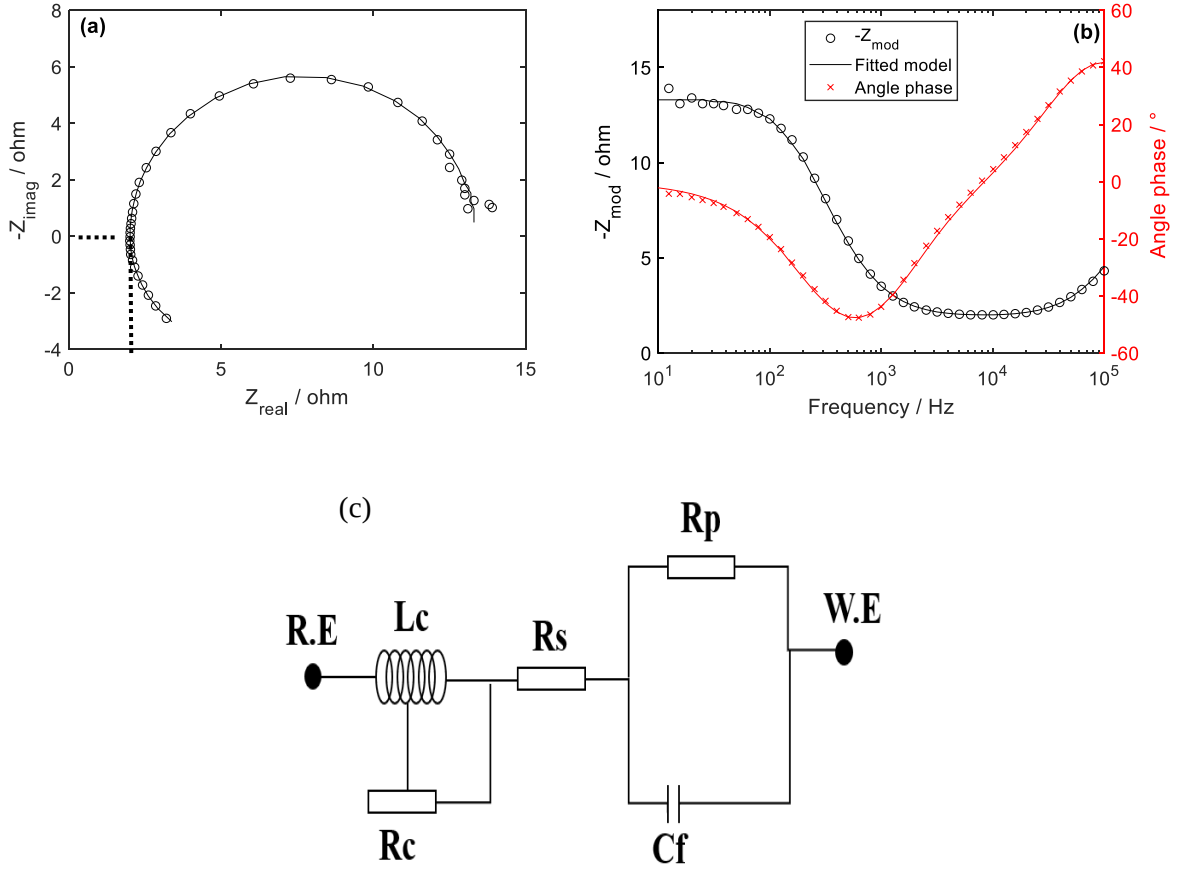

Figure 3.5: (a) The Nyquist; (b) traditional Bode plot and (c) proposed model to assume the resistance for initial hybrid EIS measurements at -5 mA cm^{-2} CO_2 reduction on a polycrystalline gold cathode in 0.2 mol L^{-1} $KHCO_3$ and CO_2 bubbling flow rate of 20 mL min^{-1}.

3.5.3 Galvanostatic vs potentiostatic CO_2 reduction

Electrochemical reduction of CO_2 can be performed by using two different methods: potentiostatic (constant potential) and galvanostatic (constant current). For potentiostatic CO_2 reduction, the potential is constant over electrolysis while the current is recorded. This

approach is an appropriate method when the goal is to identify and quantify CO_2 reduction reaction products. Additionally, this method enables us to correlate the reaction rate changes and product formation [30].

In contrast, the current is constant in a galvanostatic CO_2 reduction and the potential changes to maintain the desired current constant. This method has some advantages over the potentiostatic method where the goal of the experiment is scaling-up, or the potential changes is not significant (low current densities or low resistance). When the applied current density is high, the reaction rate surpasses the mass transport to the electrode interface and the corrected potential would change significantly [254]. The potential changes alters the product distribution throughout the electrolysis and sometimes, the potential shifts to the regions where CO_2 reduction reaction is not favourable anymore.

The potential correction in a potentiostatic CO_2 reduction was conducted by positive-feedback compensation (accounts ohmic losses). In a galvanostatic reduction, the measured electrode potential was corrected with Ohm's law:

$$E_{corrected} = E_{measured} - i_{total}\, R_s \qquad (3.1)$$

Where i_{total} is the total current and R_s is known as the solution resistance. Figure 3.6 illustrates the measured potential and the corrected potential during 4 hours galvanostatic CO_2 reduction at a constant current density of -5 mA cm^{-2} giving the total current of -10.01 mA and the solution resistance of 3.8 ohms.

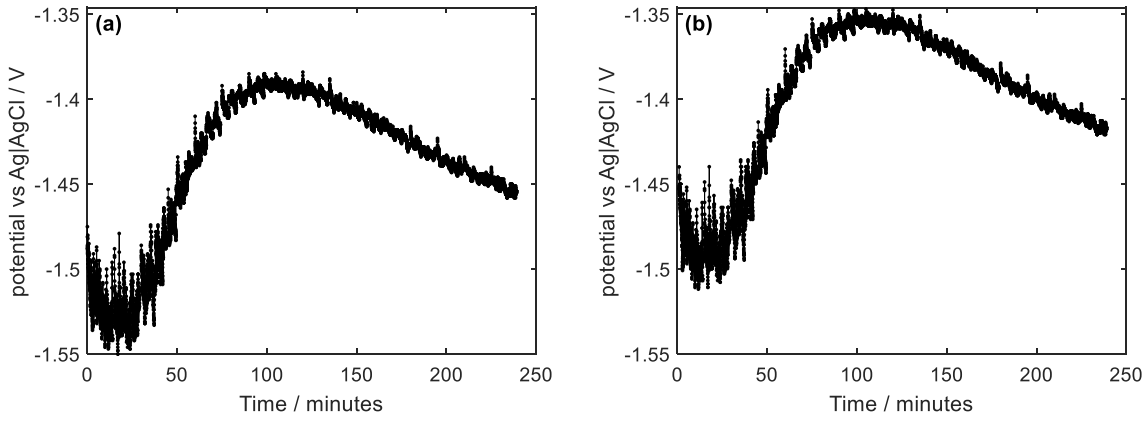

Figure 3.6: The potential changes over a galvanostatic reduction of CO_2 (-5 mA cm^{-2}) on a polycrystalline gold cathode in 0.2 mol L^{-1} $KHCO_3$ and CO_2 bubbling flow rate of 20 mL min^{-1}: (a) recorded potential, (b) potential after ohmic correction.

In this work, the below sequence is often used for a standard CO_2 reduction experiment:

1. Open circuit potential measurements
2. Potentiostatic EIS at open circuit potential to measure initial solution resistance
3. Cyclic voltammetry (sweeping the potential where no CO_2 reduction occurs, between -0.75 to 1.2 V vs Ag|AgCl (saturated KCl)) for initial characterisation
4. Sequence loop (15 minutes each loop)
    a. Potentiostatic or hybrid EIS at a fixed potential or current
    b. Chronoamperometry or chronopotentiometry
5. Cyclic voltammetry (between -1.2 to 1.2 V vs Ag|AgCl (saturated KCl)) to see the possible changes in cyclic voltammetry
6. Potentiostatic EIS at open circuit potential to estimate the final solution resistance
7. Open circuit potential measurements

3.6 CO_2 reduction product quantification

The reaction product analysis enables us to get some information about catalyst selectivity and activity in CO_2 reduction reaction. Several techniques can be used for CO_2 reduction products analysis including gas chromatography (GC), proton nuclear magnetic resonance (HNMR), high-performance liquid chromatography (HPLC), head-space gas chromatography (HSGC), ion chromatography (IC) and mass spectrometry (MS). A summary of these analytical techniques is given in Table 3.2. According to the table, it is possible to reason out why GC and HPLC were employed for gas and liquid products analysis, respectively.

3.6.1 Gas chromatography

The gas products in this study were detected by gas chromatography (GC- SRI 8610C, Multi-Gas#3 configuration) equipped with a haysep-D column with TCD and FID detectors which enables us to separate and quantify different gaseous components with rather high sensitivities [255, 256].

The separation process occurs inside the column based on the chromatography principles. First of all, a small volume of the sample (1 mL) is mixed with the carrier gas (Ar) passing through a column. Different species in the sample interact differently with the material inside the column. A strong interaction results in a long retention time while the species with a weaker interaction retain shorter. Two parameters that can influence retention times are the

column temperature and carrier gas flux. At the end of the column, gaseous components are quantified using an appropriate detector by giving a signal when the component leaves the column. Two different detectors were used in this research:

Table 3.2: Common techniques for the product analysis during electrochemical CO_2 reduction reaction.

Analysis	Details	Limitations	Products' detection
GC	• Suitable for gas phase • Low detection limit [257, 258]	Retention times changes for an inappropriate method	H_2, CO and hydrocarbons
HSGC	• Suitable for volatile compounds • Low detection limit [257, 258]	Retention times changes	C1-C4 volatlile organics
MS	• Rapid analysis • Valid for various products [124]	Invalid for some molecules [259]	Hydrocarbons, alcohols
HPLC	• Suitable for liquid phase • Small aliquot of electrolyte needed [260]	Retention times changes	Formate and alcohols
H NMR	• Suitable for a wide range of products [261, 262]	Cost Invalid for aldehyde products [263]	Formate, alcohols and ketones
IC	• Ions detection	Retention times changes Limited detection range [264]	Formate and oxalate

1. **Thermal Conductivity Detector (TCD):** The principle of quantification is based on changes in carrier gas thermal conductivity when another compound is dissolved in the carrier gas. An appropriate carrier gas thermal conductivity allows the detector to identify all the products. This detection method can be used for both organic and inorganic compounds detection. The advantage of using Ar as the carrier gas is the TCD sensitivity to H_2. So, in this work, TCD was mainly used for H_2 detection.

2. **Flame Ionisation Detector (FID):** This detection method is based on passing the samples through hydrogen flame (gas compounds ionisation) which is highly sensitive to hydrocarbons and CO_2 reduction products. As hydrogen flame is used in FID, hydrogen is not detected here. The FID is coupled to a methaniser converting CO and CO_2 to CH_4 through a nickel-based catalyst for CO detection.

The signal area depends on the nature of the gaseous product and its concentration. So, the GC was calibrated to quantify H_2, and CO. CO_2 is considered as the reactant gas which appears on FID as a large broad peak which exceeds the detection limit. It should be noted that the detection limit for GC is around 100 ppm for TCD and 10 ppm for FID detectors which equals to current efficiencies of approximately 1% for H_2 and 0.1% for CO at -5 mA cm^{-2} and CO_2 flow rate of 20 mL min^{-1}. Current / Faradaic efficiency measures the selectivity of an electrocatalyst toward a specific product and is calculated by determining the charges required to form each product dividing by the total number of coulombs passed during electrolysis. In this circumstance, the volumetric production rate from GC measurements is converted to the molar basis by ideal gas law assumptions following by a conversion to the charge basis using the Faraday constant. For example, a high Faradaic efficiency toward CO indicates the electrocatalyst is highly selective for CO production, yet does not give any information regarding its activity. Table 3.3 shows typical uncertainties for an example experiment which contributes to the uncertainties coming from Alicat mass flow controller and GC calibration. The calculations have been fully explained in details in Appendix 3.

Table 3.3: Faradaic efficiencies and their associated uncertainties for a galvanostatic (-5 mA cm^{-2}) CO_2 reduction reaction on a polycrystalline gold electrode in 0.2 mol L^{-1} $KHCO_3$ and CO_2 bubbling flow rate of 20 mL min^{-1}.

Gaseous product	Faradaic efficiency / %	Uncertainty / ±%
H_2	46.83	0.07
CO	51.2	4.63
Total	98.03	4.7

3.6.2 High Performance Liquid Chromatography (HPLC)

In addition to gaseous products, CO_2 electroreduction can also form some liquid products with very low Faradaic efficiencies. The primary liquid product using gold and Cu electrodes is formate [49, 265]. In this study, the HPLC (HP 1100 series equipped with a SUPELCOGEL^{TM} C-610H) has been employed for the detection of liquid products.

For the analysis, it requires a very small (50 µL) volume of the electrolyte from 2 mL sample vials by the needle which is mixed to the mobile phase to pass through a high-pressure column. For the carboxylic acids (such as formic and acetic acid) analysis, a dilute acid can be used as the eluent to separate the liquid products [124, 209]. The separation depends on

some factors such as column temperature, mobile phase flow and composition. The liquid components in the mixture pass through the column with different rates. At the end of the column, the separated compounds can be detected by employing an appropriate detector identifying the components based on the retention time [266, 267]. In this study, we used two types of detectors:

1. **Diode Array Detector (DAD):** The principle of this detector is based on their UV or visible light absorption. DAD detector covers a wide range of wavelength and is suitable for unsaturated components with strong UV absorption. However, the weakness of this detector is low sensitivity toward alcohols.
2. **Reflective Index Detector (RID):** The principle of this detector is based on the differences in refractive index between the mobile phase and the electrolyte. In this method, the mobile phase is considered as a reference and the second compartment's refractive index will be different giving a signal.

The formic acid detection limit in our HPLC is 0.1 mM (equals a Faradaic efficiency of 0.7% after 4 hours CO_2 reduction at -5 mA cm^{-2} in 55 mL of electrolyte). The component's concentration determination in the HPLC is very similar to a GC. In this case, The peak area is proportional to each product concentration. For HPLC calibration, different solutions of known concentration of formic acid in water and $KHCO_3$ has been used. The detailed specification for GC and HPLC (Faradaic efficiency calculations, calibration and uncertainties analysis) is provided in Appendix 3 and Appendix 4, respectively.

3.7 Conclusions

To sum up, this chapter has discussed the main challenges in CO_2 reduction reaction which are the product generation and quantification. To achieve that purpose, a careful design of the electrochemical reactor is required to maximise the product concentrations coupled to the GC. Additionally, a method for the calculation of accurate potential was proposed in a control experiment that would provide a better understanding of CO_2 reduction reaction which eventually tackles the fundamental problems of reducing the overpotential. In this chapter, all the experimental consideration for an efficient CO_2 reduction has been summarised.

4 Electrochemical CO_2 Conversion on Polycrystalline Gold

4.1 Introduction

This chapter details the fundamentals associated with electrochemical experiments on a gold cathode employing the experimental set-up shown in Figure 3.1. This chapter aims to gain more knowledge about the polycrystalline surface changes (caused by CO electrooxidation or CO_2 reduction) during electrolysis (galvanostatic / potentiostatic) or cyclic voltammetry. Furthermore, by performing electrocatalytic CO_2 reduction on different gold surfaces, we can obtain information about the impact of surface roughness on the catalytic activity and selectivity. Besides, formate formation has been investigated in details by performing cyclic voltammetry and measuring the formate concentration after electrolysis. Lastly, the cell design has been modified so that the minimal resistance achieved during electrolysis.

4.2 Results and discussion

4.2.1 CO oxidation on gold electrode

Prior to the controlled CO_2 electroreduction, several electrochemistry measurements were conducted on a gold electrode with a surface area of 3.141 cm^2 to study the reactions occurring on the gold electrode and also to observe the Au/AuO_x process used to determine the electrochemically active surface area (EASA). The CV can be taken to study the interfacial behaviour of electroactive species. Also, reactant and the product can play a role in an adsorption-desorption process.

The onset of Faradaic currents is 0.7 V vs Ag|AgCl due to gold oxide formation (peak B in Figure 4.1f) which has already been reported by many researchers in early studies [268-275]. However, many reported the onset potential for gold oxidation starts at lower potential values presumably due to the electrode structure [276], electrolyte composition [269, 275, 277] or impurities from the anolyte that can be deposited on the gold cathode so that affecting the oxygen adsorption [270].

The CV at a fixed upper potential and various lower potential (negative values) represents significant changes at the potentials around -0.13 V vs Ag|AgCl in the forward scan (Figure 4.1c and Figure 4.1d) which is attributed to CO oxidation to CO_2 while there is no carbon monoxide oxidation for other lower potential (less negative) limits (Figure 4.1a and Figure

4.1b). Given that CO (the produced CO during CO_2 reduction) adsorbs on the gold only at more negative potentials than -0.9 V vs Ag|AgCl, no CO on gold is formed at lower potentials to be oxidised. In other words, the presence of CO peak at the potential of -0.13 V vs Ag|AgCl is evidence of CO_2 reduction at the potentials higher than -0.9 V vs Ag|AgCl. Also by increasing the potential to more negative values (Figure 4.1e), more carbon monoxide adsorbs on the gold; thus, more carbon dioxide will be produced through CO oxidation at the potentials around -0.13 V vs Ag|AgCl.

For the potentials higher than -1.30 V vs Ag|AgCl, as illustrated in Figure 4.1e, the maximum CO coverage is achieved and increasing the potential does not alter the CO coverage on the gold electrode. Interestingly, using alkaline electrolytes can increase the CO coverage through the potential changes (0.5 V to more negative potentials) by higher pH values. This effect has already been highlighted by Koper *et al.* [62] who investigated CO adsorption on Au(111), Au(100) and Au(110).

Figure 4.1f clearly shows different features of a polycrystalline gold surface: CO oxidation at peak A, gold oxidation at peak B, gold reduction in the negative scan to metallic gold at peak C and a wide region of double layer charging area (non-Faradaic current) where no electrochemical reaction takes place. Additionally, if the potential is swept to more negative values, both CO_2 reduction reaction and HER cause the cathodic current falling sharply. Gold oxide formation starts at peak B and is followed by further gold dissolution by gold oxide monolayer formation like AuO [278].

The real surface area of a gold electrode can be estimated through oxygen adsorption measurements. Rand *et al.* proposed that a monolayer is approximately the oxygen coverage of the gold electrode held for 100 sec at 1.2 V vs Ag|AgCl in 1 mol L^{-1} H_2SO_4 [271, 279]. The coverage could be calculated easily by desorbing the layer through sweeping the potential to the cathodic values and integrating the charge passed. In this study, the charge value of 400 µC cm^{-2} has been assumed to produce one EASA for the electrode while in the literature different values such as 192 µC cm^{-2} [280], 386 µC cm^{-2} [281-286], 390 µC cm^{-2} [287-291], 482 µC cm^{-2} [227, 292, 293] and 723 µC cm^{-2} [149, 294-296] has been reported and a roughness factor of 1.3 was considered as a smooth gold electrode.

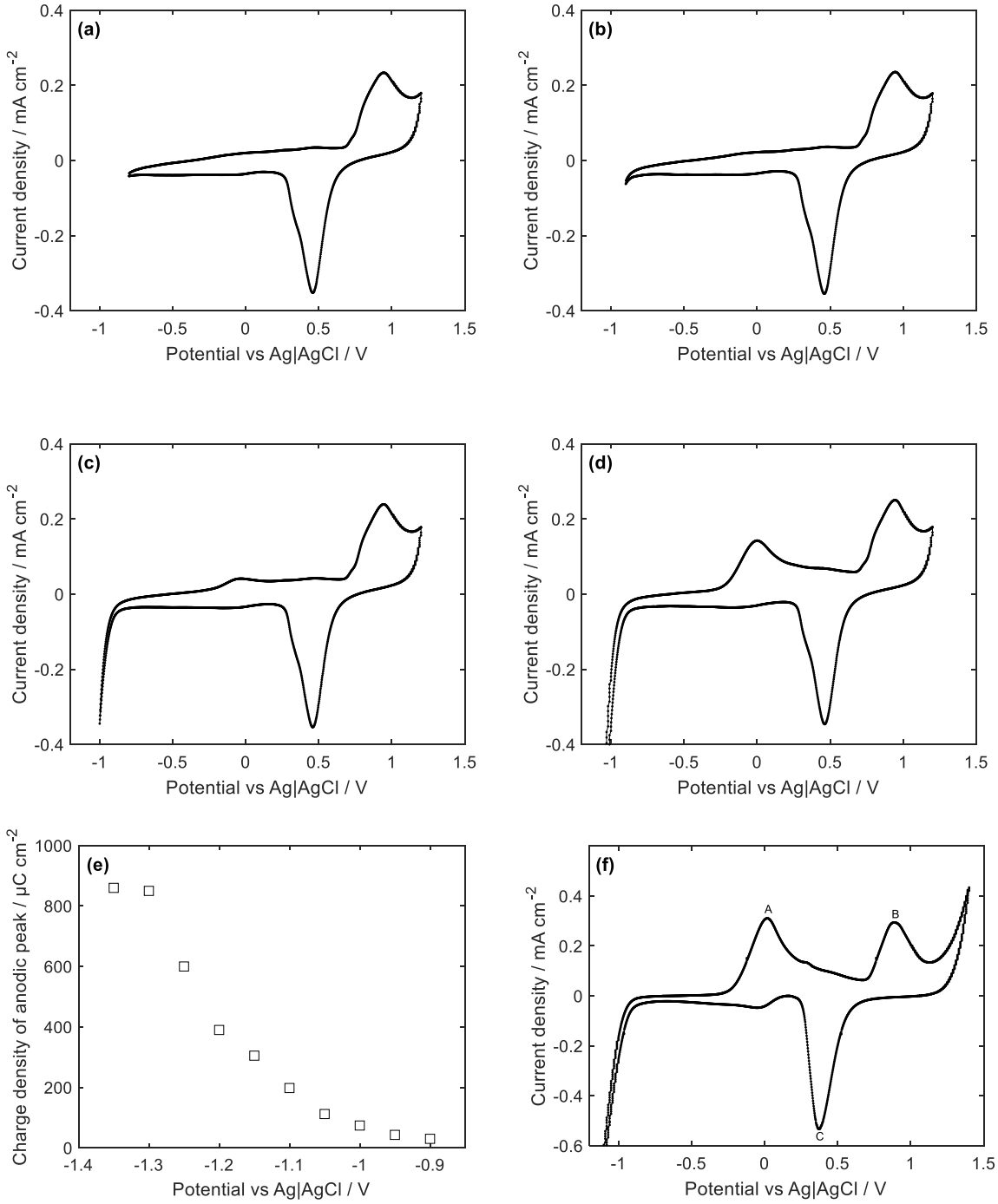

Figure 4.1: The effect of lower potential limits on CO oxidation peak using gold electrode in 0.2 mol L^{-1} $KHCO_3$ (saturated with CO_2) with the upper potential limit of 1.2 V vs Ag|AgCl and the scan rate of 100 mV s^{-1}.

4.2.2 The effect of scan rate on CV

The scan rate in a CV defines how fast the potential is recorded. A series of experiments were carried out at different scan rates relating to different film thickness and features. Obtained CV during film growth on the gold electrode at different scan rates are presented in Figure

4.2, which is consistent with the previous observations [297, 298] who reported cyclic voltammetry changes at different scan rates on carbon and gold electrodes. Our results show that the current response will change if the scan rate is altered. Each curve has the same form, but the current density increases with scan rate because of the size of the diffusion layer at different scan rates. In slower scan rates the diffusion layer grows much further from the electrode compared with faster scan rates; thus, there will be smaller flux to the electrode surface. As the current is proportional to the flux, the magnitude of the current will be higher at high scan rates [252, 299].

The kinetics of the gold electrode can be shown by the obtained voltammograms of the AuO_x films in 0.2 mol L^{-1} $KHCO_3$ at different scan rates as illustrated in Figure 4.2. As evident in Figure 4.2, the peak currents for gold oxide formation and gold oxide reduction increased with the scan rate over the range of 5 to 800 mV s^{-1}.

Another interesting aspect of the reduction peaks is that they became broader by faster scan rates and two separate peaks at scan rates faster than 400 mV s^{-1} can be observed. One explanation could be various gold oxide formation at high potentials. For slow scan rates, the time is sufficient for an electrochemical reduction of gold oxide at a fixed potential while for higher scan rates, different types of gold oxide cannot be reduced electrochemically in one potential. Hence, two separated peaks can be observed.

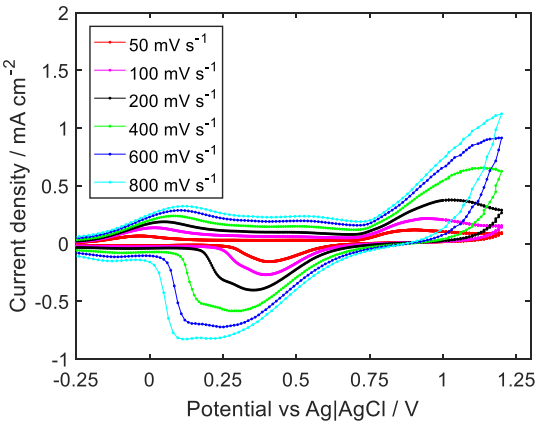

Figure 4.2: Cyclic Voltammetry at a gold electrode in 0.2 mol L^{-1} $KHCO_3$ (saturated with CO_2) with the anodic upper limit of 1.2 V vs Ag|AgCl and lower potentials of -1.2 V vs Ag|AgCl at different scan rates.

4.2.3 Galvanostatic CO_2 reduction

Thirteen galvanostatic CO_2 reduction experiments (-5 mA cm^{-2}) were performed in an aqueous 0.2 mol L^{-1} $KHCO_3$ electrolyte for 4 hours on the polycrystalline gold cathode. The average gaseous products Faradaic efficiencies and potentials are given in Figure 4.3. Given that the literature data [36, 38, 43, 151, 300] shows the main gaseous products during galvanostatic / potentiostatic CO_2 reduction on gold cathodes are CO and H_2 (with small amount of formic acid with Faradaic efficiency of <10%), the overall agreement was very good and consistent. The results also suggest that the high CO Faradaic efficiencies diminish quickly and HER becomes the dominant reaction due to deactivation (this effect will be discussed thoroughly in details in chapter 5).

From the results in Figure 4.3, we can see a huge variation in the gaseous products Faradaic efficiency and selectivity in CO_2 electroreduction and the potential changes during electrolysis. While some of these variations are attributed to the surface roughness, it is clear that significant variation in the product selectivity is found even when repeating the experiments under the same reaction conditions. Given that potential drives the reaction selectivity [43], the variation in Faradaic efficiency could be due to changes in potential (please refer section 4.2.4). Also, the different roughness factors at the start of each experiment dramatically affect the product distribution. We believe that the rougher electrodes (roughness factor 3) exhibit more activation for CO production due to more active sites favouring CO_2 reduction reaction and it takes a longer time to get deactivated while for a smoother gold electrode (roughness factor 1), the rate of deactivation is more. One explanation could be partial CO_2 adsorption on the smooth electrode under OCP, shortening the catalyst long-life [207]. This conclusion is consistent with Li *et al.* [98] study who performed CO_2 reduction on an extremely rough Cu surface. The effect of roughness factor on product distribution is illustrated in Figure 4.5.

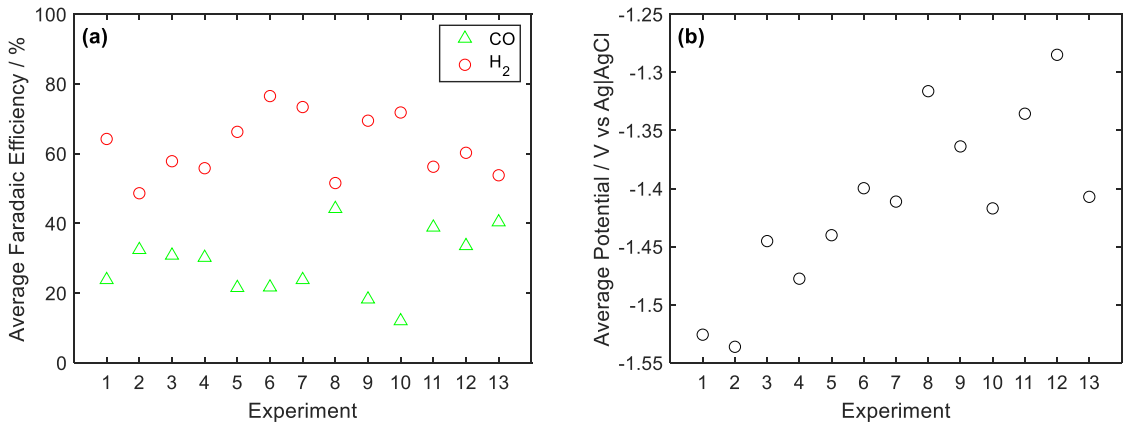

Figure 4.3: Gaseous products (a) Average Faradaic efficiency (H_2 red circle and CO green triangle); and (b) Average potential during 4 hours galvanostatic CO_2 reduction (-5 mA cm^{-2}) at the gold electrode in 0.2 mol L^{-1} $KHCO_3$.

Figure 4.4 illustrates XPS measurements taken before and after galvanostatic CO_2 reduction on gold electrodes showing the chemical state of the electrodes. XPS scans in Figure 4.4a shows only gold peak before any electrolysis confirming a clean surface without any metallic impurities was used within the experiment while performing CO_2 reduction had no effect on the gold structure except a thin layer of carbon formation on the gold cathodes which could be one explanation for the electrode deactivation (see chapter 5). Figure 4.4b shows the same position for Au 4f peak (84 eV) while small changes in gold structure (like gold oxide formation) results in Au 4f peak changes [66]. From these results, we can conclude that the gold state has not been changed over electrolysis.

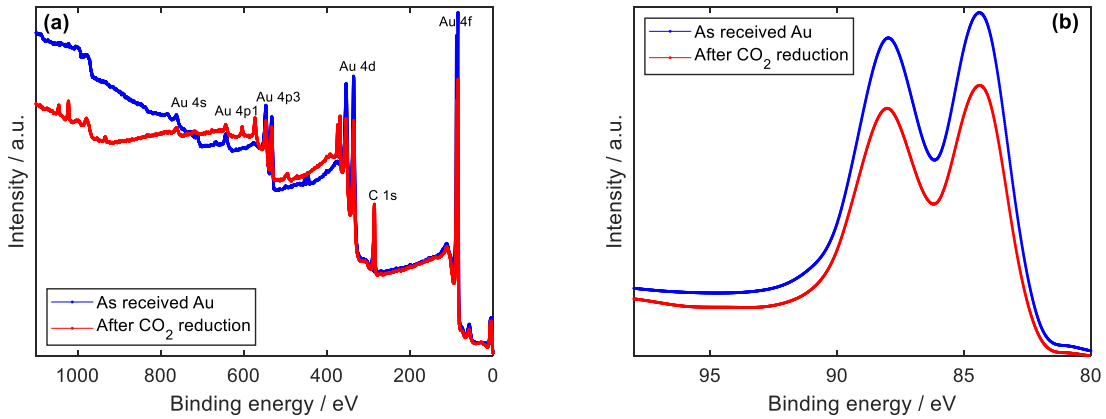

Figure 4.4: XPS spectra of the gold surface before and after 4 hours galvanostatic CO_2 reduction (-5 mA cm^{-2}) in 0.2 mol L^{-1} $KHCO_3$ saturated with CO_2; (a) full survey scan, (b) XPS high-resolution scan for Au 4f.

Galvanostatic CO_2 reduction at different current densities (Figure 4.5a and 4.5b) reveals that the Faradaic efficiency for CO production decreases by increasing the current density. The inhibition of CO production at high current densities is consistent with the potential increases to more negative values which favours HER. Also, a rougher electrode is more selective for CO production most likely due to more available sites for CO_2 reduction reaction compared with HER. This result is consistent with the experiments performed on gold nanoparticles [50, 55, 57, 58, 60] which is known as a rougher surface compared with the bulk gold.

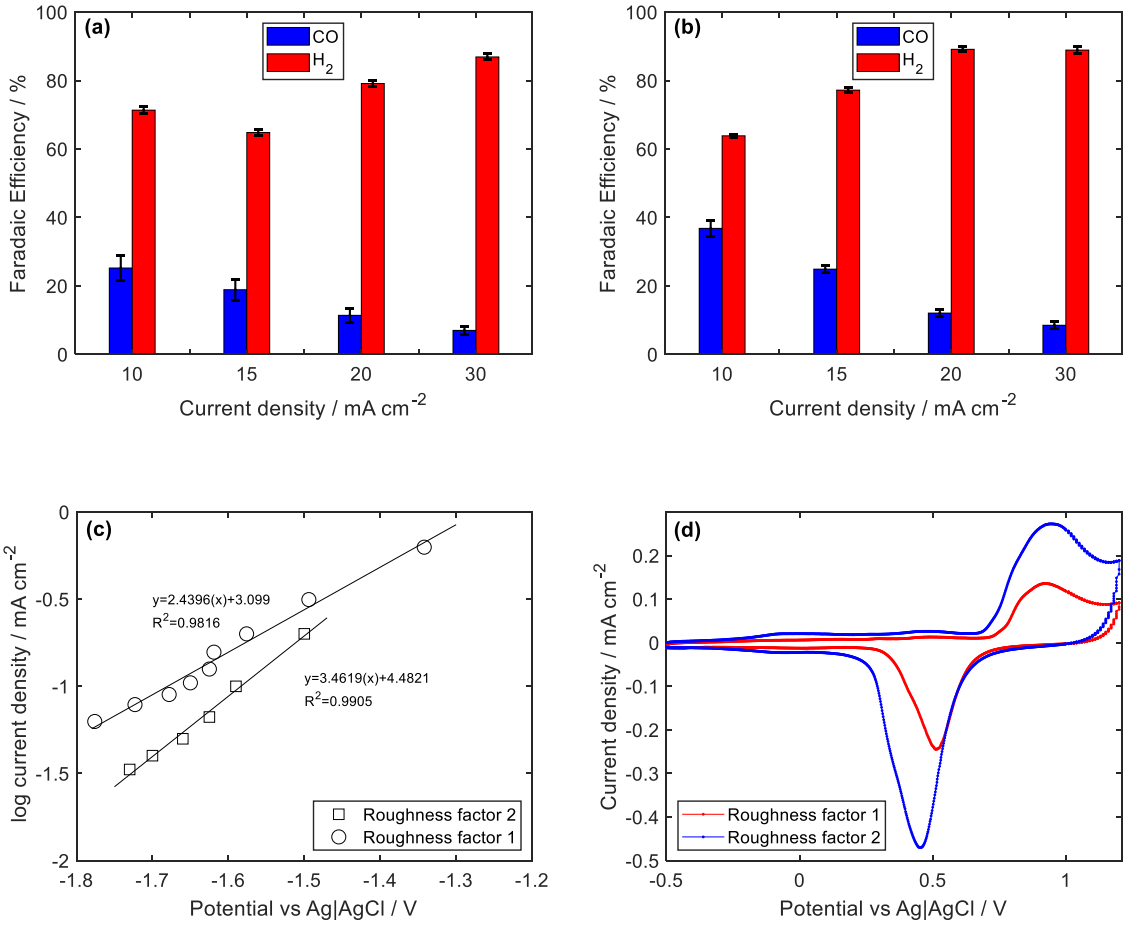

Figure 4.5: The average (a) Faradaic efficiency for different products in a galvanostatic CO_2 reduction using a gold electrode with roughness factor 1; (b) gaseous products Faradaic efficiencies during galvanostatic CO_2 reduction on a gold cathode with roughness factor 2; (c) Tafel plot for galvanostatic CO_2 reduction on gold cathode with various roughness factors after 4 hours electrolysis in 0.2 mol L^{-1} $KHCO_3$ saturated with CO_2 and (d) The voltammograms for polycrystalline gold cathodes at different roughness factor.

The Tafel plot for a polycrystalline gold electrode (roughness factor 2) has been shown in Figure 4.5c suggesting a better performance for a rougher electrode due to a sharper increase in the Tafel slope. The much higher Tafel slope of the rougher gold electrode indicating a much faster initial electron transfer of the CO_2 electroreduction to CO compared with a

smooth gold electrode [57, 128, 130]. Figure 4.5d represents the voltammograms for a polycrystalline gold electrode with different roughness factors. The gold electrode with the charge density of reduction peak at around 400 μC cm^{-2} was considered as a smooth gold (with the roughness factor of about 1) and the gold electrode with the charge density of reduction peak of 800 μC cm^{-2} was considered as gold cathode with the roughness factor of 2 (As described in section 4.2.1). In Figure 4.5d, the charge density of gold oxide reduction peak was 456 μC cm^{-2} and 890 μC cm^{-2} for the gold with roughness factor 1 and 2, respectively. It is worth noting that it is tough to obtain atomically smooth gold electrode and the charge density depends on many factors like the upper potential limit, scan rate, etc. Nevertheless, the charge density of 400 μC cm^{-2} was considered as a smooth electrode in this study and the blue CV in Figure 4.5d is twice as rough as the red CV.

4.2.4 Potentiostatic CO_2 reduction

The potentiostatic CO_2 reduction at different voltage was conducted across one-hour electrolysis to make sure no deactivation takes place, and the current is relatively stable over the experiment. Figure 4.6a shows the average gaseous products Faradaic efficiencies versus the potential over one-hour electrolysis. As can be observed, CO is more selective at the lower overpotentials (78% at -1.3 V vs Ag|AgCl) over H_2 while the product distribution changes significantly by increasing the potential. The CO Faradaic efficiency reduction at more negative potentials is accompanied by H_2 Faradaic efficiency increasing except at -1.55 V vs Ag|AgCl most likely due to stronger CO bonding to the electrode surface compared with -1.6 V vs Ag|AgCl which is expected to affect CO production over electrolysis [18, 157, 301].

Figure 4.6b represents the average current across one-hour electrolysis overlaid with a CV conducted before the CO_2 reduction experiment. The obtained current densities match very well to the CV, except at higher current density values where the currents become noisy. This is attributed to the bubbles forming on the electrode surface causing the electrode coverage and subsequently current densities fluctuation. The results are consistent with the study performed by Cave *et al.* [66], but in our case, the recorded current density is as twice as what they obtained in a flow cell. Figure 4.6c depicts typical current density changes by time over potentiostatic CO_2 reduction at different voltages. The voltage profile indicating the electrode deactivation at all potentials over electrolysis. Also, the current density values increase significantly (up to nearly -35 mA cm^{-2}) at -1.8 V vs Ag|AgCl owing to a sharp rise in HER.

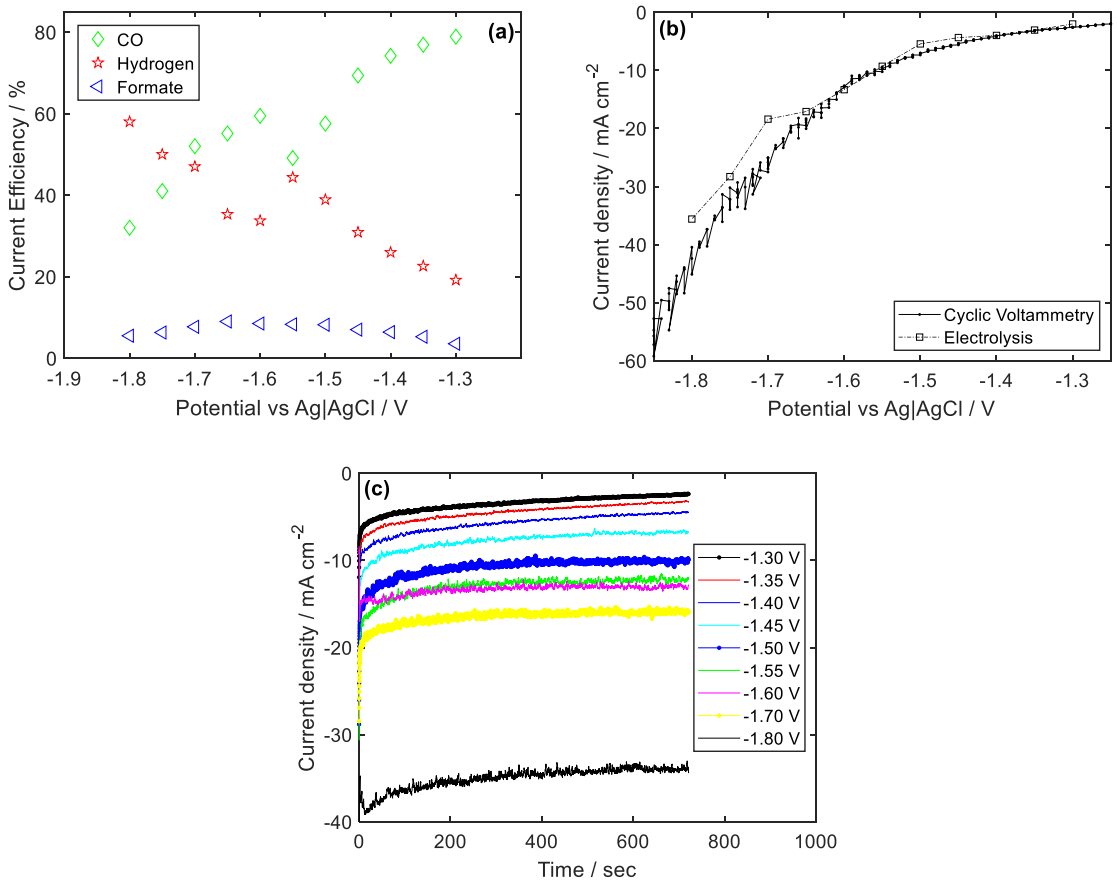

Figure 4.6: Gaseous products Faradaic efficiency and current density changes during potentiostatic CO_2 reduction at the gold electrode (roughness factor 3).

4.2.5 Formate formation on gold electrode

As can be observed in Figure 4.3a, each GC measurement takes 15 minutes to separate the gaseous products, and the first run is often under-representative of the formed gaseous products and the total charge balance no longer holds. While this 30-40 % missing charge is maybe due to the dead time between the headspace of the electrochemical cell and the GC [302-305], we believe another parameter is affecting this unaccounted charge.

The headspace volume over the electrochemical cell is clearly shown in Figure 4.7a. The mass balance for CO over a perfectly mixed headspace by ideal mixing assumption with the isothermal condition and constant gas density is:

Flow in – Flow out – Consumption + Generation = Accumulation

Hence, we have the following equation for CO:

$$0 - \dot{N}_{CO,out} - 0 + \dot{N}_{CO,gen} = \frac{dN_{CO}}{dt} \quad (4.2)$$

By dividing the equation (4.2) by the CSTR volume V[L]:

$$-\frac{C_{CO}\dot{F}_{out}}{V} + \frac{\dot{N}_{CO,gen}}{V} = \frac{dC_{CO}}{dt} \quad (4.3)$$

Where C_{CO} [M] is the CO concentration and $\dot{F}_{out}$ [L s^{-1}] is the outlet flow based on ideal mixing assumption. By considering τ [s] as residence time ($\tau = V/\dot{F}_{out}$), the above equation becomes:

$$\frac{\dot{N}_{CO,gen}}{V} = \frac{dC_{CO}}{dt} + \frac{C_{CO}}{\tau} \quad (4.4)$$

This equation can be solved by an initial condition of $C_{CO} = 0$ at t = 0. The obtained equation will be:

$$C_{CO}(t) = (\frac{\dot{N}_{CO,gen}}{V})\tau(1 - \frac{1}{e^{t/\tau}}) \quad (4.5)$$

In a typical CO_2 reduction reaction on the gold electrode, the CSTR (headspace) volume is 20 mL, and the outlet flow rate is 20 mL min^{-1}. By assuming a total current of -10 mA for which CO Faradaic efficiency is 60%, $\dot{N}_{CO,gen} = 3.11 \times 10^{-8}$ mol s^{-1}. Figure 4.7b shows the CO concentration changes by the time where steady-state conditions could be obtained after 4 minutes. By knowing that each GC measurement takes 15 minutes, the product dilution in the volume between the electrochemical cell headspace and the GC cannot completely explain the missing charge in the first few experiments. One explanation could be higher liquid products (especially formate) formation at the start of the experiment. For that reason, liquid samples were taken every 30 minutes and post-analysed. The calculated Faradaic efficiencies in both potentiostatic (-1.5 V vs Ag|AgCl) and galvanostatic (-5 mA cm^{-2}) CO_2 reduction at different electrolyte concentration are given in Figure 4.8. The results suggest that the formate Faradaic efficiency is remarkably higher at the beginning of the experiment in both galvanostatic and potentiostatic electrolysis and after an hour, the formate Faradaic efficiency gets flat and almost identical for all concentrations. The clean gold surface at the start of the electrolysis likely provides some active sites for formate formation. The formate activity is decreased due to adsorbed intermediate species on the gold surface which favour either CO or H_2 production. This effect unlikely been explored in the literature on gold or silver

electrodes but Pan *et al.* [306] observed higher formate production rate in the first two hours of the experiment in a 10 hours photochemical reduction on Cu electrodes. Herein, we believe both electrochemical cell headspace volume and higher formate formation at the start of the experiment contribute to unaccounted charges in the first few GC measurements.

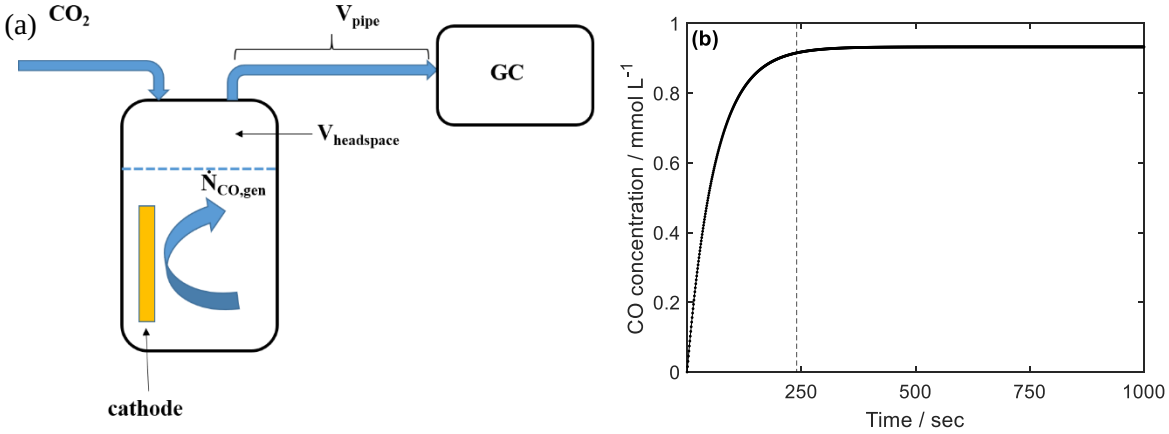

Figure 4.7: (a) The schematic photo for the headspace volume over the electrochemical cell; (b) The required time to achieve a steady-state condition in the headspace volume of 20 mL and a Faradaic efficiency of 60% for CO.

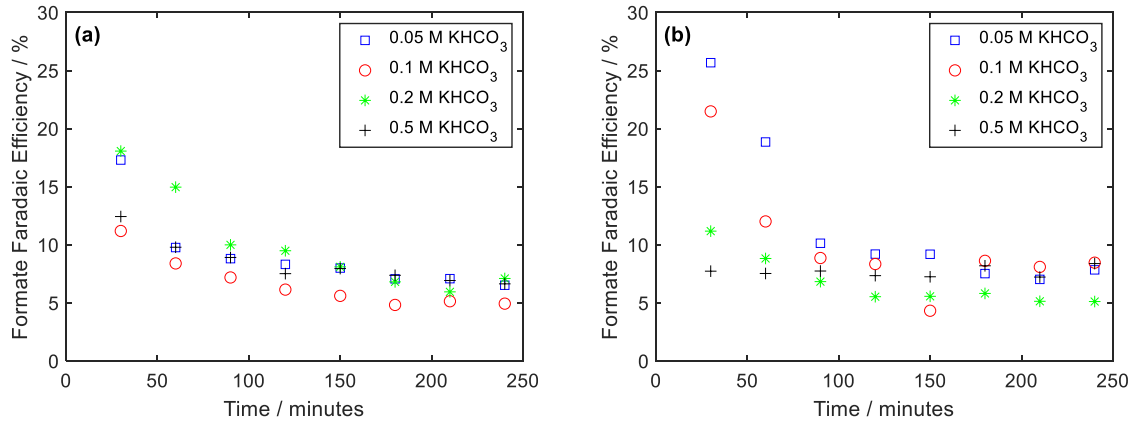

Figure 4.8: Formate Faradaic efficiency changes by time a) galvanostatic (-5 mA cm^{-2}); b) potentiostatic CO_2 reduction at -1.5 V vs Ag|AgCl (saturated with CO_2).

4.2.5.1 CV changes during formate formation

To observe the possible changes on the electrode surface during the electrolysis, CV and liquid samples were taken during the experiment. Figure 4.9 shows the cyclic voltammetry of prepared electrode in aqueous 0.2 mol L^{-1} $KHCO_3$ solution saturated with CO_2 after different periods of CO_2 reduction under the constant current density of -10mA cm^{-2}. As described

previously in Figure 4.1f, the first anodic peak at the potential of 0.9 V relates to the gold oxidation and the cathodic peak at 0.4 V indicates a reduction of gold oxide to metallic gold. Another anodic peak in the negative scan at the potential around -0.13 V has appeared which is increasing by time indicating something is being produced during the electrolysis. By liquid sample analysis, it has been observed that the peak attributes to the formate oxidation. Neither methanol nor acetic acid was detected. Increasing the formate concentration in the electrolyte did cause an increase in the peak size. The source of the peak can also be confirmed by phase diagram (Figure 2.6) for $HCOO^-$ /HCO_3^- reaction showing the same oxidation potential as can be observed in the CV in Figure 4.9.

CO adsorption/oxidation, as well as oxidation/reduction of the electrode surface significantly affects formate generation by blocking active sites for formate adsorption in the forward scan and also retarding the decomposition of adsorbed formate. Gold oxide reduction potentially provides more active sites for formate in the negative scan to be oxidised. This result is consistent with other studies on formic acid oxidation on Platinum where the formate oxidation peak was observed on the negative-going sweep [307-310].

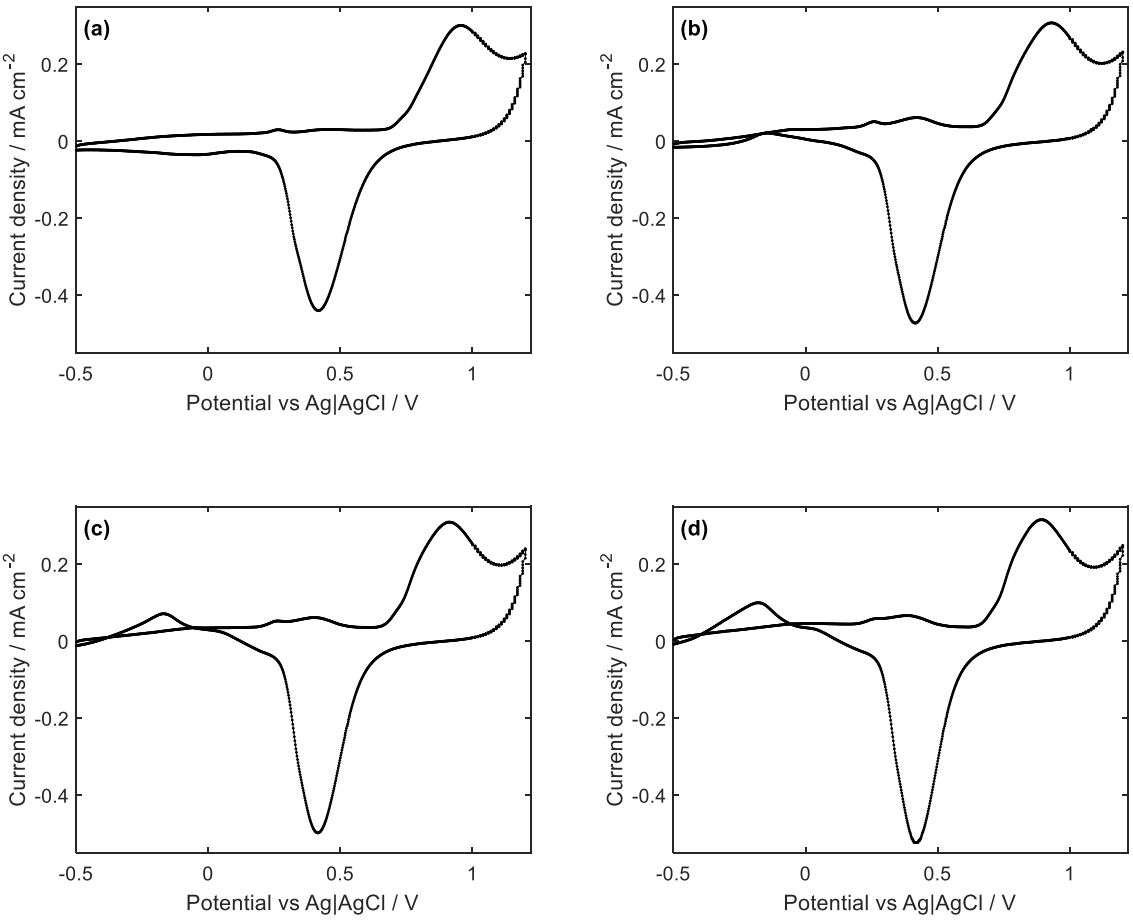

Figure 4.9: Cyclic Voltammetry changes by time at the gold electrode in 0.2 mol L^{-1} $KHCO_3$ (saturated with CO_2) with the current density of -10 mA cm^{-2} after; (a) 0 minutes, [$HCOO^-$]=0; (b) 60 minutes, [$HCOO^-$]=0.4 mM; (c) 120 minutes, [$HCOO^-$]=0.78 mM; (d) 180 minutes [$HCOO^-$]=1.30 mM.

To make sure that the peak changes are due to different formate concentration, a variety of experiments were conducted under different galvanostatic measurements at -3 mA cm^{-2}, -9 mA cm^{-2}, -13 mA cm^{-2} and -16 mA cm^{-2}. The voltammograms after 4 hours electrolysis are illustrated in Figure 4.10 and again confirming that the peak size is increasing by the applied current which is consistent with HPLC results showing more formate is produced at higher currents.

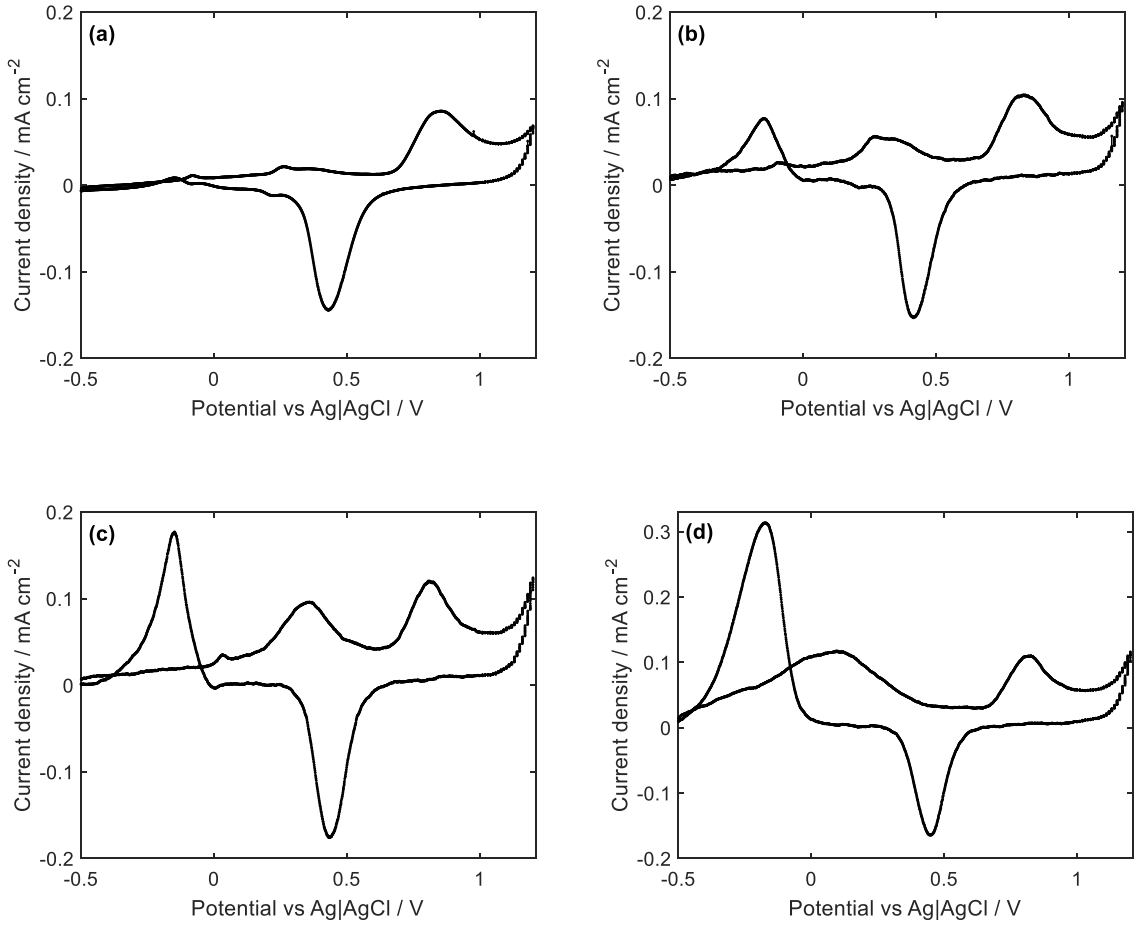

Figure 4.10: Cyclic Voltammetry after 4 hours galvanostatic CO_2 reduction at the gold electrode in 0.2 mol L^{-1} $KHCO_3$ (saturated with CO_2) at (a) -3.18 mA cm^{-2}; (b) -9.55 mA cm^{-2}; (c) -12.73 mA cm^{-2}; (d) 15.91 mA cm^{-2}.

4.2.6 The effect of different electrolyte in IR-drop

The solution resistance was continuously measured over CO_2 electroreduction using the set-up shown in Figure 3.1a. The resistance values for different galvanostatic reduction are given

in Figure 4.11a and show that the resistance decreased by time due to K^+ selective transport from the anolyte to the catholyte; hence, the electrolyte becomes more conductive. Also, the K^+ transportation rate would be higher at higher current densities, and the resistance drop would be more significant. Considerable solution resistance in this cell set-up is not ideal for galvanostatic or potentiostatic measurements and is due to the further position of the reference junction to the working electrode to avoid any inductance feature in the EIS spectra. One method to minimise the IR drop is to reduce the electrolyte resistance by increasing the solution conductivity [252]. This can be achieved by using more concentrated electrolyte (Figure 4.11b). Using 1 mol L^{-1} instead of 0.2 mol L^{-1} $KHCO_3$ can significantly reduce the solution resistance from 49 Ω to 11 Ω. One of the common issues of using higher $KHCO_3$ concentration is affecting the product distribution by forming a higher electrolyte buffer capacity which subsequently does not let the pH increase at the vicinity of the electrode surface [105, 109]. Another well-known effect of higher electrolyte concentration in CO_2 electroreduction is the CO_2 solubility reduction due to salt content [178-180] which introduces mass transport limitation to the cell and makes it more complicated with unknown effects.

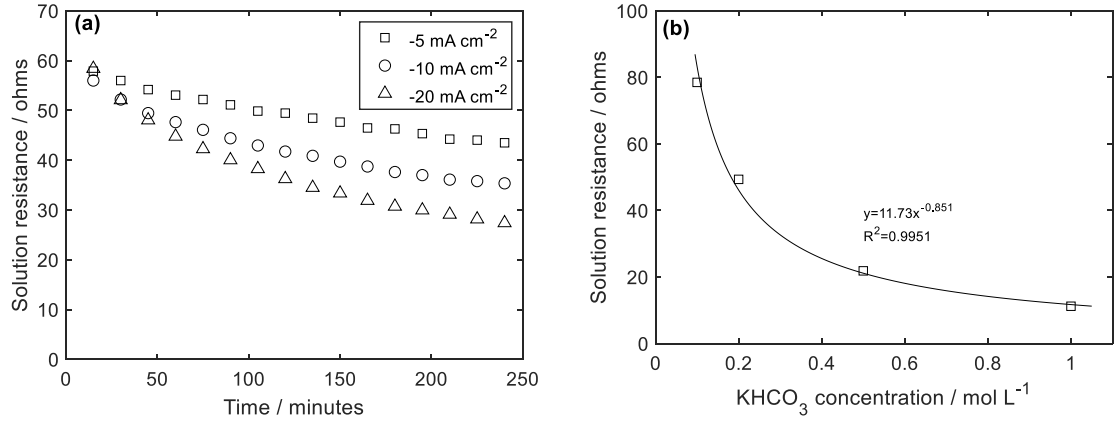

Figure 4.11: The solution resistance changes by (a) time over galvanostatic CO_2 reduction at different current densities in 0.2 mol L^{-1} $KHCO_3$; (b) $KHCO_3$ concentration over 4 hours galvanostatic (-5 mA cm^{-2}) CO_2 reduction.

In order to reduce the solution resistance, the addition of different electrolyte solutions to the original 0.2 mol L^{-1} $KHCO_3$ were examined to see how it affects the resistance. Figure 4.12a shows CV obtained in the solution with 0.2 mol L^{-1} and various KCl concentration. As can be seen, gold reacts with chlorine at lower potentials (0.7 V vs Ag|AgCl) compared with a solution contains only $KHCO_3$ which is consistent with Pourbaix diagram for $Au/AuClO_4$ reaction [163] and gold dissolution increases with KCl concentration. In fact, Cl^- makes a

complex with gold and the electrode passivates when oxygen is adsorbed [277]. However, a significant reduction in resistance could be achieved from the value of 30.6 Ω (at 0.1 mol L^{-1} KCl + 0.2 mol L^{-1} $KHCO_3$) to 10.6 Ω (at 1 mol L^{-1} KCl + 0.2 mol L^{-1} $KHCO_3$). This effect can be resolved by anionic species substitution. As illustrated in Figure 4.12b and Figure 4.12c, using the electrolyte containing 0.2 mol L^{-1} $KHCO_3$ and KF (instead of KCl) can significantly reduce the solution resistance on one hand, and generate a CV very similar to the classical cyclic voltammetry (shows the normal gold oxide/redox feature) on the other hand. Despite the resistance reduction obtained in this circumstance, the challenge still exists and due to a high K^+ concentration, a normal CO_2 electroreduction does not take place, and the electrode activity diminishes quickly (after 1 hour) due to mass transport limitation or high buffer capacities of the bulk electrolyte.

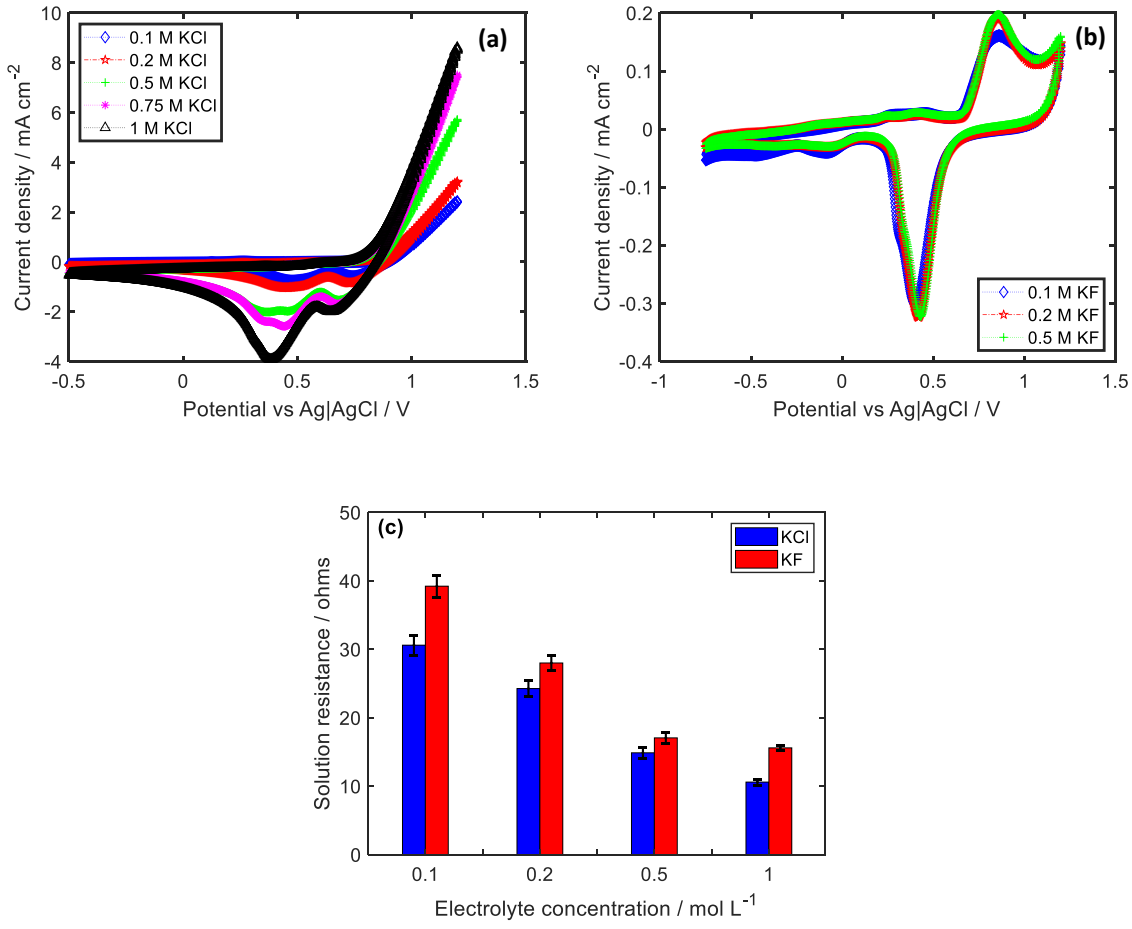

Figure 4.12: The effect of electrolyte addition to 0.2 mol L^{-1} $KHCO_3$ (a) CV changes by KCl concentration; (b) CV changes by KF concentration; (c) The electrolyte resistance changes by adding KCl and KF at different concentrations.

Hence, another cell configuration (Figure 3.1b) was designed to minimise the IR drop by using a tip at the end of the reference junction which is known as “Luggin capillary”. The luggin capillary is used to control the position of the reference electrode relative to the working one. The tip diameter is much smaller than the reference electrode and is placed as close as twice it’s diameter to the working electrode to avoid any nonhomogeneous current density. Also, the small tip diameter allows sensing the electrolyte potential at the vicinity of the working electrode. Applying all of those modifications resulted in a lower impedance (1.99 Ω) as can be observed in Figure 3.5.

4.3 Conclusions

In this chapter, a series of fundamental analysis was performed on gold electrodes to ensure the results are consistent with the literature. It was found that the electrochemical CO_2 conversion is a complex reaction which is affected not only by the cathode material but also by a range of experimental parameters. These parameters make it hard to interpret the data in an electrochemical CO_2 reduction reaction. In this chapter, the effect of the rougher surface on the product distribution has been examined. It was shown that the rougher surfaces favour CO production while on a smoother gold electrode, HER would be dominant. The observed improvements in the CO selectivity on a rough gold is attributed to the higher surface area available for the CO_2 reduction reaction, rather than HER.

It was also proposed that the initial delay in gaseous products detection is partly due to higher formate production rate at the start of the electrolysis. Formate formation on the gold cathode is poorly understood; hence, we tried to find out the unknown aspects of formate formation during electrocatalytic CO_2 reduction on gold.

5 Preventing the Deactivation on Gold Electrodes

Abstract: The electrochemical reduction of CO_2 on gold cathodes was investigated and the major products found to be CO, H_2 and formate. As expected, the current efficiency for CO production decreased slowly with time, with this deactivation accompanied by an increase in the activity of the cathode towards H_2 and formate production. The deactivation was found to be due to the deposition of Cu, Zn and possibly Fe from the electrolyte, with the presence of Fe strongly enhancing H_2 production, the Cu deposition increasing the formate production rate and Zn enhancing both H_2 and formate production. Here, it is shown that the accumulation of these poisons prevented with periodic anodic treatments as previously described in the literature. However, the process used to strip these poisons can lead to significant gold dissolution, with up to 454 ppb of gold found in the electrolyte after 4 hours of electrolysis, and thus is unsuitable for use in long-term CO_2 reduction systems. Therefore alternative electrochemical cleaning protocols (periodic cyclic voltammetry, open-circuit and low anodic current treatments) were investigated as methods to remove these poisons without significant gold corrosion occurring. The best approach to prevent the deactivation of gold cathodes during CO_2 reduction, is to cycle the potential between -0.5 V and 0.5 V vs Ag|AgCl every 15 minutes during long-term electrolysis. It is also shown that simply interrupting the CO_2 reduction process every 15 minutes with 4 minutes at open circuit can also partially prevent CO_2 reduction as will short anodic current pulses.

5.1 Introduction

The electrocatalytic reduction of CO_2 to useful chemicals on metallic electrodes has become an increasingly important area of research [100, 192, 311, 312]. While many metals have been studied for this process [29, 35, 36, 43, 110, 313], currently no metal has proved to be both highly active and selective for long periods of time [203, 205, 206, 210, 220]. Normally in aqueous media, gold cathodes exhibit high CO selectivity (current efficiency 16-91 %) at relatively low overpotentials [27, 49, 58], with formate found as a minor product (current efficiency < 10%) [35, 36, 38, 43, 151, 314]. As the other major product from CO_2 reduction of gold is hydrogen (from the parallel hydrogen evolution reaction), if even the selectively towards CO cannot reach 100%, the CO and H_2 produced can be used as a feedstock for other process requiring syngas.

Despite the high selectivity towards CO, it is clear that this is not maintained during continuous reduction [203, 222]. This deactivation is also found on other metallic cathodes and while some have developed methods to maintain CO_2 reduction activity on these other metals [181, 205, 210, 213, 220, 224, 225], there has been limited studies focusing on understanding or preventing the deactivation of gold during electrocatalytic CO_2 reduction [203, 223]. In general, the deactivation during electrocatalytic CO_2 reduction is normally attributed to the poisoning of the cathode by metallic [25, 210, 222] or organic [210] impurities within the electrolyte. Other studies have shown that this deactivation is unavoidable during continuous CO_2 reduction due to the accumulation of surface bound intermediates from the reaction [27, 86, 207, 215, 220, 302, 315], and in some cases the influence or significance of metallic impurities has been specifically discounted [184, 207, 220].

Preventing electrode deactivation has been investigated by either applying periodic anodic treatments to the cathode [203, 205, 220, 223] or by removing the impurities using pre-electrolysis of the electrolyte [210]. While pre-electrolysis has proved feasible in the laboratory environment [210] others suggest that this approach is ineffective, energy and time consuming [131, 205, 220, 221], and seems unlikely to be successful on an industrial scale due to the ultra-low level of impurities which appear to cause deactivation. While periodically interrupting the CO_2 reduction process to strip off either metallic or carbonaceous poisons via anodic treatments has also been successful for Cu, Ag and gold cathodes, little attention has been focused on the long-term stability of the cathodes due to anodic dissolution of the metal during these treatments. For example, it is clear that these anodic treatments will alter the surface morphology of gold cathodes due to gold dissolution [66, 223, 227], which occurs at high anodic potentials upon the formation of gold oxide, as well as during the reduction of gold oxide back to metallic gold [249, 250, 268, 316]. While this dissolution could arguably improve the performance of bulk gold cathodes (by enhancing the roughness factor), if gold nanoparticles are used for CO_2 reduction, the anodic treatment used to prevent deactivation will almost certainly cause dissolution and/or growth of the nanoparticles [317, 318], especially considering that gold nanoparticles can oxidise more easily than bulk gold [319, 320]. Given these factors and considering that the previous studies did not provide significant insight in the deactivation mechanism and catalyst recovery, it is clear that a systematic study of the electrochemical treatment protocol for gold cathodes during CO_2 reduction needs to be developed, with the specific aim of avoiding gold dissolution. Thus, the influence of various

periodic cleaning protocols (cyclic voltammetry, open circuit potential steps and anodic pulses), are investigated in terms of their ability to prevent the deactivation of gold cathodes for CO_2 reduction while avoid gold dissolution.

5.2 Experimental

Electrochemical experiments were performed using gold disc (99.999%) mechanically polished to a mirror finish using silicon carbide paper and alumina slurries (down to 0.05 μm). The working electrode with a geometric area of 2.01 cm^2 was used in a two-compartment gas-tight glass electrochemical cell with a graphite counter electrode, with Nafion 115 used to separate the anolyte and catholyte chamber. The potential of the cathode was measured with respect to an Ag|AgCl (saturated KCl) reference electrode held in a Luggin capillary. All the potentials in this study are referenced to the Ag|AgCl unless specifically stated. CO_2 gas (99.995%) was continuously purged at a rate of 40 mL min^{-1} for 30 minutes before each experiment to saturate the electrolyte and then the flow rate reduced to 20 mL min^{-1} during the experiment by using Alicat mass flow controller. The current efficiency (percentage of the total current going towards the formation of a certain product) was determined by gas chromatography (SRI instruments, methanizer FID and TCD detectors, Haysep-D column) every 15 minutes. High Performance Liquid Chromatography (HPLC, equipped with a SUPELCOGEL^{TM} C-610H column) was employed for post-electrolysis analysis of reduction products present within the electrolyte. In all cases, 0.2 mol L^{-1} $KHCO_3$ (99.7% ACS reagent, Sigma Aldrich) was used directly as the electrolyte without any purification. All the experiments were conducted at room temperature (23 °C) using a Gamry Reference 3000 potentiostat. Experiments were carried out at constant current densities for 4 hours, with electrochemical impedance spectroscopy (EIS) measurements (100 kHz-10 Hz, 5 mV rms amplitude) every 15 minutes to measure the electrolyte resistance and correct the measured potential. Periodically measuring the electrolyte resistance is important during long-term CO_2 electroreduction experiments as the electrolyte resistance can decrease with time due to selective K^+ ion transportation from the anolyte to the catholyte [174].

To determine the concentration of metallic impurities within the electrolyte, samples were analysed by ICP-MS (Agilent 7500cx). ICP-MS was also conducted on electrolyte samples after electrolysis to quantify the gold dissolution due to the cleaning procedures.

The impurities deposited on the surface of the gold cathodes during CO_2 reduction were examined by XPS. In all cases, after 4 hours of electrolysis, the electrodes were removed from

the electrochemical cell, rinsed thoroughly with DI water and dried under room temperature. The XPS spectra were obtained on a Kratos Axis Ultra DLD instrument using monochromated Al K_α x-rays (1486.69 eV). The anode was set at 15 kV with a 10 mA emission current and a base pressure of 5×10^{-9} torr. The survey scans were collected over the range 1300 to -5 eV in 1eV steps with a 13 minute acquisition time.

5.3 Results and discussion

5.3.1 Continuous galvanostatic CO_2 reduction on gold

During the galvanostatic reduction of CO_2 on gold cathodes , the main gaseous products were found to be CO and H_2 (Figure 5.1) which is consistent with previous reports [36, 38, 151, 223, 321]. Small amounts of formic acid were also produced with a current efficiency of <10%. As expected, the current efficiency for CO production was found to decrease over 4 hours of reduction (Figure 5.1), with this drop in current efficiency for CO production accompanied by the cathode potential becoming less negative. The deactivation of electrodes during CO_2 reduction has been reported elsewhere for gold cathodes [203] and other metals [205, 210, 322] and is normally attributed to the deposition of metals from electrolyte impurities [222] or surface bound intermediates [184, 220]. These deposited poisons either block the active sites for CO production or produce sites that favour the hydrogen evolution reaction (HER). As the cathode potential becomes more positive, the selectivity towards CO decreases and the HER increases, this indicates that the activity of the cathode for the HER increases during the deactivation process. This would be expected if elements like Fe, Cu, or C are deposited on the gold surface, as these are more selective for the HER compared to gold [27, 323]. While the bulk pH of the electrolyte does change during CO_2 reduction due to the selective transport of K^+ ions across the membrane, it seems unlikely that this contributes to the observed changes in CO vs H_2 selectivity as the bulk pH only increases from around 6.8 to 7.2 during a 4 hour CO_2 reduction experiment.

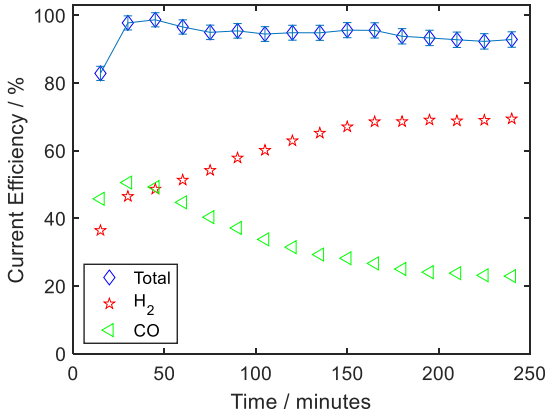

Figure 5.1: Current efficiency towards gas products during CO_2 reduction at a gold cathode in 0.2 mol L^{-1} $KHCO_3$ saturated with CO_2 at -5 mA cm^{-2}.

To investigate possible changes in the surface of the gold during the deactivation process, cyclic voltammetry was conducted before and immediately after 4 hours of galvanostatic CO_2 reduction, with significant differences in the voltammograms being observed (Figure 5.2).

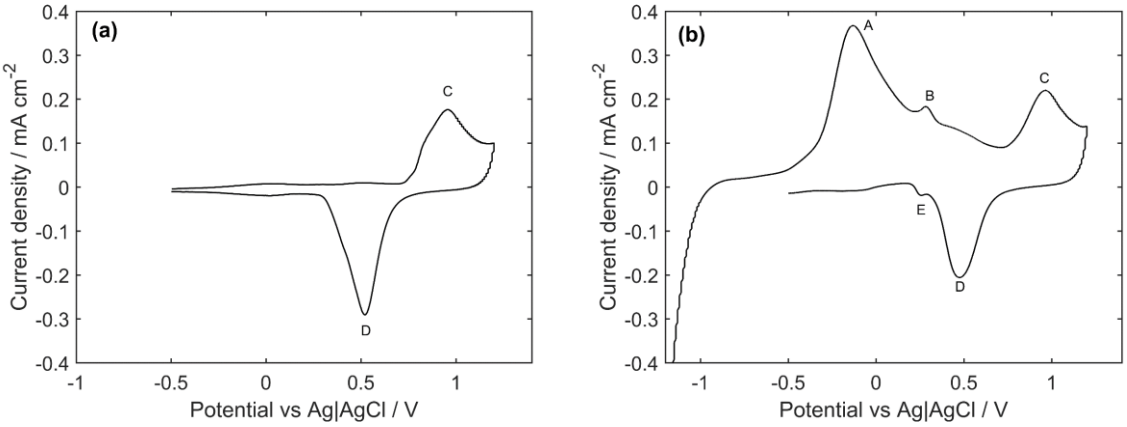

Figure 5.2: Cyclic voltammetry at the scan rate of 100 mV s^{-1} of a gold electrode in 0.2 mol L^{-1} $KHCO_3$ saturated with CO_2 (a) before and (b) after 4 hours of CO_2 reduction at -5 mA cm^{-2}.

The voltammogram of the gold cathode before CO_2 reduction exhibits the normal gold – gold oxide redox features, with peak C and D corresponding the formation and reduction of gold oxide respectively (Figure 5.2a). These peaks are still observed after 4 hours of CO_2 reduction, but are accompanied by three new peaks (Figure 5.2b). The large anodic peak at the potential around -0.13 V vs Ag|AgCl (peak A) is attributed to the oxidation of CO [61, 251, 324, 325], formed from the CO_2 reduction reaction. The size of this peak decreases significantly if the potential is held at -0.75 V for 1 minute prior to the cyclic voltammetry, suggesting that this CO is either weakly adsorbed on the cathode or dissolved CO within the diffusion layer (and

thus diffuses into the bulk during this pause at -0.75 V). The peak size also decreases on the subsequent voltammetric cycles due to the CO stripping reaction and diffusion away from the surface. It was also observed that the potential of this CO oxidation peak shifts to slightly higher potentials between the 1st and 2nd cyclic voltammetry cycles which we attribute to the high interfacial pH (which forms during CO_2 reduction [164, 174]) decreasing back to the bulk pH value during the cyclic voltammetry. Peaks B (0.28 V vs Ag|AgCl) and E only appear after prolonged reduction, suggesting these are related to the species responsible for the deactivation. Others have shown that both Cu and Zn deposit on gold cathodes, with a Zn stripping peak found at -0.5 vs Ag|AgCl and Cu stripping peaks found at -0.05 and 0.24 V vs Ag|AgCl [222].

The standard potential for Cu^{2+}/Cu reaction is reported to be 0.14 V vs Ag|AgCl [163], so together with a previous report [222], it is reasonable to suggest that peaks B and E are due to the presence of Cu^{2+} impurities present in the electrolyte. This was confirmed by ICP-MS analysis, which revealed that the 0.2 mol L^{-1} $KHCO_3$ electrolyte contained approximately 0.06 µM Cu, 0.06 µM Zn and 0.2 µM Fe. To examine if these elements altered the selectivity of the CO_2 reduction reaction on gold, an additional 1 µM of Cu^{2+}, Fe^{2+} and Zn^{2+} were added to the electrolyte prior to CO_2 reduction. By performing cyclic voltammetry after a period of prolonged CO_2 reduction, it was found that the addition of Cu^{2+} caused peaks B and E to increase in size (Figure 5.3d), confirming that Cu impurities are the source of these peaks. No additional peaks could be found by cyclic voltammetry when Fe^{2+} and Zn^{2+} were added to the electrolyte (the standard potential of the Fe^{2+}/Fe and Zn^{2+}/Zn reactions are -0.64 and -0.96 V vs Ag|AgCl [163]). However, by following the current efficiency of the CO_2 reduction reaction in the presence of either 1 µM Cu^{2+}, Fe^{2+} or Zn^{2+}, it was found that the presence of Fe^{2+} and Zn^{2+} had the most dramatic impact on the deactivation of the cathode towards CO production, a corresponding rapid increase in the current efficiency towards H_2 (Figure 5.3a). For the experiments containing additional Fe^{2+}, this seems reasonable given the much higher selectivity that Fe has towards H_2 compared to gold [38]. Interestingly, the addition of Cu^{2+} did not alter the selectivity towards the HER, but did cause the CO to decrease more rapidly compared to the control experiment (Figure 5.3b). Liquid samples taken over the course of these experiments revealed that the drop in current efficiency towards CO in the presence of Cu^{2+} can be explained by the increase in formate production rate (Fig 5.3c). The increasing formate production rate and thus activity of the electrode for formate production over the electrolysis time, suggests that the surface is continuously accumulating Cu. In the case of

Fe^{2+} additions, no changes in the formate production rate could be observed, which again is consistent with the known behaviour of Fe cathodes [38] while the additional 1 μM of Zn^{2+} caused both H_2 and formate production to increase. As this analysis suggests that Fe, Zn and Cu impurities present in the electrolyte may play a role in the deactivation of gold cathodes, XPS was used to the examine whether these elements deposited onto the surface of the gold during CO_2 reduction. This analysis (Figure 5.4) revealed that small amounts of Zn and Cu were found on the surface of the gold in agreement with others [222]. Surprisingly, despite the clear evidence that Fe^{2+} in the electrolyte causes rapid deactivation of the gold cathode towards CO_2 reduction, no evidence for Fe on the surface of the gold cathodes was found by XPS. One possible explanation for this is that the small quantity of Fe deposited on the gold during CO_2 reduction quickly re-dissolves in the short period at open circuit potential prior to the electrode being removed from the electrolyte.

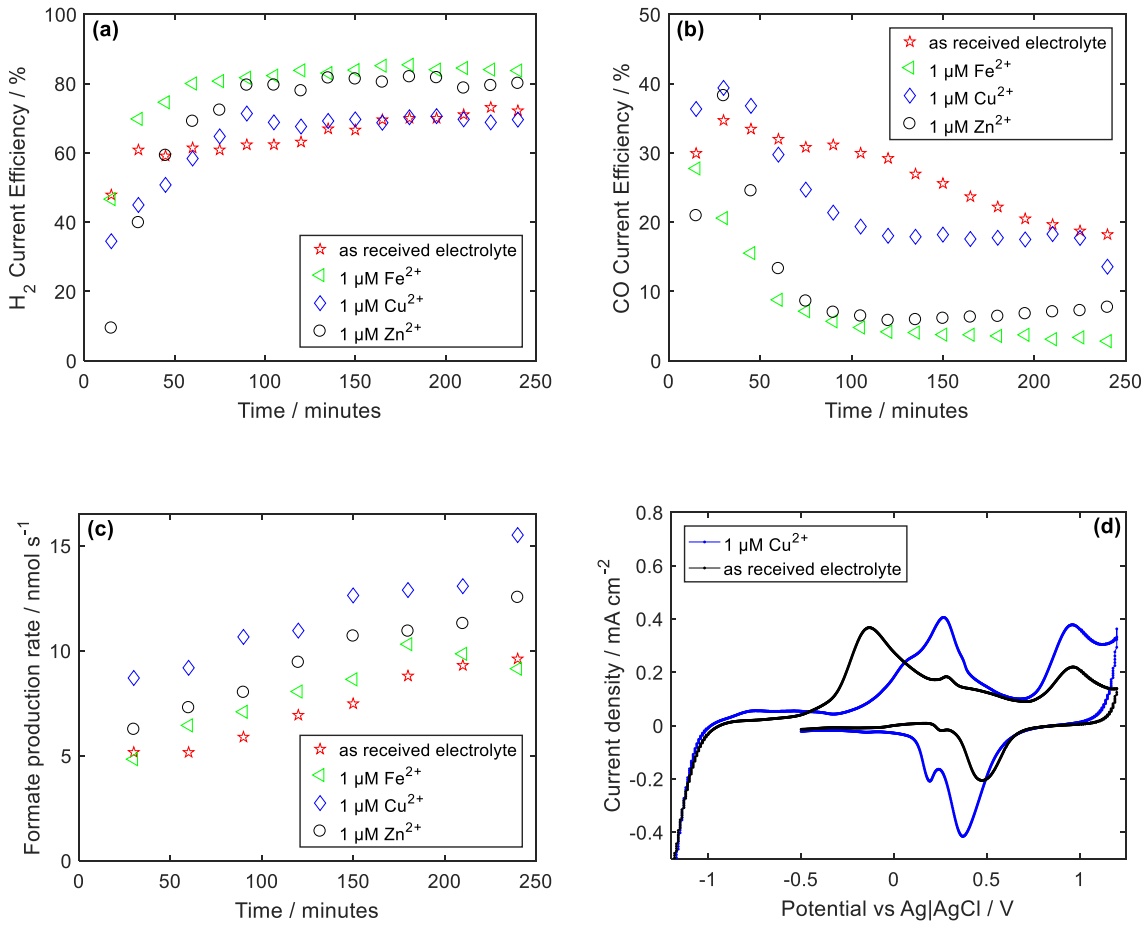

Figure 5.3: The effect of intentionally added electrolyte impurities on (a) CO current efficiency, (b) H_2 current efficiency and (c) formate production rate (d) cyclic voltammetry after 4 hours CO_2 reduction at -10 mA cm^{-2} in CO_2 saturated 0.2 mol L^{-1} $KHCO_3$ with and without the additional of 1 μM Cu^{2+}.

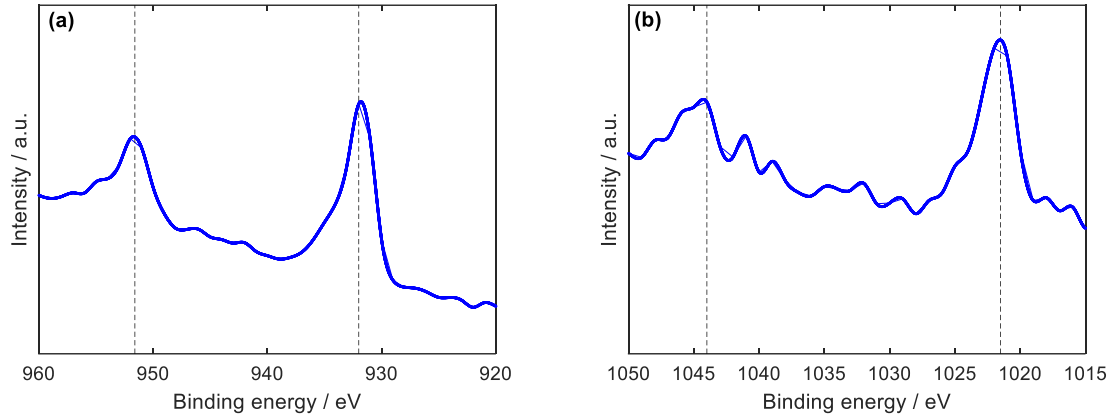

Figure 5.4: XPS 2p spectra of a) Cu and b) Zn on the gold electrode after 4 hours CO_2 electroreduction at the current density of -5 mA cm^{-2} in CO_2 saturated 0.2 mol L^{-1} $KHCO_3$. The vertical lines indicate the binding energies associated with the metallic species [222].

5.3.2 Preventing the deactivation by using periodic anodic treatments

To avoid the observed deactivation of gold electrodes during CO_2 reduction, the common approach is to periodically apply relatively positive potentials to the gold electrode in order to anodically strip the poisons responsible for deactivation. Shiratsuchi *et al.* [223] applied a repeating square-wave potential protocol of -1.5 V vs Ag|AgCl for 5 seconds (CO_2 reduction step) followed by 1 V vs Ag|AgCl for 5 seconds (cleaning step). Similarly, Kedzierzawski and Augustynski [203] used a periodic activation process wherein the potential of the gold electrode was swept from the CO_2 reduction potential (-1.65 to -0.95 V vs Ag|AgCl) to 1.1 V vs Ag|AgCl at 50 mV s^{-1} every 15 minutes in order to anodically strip any poisons off which may accumulate on gold during CO_2 reduction. Both of these approaches successfully prevent deactivation, with the current efficiency towards CO production found to be almost stable at around 60 % for 4 hours (Figure 5.5). In the case of the square-wave potential protocol proposed by Shiratsuchi *et al.* [223], in agreement with their work, it is found that while this stabilises the electrode for CO production, the net rate of H_2 production is found to be very low and the total charge balance no longer holds. This is likely due to the oxidation of a portion of the evolved H_2 when the potential is pulsed to 1 V vs Ag|AgCl. As the kinetics of hydrogen oxidation are faster than CO oxidation [326], it is not surprising that this oxidation appears to only effect the net H_2 evolution and not CO production. This oxidation of hydrogen does not seem to occur when following the method proposed by Kedzierzawski and Augustynski [203], as the oxidising or stripping potentials are obtained by sweeping the potential from the CO_2 reduction conditions (-1 V) up to 1.1 V at 50 mV s^{-1} during which time the majority of the evolved hydrogen can diffuse away from the electrode. While these

methods clearly prevent or slow the deactivation of the gold electrode, both approaches will result in the formation of gold oxide and thus lead to gold corrosion and/or severe surface restructuring [203, 223, 227, 249, 250, 268, 316]. While this may have very little effect on CO_2 reduction experiments utilising bulk gold cathodes lastly a few hours, it seems obvious that this corrosion will make long-term CO_2 reduction on gold problematic, especially if gold nanoparticles are used [317, 318]. In fact, Shiratsuchi *et al.* pointed out that their periodic cleaning procedure resulted in gold corrosion and an increase the roughness factor of the gold cathode [223]. To confirm that gold corrosion occurs during these cleaning procedures, electrolyte samples taken after 4 hours of CO_2 electrolysis were analysed by ICP-MS, with 454 ppb gold found in the electrolyte when the method of Shiratsuchi *et al.* was used, and 47 ppb gold found after 4 hours of electrolysis following the procedure of Kedzierzawski and Augustynski. The lower level of gold in the electrolyte following the Kedzierzawski and Augustynski method is due to the shorter time this method spends at potentials capable of anodic gold dissolution.

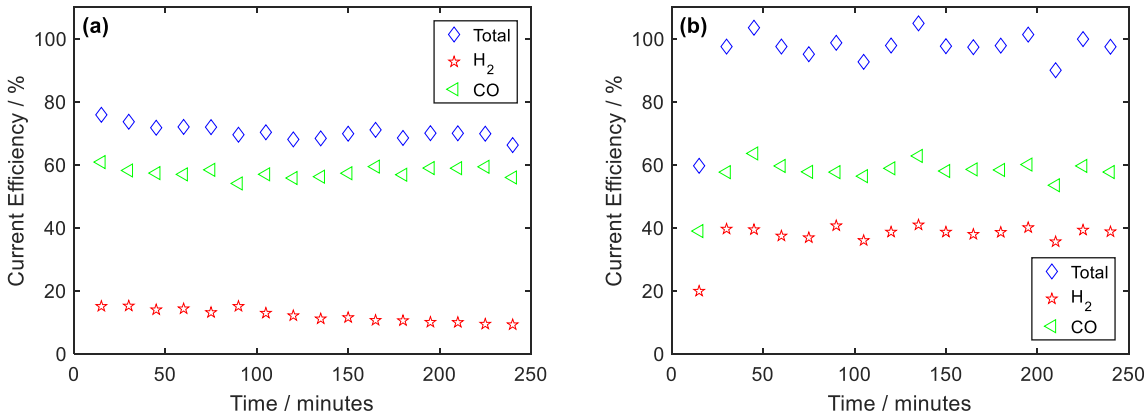

Figure 5.5: Current efficiency of gas products from CO_2 reduction at a gold cathode in 0.2 mol L^{-1} $KHCO_3$ saturated with CO_2 using periodic activation procedures. (a) Repeating sequence of -5 mA cm^{-2} for 5 sec and 1 V vs Ag|AgCl for 5 sec (Shiratsuchi *et al.* [223]), (b) CO_2 reduction at -5 mA cm^{-2}, with sweeps from -1 V to 1.1 V at 50 mV s^{-1} every 15 minutes (Kedzierzawski and Augustynski [203]).

5.3.3 Preventing deactivation without gold dissolution

From the previous section, it is clear that gold electrodes will undergo significant dissolution and very likely severe surface restructuring due to the anodic treatments applied to remove the poisons responsible for the deactivation during CO_2 reduction. As this dissolution and restructuring is due to the formation and reduction of gold oxide [249, 250, 268, 316], here

the possibility of removing the poisons without the formation of gold oxide is investigated by performing cyclic voltammetry every 15 minutes during galvanostatic CO_2 reduction. In this case, the potential was swept at 100 mV s^{-1} between -0.5 V vs Ag|AgCl and various upper potential limits. As the onset of gold oxide formation is 0.65 V vs Ag|AgCl in 0.2 mol L^{-1} $KHCO_3$ saturated with CO_2, the upper potential limit was selected to be between 0 and 0.5 V vs Ag|AgCl to ensure that no gold oxide formation or gold dissolution would occur. Thus upper potential limits of 0, 0.15, 0.35 and 0.5 V vs Ag|AgCl were selected to be more positive than the CO stripping peak, just below the stripping of Cu (peak B = 0.28 V), just after the Cu stripping potential, and well after the Cu stripping peak but below the gold oxide formation potential. While there is still some deactivation of the CO_2 reduction towards CO when the upper potential limit of the stripping voltammetry is only 0 V, by sweeping the potential to at least 0.15 V appears to stabilise the current efficiency for CO production (Figure 5.6a). This stabilisation is highlighted by the measured potential during the galvanostatic CO_2 reduction periods, where it is clear that upper potential limits of 0.35 and 0.5 V vs Ag|AgCl ensure that the potential remains essentially constant over 4 h of CO_2 reduction. For an upper potential limit 0.15 V vs Ag|AgCl, it appears that the electrode is still being deactivated as the potential during the CO_2 reduction continuously increases, as does the potential the when upper potential limit is 0 V. The increasing electrode potential coupled with a drop in the current efficiency for CO production indicates that the cathode is becoming more active towards the HER, which is consistent with the accumulation of Cu on the cathode. This is not surprising given that the cyclic voltammetry reveals that Cu is not stripped from the gold until the potential is at least 0.28 V vs Ag|AgCl. This stripping can be observed on the cyclic voltammograms used to clean the electrode, with the charge associated with the Cu stripping process (peak B) found to decrease over the five cycles, suggest that less Cu remains on the gold electrode after this cleaning process (Figure 5.7). It was also found that when the upper potential limit of the stripping voltammetry was 0.5 V vs Ag|AgCl, the formate production rate was constant at around 3 nmol s^{-1} (compare with Figure 5.3c) which confirms that this approach successfully prevents the continuous accumulation of Cu on the surface during CO_2 reduction. While the deactivation is essentially prevented when the upper potential limit of the stripping voltammetry is at least 0.35 V vs Ag|AgCl, the current efficiency for CO production is more stable (compared to Figure 5.1) even when the upper potential limit is below the Cu stripping potential. This suggests all of the stripping voltammograms used in this work have removed other poisons in addition to Cu. Given that the electrolyte also contains dissolved Fe and Zn and that these both lead to deactivation (Figure 5.6b), it seems

clear that Fe and Zn are also dissolved off the gold surface during the stripping cyclic voltammetry. This is consistent with the expected potential required to strip Fe and Zn off the gold (-0.64 and -0.96 V vs AgAgCl). This was confirmed by XPS which revealed that no Fe, Zn and Cu impurities were found on the gold surface when the upper potential limit of voltammetry is 0.35 V vs Ag|AgCl. Finally, unlike the two previously report cleaning processes [203, 223], ICP-MS analysis showed that no significant gold corrosion occurs during the cleaning process that has been applied in this work, suggesting that this approach can be used to prevent the deactivation during long-term CO_2 reduction processes.

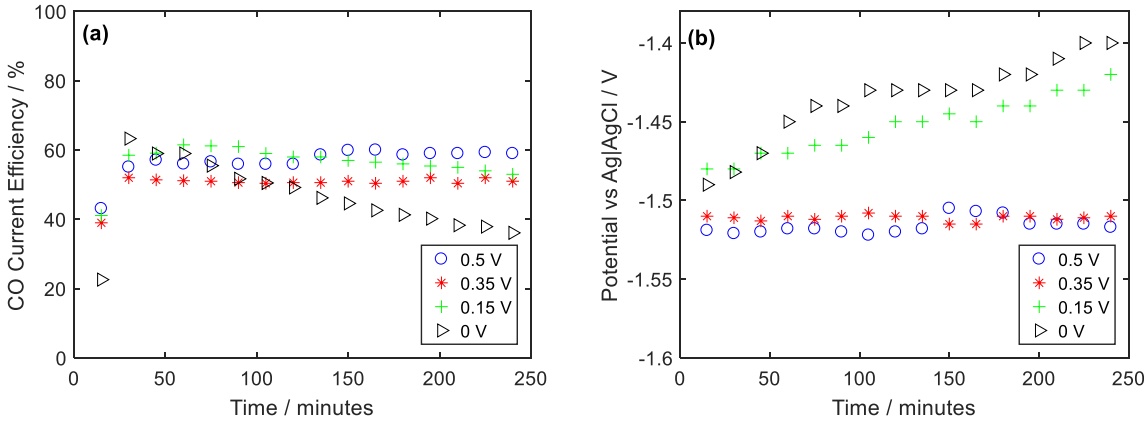

Figure 5.6: (a) Current efficiency for CO production and (b) potential vs time during CO_2 reduction at a gold cathode in 0.2 mol L^{-1} $KHCO_3$ saturated with CO_2 at -5 mA cm^{-2} with cyclic voltammetry every 15 minutes between -0.5 V and an upper potent limit of (⊳) 0 V, (+) 0.15 V, (*) 0.35 V and (o) 0.5 V vs Ag|AgCl.

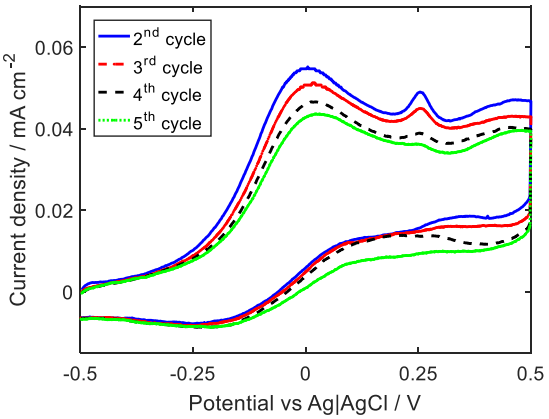

Figure 5.7: Stripping cyclic voltammetry on a gold cathode during CO_2 reduction in 0.2 mol L^{-1} $KHCO_3$ saturated with CO_2 at -5 mA cm^{-2}. The stripping voltammetry was performed every 15 minutes at 100 mV s^{-1}. The anodic current between 0.5 V and -0.25 V during the scan in the negative direction is most likely due to oxidation of residual CO not completely oxidized during the scan in the positive direction.

5.3.4 Using periodic open circuit or anodic treatments to prevent deactivation

While using cyclic voltammetry over an appropriate potential range is an effective method to prevent the deactivation of gold cathodes during CO_2 reduction, using a method requiring a reference electrode is unlikely to be applied in an industrial electrolysis process. Given that the gold cathode is poisoned by Zn, Fe, and Cu, it is proposed that any simple two electrode method which results in the potential of the gold electrode being more positive than -0.96, -0.64 or 0.28 V vs Ag|AgCl will be enough to remove the Zn, Fe, and Cu poisons respectively. Therefore, interrupting galvanostatic CO_2 reduction with periods of open circuit or low anodic currents has been investigated as possible simple cleaning methods.

By interrupting CO_2 reduction every 15 minutes with 4 minutes at open circuit, the deactivation of the gold cathode is found to be less severe than without the interruptions (Figure 5.8a). By measuring the potential during the 4 minute open circuit interruptions, it is found that over the entire 4 hour period of CO_2 reduction, the potential at the end of each 4 minute open circuit interruption is approximately between -0.31 and -0.36 V (Figure 5.8b). Thus it is concluded that the small improvement in the stability of the current efficiency for CO production is due to the removal of Fe and partial removal of Zn (both of which should occur at potentials above -0.64 V). Clearly as the maximum potential during the open circuit interruptions below that required to remove the Cu, the remaining deactivation is likely due to the accumulation of Cu, with cyclic voltammetry and XPS analysis confirming that Cu indeed remains on the surface after these open circuit periods. In addition to the Cu, XPS also showed the presence of Zn on the gold despite the fact that the achieved potential during open circuit potential periods is more positive than the Zn/Zn^{2+} potential. As Zn passivates at pH=7 and -0.36 V vs Ag|AgCl [163], it is likely that the Zn remaining on the gold surface is ZnO rather than metallic Zn. While this passive ZnO forms during OCP interruptions, we propose that the formation of this passive ZnO is avoided during periodic stripping voltammetry cleaning process. This is because the pH-potential window where the passive ZnO can form is very small [163] and the surface pH will be higher than 7, immediately after a period of CO_2 reduction [164, 174].

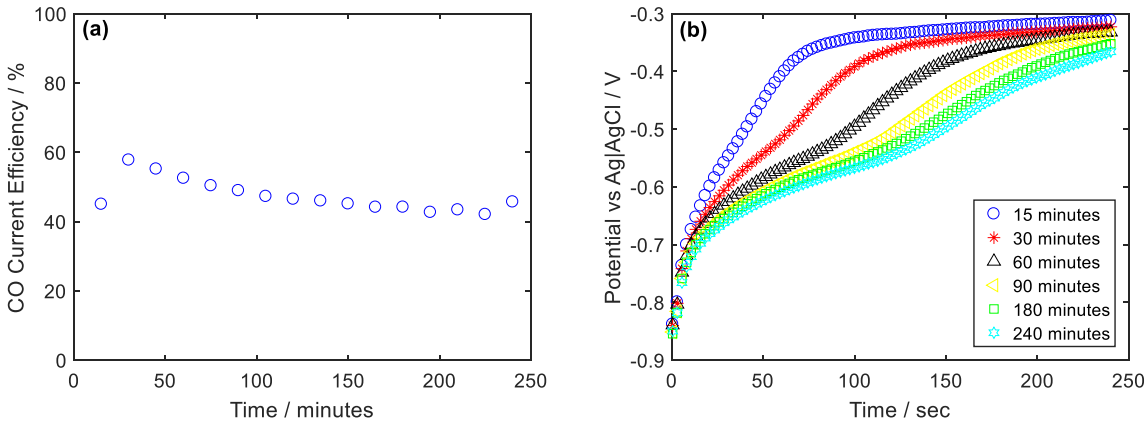

Figure 5.8: The effect of interrupting CO_2 reduction at -5 mA cm^{-2} with 4 minutes of open circuit potential every 15 minutes. (a) Current efficiency for CO production, and (b) the open circuit potential during the CO_2 reduction interruption at various times over the 4 h period of CO_2 reduction.

As the open circuit periods were not found to remove all of the Zn and Cu poisons, the CO_2 reduction was instead interrupted every 15 minutes with short periods of anodic current. The currents and treatment times were based on the charge associated with the CO oxidation peak and Cu stripping peak found by cyclic voltammetry (Figure 5.7). By interrupting the galvanostatic CO_2 reduction every 15 minutes with a 25 µA cm^{-2} anodic current for between 10 and 50 seconds (250-1250 µC cm^{-2} of anodic charge), it was found potential of the gold electrode could reach between -0.15 V and 0.55 V (Figure 5.9a) which is enough to partially strip Fe, Zn and at higher potentials Cu. As with the open circuit interruptions, this resulted in an improved stability, but did not completely prevent deactivation with the current efficiency for CO production dropping from an average maximum of 53 % to an average of 46%. (Figure 5.9b). XPS revealed that no Fe or Cu was on the gold surface following this cleaning protocol (when the achieved potential is around 0.3 V vs Ag|AgCl), and again it is suggested that the Zn remaining on the surface is in the form of ZnO which is resistant to corrosion at the pH and potentials found during this cleaning process.

Finally, an interestingly observation made during this work was that electrodes were generally found to be more stable for CO production when the electrodes were less active for CO production. While the initial differences in the current efficiency for CO production between experiments are likely to be due to slight variations between the electrode themselves (*e.g.* surface roughness factor or crystal facets) no clear trend between the initial electrode structure (based on cyclic voltammetry recorded before the CO_2 reduction) and the initial current efficiency could be found. Despite this, the observation that less active electrodes were less

susceptible to poison may suggest that only certain sites on the gold electrodes are readily poisoned.

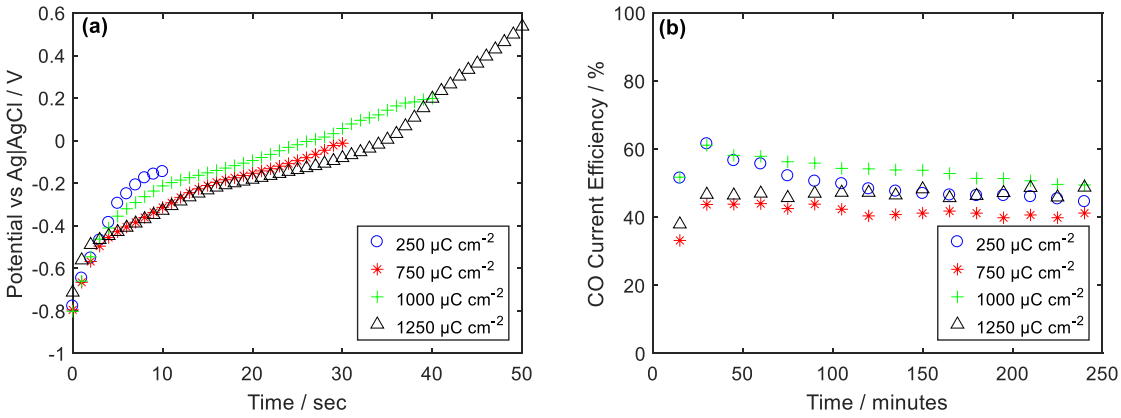

Figure 5.9: The effect of anodic treatments applying various charges on (a) potential during treatment procedure and (b) current efficiency for CO production. The anodic treatments were applied every 15 minutes during CO_2 reduction at -5 mA cm^{-2} in 0.2 mol L^{-1} $KHCO_3$ saturated with CO_2.

5.4 Conclusion

Electrochemical CO_2 reduction on gold can produce CO, H_2 and formate, although the current efficiency towards CO decreases over time due to the deactivation of gold cathode. This deactivation results in higher H_2 production and a continuously increasing formate production rate. XPS analysis shows that this deactivation is caused by the deposition of Cu and Zn from trace amounts of these elements in the electrolyte. Surprisingly, no Fe could be found on gold cathode by XPS after prolonged CO_2 reduction, despite the fact that the Fe concentration in the electrolyte is higher than that of Zn and Cu and that intentional addition of Fe^{2+} to the electrolyte leads to severe deactivation. Seems that Fe deposition on gold is harder than other metallic impurities present in the electrolyte. Thus it is concluded that Zn, Cu and Fe all contribute to the deactivation of gold cathodes for CO_2 reduction. This deactivation can be prevented by periodically increasing the potential of the gold electrode to anodically strip these poisons from the surface. Unfortunately, this treatment can lead to significant gold dissolution if the potential exceeds approximately 0.65 V vs Ag|AgCl at pH 7, which would make long-term electrolysis very difficult. However, by periodically interrupting CO_2 reduction with cyclic voltammetry every 15 minutes between -0.5 and 0.5 V vs Ag|AgCl, the metallic impurities can be stripped and the deactivation prevented without leading to gold dissolution. Partial prevention of the CO_2 reduction deactivation can also be achieved with

periodic open circuit periods or short anodic current treatments, although further work needs to be conducted to optimise these simple cleaning protocols.

5.5 Additional material

In addition to the results depicted in Figure 5.9, some more experiments were conducted at the same anodic charge, and the galvanostatic CO_2 reduction was interrupted by applying equal anodic pulse (750 µC cm^{-2}) every 15 minutes. As can be observed in Figure 5.10, incorporating a brief chronopotentiometry treatment at a very gentle anodic current during galvanostatic CO_2 reduction has a substantial effect on the CO formation. The potential changes during the short anodic pulse (Figure 5.10a) depict the final voltage at the end of treatment is identical when the passed charge is the same (in this case, the potential is enough to strip off Zn and Fe impurities). Also, the CO selectivity is almost the same in an equal amount of charge as can be observed in Figure 5.10b. This is consistent with the results in Figure 5.9 showing the electrode activation is dependent on the passed charge during the treatment. Hence, the gold surface can back to an earlier state if an appropriate pass charged is employed. Here we can propose that using the charge density of 1000 µC cm^{-2} can guarantee high CO selectivity over long-term electrolysis.

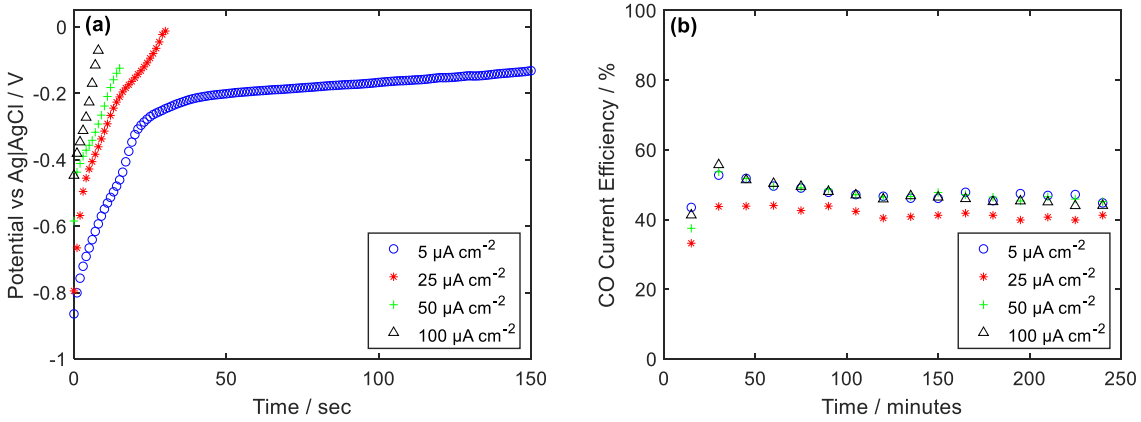

Figure 5.10: The effect of anodic treatments applying identical charges at various current densities on (a) potential during the treatment procedure and (b) current efficiency for CO production. The anodic treatments were applied every 15 minutes during CO_2 reduction at -5 mA cm^{-2} in 0.2 mol L^{-1} $KHCO_3$ saturated with CO_2.

Similarly, a series of voltammograms were used to probe the electrochemically adsorbed CO on the gold surface as earlier discussed in section 4.3.1. Initially, the applied potential was from 1.2 V to -1.2 V vs Ag|AgCl (Figure 5.11a) to drive the voltage to CO_2 reduction potential

to form CO (Figure 5.11b), after 1 minute constant potential at -0.75 V vs Ag|AgCl, another potential sweeping range was used (-0.75 to 1.2 V vs Ag|AgCl) to see any evidence of adsorbed CO on the gold surface by using voltammograms. This one-minute potentiostatic step allows the surface condition to equilibrate with the bulk solution. Figure 5.11c illustrates that holding the potential at the point where no CO_2 reduction occurs, desorbs CO from the gold surface. The result is consistent with other studies showing the fact that *CO bonds on the gold electrodes are weak so that cannot be reduced further to produce any hydrocarbons [27, 38, 157, 158]. Hence, by keeping the potential at -0.75 V vs Ag|AgCl for 1 minute, CO oxidation peak is absent (Figure 5.11c) and it is unlikely any CO intermediates would be presented in our experiment in this condition.

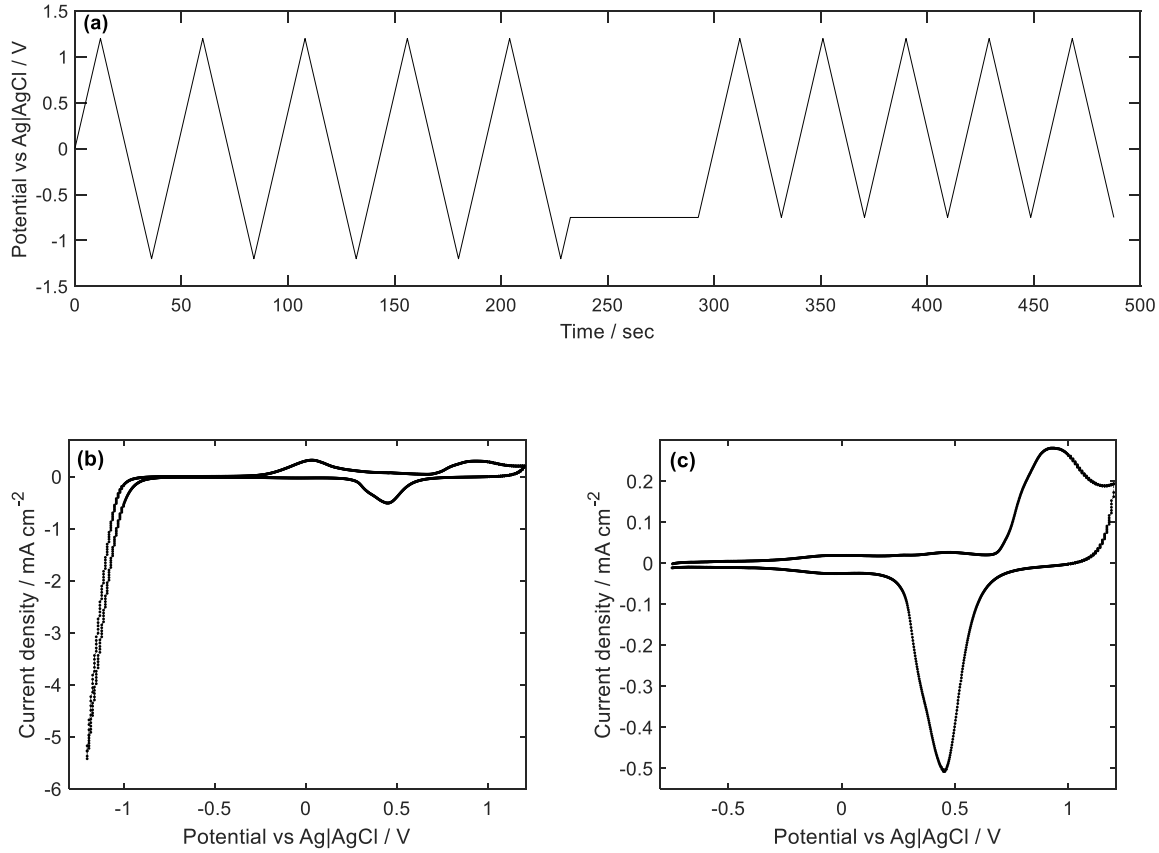

Figure 5.11: Cyclic Voltammetry changes at different potential ranges at gold electrode in 0.2 mol L^{-1} $KHCO_3$ (saturated with CO_2) and the scan rate of 100 mV s^{-1}. (a) the potential changes by time at different potential ranges; (b) the effect of potential range on the current density before one-minute pause; (c) the impact of potential range on the current density after one-minute pause.

The following strategy has been applied afterwards to see what reason makes the gold electrode poisonous. Figure 5.12a showed a time course of current efficiency when

galvanostatic CO_2 reduction was interrupted by a one-minute pause at a constant potential of -0.75 V vs Ag|AgCl every 15 minutes. As illustrated in Figure 5.11a, that time is enough for desorbing all CO intermediates (and possibly some part of Zn) from the gold electrode surface; consequently, only metallic impurities (like Fe and Cu) are presented on the electrode surface. Nevertheless, a considerable amount of deactivation is observed in Figure 5.12a while in Figure 5.12b the current efficiency for CO is interestingly stable as we have used one minute constant potential at -0.75 V vs Ag|AgCl (to remove CO) and also the charge density of 250 µC cm^{-2} (25 µA cm^{-2} for 10 sec). In this circumstance, the potential (as the driving force) would be essentially stable over electrolysis (the red triangles in Figure 5.12c). Also, the measured potential during treatment steps was still cathodic showing the fact that no gold oxide has been formed. These results are supposedly suggesting a significant influence of metallic impurities (coming from the electrolyte) compared with CO-related intermediates on the gold electrode deactivation. However, we believe that the deactivation mechanism is unlikely the same for other electrodes (like Cu) as CO bonds are stronger compared with gold electrodes [158].

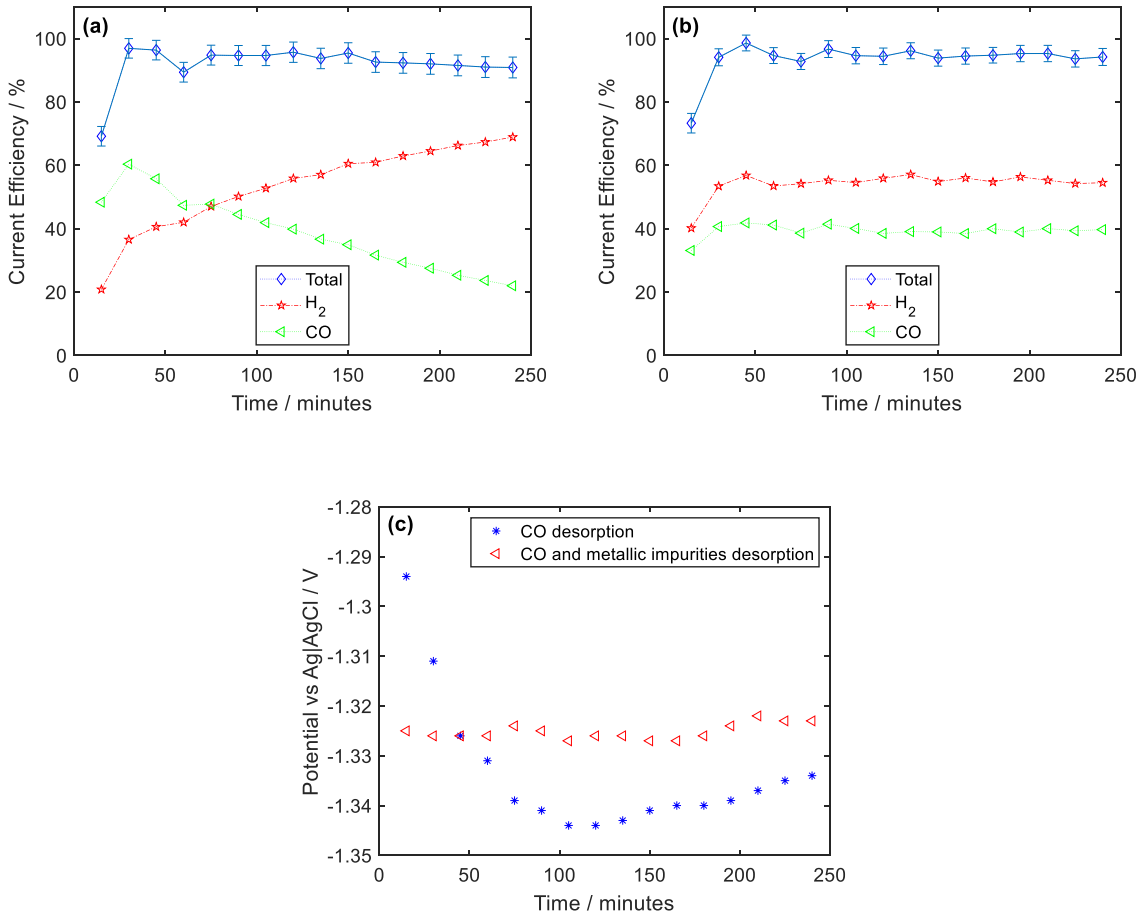

Figure 5.12: Current efficiency changes of gaseous products by time for CO_2 reduction using gold electrode in 0.2 mol L^{-1} $KHCO_3$ (saturated with CO_2) at -5 mA cm^{-2}; (a) with 1 minute pause at the potential of -0.75 V vs Ag|AgCl; (b) with 1 minute pause at the potential of -0.75 V vs Ag|AgCl and 10 second anodic pulse at 25 µA cm^{-2}; (c) potential changes during electroreduction for both methods.

6 Electrocatalytic CO_2 Reduction in a Continuous Flow Electrochemical Cell

This chapter was originally published in the Electrochemistry Communications under the title "Comparing the electrocatalytic reduction of CO_2 to CO on gold cathodes in batch and continuous flow electrochemical cells", corresponding to reference [327] in this thesis. Section 6.5 provides additional information which has not been included in the original paper.

DOI: https://doi.org/10.1016/j.elecom.2019.03.005

Abstract: The electrocatalytic reduction of CO_2 on gold cathodes was found to differ significantly between a standard batch electrochemical cell and a flow cell incorporating a porous gold cathode. While the well-known influence of $KHCO_3$ concentration on product selectivity was observed in the batch cell, the selectivity of the CO_2 reduction reaction was shown to be independent of $KHCO_3$ concentration in the flow cell. The Faradaic efficiency for CO production was found to be 80-90% regardless of the $KHCO_3$ concentration whereas in the batch cell it decreased from 75% to 35% as the $KHCO_3$ concentration is increased from 0.05 to 0.5 mol L^{-1}. The current density was found to be independent of $KHCO_3$ concentration and similar in both cells (-4 to -10 mA cm^{-2} at -1.3 V vs Ag|AgCl). As the $KHCO_3$ concentration effect is normally attributed to changes in the local pH at the cathode-electrolyte interface brought about by the buffering action of the electrolyte, the results found in this work suggest that pH buffering can be suppressed or manipulated in some cell/electrode configurations. In the flow cell used in this work, it is suggested that poor transport of the $KHCO_3$ through the porous cathode support to the active surface results in higher local pH than that found at the surface of a cathode immersed in a traditional batch cell.

6.1 Introduction

The electrocatalytic reduction of CO_2 into fuels and industrial chemicals has become an important area of research, as it can be used to store renewable energy as chemical energy [14, 94, 328]. Electrocatalytic CO_2 reduction in aqueous electrolytes has many advantages

over traditional chemical conversion including simple process design, direct control of surface free energy and also operating under ambient conditions [17, 329, 330]. While many [60, 131, 331-333] have focused on modifying the activity and selectivity through electrocatalytic design and development, others proposed that the ionic species in the electrolyte can play a key role in controlling the CO_2 reduction reaction by affecting the pH and CO_2 concentration close to the electrode surface [34, 105, 108, 109, 166, 170, 334].

As the hydrodynamics at electrode-electrolyte interface can directly influence the interfacial pH and CO_2 concentration [164, 174], it must be expected that the electrochemical cell configuration (*e.g.* electrolyte agitation / flow, electrode geometry) will influence the behaviour of the electrocatalytic CO_2 reduction reaction. In literature, the most commonly used cell configuration is a batch type cell, with the reduction reaction occurring at the cathode within a CO_2 saturated electrolyte [36, 181, 184]. While some specifically mention using some form of electrolyte agitation [19, 72, 174, 335] , in most cases the electrode-electrolyte interface will not be stagnant due to the CO_2 purged into the cell or the gas bubbles evolved off the cathode. In a few cases, electrocatalytic CO_2 reduction has been conducted in a flow cell configuration, wherein gas or CO_2 saturated electrolyte is continuously pumped through the electrochemical cell (which normally consists of electrode separated by a membrane) [30, 173, 336]. It is important to note that in these previous reports of CO_2 reduction in flow cells, the electrolyte flows directly over the surface of the cathode, and thus increasing the gas or electrolyte flow rate to enhance CO_2 transport to the cathode surface will also increase the buffering action of electrolyte on the interfacial pH [164, 174].

Despite the overwhelming evidence that the interfacial pH influences electrochemical CO_2 reduction [34, 109, 172-174, 302], and the fact that cell configuration / electrolyte hydrodynamic is likely to impact this interfacial pH, there are no studies which compare identical electrodes in different electrochemical cells. Thus this investigation compares the electrocatalytic CO_2 reduction at gold electrodes in a typical batch cell to the performance of gold electrodes in a flow cell designed to maximize the interfacial pH at the surface of the cathode.

6.2 Experimental

6.2.1 Electrochemical cell configuration

Electrocatalytic CO_2 reduction was performed using two different cell configurations; a batch cell and a zero-gap flow cell. In this work, gold was chosen as the cathode material as it is known to be very selective for CO production and its electrochemically active surface area can be easily determined by cyclic voltammetry [227, 282, 337]. The batch cell was based on a two-compartment gas-tight glass electrochemical cell using a gold disc cathode (99.999%, 16mm diameter) separated from a graphite counter electrode by a Nafion 115 membrane. A reference electrode (Ag|AgCl saturated KCl) held in a luggin capillary was placed in the cathode chamber. The gold cathode was polished to a mirror finish using silicon carbide paper and alumina slurries (down to 0.05 µm) prior to use. As a comparison, a flow cell consisting of a cathode flow chamber machined in a graphite plate and PTFE anolyte chamber was constructed (Figure 6.1). Vertical flow channels (1×1 mm) were machined into the graphite plate with the electrolyte entering at the base of the flow channels and existing at the top. A gold coated carbon paper (20 mm diameter) was used as the cathode, with the gold coating pressed against the Nafion 115 membrane used to separate the cathode flow chamber from the anolyte chamber. In this flow cell design, CO_2 saturated $KHCO_3$ was recirculated from a 60 mL reservoir at 10-50 mL min^{-1} through the flow channels machined in to graphite plate and over the backside of the gold coated carbon paper. The anolyte chamber contained the reference electrode and a mixed-metal oxide titanium mesh anode (Ti-shop.com) as the counter electrode. The carbon paper (SIGRACET GDL 10 AA, Ion Power) was coated by gold using a EMS150T ES sputter coater to a mass loading of 0.09 mg cm^{-2}.

6.2.2 Electrolysis measurements

Electrocatalytic CO_2 reduction was performed at between -1.1 V and -1.5 V vs Ag|AgCl using a Gamry Reference 3000 potentiostat. CO_2 gas (99.995 vol%) was continuously purged through the electrolyte at a rate of 40 mL min^{-1} for 30 minutes before each experiment to ensure that the electrolyte was saturated. This flow was reduced to 20 mL min^{-1} during the experiment and controlled by a mass flow controller (Alicat, MC-20SCCM-D). Different concentrations of $KHCO_3$ (99.7% ACS reagent, Sigma Aldrich) was directly used as the electrolyte, without any purification, and was prepared with 18.2 MΩ cm deionized water. Electrochemical impedance spectroscopy was used to determine the resistance between the

cathode and reference electrode, with this then compensated by positive feedback during the potentiostatic electrolysis. All experiments were conducted at room temperature (23 °C).

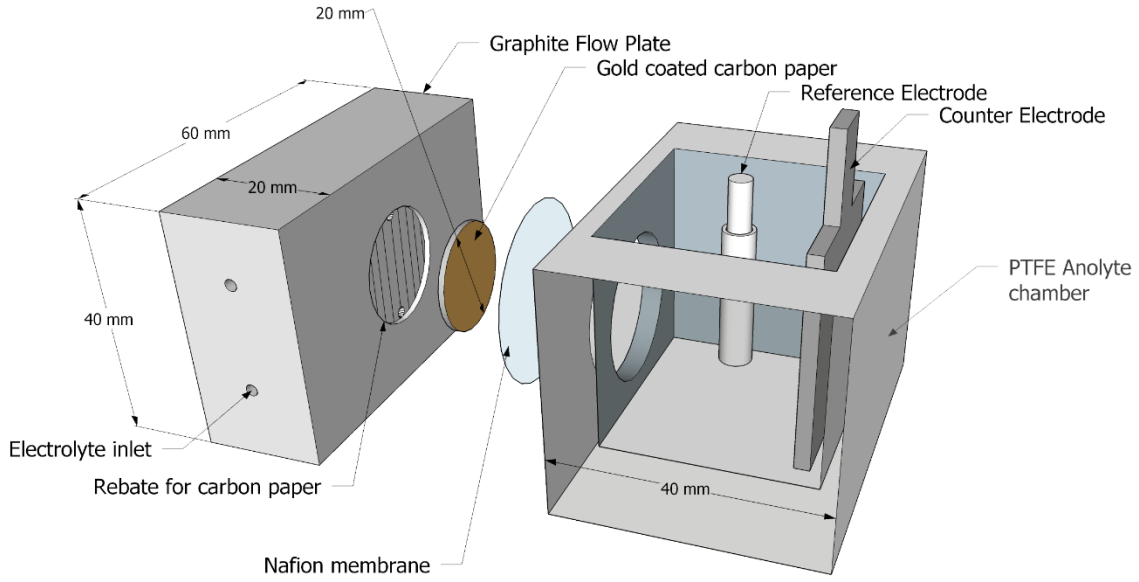

Figure 6.1: Schematic diagram of the electrochemical flow cell.

6.2.3 Product Quantification

The gas samples were injected into a gas chromatograph (SRI 8610C) equipped with a Haysep-D column, Ar carrier gas, methanizer FID and TCD detectors to quantify CO and H_2 every 15 minutes during the electrolysis experiments. The Faradaic efficiency was then calculated from the ratio of charge needed to produce a certain product to the measured charge passed during the sampling time. High Performance Liquid Chromatography (SUPELCOGEL^{TM} C-610H column) was employed for post-electrolysis analysis of reduction products present within the electrolyte.

6.3 Results

6.3.1 The Effect of Electrolyte Concentration

In both the batch and flow cells, potentiostatic CO_2 reduction between -1.1 V and -1.5 V vs Ag|AgCl (-0.5 to -0.9 V vs RHE at pH=6.8) resulted in the production of CO and H_2 with trace amounts of formate. Typically, the Faradaic efficiency for formate production was less than 10%, and in all experiments, the overall mass-charge balance was found to be satisfied (within the experimental uncertainties). In both cells, the current density was found to be

independent of $KHCO_3$ concentration and flow rate (in the flow cell), and typically the current density was between -4 and -10 mA cm^{-2} at -1.3 V vs Ag|AgCl.

Consistent with others [108, 109], in the batch cell at -1.3 V, as the concentration of $KHCO_3$ increased, the Faradaic efficiency for CO production decreases (Figure 6.2a), with this effect also seen at -1.1 and -1.5 V. This effect is widely reported to be directly due to the increased buffering capacity of the $KHCO_3$ electrolyte which suppresses the localised increase in pH caused by the cathodic reactions [29, 164, 166]. Surprisingly, in the flow cell configuration, this well-known buffering capacity effect is not observed, with the Faradaic efficiency for CO production remaining constant over electrolyte concentrations between 0.05 and 0.5 mol L^{-1} (Figure 6.2b). This observation is proposed to be due to poor transport of the electrolyte from the flow channels through the carbon paper to the active gold surface, which essentially would mean that a high pH at the gold surface can be maintained despite the increased buffering capacity of the electrolyte. It is also found that the Faradaic efficiency towards CO production is higher in the flow cell compared to the batch cell, which has important implications for measuring and reporting the performance of cathodes for CO_2 reduction.

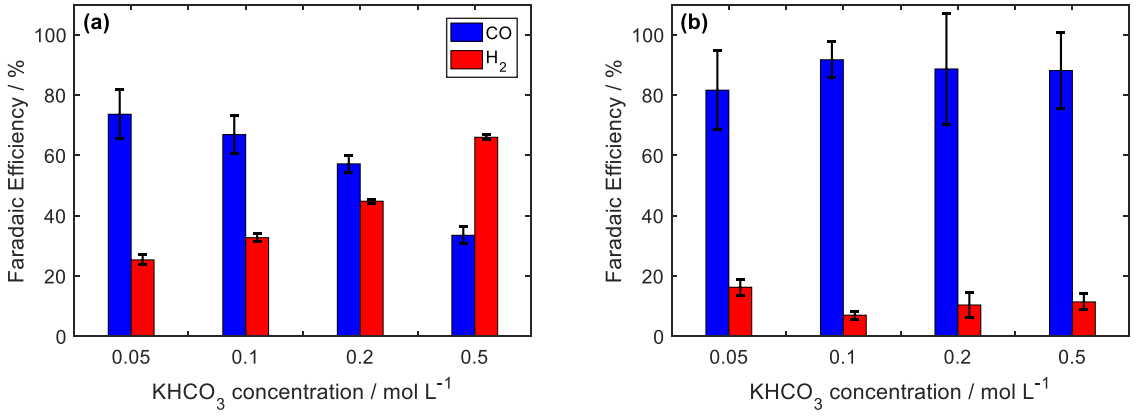

Figure 6.2: Faradaic efficiency for CO and H_2 production in the batch cell with different $KHCO_3$ concentrations at -1.3 V vs AgAgCl in (a) the batch cell; (b) the flow cell.

To confirm that the hydrodynamic conditions in the flow cell is the cause of the observed differences in Faradic efficiency between the two cells, the performance of a gold-coated carbon paper cathode was also measured in the standard batch cell. The performance was essentially the same as the polished gold disc (*i.e.* lower CO selectivity at higher $KHCO_3$ concentrations), which confirms that the electrode itself (gold-coated carbon paper vs a polish gold disc) is not the cause for the differences between the two electrolysis cells.

6.3.2 The Effect of Electrolyte Flow Rate

To examine the hydrodynamics at the active cathode surface in the flow cell, the flow rate of electrolyte through the cell was varied over an 8 h electrolysis period. It was reasoned that if the electrolyte was being forced through the porous carbon paper by the flow, then the flow rate should directly alter the CO_2 reduction performance by manipulating the interfacial surface pH in a similar way to that achieved at rotating electrodes [174]. These results show that the selectivity of the reaction in this cell is unaffected by electrolyte flow rates between 10 and 50 mL min^{-1} (Figure 6.3), which supports the proposal that the transport of species to and from the active electrode surface is restricted to diffusion through the porous carbon paper, rather than by the forced convection of electrolyte (Figure 6.4). This is similar to the proposed mechanism at porous electrodes (immersed in electrolytes), wherein the restricted transport of species within the electrode pores is believed to enhance CO_2 reduction [126, 338]. While we have not attempted to optimize the transport behaviour through the carbon paper electrode support, others have showed that the transport of CO_2 through carbon paper electrodes can be improved by using thinner electrodes [53, 336].

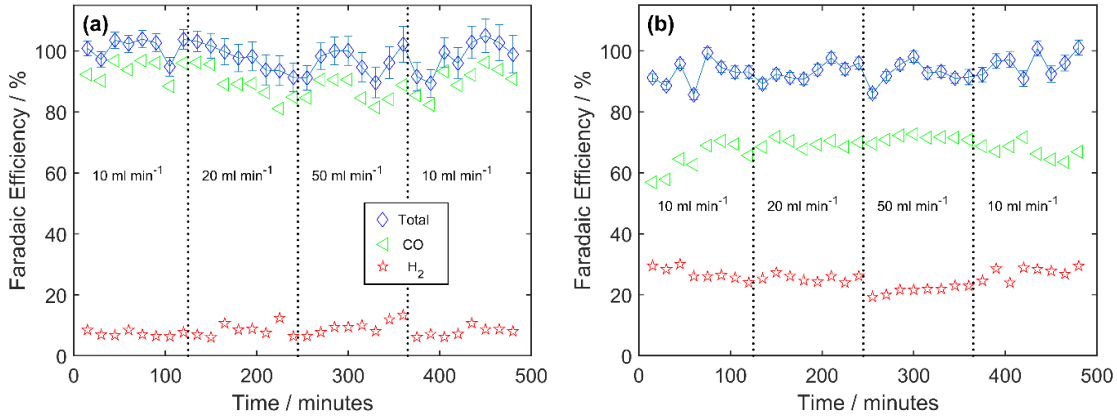

Figure 6.3: Faradaic efficiency changes in the flow cell by time at: (a) -1.3 V; (b) -1.5 V using 0.2 mol L^{-1} $KHCO_3$ as the catholyte and a CO_2 bubbling flow rate of 20 ml min^{-1}.

These findings have important implications for the development and comparison of electrocatalysts and strongly support previous proposals that standardization of CO_2 electrolysis cells is required [173]. Furthermore, it should not be unexpected that the selectivity of other electrode reactions will also be influenced by cell design.

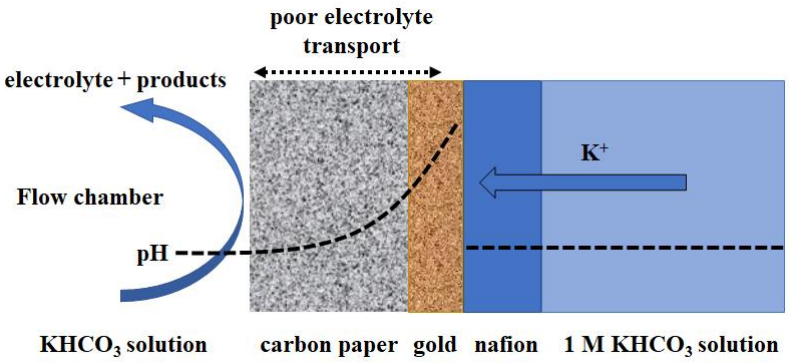

Figure 6.4: Proposed transport phenomena in the flow cell which leads to enhanced CO_2 reduction.

6.4 Conclusion

Understanding and controlling the hydrodynamics at the electrolyte-electrode interface during electrocatalytic CO_2 reduction is clearly important. In particular, it is shown that the performance of gold cathodes depends strongly on the configuration of the electrolysis cell. It is also shown that the well-known effect of $KHCO_3$ concentration on the Faradaic efficiency of CO production on gold cathodes can be completely negated by using the gold cathode within a flow cell designed to restrict facile transport of the electrolyte species to the electrode surface. These results have important implications for all working on electrocatalytic CO_2 reduction: clearly the comparison of results between research groups requires identical electrochemical cells / electrode geometries to be used. We also suggest that conclusions regarding the influence of electrocatalytic material on product selectivity may not be related to the material itself but rather the cell or electrode configuration / geometry.

6.5 Additional material

In addition to the results presented in Figure 6.2, some more potentiostatic (at -1.5 V vs Ag|AgCl) CO_2 reduction experiments were conducted to support the fact that the electrolyte composition influences the product distribution in the batch and flow cell (Figure 6.5). As clearly evident, the results clearly support the previous findings and suggest higher CO production in lower buffer capacities. The results also propose that higher potentials have a negative impact on CO Faradaic efficiencies and H_2 production will be dominant (it is more evident in the case of batch cell).

Interestingly, the results obtained from the flow cell (Figure 6.5b and Figure 6.2b) reveal that this type of cell is more selective toward CO production; however, it is less sensitive toward

applied potential while the electrolyte concentration has almost no effect on the product distribution. It is believed that both CO_2 reduction reaction and HER can cause an increase in the surface pH by producing OH^- which shifts the CO_2 equilibrium toward bicarbonate production; hence the local bicarbonate concentration will be decreased [29, 164, 166]. Also, in the concentrated $KHCO_3$ solutions, there are enough $HCO3^-$ agents to neutralise the produced OH^- and the pH will be constant at the electrode surface. A less concentrated buffering agent leads to an increase in the local pH close to the cathode in non-equilibrium situations, decreasing the concentration of dissolved CO_2.

The flow cell has been designed so that the dissolved CO_2 reaches the gold surface via diffusion through a high pH region. In this circumstance, it is proposed that the electrolyte conditions would influence the product distribution. Experimentation suggests that the mode of dissolved CO_2 transport to the gold active site can be controlled by diffusion.

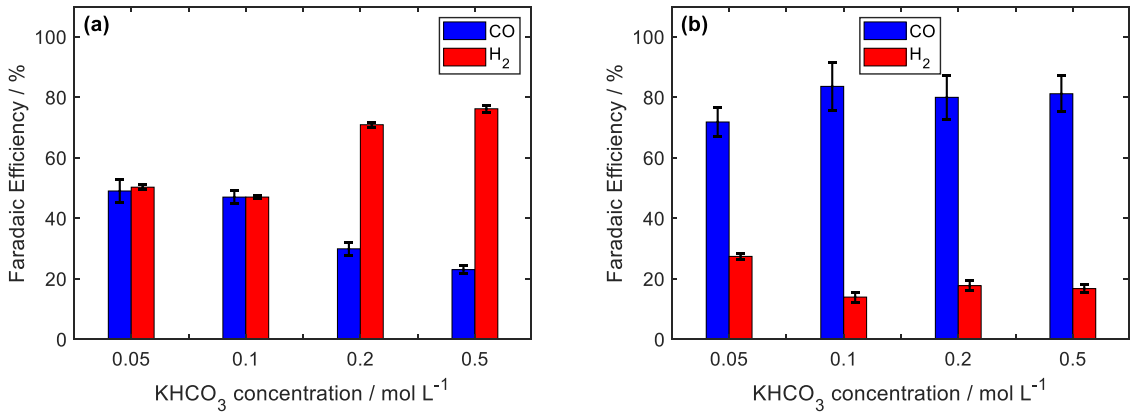

Figure 6.5: Faradaic efficiency for CO production in the batch cell with different $KHCO_3$ concentration using chronoamperometry at: a) -1.5 V batch cell and b) -1.5 V flow cell and CO_2 bubbling flow rate of 20 mL min^{-1}.

To lend further support to the effect of cell hydrodynamics in CO production, galvanostatic (-5 mA cm^{-2}) CO_2 reduction on polycrystalline gold electrode was carried out at different $KHCO_3$ electrolytes (0.05, 0.1, 0.2, 0.5 and 1 mol L^{-1}) for 4 hours at each electrolyte concentration using batch cell and flow cell. Unlike the potentiostatic experiments, the galvanostatic experiments (Figure 6.6) showed a significant influence of $KHCO_3$ concentration on the product distribution when the flow cell was used. But while this may appear to be due to $KHCO_3$ concentration, the potential (which directly influences selectivity) also changes. Hence, the changes in the product selectivity could be explained by the potential changes during galvanostatic reduction. Also, the obtained results for the batch cell are

consistent with our previous findings presented in Figure 6.2 and with the proposal that a higher surface pH favours CO_2 reduction reaction (this effect has already been discussed in section 6.3.1).

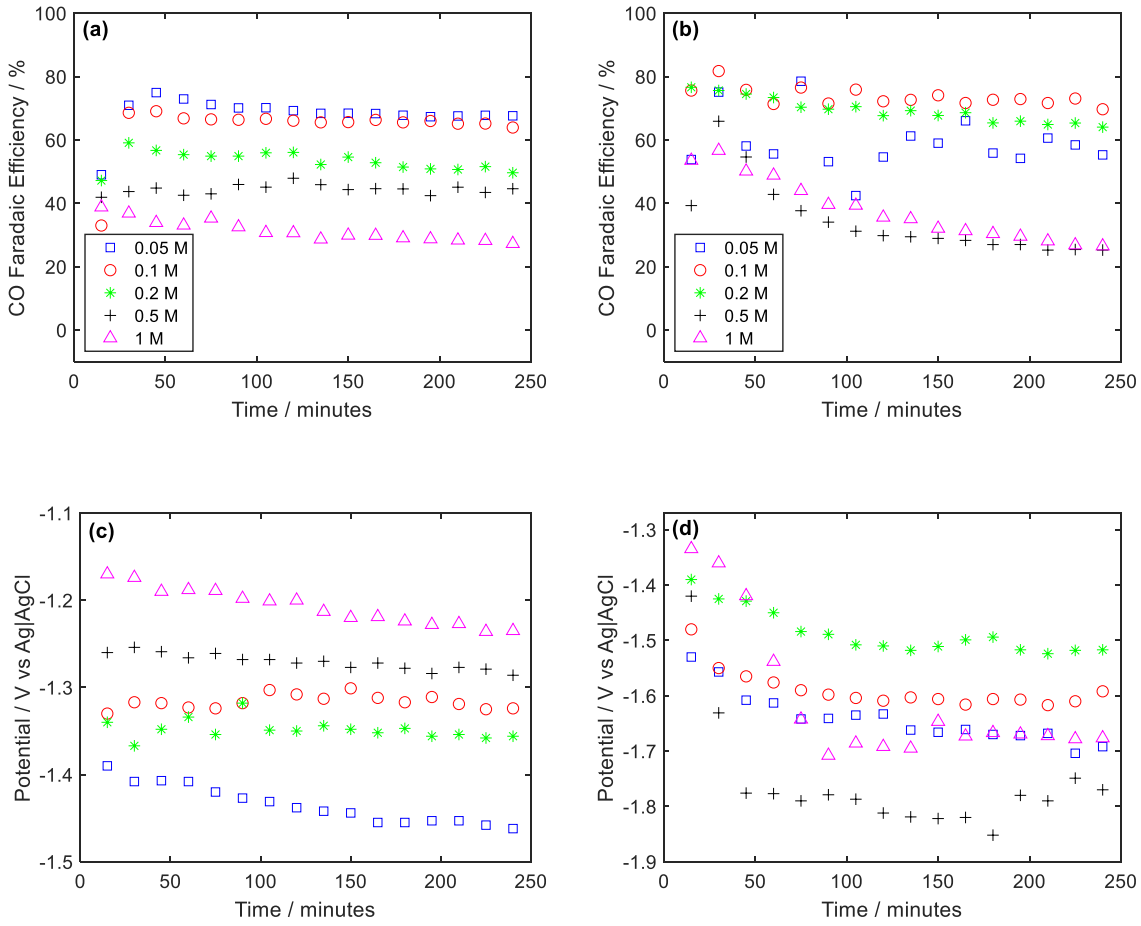

Figure 6.6: CO Faradaic efficiency using :(a) batch cell; (b) flow cell, and the electrode potential changes using: (c) batch cell ;(d) flow cell by time for CO_2 reduction at -5 mA cm^{-2} in different $KHCO_3$ concentration.

To ensure that the enhanced performance in the flow cell (because of higher CO Faradaic efficiency) is for the hydrodynamic effects (not for the porous nature of the carbon paper), a potentiostatic (at -1.5 V vs Ag|AgCl) CO_2 reduction was conducted in 0.2 mol L^{-1} $KHCO_3$ using a gold-coated carbon paper in the batch cell. As illustrated in Figure 6.7, the results have been compared with the normal polycrystalline bulk gold and show almost the same performance confirming the electrode is not the reason for different behaviours between the batch and flow cells.

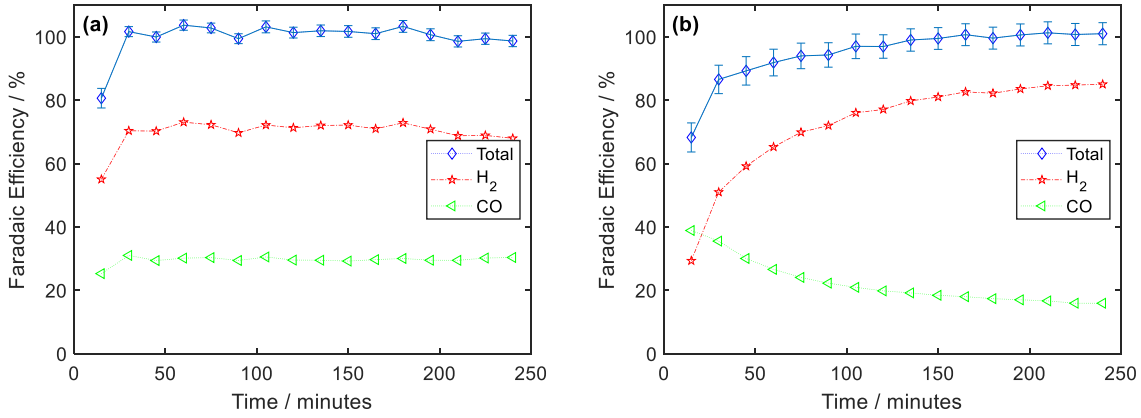

Figure 6.7: The effect of porous electrode design on CO_2 electroreduction in the batch cell in 0.2 mol L^{-1} $KHCO_3$ and CO_2 bubbling flow rate was 20 ml min^{-1} at -1.5 V vs Ag|AgCl. (a) the product distribution using polycrystalline gold electrode; (b) using gold coated (0.091 mg cm^{-2}) on carbon paper placed in the batch cell.

Figure 6.8 provides more details for the results previously discussed in Figure 6.3. As can be observed, the current density is continuously decreasing by increasing the flow rate (over time) and seems to be due to the cathode deactivation because the initial solution flow rate (10 mL min^{-1}) has been examined after 6 hours while the current density was remarkably lower than that of initial values. Also, the recorded current densities show a notably higher current density value at higher potentials suggesting higher production rate for the products in line with the dependence of the CO_2 reduction reaction to the potential (see section 2.3).

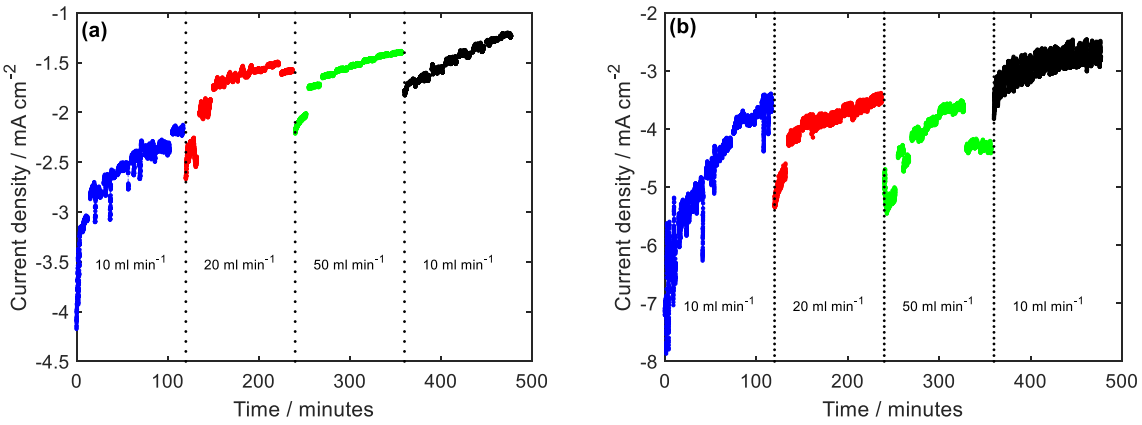

Figure 6.8: Current density changes in the flow cell by time at: (a) -1.3 V; (b) -1.5 V using 0.2 mol L^{-1} $KHCO_3$ as the catholyte and a CO_2 bubbling flow rate of 20 mL min^{-1}.

Another interesting observation is the dependency of CO_2 electroreduction on the gold loading coated on the carbon paper. Observations show a linear increase of the gold content on the carbon paper over sputtering time (Figure 6.9a). The EASA analysis in Figure 6.9b

presents a logarithmic increasing of the charge density of the gold oxide reduction peak (the charge corresponding to the number of electrons required to entirely reduce the gold oxide surface to a metallic gold surface) showing that not necessarily all of the surface is involved in the electrochemical reaction, especially at higher gold loadings. To investigate the effect of gold loading on CO Faradaic efficiency, the potentiostatic reduction was performed at -1.3 V vs Ag|AgCl (Figure 6.9c) and -1.5 V vs Ag|AgCl (Figure 6.9d). As highlighted, even a small amount of gold (5 µg cm^{-2}) on carbon paper eventuated 75% CO Faradaic efficiency at -1.3 V vs Ag|AgCl. It seems likely that the reason for HER is the carbon paper itself and is not from the gold which is reasonable as carbon is a suitable catalyst for HER. The results are consistent with the outcomes shown in Figure 6.2b and Figure 6.5b again confirming that at the same gold loading, CO Faradaic efficiency is decreasing by increasing the potential to a more negative value. Also, a higher amount of loading did cause an increase in the CO Faradaic efficiency as well as stability, most likely because of more available sites favouring CO_2 reduction reaction compared to HER. The obtained current densities for these experiments have been depicted in Figure 6.9e (for -1.3 V vs Ag|AgCl) and Figure 6.9f (for -1.5 V vs Ag|AgCl) at different gold loadings over 4 hours electrolysis. The result is suggesting that higher overpotentials (more negative values) generally shift the current densities to higher values which is in line with the previous findings in this chapter. Also, it can be concluded that the current density values are generally higher at more gold loadings most likely due to more available sites for the reactions.

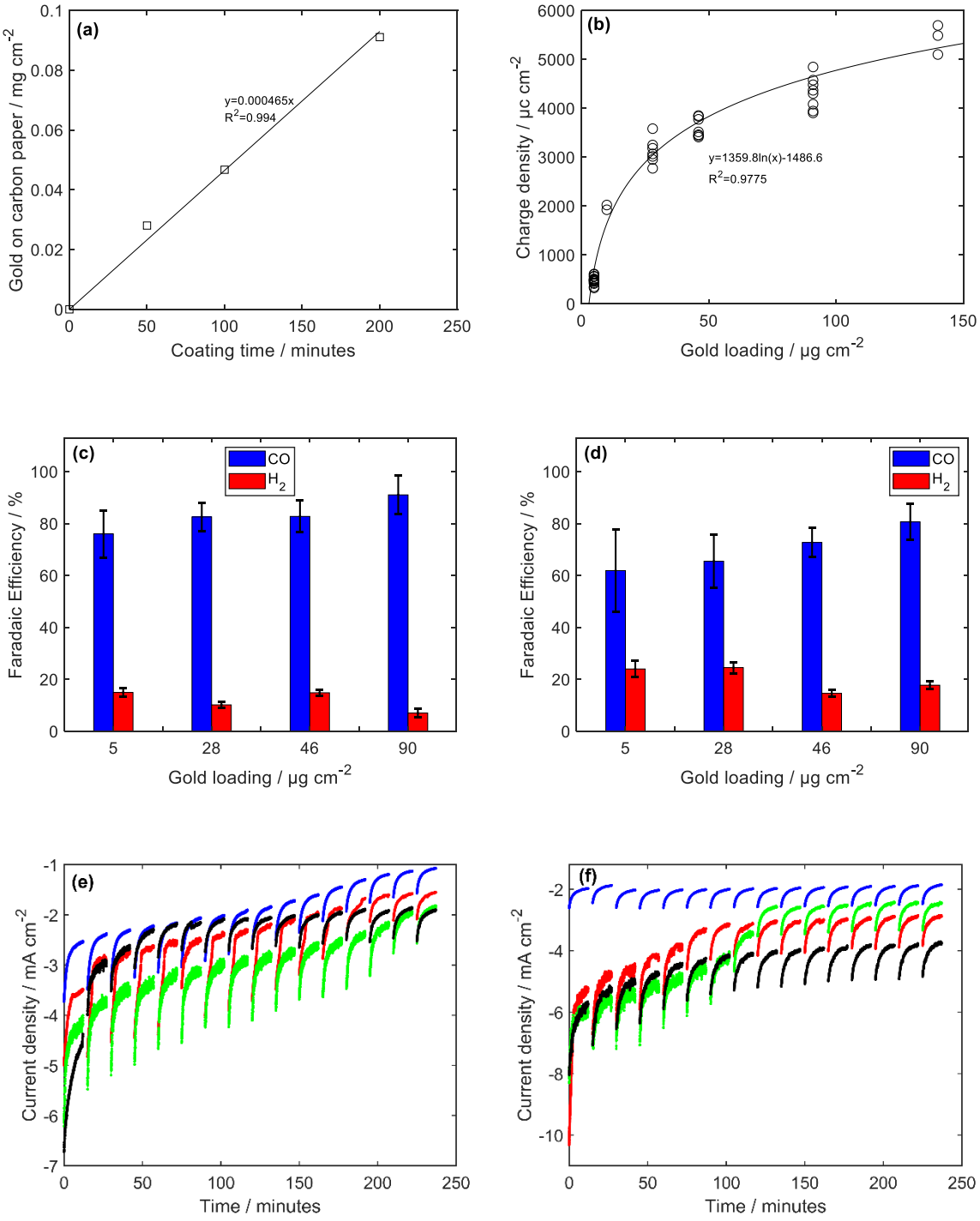

Figure 6.9: The effect of gold loading time on: a) the amount of gold on carbon paper; b) charge density of the reduction peak; c) CO Faradaic efficiency at -1.3 V; d) CO Faradaic efficiency at -1.5 V; e) current density at -1.3 V; f) current density at -1.5 V. The electrolyte was 0.2 mol L^{-1} $KHCO_3$ and CO_2 bubbling flow rate was 20 ml min^{-1}.

7 Electrochemical CO_2 Reduction Using Atomically Precise Gold Clusters

Abstract: The atmospheric CO_2 concentration increasing has raised serious environmental concerns and has detrimental effects on human health. Researchers in the last three decades have shown that CO_2 can be a potential source of carbon for the production of fuels and chemicals. The metal surfaces have shown excellent size-dependent catalytic activities for electrochemical reduction of CO_2. Recently, atomically precise clusters have attracted increasing research interest in the field of catalysis due to their size-dependent electronic and chemical properties. Their catalytic activity and selectivity for a chemical reaction can be fine-tuned with a minor change in the cluster composition, *e.g.* change in the number of atoms in metal-core. In this chapter, we synthesised the atomically precise $[Au_6(dppp)_4](NO_3)_2$, $[Au_9(PPh_3)_8](NO_3)_3$, $[Au_{13}(dppe)_5Cl_2]Cl_3$ and $Au_{101}(PPPh_3)_{21}Cl_5$ clusters. The identity of clusters was confirmed using NMR, ESI-MS and UV-Vis spectroscopy. The clusters deposited on carbon paper served as a cathode material for electrochemical reduction of CO_2 in a three-electrode system. XPS spectra suggests the clusters deposited on carbon paper were still intact. The Au_{13} based catalyst showed up to 95% selectivity for CO production over hydrogen evolution reaction. Calcination of clusters lowers the activity, which can be attributed to the agglomeration of small clusters to larger particles. The agglomeration was also confirmed by XPS, SEM and cyclic voltammetry before and after the catalytic reaction. These findings demonstrate the possibility of employing atomically precise metal clusters for selective reduction of CO_2 to CO.

7.1 Introduction

With the increase in population and constant urbanisation, the demand for energy is continuously increasing. More than 80% of contemporary global energy demand is supplemented by burning fossil fuels which harm the environment as well as human health [66, 339]. The world is dumping billions of tons of CO_2 to the atmosphere, recycling of CO_2 for producing fuels and chemical can be a sustainable solution to meet energy demand along with alleviating environmental concern. However, the thermodynamic uphill nature of CO_2 reduction reaction (CO_2RR) questions the economic feasibility of this process [340, 341]. Research in the last two decades in photocatalytic and electrocatalytic reduction pathway has

paved a way to an effective reduction of CO_2. The electrocatalytic reduction of CO_2 involves complicated multiple electron processes. This may lead to formation of variety of products such as carbon monoxide (CO), formic acid (HCOOH), formaldehyde (HCHO), methanol (CH_3OH), methane (CH_4), ethylene (C_2H_4), ethanol (C_2H_5OH) and oxalic acid ($H_2C_2O_4$). The activity of CO_2 reduction reaction and the product distribution strongly depends on the nature of the electrode surface and the electrolyte [341, 342].

Hori and co-worker studied and reviewed the electrochemical reduction of CO_2 on various metal surfaces; and concluded that invariably metal surfaces are selective to specific products [27]. This effect has also been highlighted by many research groups in early studies who classified the metallic electrodes based on the product distribution [36, 43]. The selectivity of the product was dependent on the ability of a metal surface to adhere to the intermediate and relative overpotential for competing reactions such as hydrogen evolution reaction (HER). For example, silver (Ag), gold (Au), and Pd are selective towards CO production whereas H_2 is the major product on the surface of Ni, Fe and Pt. Also, a variety of products are observed on Cu surface [131, 159, 343-345]. However, the activity of bulk materials was unsatisfactory due to the relatively smaller active surface area. This problem is being addressed by exploring materials with subnanometer dimensions. Zhu *et al.* demonstrated size dependence on the selectivity of CO_2RR in the electrochemical reduction of CO_2 using different size gold nanoparticles (4, 6, 8 and 10 nm); they showed that 8 nm gold nanoparticle was the best catalyst in terms of selectivity [58]. This behaviour was explained by DFT calculations on Au_{13} suggesting the edge sites on gold nanoparticle surface promote CO_2 reduction whereas corner sites favour competitive HER [58]. In a similar work, Mistry *et al.* studied the electrocatalytic reduction of CO_2 on gold nanoparticles ranging from 1.1 nm to 7.7 nm in diameter. It was concluded that gold nanoparticles with a particle size less than 5 nm have significantly higher activity compared with the bulk gold. The smaller particles (<5 nm) were reported to have higher H_2/CO ratio [346]. The product distribution of the Cu surface strongly depends on the particle size. The selectivity of hydrocarbons decreased with a reduction in the particle size and almost vanished below 2 nm [125]. The shape of the catalyst is another factor that significantly influences the reactivity. The particular shape has some prominent exposed reactive sites, and it can induce strain leading to the variation in the electronic structure of the material. Liu *et al.* demonstrated the comparison of activity for CO_2 reduction reaction for similar size bulk silver, triangular silver nanoplates and gold nanoparticles. The triangular silver nanoplates (Tri-Ag-NPs) were reported achieving a Faradic efficiency for

CO up to 96.8%, and the improved energy density with a small overpotential (96 mV) along with durability up to 7 days. The DFT calculations indicate the enhanced activity of Tri-Ag-NPs was due to both optimum edges-to-corner ratio and domination of Ag(100) facet [347]. Huang and co-worker studied the electrochemical reduction of CO_2 on icosahedral and octahedral palladium nanoparticles of similar size deposited on carbon. The icosahedral palladium nanoparticles were reported to achieve both higher Faradic efficiency and higher CO partial current densities. DFT calculations suggested the boost in catalytic activity on icosahedra shape most likely due to the shifting of d-band because of strain; thus, enhancing the absorption of COOH* intermediate [348].

Nanoclusters (NCs) are ultra-small nanoparticles with atomically precise chemical composition. The geometrical, electronic, magnetic and optical properties of clusters are strongly dependent on their size. Thus, these materials have attracted huge interest in catalysis as the catalytic activity or selectivity of a chemical reaction can be fine-tuned *via* a minor change in the composition of the catalyst [349, 350]. Vajda *et al.* reported size selected Cu_4 deposited on Al_2O_3 exhibits superior activity for catalytic hydrogenation of CO_2 to methanol at low pressure [351]. The CO_2 reduction reaction activity of CO_2 was strongly dependent on the size of clusters. Cu_3 had only one less atom than Cu_4, but its activity was almost half of that for Cu_4 activity [352]. The redox behaviour of metal clusters has been previously reported for electrocatalytic or electron transfer reactions. For example, Chen and Chen used a range of ligand-protected gold clusters (from Au_{11} to Au_{140}) for electrochemical reduction of oxygen [135]. The smaller size gold clusters showed higher activity. The similar results were obtained using silver clusters for oxygen reduction reaction [136]. Kwak *et al.* reported the use of $PtAu_{24}(SC_6H_{13})_{18}$ cluster for a reasonably high activity for HER [137]. $Au_{25}(SR)_{18}$ clusters were reported to enhance the activity of MoS_2 for HER due to favourable charge transfer and electronic interaction between cluster and support [138]. Deposition of glutathione-capped gold clusters on the titania nanotube arrays synergistically improved the visible light photocatalytic and photoelectrochemical activities [353]. There have been some computational and experimental studies for catalytic and electrocatalytic reduction of CO_2 using metal clusters [140, 141]. Kaufmann *et al.* studied the electrochemical reduction of CO_2 on thiol-protected $[Au_{25}(SC_2H_4Ph)_{18}]^-$ clusters. The combination of electrochemical, spectroscopic and computational studies indicate that the optical and electrochemical changes produced by absorption of CO_2 on the clusters were similar to those observed during cluster oxidation. This ultrasmall cluster was found as selective towards CO (contrary to Mistry *et*

al. [346]), and producing CO at relatively low overpotential (~90mV), and the production rate of CO and current was 7-700 times higher than the bulk gold catalyst [50]. The same group explained that the ligand protected clusters require relatively high electrochemical potential for the carboxyl intermediate formation. Thus, delegation is a necessary step for electrochemical reduction [354]. Jin and co-workers studied the effect of charge ($Au_{25}(SR)_{18}^{q}$ q=-1,0,+1) on electrochemical reduction of CO_2. The results suggested that the clusters are inactive for CO_2 reduction unless they are fully covered with ligand [355]. Kauffman *et al.* studied the electrochemical reduction of CO_2 along with competing for HER using DFT calculations. It was found that the particles with smaller size have higher stabilities for *COOH and *CO intermediates [142].

In summary, the clusters are promising materials for electrochemical reduction of CO_2. However, the electrochemical reduction of CO_2 on metal clusters have not been explored enough. To the best of our knowledge, there is no report on the use of phosphine capped gold cluster for CO_2 reduction. Herein, we report an electrochemical reduction of CO_2 using phosphine capped gold clusters in aqueous solution. gold clusters $[Au_6(dppp)_4](NO_3)_2$, $[Au_9(PPh3)_8](NO_3)_3$, $[Au_{13}(dppe)_5Cl_2]Cl_3$ and $Au_{101}(PPPh3)_{21}Cl_5$ (referred as Au_6, Au_9, Au_{13} and Au_{101} in this paper) were synthesized and deposited on carbon paper which served as cathode material for CO_2 reduction system. The clusters show almost identical selectively towards CO, with a minor improvement with Au_{13} cluster. The selectivity of CO was invariably lower for a calcined (200 ˚C) samples. This might be due to the agglomeration effect, which was confirmed via cyclic voltammetry and shift in Au 4f binding energy (as measured by XPS spectra).

7.2 Experimental

Electrochemical CO_2 reduction was performed in a custom made three-electrode based electrochemical flow cell as fully explained in our previous paper [327]. Briefly, the potentiostatic reduction was carried out at -1.5 V vs Ag|AgCl using a Gamry Reference 3000 potentiostat. The cell consists of metal clusters based catalyst as a cathode and a mixed-metal oxide titanium mesh as the counter electrode and Ag|AgCl as the reference electrode. The gold clusters coated on the carbon paper (SIGRACET GDL 10AA, Ion Power). The full description of the cluster synthesis is given in Appendix 5.

The electrolyte was continuously bubbled by CO_2 gas (99.995 vol%) at 20 mL min^{-1} during the experimentation using a mass flow controller (Alicat, MC-20SCCM-D). The electrolyte was 0.2 mol L^{-1} $KHCO_3$ without any purifications and was prepared with 18.2 MΩ deionised water. All the experiments were carried out at the room temperature (23 ˚C).

The gaseous products were analysed using a gas chromatograph (SRI 8610C) equipped with a haysep-D column, TCD and FID detectors to quantify H_2 and CO during the electrolysis. The Faradaic efficiency was calculated based on the charge needed to produce a particular product to the total charge passed during the electrolysis.

7.3 Results and discussions

7.3.1 Deposition of clusters

The gold clusters were synthesised following previously reported methods in the literature. Their structural identity was confirmed by NMR and ESI-MS. Also, the detailed synthesised and characterisations can be seen in Appendix 5. The Au_6, Au_9, Au_{13} were atomically precise and capped with phosphine, whereas Au_{101} was also phosphine ligand protected with narrow particle size distribution. The crystal structure of Au_6, Au_9 and Au_{13} are shown in Figure 7.1. These metal clusters were dissolved in dichloromethane and deposited on a carbon paper to achieve the desired concentration.

To study the particle size, XPS spectra have been recorded at the Au 4f, phosphorous 2p, and carbon 1s and oxygen 1s regions for Au_n clusters deposited on carbon paper. The collected XPS data was fitted in the following manner. We assigned C 1s peak to 285 eV and used this to calibrate the peak positions of other elements [356]. A Shirley background was subtracted from raw data. A Lorentzian function was fitted for all peaks. The splitting was fixed at 3.67 eV for Au 4f and 0.84 eV for P 2p. The full width at half maximum (FWHM) for a doublet was kept constant but was allowed to vary for two different doublets. The binding energy peak of Au $4f_{7/2}$ for bulk gold is reported around 84±0.2 eV in most of the literature [356, 357]. However, the peak position is dependent on the substrates. The Au 4f peak position is within ±0.2 eV when deposited on non-interacting surfaces whereas the shift as much as 1.5 eV shift is observed for interacting surface [358-360].

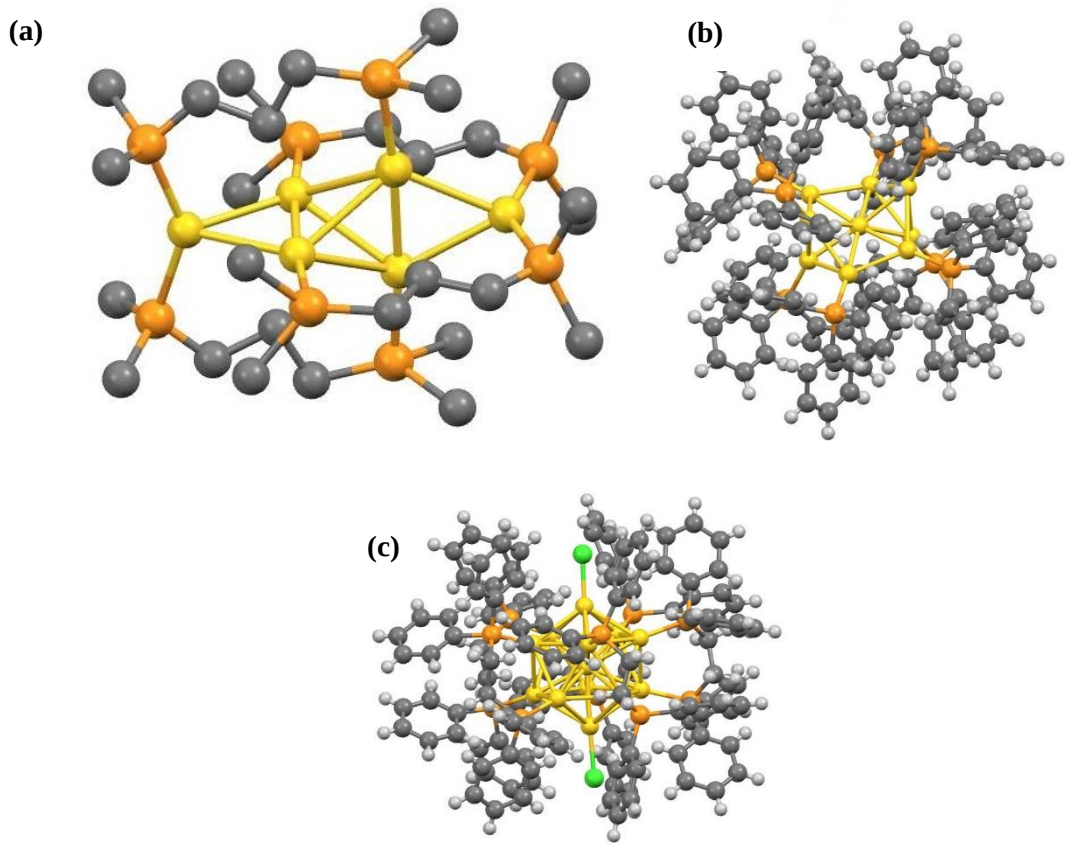

Figure 7.1: Crystal structures of Au_6 (a), Au_9 (b) and Au_{13} (c) clusters showing the exact number of gold atoms per cluster core. The atomic colour scheme is gold (Au), orange (P), green (Cl), and black (C).

Since the clusters were heated at high temperatures, we can assume the clusters agglomerated to form larger size nanoparticles (can be seen in SEM image Figure A5.6). We observed the peak position for the calcined Au_9 sample at 84.60 eV and no phosphorus was found in the survey spectrum. In this study, we compare the peak positions of all the clusters relative to calcined Au_9 clusters. As illustrated in Table 7.1, Au $4f_{7/2}$ peak position of XPS spectra for all the clusters (except Au_{101}) deposited on carbon paper was at higher binding energy than that of calcined Au_9/C-paper. Also, the FWHM for clusters was higher than that of calcined Au_9 cluster. Similarly, a shift to higher binding energy and increase in FWHM was reported previously for small size gold nanoparticles; our results are consistent with these findings [356, 359, 361, 362]. As shown in Figure 7.2, the XPS spectra were fitted with two peaks for each for the Au $4f_{7/2}$ and Au $4f_{5/2}$ components. We attribute the origin of a smaller peak to partial removal of the phosphine ligands from gold surface. Thus, resulting in direct contact between gold and carbon paper. We observed phosphine removal upon deposition on support in our previous works [356]. It is interesting to note that the peak position of the minor peak

is at lower binding energy for monodentate ligands whereas it is at higher binding energy for the bidentate ligand.

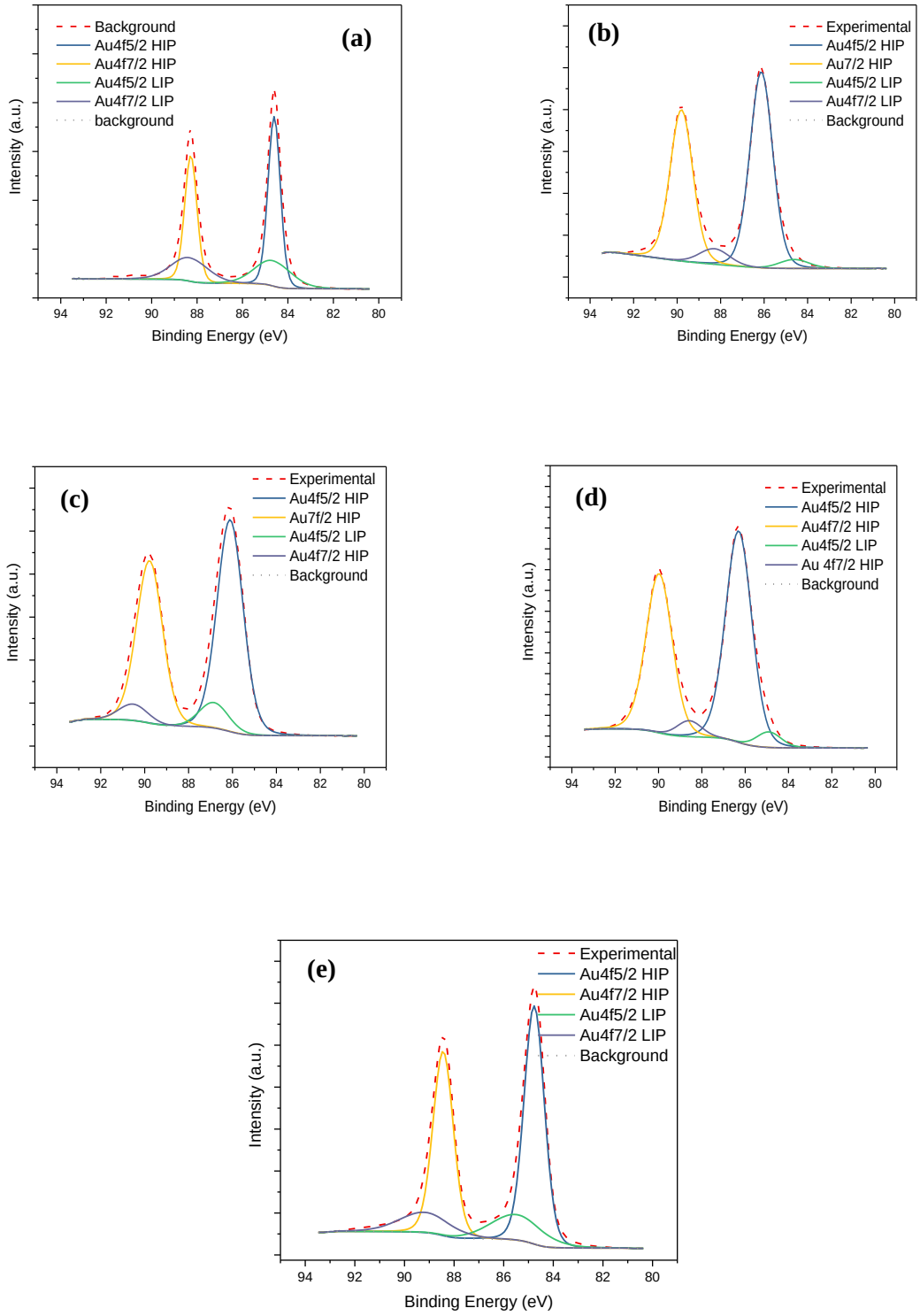

Figure 7.2: The XPS spectra for Au 4f on different clusters; (a) calcined Au_9, (b) Au_6, (c) Au_9, (d) Au_{13} and (e) Au_{101}.

Table 7.1 The peak position obtained from XPS spectra for Au 4f on different gold clusters.

	Binding energy	FWHM
Calcined Au_9	84.60	0.64
Au_6	86.13	1.23
Au_9	86.11	1.40
Au_{13}	86.30	1.42
Au_{101}	84.77	0.96

7.3.2 Electrocatalytic reduction of CO_2 on gold clusters

To study the activity of clusters, the clusters deposited on carbon paper were studied for the electrochemical reduction of CO_2. The electrochemical CO_2 reduction performance was first evaluated in a potentiostatic reduction (at -1.5 V vs Ag|AgCl) at a calcined Au_9 on carbon paper (low loading 0.09 mg cm^{-2}) (Figure 7.3a). As evident, the major products were CO and H_2, with a stable Faradaic efficiency of 68% and 25%, respectively. The current and the activity remained stable for 4 hours experiment without significant deactivation. We could not observe any formate formation after 4 hours electrolysis, suggesting the unaccounted Faradaic efficiency to be around 7% which can be attributed to the measurement errors as shown by uncertainties bar.

The loading dependent CO_2 reduction reaction has been investigated to respect of the exact amount of gold catalyst mass per geometric carbon paper area. So, higher gold loading was used to see how it affects CO_2 reduction reaction. Similarly, higher loadings did not increase the Faradaic efficiency as depicted in Figure 7.3.c showing that not necessarily higher gold clusters loading provide more active sites for CO_2 reduction reaction. This finding is in contrast with Nursanto *et al.* [139] where they achieved higher CO selectivity at higher gold loadings. The possible changes on the gold surface were further examined via CV before and after electrolysis at the scan rate of 100 mv s^{-1} as can be observed in Figure 7.3b and Figure 7.3d. The atomically precise metal clusters have well-defined shape; thus, provide a similar environment for all the competing reactions that can explain the strikingly similar selectivity over metal clusters. The voltammograms show normal gold oxide / redox feature with no apparent changes over electrolysis indicating the electrode surface active sites for either CO_2 reduction reaction or HER are almost identical before and after electroreduction.

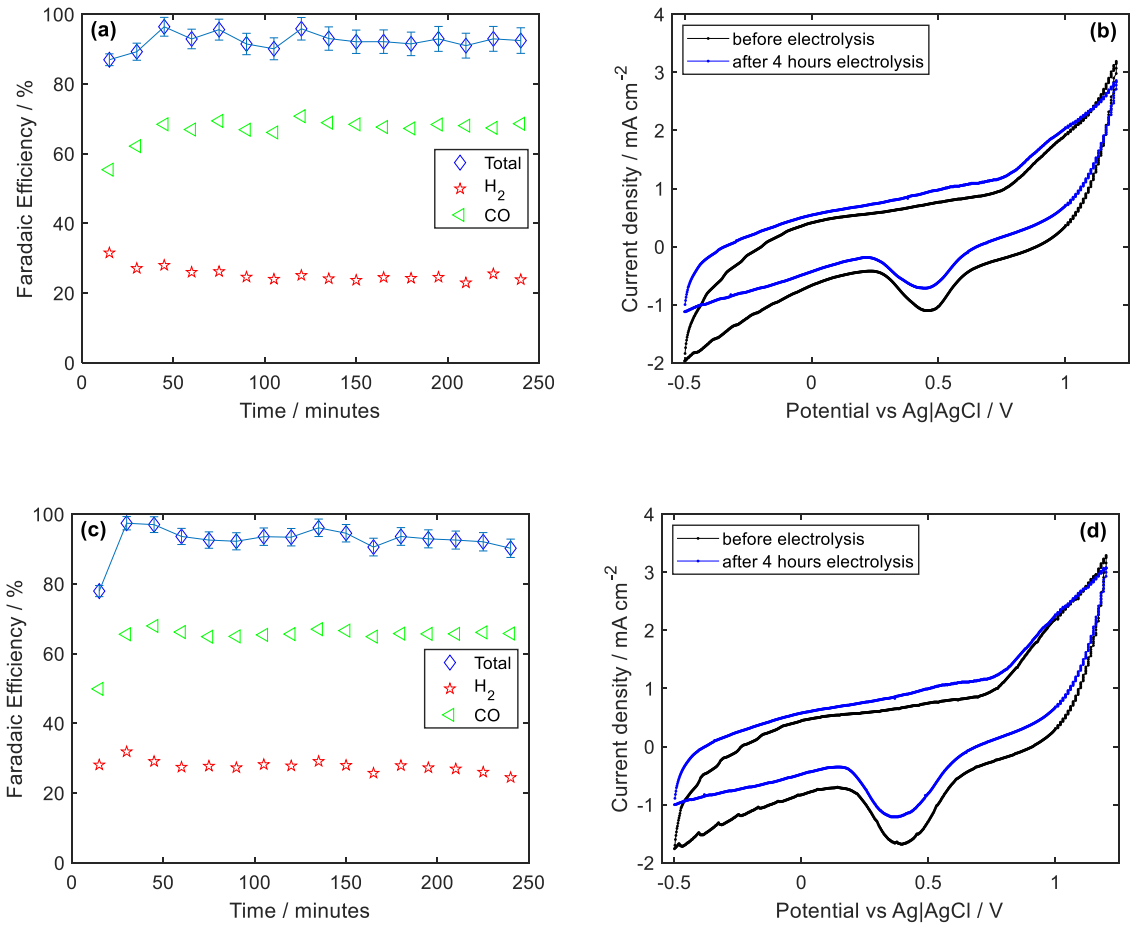

Figure 7.3: Potentiostatic (at -1.5 V vs Ag|AgCl) CO_2 reduction on calcined Au_9; (a) the product distribution with the gold loading of 0.09 mg Au cm^{-2}; (b) CV before and after 4 hours electroreduction with the gold loading of 0.09 mg Au cm^{-2}; (c) the product distribution with the gold loading of 0.18 mg Au cm^{-2}; (d) CV before and after 4 hours electroreduction with the gold loading of 0.18 mg Au cm^{-2}, in 0.2 mol L^{-1} $KHCO_3$ saturated with CO_2.

We also prepared different loadings Au_9 samples without any heat treatment (uncalcined). It is interesting to note that the protecting ligands, can modify the clusters catalytic activity [363]. It is in line with Chen and Chen studies which highlighted that phosphine ligands do not block the O_2 for oxygen reduction reaction on gold clusters [135]. Furthermore, the results (Figure 7.4a and Figure 7.4c) suggested that relatively higher CO selectivity could be achieved compared with the calcined samples (Figure 7.3a and Figure 7.3c). This can be attributed to the agglomeration of clusters as observed from XPS spectra (Table 7.1) and SEM (Figure A5.6a, A5.6b). The agglomeration of calcined clusters reduces the number of active sites. While the voltammograms (Figure 7.4b and Figure 7.4d) show the gold oxide / redox potential consistent with bulk gold [282, 364] and calcined Au_9 (Figure 7.3b and Figure 7.3d), CV changes significantly over electrolysis which is most likely due to either clusters reconstruction to more stable geometries or surface cleaning. The SEM image of clusters

before and after electrolysis can be observed in Figure A5.6c and Figure A5.5d. Also, a small variation at the potential of around -0.1 V vs Ag|AgCl is attributed to the presence of phosphine ligands [318] which could be observed in all uncalcined samples in line with the XPS results (Figure 7.2).

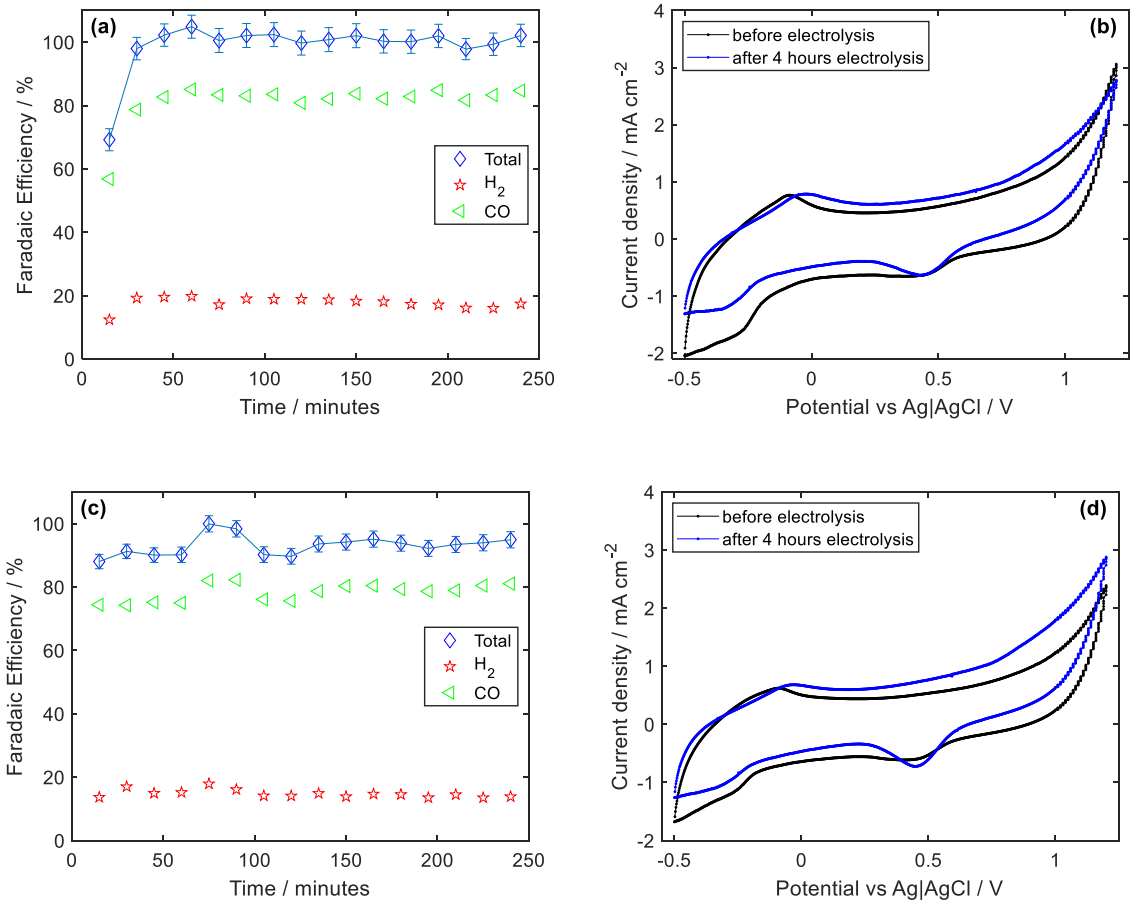

Figure 7.4: Potentiostatic (at -1.5 V vs Ag|AgCl) CO_2 reduction on uncalcined Au_9; (a) the product distribution with the gold loading of 0.09 mg Au cm^{-2}; (b) CV before and after 4 hours electroreduction with the gold loading of 0.09 mg Au cm^{-2}; (c) the product distribution with the gold loading of 0.18 mg Au cm^{-2}; (d) CV before and after 4 hours electroreduction with the gold loading of 0.18 mg Au cm^{-2}, in 0.2 mol L^{-1} $KHCO_3$ saturated with CO_2.

The same potentiostatic experiments have been conducted using different gold clusters and are presented in Figure 7.5. As the only structural differences in each gold clusters in Figure 7.5 is the protecting ligands, that offers an ideal experiment to see the effect of ligands on CO_2 electroreduction. As illustrated, uncalcined samples showed better performance for CO production in all cases while increasing the gold loading did not alter the product distribution (except calcined Au_6). Moreover, Au_{13} showed the highest CO selectivity. The Faradaic efficiency for CO production was found to be 93% at -1.5 V vs Ag|AgCl in 0.2 mol L^{-1} $KHCO_3$ using relatively low gold loadings (Figure 7.5b and Figure 7.5d). As evident,

different gold clusters contain various coordination environment. The less low-coordinated gold atoms enhance CO production over unwanted HER. These results are consistent with previous observations suggesting the smaller gold nanoparticles showed better performance toward HER [58, 346]. Au_{13} nanocluster consists of precisely 13 gold atoms which is the best among others for CO_2 reduction reaction. The improved catalytic performance for atomically precise Au_{13} provides opportunities for further research over gold-based nanoclusters.

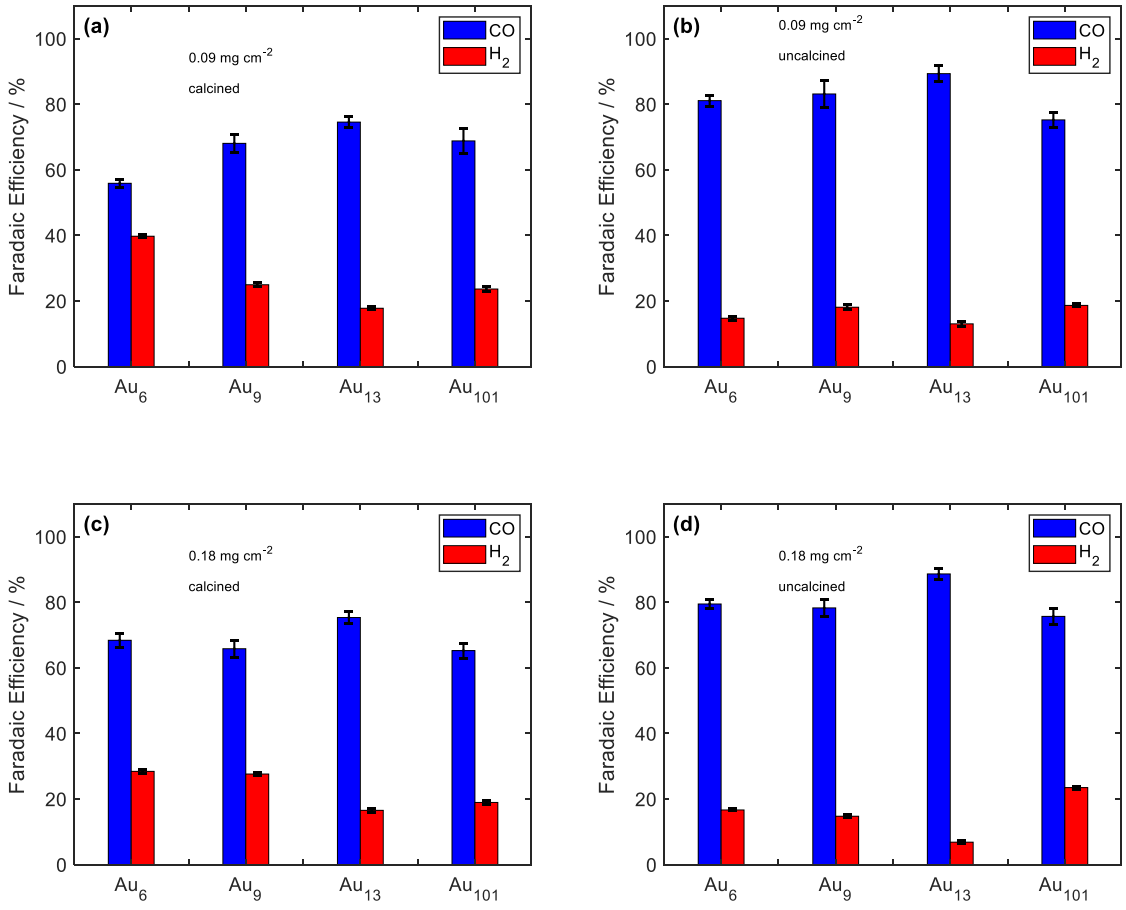

Figure 7.5: Gaseous products distribution in a potentiostatic (at -1.5 V vs Ag|AgCl) CO_2 reduction using various gold cathodes in 0.2 mol L^{-1} $KHCO_3$ saturated with CO_2 under (a) Calcined sample with the gold loading of 0.09 mg Au cm^{-2}; (b) Uncalcined sample with the gold loading of 0.09 mg Au cm^{-2}; (c) Calcined sample with the gold loading of 0.18 mg Au cm^{-2}; (d) Uncalcined sample with the gold loading of 0.18 mg Au cm^{-2}.

The catalyst loading on different gold clusters can be used to tune the activity and selectivity of the CO_2 electroreduction. The average current density over potentiostatic (at -1.5 V vs Ag|AgCl) CO_2 reduction suggesting a relatively higher current density for higher gold loading. Furthermore, the current densities for the calcined and uncalcined samples were almost the same. These results are consistent with previous studies [365-368] who found that

the activity would be increased by increasing the catalyst loading most likely due to higher surface area and better reactivity.

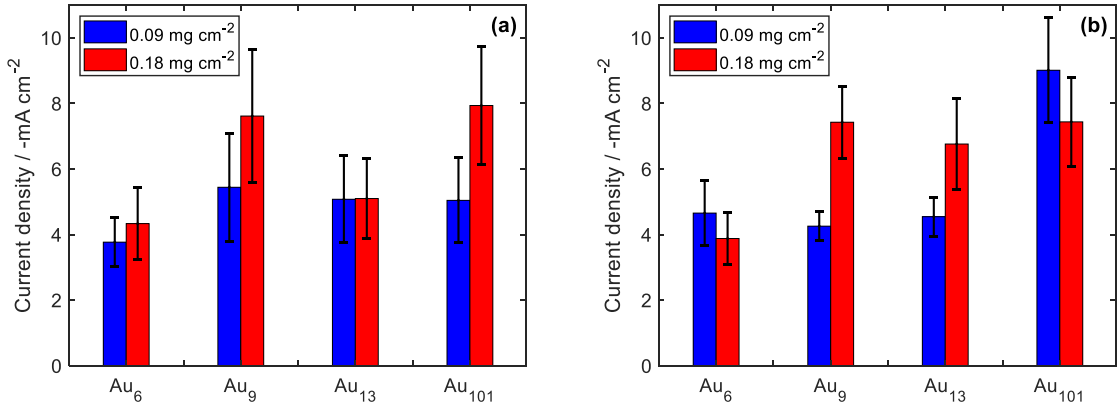

Figure 7.6: The effect of sample preparation on the average current density in a potentiostatic (at -1.5 V vs Ag|AgCl) CO_2 reduction in an aqueous 0.2 mol L^{-1} $KHCO_3$ at different gold clusters and loadings under (a) calcination, (b) without calcination.

In order to gain further insights into the key factors affecting the selectivity and the activity, the electrochemically active surface area (EASA) was estimated. As evident for the calcined samples, the charge density of gold oxide reduction peak increases by gold loading (except for Au_{13}) showing more available gold for CO_2 reduction. Also, the EASA was unchanged (or showed less value) over electrolysis for calcined samples while for uncalcined samples, the clusters do undergo partial agglomeration over electrolysis and showed higher EASA. These findings are not consistent with Kauffman [366] results where ligand-protected gold clusters can protect the clusters against agglomeration in long-term electrolysis.

Our results demonstrate high catalytic activity and selectivity for ligand protected and ligand-free gold nanoparticles for the electrochemical CO_2 conversion to CO in aqueous $KHCO_3$ electrolytes. Phosphine-protected clusters were found to be active and selective for electrocatalytic CO_2 reduction at relatively low loadings. Additionally, such understanding is critical for designing highly selective and active gold nanostructured catalysts which decrease noble metal consumption on one hand and maintain the catalytic activity over long-term electrolysis on the other hand. The elegant and straightforward approach as proposed here provides a scalable and novel route for electrochemical reduction of CO_2. The easy, durable and cheap synthesising method is highly desirable for practical implications.

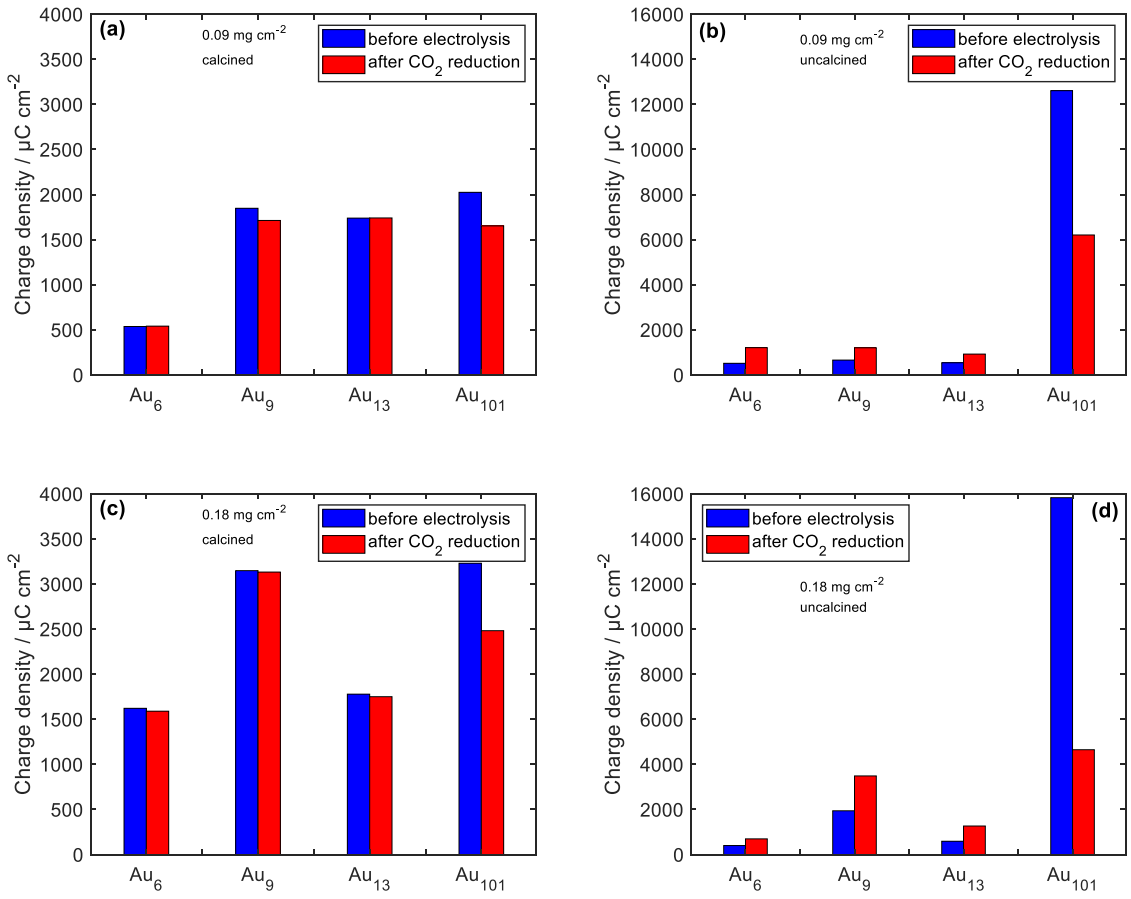

Figure 7.7: The charge density of a gold oxide reduction peak before and after electrolysis in 0.2 mol L^{-1} $KHCO_3$ saturated with CO_2 under (a) Calcined sample with the gold loading of 0.09 mg Au cm^{-2}; (b) Uncalcined sample with the gold loading of 0.09 mg Au cm^{-2}; (c) Calcined sample with the gold loading of 0.18 mg Au cm^{-2}; (d) Uncalcined sample with the gold loading of 0.18 mg Au cm^{-2}.

8 Conclusions and Recommendations

The results presented in this thesis try to extend our knowledge of the CO_2 electroreduction reaction. The following chapter aims to conclude the major findings of this work. Also, it provides some recommendations for future research on electrocatalytic CO_2 reduction.

In chapter 4, CO electrooxidation on gold electrodes was studied experimentally at various potential limits in 0.2 mol L^{-1} $KHCO_3$. The experimental results clearly showed that the CO electrochemically adsorbs on gold when CO_2 reduction reaction occurs (at -0.9 V vs Ag|AgCl or more negative potentials) and the peak associated to CO adsorption increases by higher potentials in which the maximum CO coverage is achieved at -1.30 V vs Ag|AgCl. Also, the maximum current density was found to increase linearly by the scan rate, probably due to different diffusion layer formation. Galvanostatic and potentiostatic measurements confirmed the dependency of the product selectivity on potentials. CO production (the product of interest) was found to decrease by increasing the potential. Furthermore, rougher surfaces showed higher activity for CO production. Additionally, our measurements of the formate formation over electrolysis revealed that the formate Faradaic efficiency decreased significantly by time and became constant after 30 minutes of electrolysis. The fact that the total Faradaic efficiency of the first 30 minutes of the electrolysis does not reach to 100% had prompted us to adopt that it could be due to higher formate formation at the start of electrolysis.

In chapter 5, an important issue of the electrochemical CO_2 reduction was resolved. We investigated deactivation during the electrolysis and showed that on gold cathodes, this occurs due to Fe, Zn and Cu deposition from the trace impurities within the $KHCO_3$ electrolyte. We proposed that Fe and Zn impurities resulted in higher H_2 selectivity, and the accumulation of Cu increased the formate production rate, at the expense of CO. We also showed the two published methods [203, 223] used to prevent deactivation led to significant corrosion of the gold (up to 450 ppb gold is found in the electrolyte after only 4 hours of electrolysis), as relatively high potentials should be employed to strip the deposited poisons. Such gold corrosion would make any long-term CO_2 electrolysis impractical. Instead, we showed that these poisons could be removed and the activity for CO production maintained by interrupting the CO_2 reduction process every 15 minutes with cyclic voltammetry between -0.5 and 0.5 V

vs Ag|AgCl. We also showed that periods of open circuit or short anodic pulses (avoiding gold corrosion) could also partially reduce but not completely prevent deactivation.

In chapter 6, we investigated CO_2 reduction on gold cathodes in a typical H-cell (the most common cell for studying electrochemical CO_2 reduction) and a flow cell and showed these could give very different CO_2 reduction behaviour. While it is well-known that the $KHCO_3$ electrolyte concentration has a strong influence on the Faradaic efficiency for CO_2 reduction in H-cells with planar electrodes, we showed that in a flow cell configuration, the $KHCO_3$ concentration has no impact on the reaction selectivity. We proposed that this is due to the mass transport within the porous cathode, which essentially negates the buffering action of the $KHCO_3$ electrolyte that occurs typically in the H-cell. These results suggest that the cell configuration can play a key role in determining the CO_2 reduction reaction performance, and thus we conclude that to compare results across research groups, consideration or standardisation of electrochemical cells / electrode geometry is needed.

In chapter 7, atomically precise ligand-protected gold clusters (Au_6, Au_9, Au_{13} and Au_{101}) have been chemically synthesised and adsorbed onto carbon paper substrates. These cluster-coated electrodes were then used for CO_2 reduction in aqueous $KHCO_3$ electrolytes, and have shown very high Faradaic efficiency towards CO (80 - 90 %) at -1.5 V *vs.* Ag|AgCl, using relatively low gold loadings (90 mg cm^{-2}). Importantly, while these gold clusters do undergo partial aggregation during the CO_2 reduction reaction, the clusters maintain high selectivity over 4 hours of electrolysis, with both cyclic voltammetry and XPS analysis suggested that these cathodes still exhibit some cluster specific properties. While all four clusters (Au_6, Au_9, Au_{13} and Au_{101}) have almost identical selectively towards CO, when the cluster-coated electrodes are calcined at 200 ˚C, the selectivity towards CO decreases, with this loss in selectively was more significant for the smaller clusters. This was accompanied by a clear shift in the Au 4f binding energies towards values typical for bulk gold (as measured by XPS), suggesting that the high selectively is due to active sites unique to the gold clusters.

Some recommendations are suggested in light of the results of this work for the future work on electrochemical CO_2 reduction.

- Further experimental studies could be performed on the different Au alloys (like Au/Pd with different concentrations) to find out what conditions can affect CO/H_2 ratios.

- It would be interesting to test gas diffusion electrodes by the results found in this study. If the method to prevent the deactivation is applied for a gas diffusion electrode, high current densities can be achieved in one hand, and it would be stable over long-term electrolysis.
- Performing some experiments to investigate the effect of mass transfer limitation in the flow cell performance. To achieve this, the carbon paper with various porosity can be used.
- The effect of mass transfer on CO_2 electroreduction could also be modelled numerically. This would give a better understanding of the interfacial species concentrations (like pH and CO_2 concentration) which can cause an enhanced activity and selectivity.
- Conducting in-situ measurements during electrolysis can provide valuable information regarding the surface reactions or adsorption of molecules as it is hard to detect them by using electrochemical methods.

Appendix 1: The thermodynamic potentials

The standard reduction potential for various CO_2 reduction reactions presented in Table 1.2 is a simple calculation. To find out the standard half-cell reduction potential for CO from CO_2, equation (1.4) is written as below:

$$CO_{2(g)} + 2H^+ + 2e^- \leftrightarrow CO_{(g)} + H_2O_{(l)} \quad \text{(A1.1)}$$

The Gibbs free energy of formation ($\Delta G_{formation}$) can be calculated by the following formula:

$$\Delta G_{formation} = \sum \Delta G_{formation,products} - \sum \Delta G_{formation,reactants} \quad \text{(A1.2)}$$

So, the Gibbs free energy of formation for the equation (A1.1) and using values from [175] would be:

$\Delta G_{formation} = \Delta G(CO) + \Delta G(H_2O) - \Delta G(CO_2) = (-137169-(237129))+(394359)= 20061$ J mol^{-1}

Through the electrochemical cell, The relationship between Gibbs free energy and the reduction potential is given by the following equation:

$$E=(-\Delta G/nF) \quad \text{(A1.3)}$$

So, the reduction potential for CO production would be

$E= (-20061/(2)\times(96485))= -0.103$ V

Where n is the number of moles of electrons and F is the Faraday constant (96485 C per mol e^-).

This potential shows the CO production potential at standard condition (pH=0) and SHE scale. To convert the potential to Ag|AgCl scale and the pH range (pH=7) in our experiments, the following equations could be used showing the reduction potential shifts 59 mV per pH unit [11].

$$E_{(SHE\ at\ pH=0)} = 0.197 + 0.0592 \times pH + E_{(Ag|AgCl\ at\ pH=7)} \quad \text{(A1.4)}$$

Where 0.197 is the potential difference between the SHE and Ag|AgCl scale. The same method was used for other products reduction potential including CH_4, HCOOH, etc as can be observed in Table 1.2.

Appendix 2: Making reference electrodes

The self-made Ag|AgCl reference electrode in this study is cheap and easy to make. Additionally, its potential is stable with time enabling us to measure the correct potential during electrolysis. To be able to make a reference electrode, the following materials are needed:

- Silver wire (diameter ~ 1mm, length ~ 10cm)
- Copper wire to make the electrical connection with the silver wire
- Saturated KCl solution
- Nitric acid
- Vycor frit and heat shrink tubing
- Epoxy glue
- Glass or plastic tube

Firstly, the silver wire was placed into nitric acid for 10 seconds following by rinsing with DI water. This step aims to roughen the silver wire as well as general cleaning purposes. The next step was to secure the silver wire in a suitable glass or plastic tube using a rubber seal. The glass tube was sealed with epoxy glue and was exposed to the air for 2 hours. This step was followed by the silver wire connection to a copper wire. The glass tube was then filled with the saturated KCl from the bottom end and secured with a Vycor frit acting as a conductive pathway between the electrolyte and the reference electrode.

The silver wire should be coated with Ag|AgCl at this step. To do that, a gentle anodic current (50 μA) was applied for 12 hours to the reference electrode. In this circumstance, the reference electrode was considered as a working electrode and the reference and counter leads of the potentiostat connected to a Pt wire as the counter electrode, all placed in a container with saturated KCl solution.

After anodisation, the fresh reference electrode should be compared with another reference electrode to make sure that the potential is correct.

Appendix 3: Gas Chromatography

The used GC in this thesis is a SRI 8610C gas chromatograph (Multi-Gas#3 configuration) equipped with FID and TCD detectors. However, this GC has been designed to use two columns (including molecular sieve column for light gases separation like H_2, air, CO, CH_4 and a haysep-D column for the heavy gasses separation like CO_2, C_2H_4) for the gaseous products separation, we only used haysep-D column to increase the reproducibility [176]. Additionally, the air peak (overlap slightly with CO peak in TCD) would not appear in the FID; hence, CO quantification could be done by the FID detector which is considered as a well-known issue in the case of air contamination. The used GC parameters in this study are given in Table A3.1.

Table A3.1 The used GC parameters for gaseous products analysis in this thesis

Parameter	Value
Ar (carrier gas)	20 mL min^{-1}
H_2	20 mL min^{-1}
Valve temperature	60 ˚C
TCD temperature	150 ˚C
FID temperature	300 ˚C
Methaniser temperature	300 ˚C
Column temperature	Initial: At 40 ˚C for 2.5 minutes Ramp up: To 90 ˚C (at 30 ˚C min^{-1}) holding for 3 minutes Ramp down: To 40 ˚C (at -140 ˚C min^{-1}) holding for 7 minutes
Sample size	1 mL

GC needs to be recalibrated regularly due to the changes in the columns' retention time and detectors' sensitivity. The GC was calibrated with a custom gas sample with specification shown in Table A3.2. To do that, a five-point calibration gas mixture (2%, 4%, 6%, 8% and 10% of calibration gas) was chosen. The required calibration gas flow rate based on the points was set for the total flow rate of 20 mL min^{-1} as clearly shown in Table A3.2 and Table A3.3. In this study, CO_2 was used to dilute the calibration gas mixture to obtain several points of calibration. The calibration graphs for each component are given in Figure A3.1. The peak areas can be obtained by using Peak-Simple software by integrating the respective peaks. It

is also worth to note that the H_2 data collected from TCD measurements, while other gaseous products were measured from the FID.

Table A3.2 The composition of various gaseous components in the custom calibration gas mixture

Gas	Concentration / volume %	Uncertainty / ±%
H_2	5	0.02
CO	5	0.03
CH_4	5	0.03
C_2H_4	5	0.03
C_2H_6	5	0.03
CO_2	Balance = 75	-

Table A3.3 Composition of custom calibration gas mixture at each calibration point

Gaseous species concentration[a] / volume %	Calibration gas flow rate / mL min^{-1}	CO_2 flow rate / mL min^{-1}	Uncertainty[b] / volume %
0.1	0.4	19.6	0.010
0.2	0.8	19.2	0.011
0.3	1.2	18.8	0.012
0.4	1.6	18.4	0.013
0.5	2	18	0.014

[a] As the composition of gaseous components in the calibration gas is identical (Table A3.2), the concentration of each gas is equal at the defined calibration point.

[b] These uncertainties in the calibration gas blends caused by mass flow controller and calibration gas mixture.

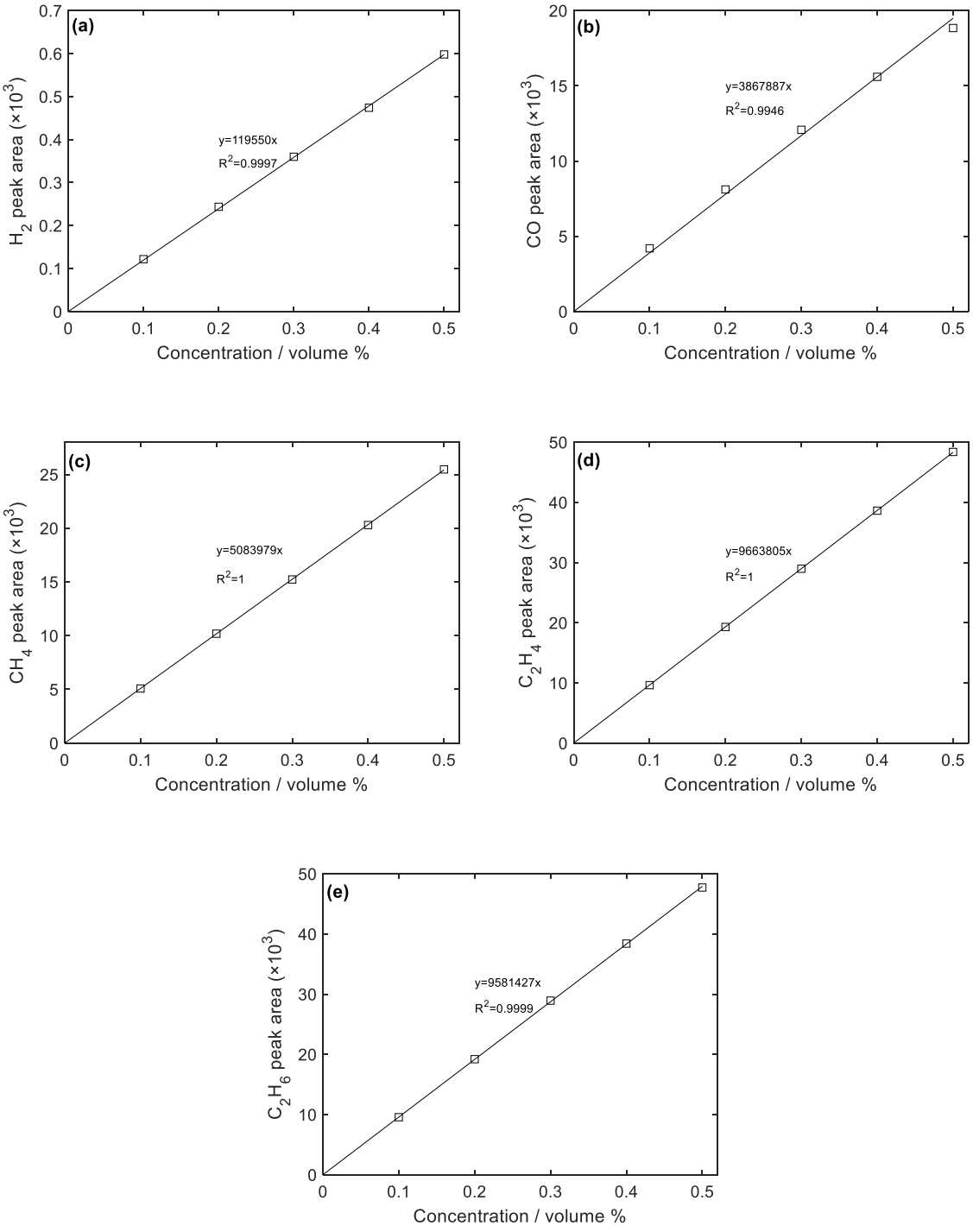

Figure A3.1: The GC calibration graphs for various gaseous components: (a) H_2; (b) CO; (c) CH_4; (d) C_2H_4; (e) C_2H_6. All gases were measured from the FID except H_2 which was measured from the TCD.

The uncertainties calculations from the calibration data (gas concentration) can be done by using equation A3.1 (this equation can be used when y value changes linearly with x values) as can be seen below [369]:

$$\Delta x = \frac{SE_{yx}}{m}\sqrt{\left[\frac{1}{k}+\frac{1}{n}+\frac{(y_0-\bar{y})^2}{m^2 s_x^2(n-1)}\right]} \quad \text{(A3.1)}$$

Where:

- Δx is the uncertainties value obtained from the linear calibration data
- SE_{yx} is the standard uncertainty of regression
- m is the linear calibration slope
- y_0 is the mean value of y measurements
- $\bar{y}$ is the mean value of the calibration data points
- k is the number of replicate experiments for y measurements
- n is the number of calibration data points
- s_x is the sample variance (or square of standard deviation) of x values related to the calibration data point

The current efficiencies uncertainties could be estimated afterwards through the error propagation method:

$$\Delta f = \sqrt{\frac{\partial f}{\partial u}(\Delta u)^2 + \frac{\partial f}{\partial v}(\Delta v)^2 + \cdots} \quad \text{(A3.2)}$$

Where Δf is the calculated uncertainties from other variables (like u and v). Table A3.4 represents the statistical values of the data shown in Figure A3.1.

Table A3.4 The calibration data statistics shown in Figure A3.1.

Product	m	SE_{yx}	n	s_x	$\bar{y}$
H_2	119550	2.934	5	2.5E-06	359.48
CO	3867887	522.803	5	2.5E-06	11904.5
CH_4	5083979	39.961	5	2.5E-06	15249.53
C_2H_4	9663805	34.06	5	2.5E-06	28980
C_2H_6	9581427	150	5	2.5E-06	28762.42

The above information was used to calculate the current efficiencies uncertainties as can be observed in Table A3.5. These results relate to a typical galvanostatic (at -5 mA cm^{-2}) CO_2 reduction on a gold cathode with the total gas flow rate of 20 mL min^{-1}. Obviously, there is

no information for C_2H_4 and C_2H_6 uncertainties because those gaseous products are not produced on the gold electrodes.

Table A3.5 Example calculations for the uncertainties associated to the current efficiency for a GC measurement during galvanostatic CO_2 reduction.

Product	Peak area	Concentration / volume %	Δx / ±%	i / mA	Δi / ±mA	CE / %	ΔCE / ±%
H_2	240.34	0.201	2.8E-05	5.46	0.0925	34.77	0.5
CO	14029	0.3627	1.5E-04	9.851	0.4182	62.73	2.66
CH_4	30.52	0.0006	1.1E-05	0.065	0.123	0.4	0.7

The details for the above calculation are as below:

- The peak area can be directly read through GC measurements
- The concentration can be obtained from calibration data. For example, CO would give:

  $$concentration = \frac{peak\ area}{slope} = \frac{14029}{3867887} = 0.3627\%$$

- Δx can be calculated simply by using equation (A3.1). For CO we have:

  $$\Delta x = \frac{SE_{yx}}{m}\sqrt{\left[\frac{1}{k}+\frac{1}{n}+\frac{(y_0-\bar{y})^2}{m^2 s_x^2(n-1)}\right]} =$$

  $$\frac{522.8}{3867887}\times\sqrt{\frac{1}{1}+\frac{1}{5}+\frac{(14029-11904.5)^2}{3867887^2(2.5\times10^{-6})(5-1)}} = \pm 0.00015$$

- In order to calculate the current and current efficiency, the concentration (volume %) should be converted into the molar basis, and then the required coulombs could be calculated by Faraday constant. To do that, the ambient conditions (1 atm and 298.15 K) and ideal gas law (PV=nRT) are assumed for. Also, 1 mole CO requires 2 mole e^- (Z=2); hence, the CO partial current would be 9.851 mA:

$$i_{CO} = \frac{PV}{RT}(Z_{CO})(F) = \left[\left(\frac{101325\times(20.66\times0.003627}{8.314\times298.15}\right)\left(\frac{1}{60\times10^6}\right)\right](2)(96485)(1000) = 9.851$$ mA

By considering the fact that V is volumetric flow rate (m^3/s), P is pressure (Pa), R is the gas constant (J/mol×K) and $\left(\frac{1}{60\times10^6}\right)$ is the conversion factor of mL/min to m^3/s and (1000) is the conversion factor of A to mA.

- The contribution uncertainties for each gas can be calculated by the gas concentration and the total gas flow rate. Also, the uncertainty for the overall gas flow rate relates to the mass flow controller which is defined by the manufacturer and in this example it is ±0.2 mL min^{-1}. For CO:

$$\Delta i_{CO} = i_{CO} \times \sqrt{\left(\frac{\Delta x}{concentration}\right)^2 + \left(\frac{\Delta V_{total}}{V_{total}}\right)^2} = 9.851 \times \sqrt{\left(\frac{0.00015}{0.3627}\right)^2 + \left(\frac{0.2}{20.66}\right)}$$
$$= \pm 0.4182\ mA$$

- The CO current efficiency can be considered as the ratio of the current goes to CO formation to the total current:

$$CO\ CE = \frac{i_{CO}}{i_{total}} = \frac{9.851}{15.7} = 62.7\%$$

- The last step would be the uncertainties associated with the CO current efficiency which can be calculated as below:

$$\Delta CE_{CO} = \frac{\Delta i_{CO}}{i_{total}} = \frac{0.4182}{15.7} = \pm 2.66\%$$

A typical chromatogram during galvanostatic CO_2 reduction (at -10 mA cm^{-2}) is shown in Figure A3.2 for both FID and TCD detectors. As evident, CO can be dedetcted in FID while H_2 is detected in a TCD detector.

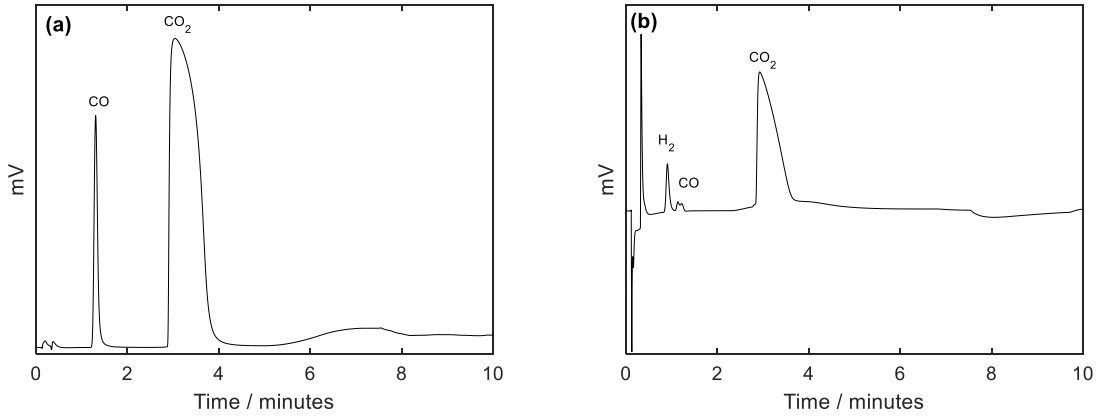

Figure A3.2: The GC results showing the gas separation during a typical CO_2 reduction using the gold electrode at the CO_2 flow rate of 20 mL min^{-1}. (a) FID detector; (b) TCD detector. The detection limit is around 10 ppm for CO and 100 ppm for H_2.

Appendix 4: High Performance Liquid Chromatography

The used HPLC in this study is a HP 1100 equipped with a SUPELCOGEL^{TM} C-610H column with two detectors. The UV/Vis detector was used for formic acid detection as it is less noisy. RI detector was also used to see if any other liquid products (most likely methanol) are formed during electrolysis or not. The used HPLC parameters in this study are given in Table A4.1.

Table A4.1 The used HPLC parameters for formate / formic acid analysis in this thesis

Parameter	Value
Mobile phase	0.1% H_3PO_4
Sample size	10 µL
Flow rate	0.5 mL min^{-1}
Working temperature	30 ˚C
Working pressure	About 45 bar
UV/Vis detector wavelength	210 nm
Sample run time	30 minutes

During the liquid analysis, the retention time for formate / formic acid was found to be 19.3 minutes; hence, 30 minutes run would give the detector enough time to identify formate / formic acid. The calibration graph for formate / formic acid is shown in Figure A4.1.

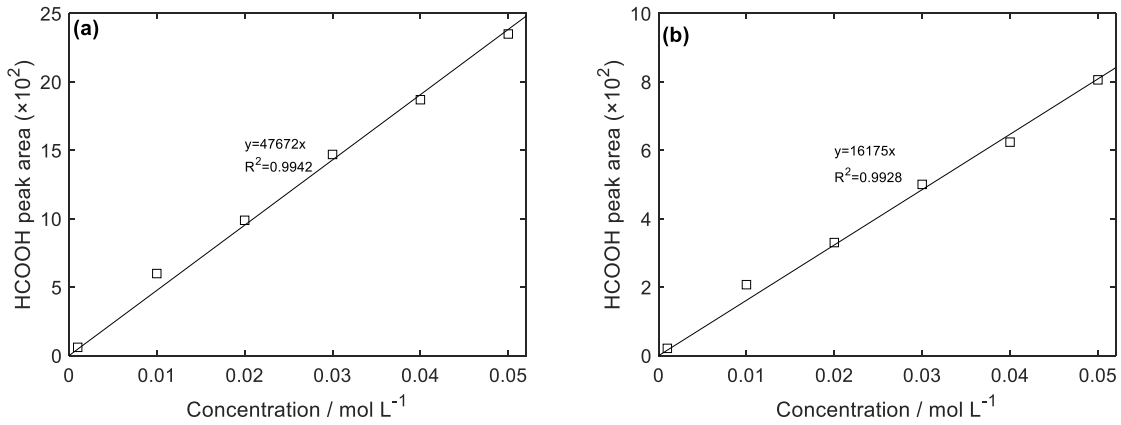

Figure A4.1: The HPLC calibration graphs for formic acid; (a) UV/Vis detector; (b) RI detector.

The formic acid Faradaic efficiency can be calculated by knowing the measured concentration over the electrolysis and the number of electrons needed for formic acid production (n=2 based on Table 1.2). For example, the formic acid concentration after 4 hours of electrolysis at -10 mA in 50 mL of 0.2 mol L^{-1} $KHCO_3$ in a typical experiment was 0.002062 mol L^{-1}, the total charge going to produce formic acid is:

$$\frac{50}{1000} L \times 0.002062 \frac{mol_{HCOOH}}{L} \times 2 \frac{mol\ e^-}{mol_{HCOOH}} \times 96485 \frac{C}{mol\ e^-} = 19.892C$$

The formic acid Faradaic efficiency can be considered as the ratio between the charge goes to formate formation and the total charge passed over the electrolysis:

$$\frac{19.892C}{\frac{10}{1000}\frac{C}{s} \times (4 \times 3600)} = 13.81\%$$

A typical chromatogram obtained after 4 hours electrolysis can be seen in Figure A4.2.

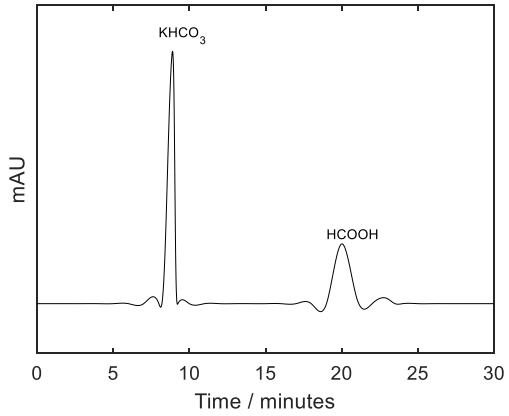

Figure A4.2: A typical chromatogram using UV/Vis detector after 4 hours potentiostatic (at -1.5 V vs Ag|AgCl) CO_2 reduction on a gold cathode in a batch cell configuration.

Appendix 5: Gold cluster synthesis

a. Characterisation

The used analytical instruments for the characterisation are as below:

NMR: Proton and phosphorous nuclear magnetic resonance (^{1}H, and ^{31}P) spectra were recorded on Bruker AV400 (400 MHz) spectrometer. All chemical shifts were reported in ppm respect to 85% H_3PO_4.

ESI-MS: The mass spectra (ESI-MS) were recorded on a maXis 3G UHR-Qq-TOF mass spectrometer (Bruker) coupled to a Dionex Ultimate 3000 LC system (Thermo Fisher).

UV-Vis Spectra: The UV-Vis spectra were recorded on GBG Scientific Equipment Cintra 4040 UV-Vis spectrophotometer.

XPS Spectra: The survey spectra were recorded on a Kratos Axis UltraDLD XPS instrument (Kratos Analytical, Wharfside, Manchester, UK) housed in the Research Centre for Surface and Materials Science at The University of Auckland. The data were excited using monochromated Al K_α X-rays. (1486.69 eV). The anode was at accelerated at 15kV with 10 mA emission current. The survey scans were collected over the range of 1300 to -5 eV in 1 eV steps with 180 seconds acquisition time. The chamber base pressure is in the high 10^{-10} Torr to low 10^{-9} Torr range.

Scanning Electron Microscopy: The microstructure and surface morphology of the gold clusters on carbon paper samples were recorded by SEM instrument (JEOL JSM-7000 F) operated at accelerating voltage of 15 kV.

b. Materials and Methods

All the necessary chemicals were purchased from well-established suppliers (Merck, Fisher chemical and Sigma Aldrich) and used without any further purification. Tetrachloroauric acid was prepared using 99.99% pure gold (Regal Casting Ltd.,99/99%) following the method reported by Brauer *et al.* [370].

$AuPPh_3Cl$: $AuPPh_3Cl$ was synthesised following the method described by Anderson *et al.* [356]. 2.8 g of triphenylphosphine (10 mmol) was dissolved in 70 mL ethanol. 2 g of $HAuCl_4$ (5 mmol) was dissolved in 9 mL ethanol and 1 mL H_2O was added to the stirring solution. The colour of the solution changes from yellowish to cloudy white. The reaction mixture was stirred for 30 minutes. The white precipitate was collected by centrifugation. The product was washed with ethanol (3 × 50 mL), dissolved in 30 mL chloroform, centrifuged, the supernatant dried using rotary evaporator. The crude was then dissolved in 10 mL dichloromethane, and crystalised via vapour diffusion using 50 mL diethyl ether in 100 mL jar for five days. The yield of product is *ca.* 2.1 g (72% by gold atoms). The identity of the cluster was confirmed by ^{31}P NMR ($CDCl_3$) with a singlet at 33 ppm (w.r.t. 85% H_3PO_4).

$AuPPh_3NO_3$: $AuPPh_3NO_3$ was synthesised following the method reported by Anderson *et al.* [356]. 1.2 g of $AuPPh_3Cl$ (2.4 mmol) was dissolved in 50 mL in chloroform. A suspension of $AgNO_3$ (1g, 6 mmol) in ethanol (50 mL) was added to the stirring solution. Addition of $AgNO_3$ in turns the solution whitish cloudy as AgCl formed, the reaction mixture was stirred for 1 hour. The product was collected by centrifugation; the supernatant was dried under vacuum. The crude was washed with water (4 × 25 mL) and ethanol (3 × 25 mL). The product was then dried in vacuum. Total of 700 mg of $AuPPh_3NO_3$ (*ca.* 70% w.r.t Au atom) was obtained. The identity of the product was confirmed by ^{31}P NMR ($CDCl_3$) with singlet at δ = 25 ppm (w.r.t. 85% H_3PO_4).

Au(THT)Cl: Au(THT)Cl was synthesised following the method reported by Uson *et al.* [371]. 2.2 g of $HAuCl_4$ was dissolved in 16 mL of methanol and 4 mL of water. 1.5 mL of tetrahydrothiophene (THT) was then added under N_2 flow. The colour of the solution changes from yellowish to reddish briefly and immediately changes to white. The stirring continued for 30 minutes. The product was collected via centrifuge and washed with methanol (4 × 25 mL), followed by ice-cold THF (2 × 25mL). The product was dried in vacuum, dissolved in 100 mL 3:1 methanol: acetone (*ca.* 50 ˚C) mixture and crystalised at 0 ˚C. The yield was *ca.* 1.1 g of Au(THT)Cl (*ca.* 56% w.r.t. gold atom).

$Au_2(dppe)Cl_2$: $Au_2(dppe)Cl_2$ was prepared following the method described by Brandys *et al.* [372]. 970 mg of Au(THT)Cl was dispersed in 20 mL methanol. 600 mg of 1,2-bis(diphenylphosphino)ethane (dppe) was added to stirring solution under N_2 flow. The reaction mixture was stirred for 1.5 hours and off-white (a bit of reddish touch) precipitate was collected via centrifugation. The product was washed with methanol (4 × 25 mL) and ice-

cold THF (2 × 25 mL). The product was partially dissolved in DCM (50 mL), and the solvent was removed under vacuum. The crude product was washed with 9:1 pet ether: DCM mixture (2 × 50 mL). The product was then dissolved in 500 mL 3:1 methanol: acetone (*ca.* 50 ˚C) mixture. The product was crystalised slowly in the ambient conditions for a few hours and then transferred to the fridge 0 ˚C, where it was crystalised overnight. The identity of the product was confirmed by ^{31}P NMR (in $CDCl_3$) with a singlet at 32.5 ppm (w.r.t. 85% H_3PO_4). The yield of product is *ca.* 1000 mg of $Au_2(dppe)Cl_2$ (*ca.* 76% w.r.t. gold).

$[Au_9(PPh_3)_8](NO_3)_3$: $[Au_9(PPh_3)_8](NO_3)_3$ was prepared following a report from Anderson *et al.* [356]. 1 g of gold phosphine nitrate ($AuPPh_3NO_3$) was dissolved in 75 mL ethanol. 18 mg $NaBH_4$ dissolved in 5 mL ethanol was added to the reaction mixture. The colour of the solution immediately turns to red and darkens quickly to deep red. The reaction mixture was stirred for 3 hours. The red colour mixture was centrifuged, any solid discarded. The supernatant was dried using a rotary evaporator. The crude product was dissolved in 25 mL dichloromethane, centrifuged; any solids discarded. The solvent was removed under using a rotary evaporator without heating. The red colour residue was washed with 2 × 25mL tetrahydrofuran (THF) yielding a green colour product. This green colour product was further washed with 3 × 25mL petroleum ether. The crude product was dried and dissolved in 10 mL methanol and crystallised *via* vapour diffusion crystallisation using 60 mL diethyl ether in an 80 mL jar over a week. The obtained crystal was washed with diethyl ether (Et_2O) and dried in vacuum. The yield of $[Au_9(PPh_3)_8](NO_3)_3$ was 190 mg (*ca.*23 % w.r.t. gold atom). The identity of the cluster was confirmed by ^{31}P NMR in CDCl3 with a single peak at δ= 57 ppm (w.r.t. 85% H_3PO_4), and presence of $[Au_9(PPh_3)_8]^{3+}$ (m/z≈1240) in ESI-MS. The UV-Vis absorption was observed at 442 nm, 424 nm, 354 nm and 316 nm (Figure A5.1).

(a)

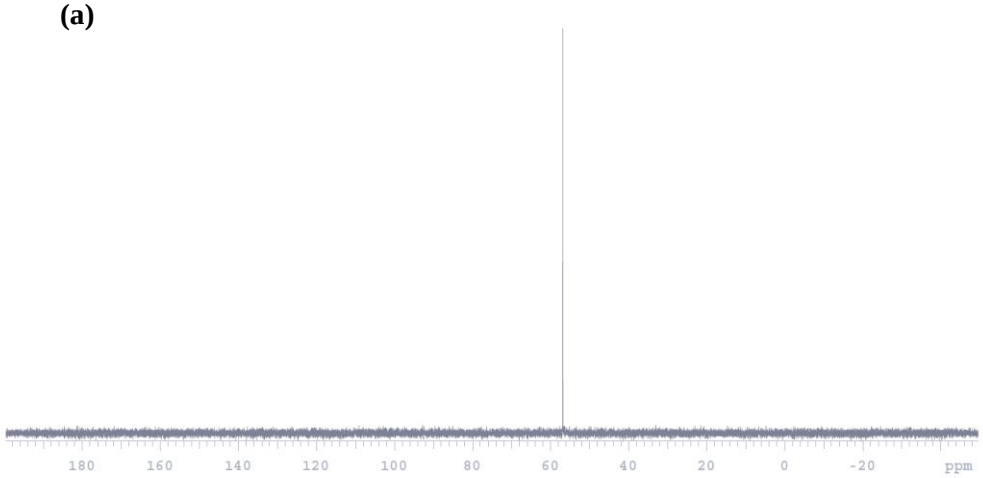
180
160
140
120
100
80
60
40
20
0
-20
ppm

(b)

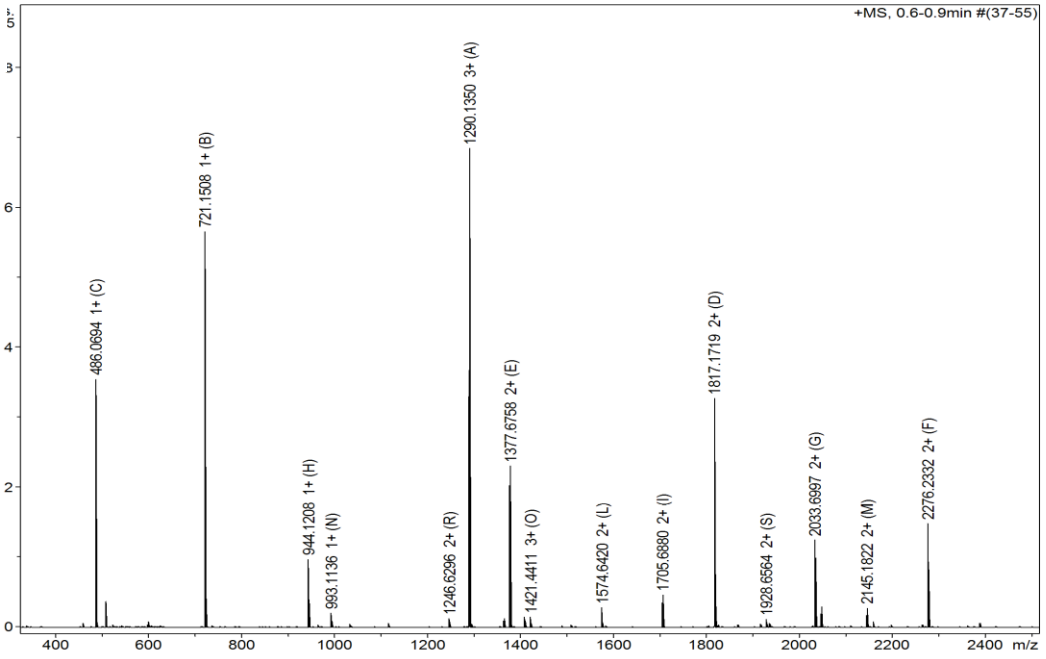
+MS, 0.6-0.9min #(37-55)
486.0694 1+ (C)
721.1508 1+ (B)
944.1208 1+ (H)
993.1136 1+ (N)
1246.6296 2+ (R)
1290.1350 3+ (A)
1377.6758 2+ (E)
1421.4411 3+ (O)
1574.6420 2+ (L)
1705.6880 2+ (I)
1817.1719 2+ (D)
1928.6564 2+ (S)
2033.6997 2+ (G)
2145.1822 2+ (M)
2276.2332 2+ (F)
400
600
800
1000
1200
1400
1600
1800
2000
2200
2400
m/z

(c)

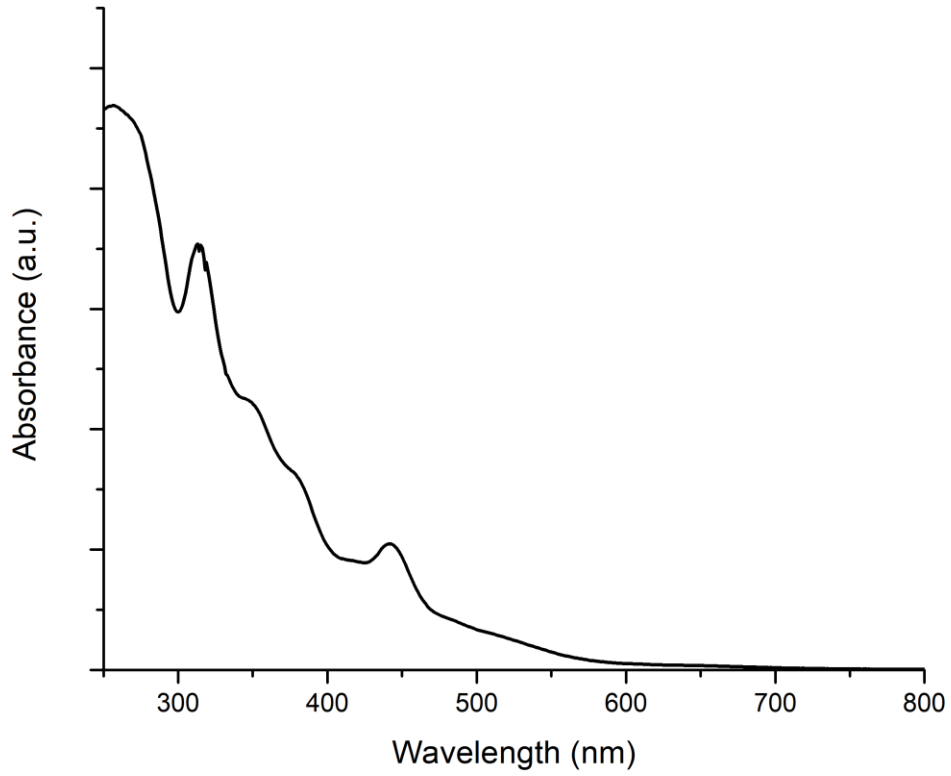

Figure A5.1: (a) ^{31}P NMR of $[Au_9(PPh_3)_8](NO_3)_3$ (b) ESI-MS of $Au_9(PPh_3)_8](NO_3)_3$ (c) UV-Vis spectra of $[Au_9(PPh_3)_8](NO_3)_3$.

$[Au_6(dppp)_4](NO_3)_2$: $[Au_6(dppp)_4](NO_3)_2$ was synthesised following the method reported in the literature [373]. Briefly, 100 mg of $[Au_9(PPh_3)_8](NO_3)_3$ was dissolved in 10 mL dichloromethane (DCM). 200 mg of 1,3-bis(diphenylphosphino)propane (20-fold molar excess) dissolved in 5 mL DCM was added to the stirring solution. The colour of the solution change from reddish to orangish briefly and immediately changed to blue indicating the ligand exchange. The reaction mixture was further stirred for 30 minutes and subsequently was poured into a 100 mL petroleum ether. The obtained product was precipitated at 0 ˚C overnight. The blue colour solids were then collected by centrifugation. The product was washed with petroleum ether (2 × 20 mL), a 9:1 petroleum ether / CH_2Cl_2 mixture (2 × 10 mL) and finally by diethyl ether (3 × 20 mL). The product was dissolved in 5 mL of methanol and crystallised by vapour diffusion of 40 mL of diethyl ether (Et_2O) over a week in 60 mL jar. The yield of product was ca. 50 mg (*ca.* 4633% yield by gold atom). The identity of the cluster was confirmed by ^{31}P NMR (in CD_3OD) with two singlets of equal intensity at δ_1=54

ppm and δ_2= 62 ppm (w.r.t. 85% H_3PO_4) as shown in Figure A5.2. The UV-Vis absorption spectra of the clusters have peaks at 325 nm, 430 nm, 507 nm and 589 nm.

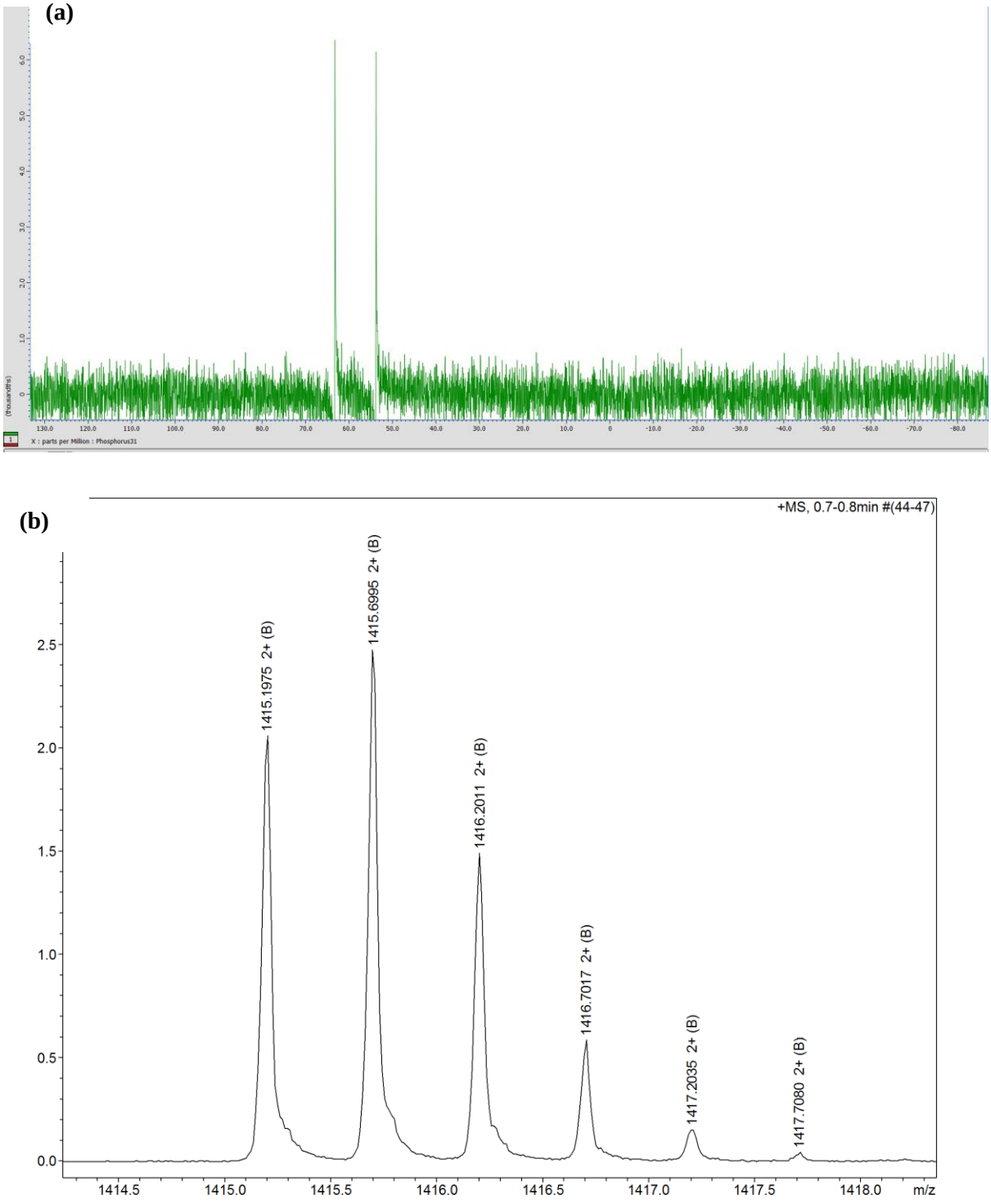

(c)

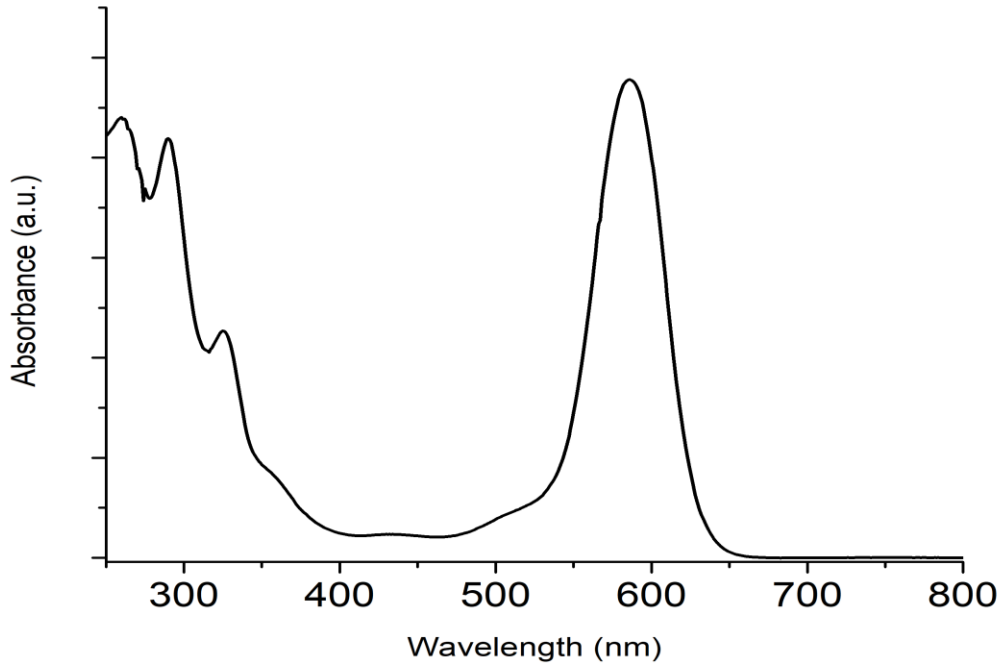

Figure A5.2: (a) ^{31}P NMR of $[Au_6(dppp)_4](NO_3)_2$ (b) ESI-MS of $[Au_6(dppp)_4](NO_3)_2$ (c) UV-Vis spectra of $[Au_6(dppp)_4](NO_3)_2$.

$[Au_{13}(dppe)_5Cl_2]Cl_3$: Synthesis of $[Au_{13}(dppe)_5Cl_2]Cl_3$ was performed following the method reported by Shichibu and Konishi [374]. 300 mg of $Au_2(dppe)Cl_2$ was dissolved in 240 mL, and then $NaBH_4$ (66 mg) suspension in ethanol (10 mL) was added to this solution. The colour of the solution changes to dark red, the stirring continued for 3 hours. The reaction mixture was centrifuged (any solids discarded) and the supernatant was dried by rotary evaporation. The product was extracted using ethanol (50 mL), centrifuged and 1 mL of neat HCl was added and stirred overnight. The solvent was removed using a rotary evaporator; the product was then precipitated from diethyl ether (100 mL) overnight at 0 ˚C. ^{31}P NMR of the crude product in CD_3OD had a peak at δ=37 ppm indicating the presence of $Au_2dppeCl_2$. The product was precipitated again in Et_2O and washed with 9:1 petroleum ether/DCM mixture (4 × 50 mL). Finally, the product was dissolved in methanol (8mL) and crystallised via vapour diffusion of diethyl ether (50 mL) in a 100 mL jar for seven days. The yield of product was ca. 70 mg (*ca.* 28% by gold atom). The identity of the cluster was confirmed using ^{31}P NMR of the product (Figure A5.3) and ESI-MS (m/z=1541 corresponding $[Au_{13}(dppe)_5Cl_2]^{3+}$). The UV-Vis spectra found the peaks at 306, 366 nm, 486 nm.

(a)

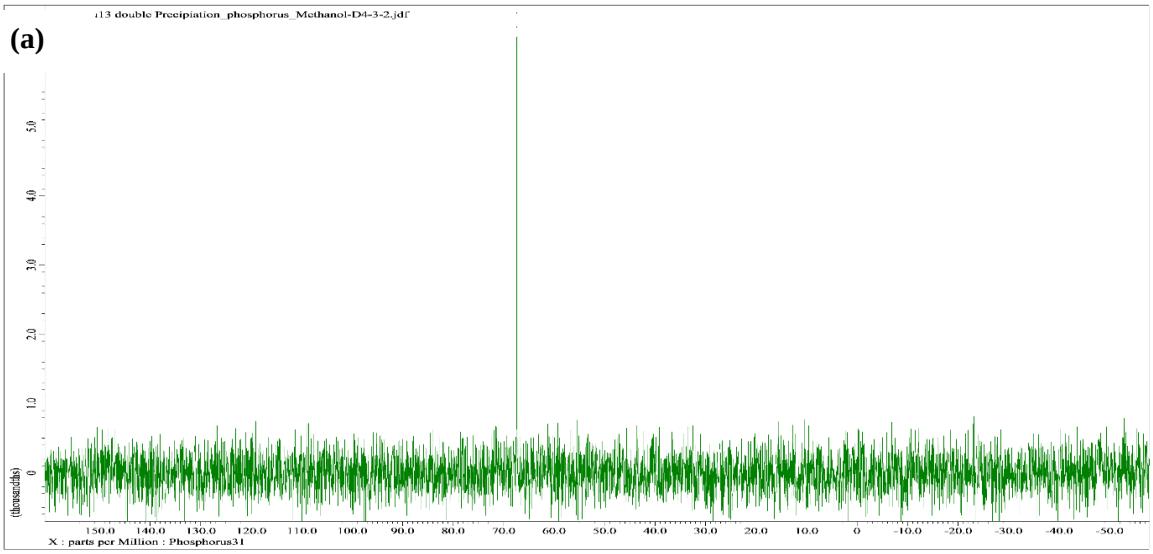
113 double Precipiation_phosphorus_Methanol-D4-3-2.jdf
(Normalized Counts)
X : parts per Million : Phosphorus31

(b)

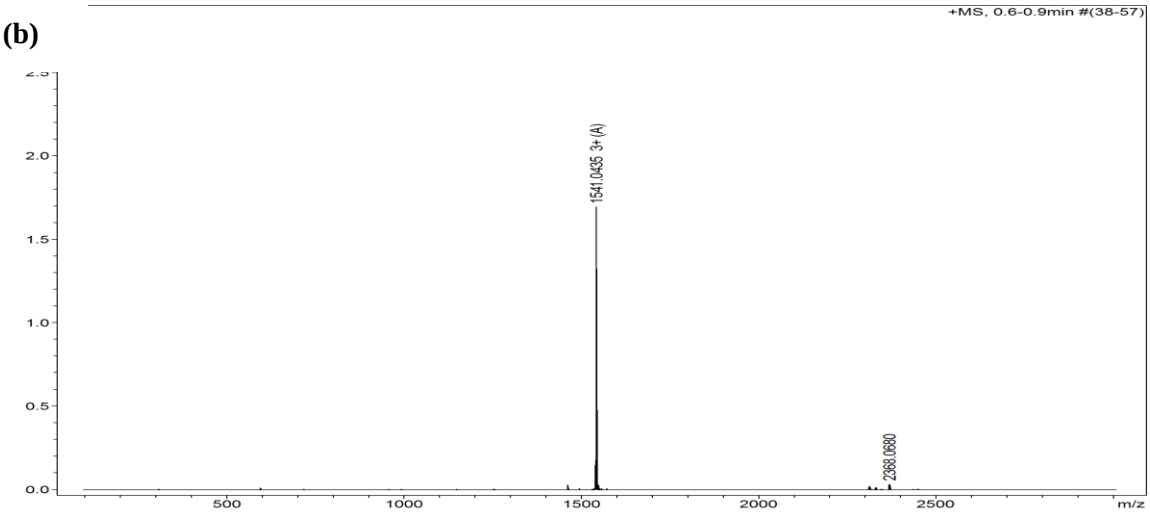
+MS, 0.6-0.9min #(38-57)
1541.0435 3+ (A)
2368.0880
m/z

(c)

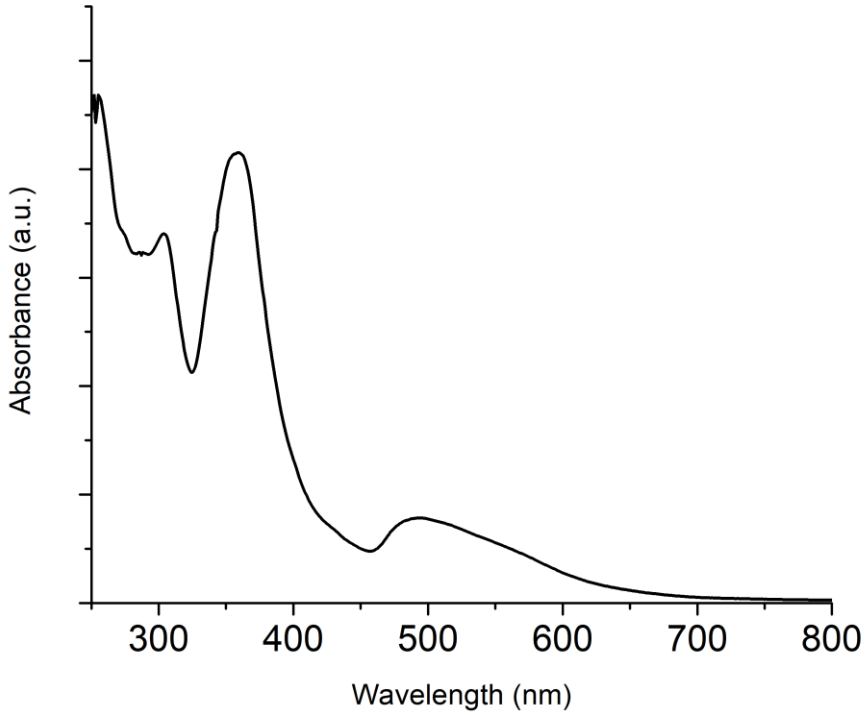

Figure A5.3: (a) ^{31}P NMR of Au_{13}, (b) ESI-MS spectra of $[Au_{13}(dppe)_5Cl_2]Cl_3$ (c) UV-Vis spectra of $[Au_{13}(dppe)_5Cl_2]Cl_3$.

1.5 nm gold cluster $Au_{101}(PPh_3)_{25}Cl_5$: $Au_{101}(PPh_3)_{25}Cl_5$ was synthesised following the method reported by Anderson *et al*.[356, 375]. Chloroauric acid (1g) was dissolved in 60 mL of water, and 60 mL toluene added. 1.4 g tetraoctylammonium bromide was added to stirring solution as the phase transfer agent. After 10 minutes of stirring, 2.3 g triphenyl phosphine added changed the colour of the solution to dark red. The reaction mixture was stirred for 3 hours. The organic phase was separated using a funnel and washed with aqueous NaCl saturated solution (2 × 50mL) and water (3 × 50mL). The organic phase was dried using a rotary evaporator without heating. The product was dissolved in 35mL chloroform, centrifuged (any solid discarded), and precipitated in 500 mL pentane at 0 ˚C. The precipitate was collected with centrifugation and washed with various solvent/solvent-mixtures to remove $AuPPh_3Cl$ impurities as follows.

100 mL hexanes followed by 100 mL 2: 3 MeOH: H_2O (two times)

100 mL hexanes followed by 100 mL 1: 1 MeOH: H2O (two times)

150 mL 3: 1 pentane: chloroform (two times)

150 mL 2: 1 pentane: chloroform (two times)

150 mL 1: 1 pentane: chloroform (two times)

Finally, the crude product was dissolved in 30 mL chloroform, centrifuged (any solid discarded) and dried under reduced pressure. The purity of the product was studied with ^{1}H NMR spectra of the product with the minimum. Total of 240 mg (*ca.* 47% yield w.r.t. gold atom) clusters was obtained. UV-Vis confirmed the identity of the cluster as shown in Figure A5.4.

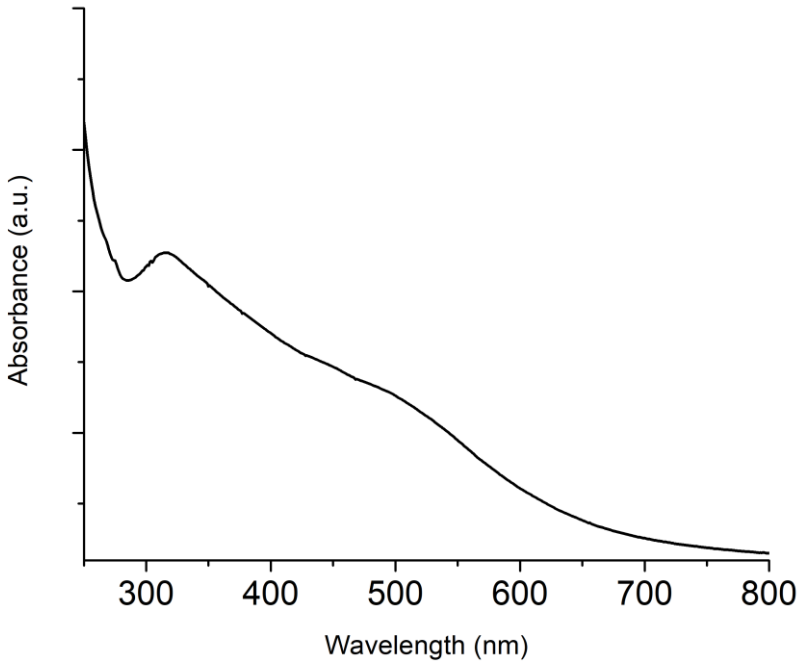

Figure A5.4: UV-Vis spectra of Au_{101}.

c. Electrochemical Studies

The cathode material electrochemical reduction of carbon dioxide (CO_2) was prepared by depositing gold cluster on carbon paper. Briefly, the synthesised metal clusters were dissolved in dichloromethane, and the solution was drop-casted on carbon paper. The clusters were gently dried under vacuum overnight. A similar deposition method was previously reported

by Chen and Chen [135]. The heat treatment of the cluster was performed at 200 ˚C in the air for 2 hours.

The electrochemical reduction CO_2 was studied in a homemade three-electrode based electrochemical flow cell. The cell consists of metal clusters based catalyst as a cathode, Pt counter electrode and Ag|AgCl as the reference electrode. The electrochemical CO_2 reduction was studied for catholyte a flow rate of 20 mL min^{-1}. The catalyst consists of 0.2 mol L^{-1} $KHCO_3$ continuously bubbled with CO_2 (20 cm^3 min^{-1}). CO_2 bubbling was started at least 20 minutes before starting the experiment. The equivolume mixture of 0.5 mol L^{-1} NaF and 0.5 mol L^{-1} $KHCO_3$ was used as anolyte. All the electrochemical measurements were carried out at room temperature.

d. Fitting P2p spectra

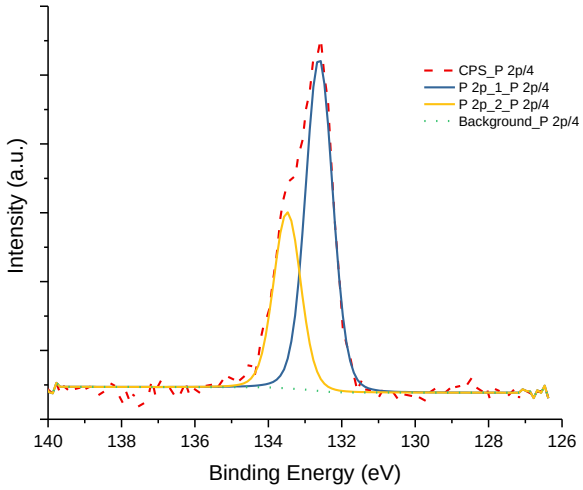

Figure A5.5: P2p spectra for Au_6

e. SEM studies

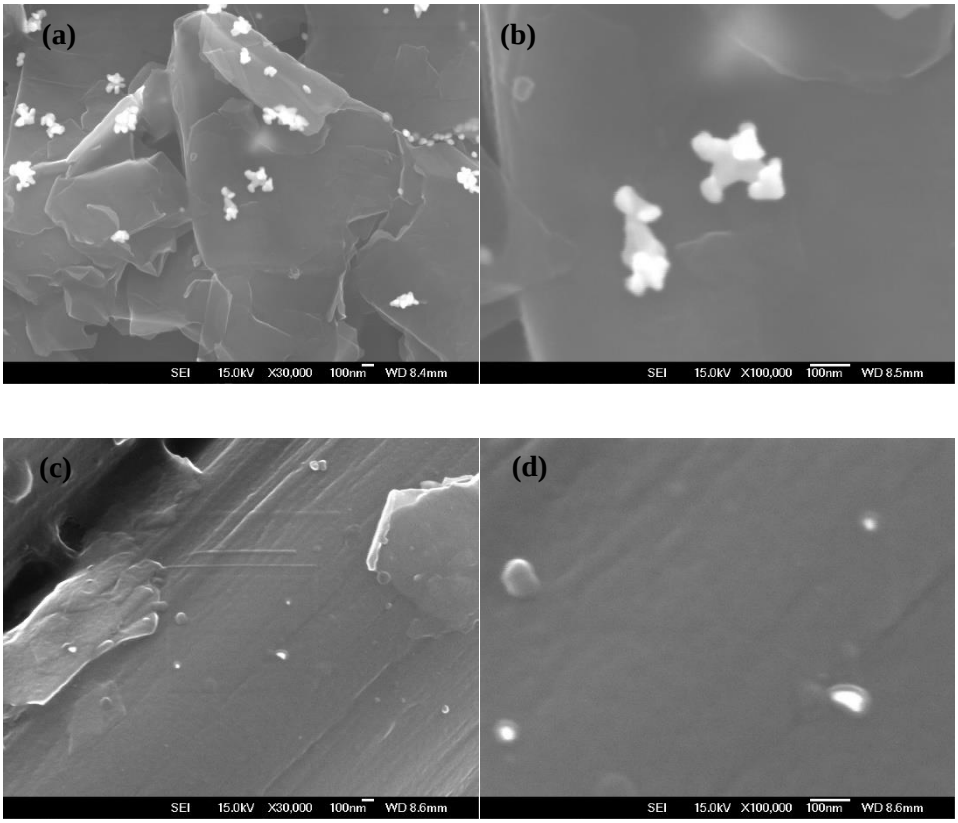

Figure A5.6: Scanning electron microscopic image of (a) calcined Au_9/Carbon paper (0.18 mg cm^{-2}); (b) used Au_9/carbon paper (0.18 mg cm^{-2}); (c) uncalcined Au_9/Carbon paper (0.18 mg cm^{-2}); (d) used uncalcined Au_9/carbon paper (0.18 mg cm^{-2}).

Appendix 6: Copyright permissions

Copyright licence for Figure 2.3.

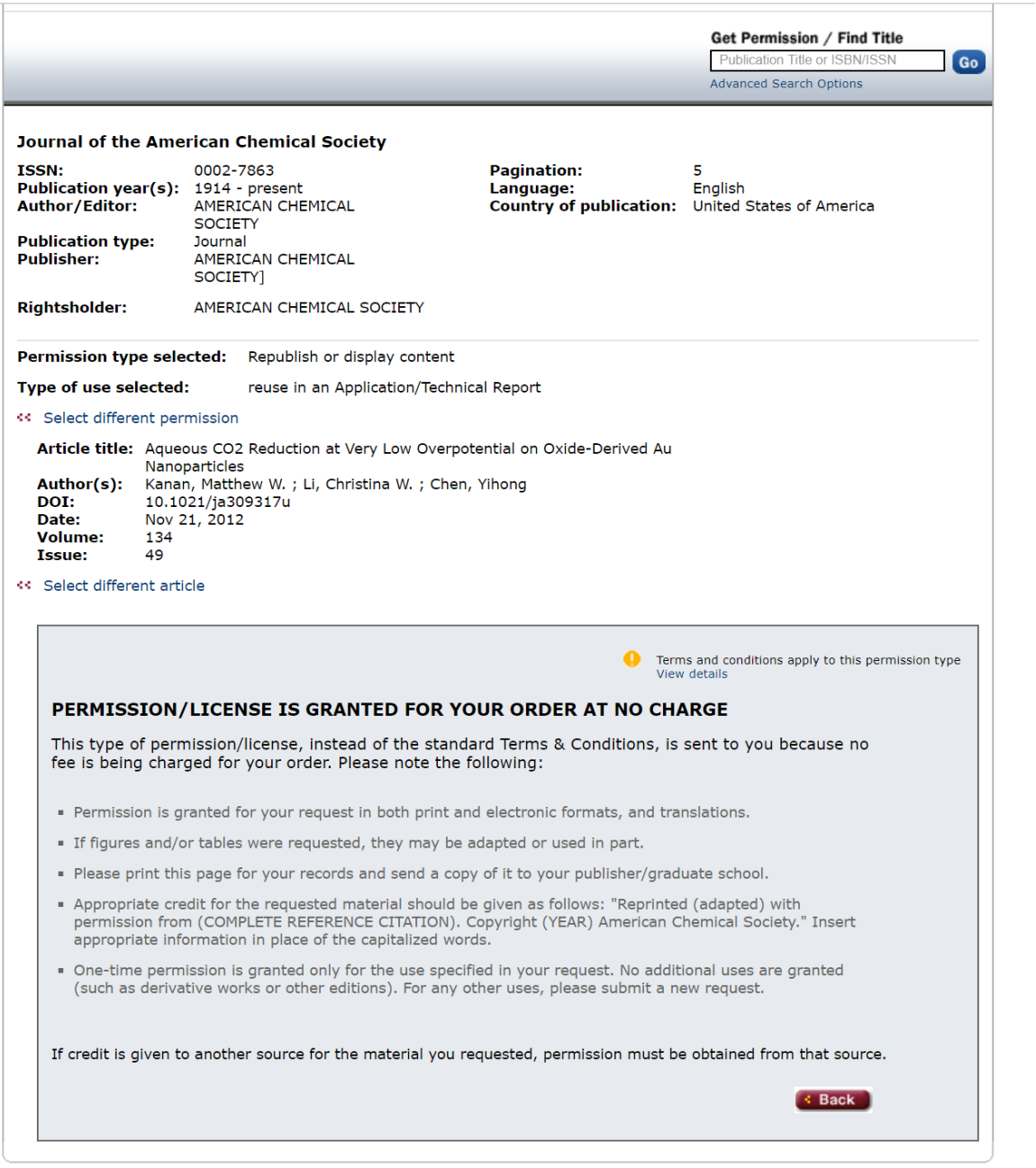

Get Permission / Find Title

Publication Title or ISBN/ISSN Go

Advanced Search Options

Journal of the American Chemical Society

ISSN:	0002-7863	**Pagination:**	5
Publication year(s):	1914 - present	**Language:**	English
Author/Editor:	AMERICAN CHEMICAL SOCIETY	**Country of publication:**	United States of America
Publication type:	Journal		
Publisher:	AMERICAN CHEMICAL SOCIETY]		
Rightsholder:	AMERICAN CHEMICAL SOCIETY		

Permission type selected: Republish or display content

Type of use selected: reuse in an Application/Technical Report

Select different permission

Article title: Aqueous CO2 Reduction at Very Low Overpotential on Oxide-Derived Au Nanoparticles
Author(s): Kanan, Matthew W. ; Li, Christina W. ; Chen, Yihong
DOI: 10.1021/ja309317u
Date: Nov 21, 2012
Volume: 134
Issue: 49

Select different article

Terms and conditions apply to this permission type
View details

PERMISSION/LICENSE IS GRANTED FOR YOUR ORDER AT NO CHARGE

This type of permission/license, instead of the standard Terms & Conditions, is sent to you because no fee is being charged for your order. Please note the following:

- Permission is granted for your request in both print and electronic formats, and translations.
- If figures and/or tables were requested, they may be adapted or used in part.
- Please print this page for your records and send a copy of it to your publisher/graduate school.
- Appropriate credit for the requested material should be given as follows: "Reprinted (adapted) with permission from (COMPLETE REFERENCE CITATION). Copyright (YEAR) American Chemical Society." Insert appropriate information in place of the capitalized words.
- One-time permission is granted only for the use specified in your request. No additional uses are granted (such as derivative works or other editions). For any other uses, please submit a new request.

If credit is given to another source for the material you requested, permission must be obtained from that source.

Back

Copyright licence for Figure 2.4.

Copyright Clearance Center

Note: Copyright.com supplies permissions but not the copyrighted content itself.

1 PAYMENT 2 REVIEW 3 CONFIRMATION

Step 3: Order Confirmation

Thank you for your order! A confirmation for your order will be sent to your account email address. If you have questions about your order, you can call us 24 hrs/day, M-F at +1.855.239.3415 Toll Free, or write to us at info@copyright.com. This is not an invoice.

Confirmation Number: 11800121
Order Date: 03/19/2019

If you paid by credit card, your order will be finalized and your card will be charged within 24 hours. If you choose to be invoiced, you can change or cancel your order until the invoice is generated.

Payment Information

Hani Taleshiahangari
University of Canterbury
hanitaleshi@gmail.com
+64 224306951
Payment Method: n/a

Order Details

Journal of applied electrochemistry

Order detail ID:	71855753
Order License Id:	4552791145513
ISSN:	1572-8838
Publication Type:	e-Journal
Volume:	
Issue:	
Start page:	
Publisher:	KLUWER ACADEMIC PUBLISHERS (DORDRECHT)

Permission Status: Granted
Permission type: Republish or display content
Type of use: Thesis/Dissertation

Requestor type	Academic institution
Format	Electronic
Portion	image/photo
Number of images/photos requested	1
The requesting person/organization	Hani Taleshi
Title or numeric reference of the portion(s)	Chapter 2, Figure 2.4
Title of the article or chapter the portion is from	Literature Review
Editor of portion(s)	N/A
Author of portion(s)	N/A
Volume of serial or monograph	N/A

Copyright licence for Figure 2.5.

ACS catalysis

ISSN:	2155-5435	**Language:**	English
Publication year(s):	2011 - present	**Country of publication:**	United States of America
Author/Editor:	American Chemical Society		
Publication type:	e-Journal		
Publisher:	American Chemical Society		
Rightsholder:	AMERICAN CHEMICAL SOCIETY		

Permission type selected: Republish or display content

Type of use selected: reuse in an Application/Technical Report

Select different permission

Article title: Understanding Selectivity for the Electrochemical Reduction of Carbon Dioxide to Formic Acid and Carbon Monoxide on Metal Electrodes
Author(s): Jaramillo, Thomas F. ; et al
DOI: 10.1021/acscatal.7b00687
Date: Jun 22, 2017
Volume: 7
Issue: 7

Select different article

Terms and conditions apply to this permission type
View details

PERMISSION/LICENSE IS GRANTED FOR YOUR ORDER AT NO CHARGE

This type of permission/license, instead of the standard Terms & Conditions, is sent to you because no fee is being charged for your order. Please note the following:

- Permission is granted for your request in both print and electronic formats, and translations.
- If figures and/or tables were requested, they may be adapted or used in part.
- Please print this page for your records and send a copy of it to your publisher/graduate school.
- Appropriate credit for the requested material should be given as follows: "Reprinted (adapted) with permission from (COMPLETE REFERENCE CITATION). Copyright (YEAR) American Chemical Society." Insert appropriate information in place of the capitalized words.
- One-time permission is granted only for the use specified in your request. No additional uses are granted (such as derivative works or other editions). For any other uses, please submit a new request.

If credit is given to another source for the material you requested, permission must be obtained from that source.

Back

Copyright licence for Figure 2.7.

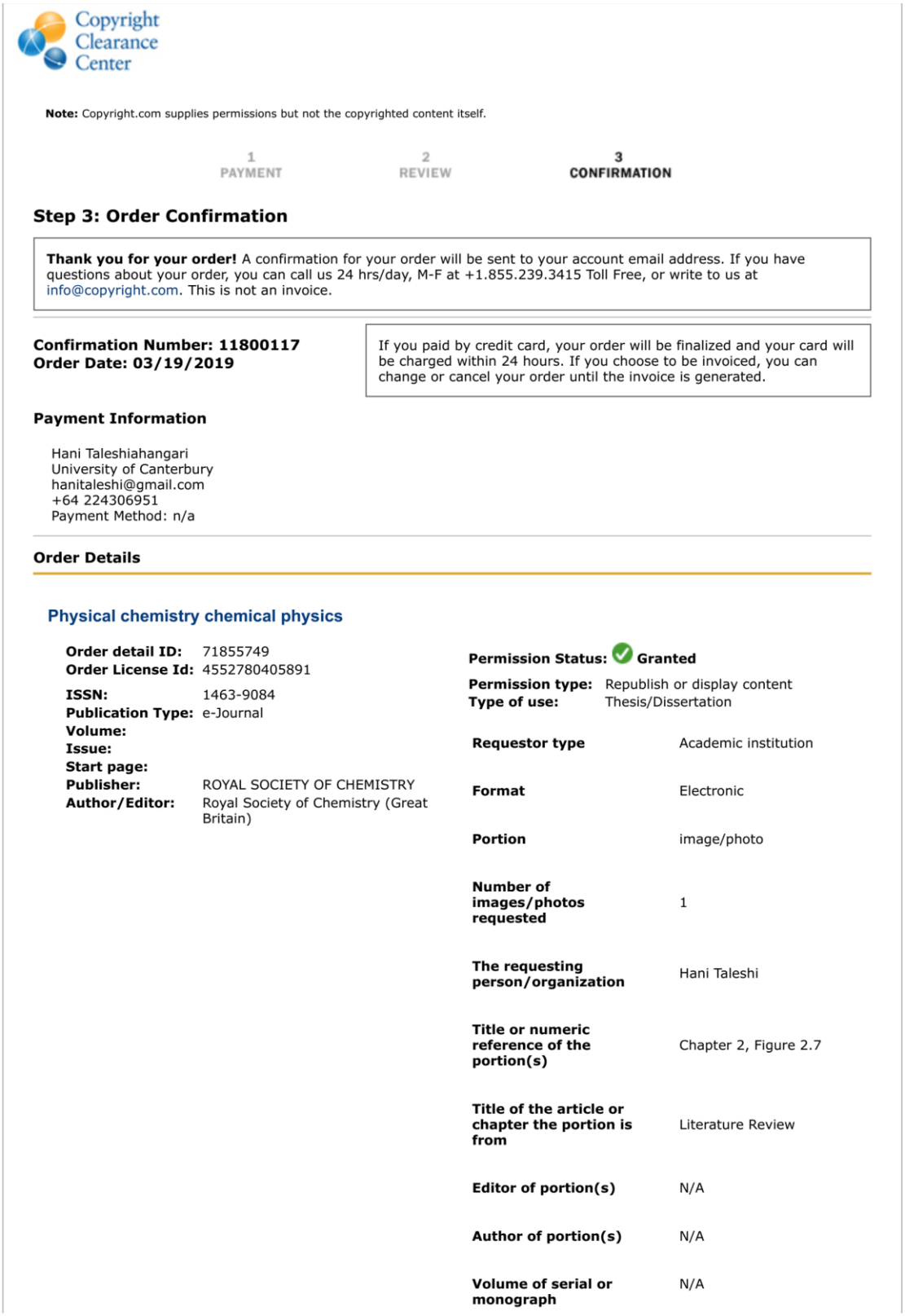

Copyright Clearance Center

Note: Copyright.com supplies permissions but not the copyrighted content itself.

1 PAYMENT 2 REVIEW 3 CONFIRMATION

Step 3: Order Confirmation

Thank you for your order! A confirmation for your order will be sent to your account email address. If you have questions about your order, you can call us 24 hrs/day, M-F at +1.855.239.3415 Toll Free, or write to us at info@copyright.com. This is not an invoice.

Confirmation Number: 11800117
Order Date: 03/19/2019

If you paid by credit card, your order will be finalized and your card will be charged within 24 hours. If you choose to be invoiced, you can change or cancel your order until the invoice is generated.

Payment Information

Hani Taleshiahangari
University of Canterbury
hanitaleshi@gmail.com
+64 224306951
Payment Method: n/a

Order Details

Physical chemistry chemical physics

Order detail ID:	71855749
Order License Id:	4552780405891
ISSN:	1463-9084
Publication Type:	e-Journal
Volume:	
Issue:	
Start page:	
Publisher:	ROYAL SOCIETY OF CHEMISTRY
Author/Editor:	Royal Society of Chemistry (Great Britain)

Permission Status: Granted
Permission type: Republish or display content
Type of use: Thesis/Dissertation

Requestor type	Academic institution
Format	Electronic
Portion	image/photo
Number of images/photos requested	1
The requesting person/organization	Hani Taleshi
Title or numeric reference of the portion(s)	Chapter 2, Figure 2.7
Title of the article or chapter the portion is from	Literature Review
Editor of portion(s)	N/A
Author of portion(s)	N/A
Volume of serial or monograph	N/A

References

1. Hoegh-Guldberg O. , et al., *Carol reefs under rapid climate change and ocean acidification.* Science, 2007. **318**(5857): p. 1737-1742.
2. Davis S.J. , Calderina K. , and Mathews H.D. , *Future CO_2 emmisions and climate change from existing energy infrastructure.* Science, 2010. **329**(5997): p. 1330-1333.
3. Hall-Spencer J.M. , et al., *Volcanic carbon dioxide vents show ecosystem effects of ocean acidification.* Nature, 2008. **454**: p. 96-99.
4. Orr J.C. , et al., *Anthropogenic ocean acidification over the twenty-first century and its impact on clacifying organism.* Nature, 2005. **437**: p. 681-686.
5. Karl T.R. and Trenberth K.E. , *Modern global climate change.* Science, 2003. **302**(5651): p. 1719-1723.
6. Olah G. , Geoppert A. , and Prakash S. , *Chemical recycling of carbon dioxide to methanol and dimethyl ether: from greenhouse gas to renewable environmentally carbon neutral fuels and synthetic hydrocarbons.* The Journal of Organic Chemistry, 2009. **74**(2): p. 487-98.
7. Kelemen P.B. and Matter J. , *In situ carbonation of peridotite for CO_2 storage.* Proceedings of the National Academy of Science, 2008. **105**(45): p. 17292-17300.
8. Aresta M. , Dibenedetto A. , and Angelini A. , *Catalysis for the valorization of exhaust carbon: from CO_2 to chemicals, materials, and fuels. Technological use of CO_2.* Chemical Reviews, 2014. **114**(3): p. 1709-1742.
9. Hernandez S. , et al., *Syngas production from electrochemical reduction of CO_2: current status and prospective implemention.* Green Chemistry, 2017. **19**: p. 2326-2346.
10. Mills R. , *Capturing carbon: The new weapon in the war against climate change*. 2011, Columbia University Press.
11. Kuhl K.P. , *Electrochemical reduction of carbon dioxide on transition metal surfaces*, in *The Department of Chemistry*. 2013, Stanford University.
12. Song Ch. , *CO_2 conversion and utilization: An overview*. 2002, ACS Symposium Series. p. 2-30.
13. Gattrell M. and Gupta N. , *Electrochemical reduction of CO_2 to hydrocarbons to store renewable electrical energy and upgrade biogas.* Energy Conversion and Management, 2007. **48**: p. 1255-65.

14. Whipple D.T. and Kenis P. , *Prospects of CO_2 utilization via direct heterogeneous electrochemical reduction.* The Journal of Physical Chemistry Letters, 2010. **1**: p. 3451-3458.
15. Ganesh I. , *Conversion of carbon dioxide into methanol- a potential liquid fuel: Fundametal challenges and opportunities.* Renewable and Sustainable Energy Reviews, 2014. **31**: p. 221-257.
16. Lu X. , et al., *Electrochemical reduction of carbon dioxide to formic acid.* Chemelectrochem, 2014. **1**: p. 836-849.
17. Spinner N. , Vega J. , and Mustain W. , *Recent progress in the electrochemical conversion and utilization of CO_2.* Catalysis Science & Technology, 2012. **2**: p. 19-28.
18. Peterson A.A. , et al., *How copper catalyzes the electroreduction of carbon dioxide into hydrocarbon fuels.* Energy and Environmental Science, 2010. **3**: p. 1311-1315.
19. Kim J.J. , Summers D.P. , and Frese J.K.W. , *Reduction of CO_2 and CO to methane on Cu foil electrodes.* Journal of Electroanalytical Chemistry and Interfacial Electrochemistry, 1988. **245**: p. 223-44.
20. Hori Y. , *CO_2 reduction, catalyzed by metal electrodes, Handbook of Fuel Cells*. 2010: John Wiley & Sons Ltd.
21. Wenzhen L. , *Electrocatalytic reduction of CO_2 to small organic molecule fuels on metal catalysts*, in *Journal of American Chemical Society*. 2010, ACS Publications.
22. Surdhar P.S. , Mezyk S.P. , and Armstrong D.A. , *Reduction potential of the carboxyl radical anion in aqueous solutions.* The Journal of Physical Chemistry, 1989. **93**(8): p. 3360-3363.
23. Schwarz H.A. and Dodson R.W. , *Reduction potentials of CO_2- and the alcohol radicals.* The Journal of Physical Chemistry, 1989. **93**(1): p. 409-414.
24. Lamy E. , Nadjo L. , and Saveant J.M. , *Standard potential and kinetic parameters of the electrochemical reduction of carbon dioxide in dimethylformamide.* Journal of Electroanalytical Chemistry and Interfacial Electrochemistry, 1977. **78**(2): p. 403-407.
25. Sullivan B.P. , Krist K. , and Guard H.E. , *Electrochemical and electrocatalytic reactions of carbon dioxide*. 1993, Amsterdam: Elsevier Science Publishers B.V.
26. Centi G. and Perathoner S. *Green carbon dioxide: Advances in CO_2 utilization*. 2014.
27. Hori Y. , *Modern Aspects of Electrochemistry*. Vol. 42. 2008, New York: Springer. 89-189.

28. Noda H. , et al., *Potential dependencies of the products on electrochemical reduction of carbon dioxide at a copper electrode.* Chemistry Letters, 1989. **18**(2): p. 289-292.
29. Hori Y. , Murata A. , and Takahashi R. , *Formation of hydrocarbons in the electrochemical reduction of carbon dioxide at a copper electrode in aqueous solution.* Journal of the Chemical Society, Faraday Transactions, 1989. **85**(8): p. 2309-26.
30. Kuhl K.P. , et al., *New insights into the electrochemical reduction of carbon dioxide on metallic copper surfaces.* Energy and Environmental Science, 2012. **5**(5): p. 7050-9.
31. Chen C.S. , et al., *Stable and selective electrochemical reduction of carbon dioxide to ethylene on copper mesocrystals.* Catalysis Science & Technology, 2015. **5**(1).
32. Kim D. , et al., *Synergistic geometric and electronic effects for electrochemical reduction of carbon dioxide using gold-copper bimetallic nanoparticles.* Nature Communications, 2014. **11**(5).
33. kwon Y. , et al., *CO_2 electroreduction with enhanced ethylene and ethanol selectivity by nanostructuring polycrystalline copper.* Chemelectrochem, 2016. **3**(6).
34. Varela A.S. , et al., *Controlling the selectivity of CO_2 electroreduction on copper: The effect of the electrolyte concentration and the importance of the local pH.* Catalysis Today, 2016. **260**: p. 8-13.
35. Hori Y. , Kikuchi K. , and Suzuki S. , *Production of CO and CH_4 in electrochemical reduction of CO_2 at metal electrodes in aqueous hydrocarbonate solution.* The Chemical Society of Japan, 1985: p. 1695-8.
36. Azuma M. , Hashimoto K. , and Hiramoto M. , *Electrochemical reduction of carbon dioxide on various metal electrodes in low-temperature aqueous $KHCO_3$ media.* Journal of the Electrochemical Society, 1990. **137**(6): p. 1772-8.
37. Azuma M. , et al., *Carbon dioxide reduction at law temperature on various metal electrodes.* Journal of Electroanalytical Chemistry, 1989. **260**: p. 441-5.
38. Hori Y. , et al., *Electrocatalytic process of CO selectivity in electrochemical reduction of CO_2 at metal electrodes in aqueous media.* Electrochimia Acta, 1994. **39**(11-12): p. 1833-9.
39. Hoshi N. , Kato M. , and Hori Y. , *Electrochemical reduction of CO_2 on single crystal electrodes of silver Ag(111), Ag(100) and Ag (110).* Journal of Electroanalytical Chemistry, 1997. **440**(1-2): p. 283-286.

40. Hori Y. , et al., *Selective formation of C2 compounds from electrochemical reduction of CO_2 at a series of copper single crystal electrodes.* The Journal of Physical Chemistry, 2002. **106**(1): p. 15-17.
41. Xiao J. , et al., *CO_2 reduction at low overpotential on Cu electrodes in the presence of impurities at the subsurface.* Journal of Materials Chemistry A, 2014. **2**: p. 4885-9.
42. Hatsukade T. , et al., *Insight into the electrocatalytic reduction of CO_2 on metallic silver surfaces.* Physical Chemistry Chemical Physics, 2014. **16**: p. 13814-19.
43. Noda H. , et al., *Electrochemical reduction of carbon dioxide at various metal electrodes in aqueous potassium hydrogen carbonate solution.* The Chemical Society of Japan, 1990. **63**(9): p. 2459-2462.
44. Roberts J.L. and Sawyer D.T. , *Electrochemical oxidation of carbon monoxide at gold electrodes.* Electrochimia Acta, 1965. **10**: p. 989-1000.
45. Hutchings G.S. , *Vapor phase hydrochlorination of acetylene: Correlation of catalytic activity of supported metal chloride catalysts.* Journal of Catalysis, 1985. **96**(1): p. 292-295.
46. Haruta M. , et al., *Novel gold catalysts for the oxidation of carbon monoxide at a temperature far below 0 C.* Chemistry Letters, 1987. **16**(2): p. 405-8.
47. Hashmi A.S.K. and Hutchings G.S. , *Gold Catalysis.* Angewandte Chemie International Edition, 2006. **45**(47): p. 7896-7936.
48. Delacourt C. , Ridgway P.L. , and NEwman J. , *Mathematical modeling of CO_2 reduction in aqueous electrolytes. I. Kinetic study on plannar silver and gold electrodes.* Journal of the Electrochemical Society, 2010. **157**(12): p. B1902-B1910.
49. Hori Y. , et al., *Electrochemical Reduction of Carbon Dioxide to Carbon Monoxide at a Gold Electrode in Aqueous Potassium Hydrogen Carbonate.* Journal of Chemical Society, chemical Communications, 1987. **10**: p. 728-9.
50. Kauffman D.R. , et al., *Experimental and computational investigation of Au_{25} clusters and CO_2: A uniqe interaction and enhanced electrocatalytic activity.* Journal of the American Chemical Society, 2012. **134**(24): p. 10237-10243.
51. Steven J.T. , *The electrochemical and electrocatalytic behaviour of gold nanoparticles,* in *Chemical and Process Engineering Department*. 2017, University of Canterbury.
52. Ohmori T. , et al., *Influence of sputtering parameters on electrochemical CO_2 reduction in sputtered Au electrodes.* Journal of Electroanalytical Chemistry, 2001. **514**: p. 51-55.

53. Hall A.S. , et al., *Mesostructure-induced selectivity in CO_2 redcution catalysis.* Journal of the American Chemical Society, 2015. **137**(47): p. 14834-14837.
54. Stevens G.B. , Reda T. , and Raguse B. , *Energy storage by the electrochemical reduction of CO_2 to CO at a porous Au film.* Journal of Electroanalytical Chemistry, 2002. **526**: p. 125-133.
55. Zhu W. , et al., *Active and selective conversion of CO_2 to CO on ultrathin Au nanowires.* Journal of the American Chemical Society, 2014. **136**(46): p. 16132-16135.
56. Huan T.N. , et al., *CO_2 reduction to CO in water: carbon nanotube-gold nanohybrid as a selective and efficient electrocatalyst.* ChemSusChem, 2016. **9**(17): p. 2317-2320.
57. Chen Y. , Li C.W. , and Kanan M.W. , *Aqueous CO_2 reduction at very low overpotential on oxide-derived Au nanoparticles.* Journal of the American Chemical Society, 2012. **134**(49): p. 19969-72.
58. Zhu W. , et al., *Monodisperse Au nanoparticles for selective electrocatalytic reduction of CO_2 to CO.* Journal of the American Chemical Society, 2013. **135**: p. 16833-16836.
59. Jovanov Z.P. , et al., *Opportunities and challenges in the electrocatalysis of CO_2 and CO reduction using bifunctional surfaces: A theoretical and experimental study of Au-Cd alloys.* Journal of Catalysis, 2016. **343**: p. 215-231.
60. Lu Qi. , Rosen J. , and Jiao F. , *Nanostructured metallic electrocatalysts for carbon dioxide reduction.* ChemCatChem Catalysis, 2015. **7**: p. 38-47.
61. Rodriguez P. , Araez N.G. , and Koper M. , *Self-promotion mechanism for CO electrooxidation on gold.* Physical Chemistry Chemical Physics, 2010. **12**: p. 9373-80.
62. Rodriguez P. , et al., *CO electroxidation on gold in alkaline media: A combined electrochemical, spectroscopic, and DFT study.* Journal of the American Chemical Society, 2010. **26**(14): p. 12425-12432.
63. Cuesta A. , Lopez N. , and Gutierrez C. , *Electrolyte electroflectance study of carbon monoxide adsorption on polycrystalline silver and gold electrodes.* Electrochimia Acta, 2003. **48**(20-22): p. 2949-56.
64. Blizanac B.B. , et al., *Surface Electrochemistry of CO on reconstructed gold single crystal surfaces studies by infrared reflection absorption spectroscopy and rotating disk electrode.* Journal of the American Chemical Society, 2004. **126**(32): p. 10130-41.

65. Rodriguez P. , Feliu J. M. , and Koper M. , *Unusal adsorption state of carbon monoxide on single-crystalline gold electrodes in alkaline media.* Electrochemistry Communications, 2009. **11**: p. 1105-8.
66. Cave E.R. , et al., *Electrochemical CO_2 reduction on Au surfaces: mechanistic aspects regarding the formation of major and minor products.* Physical Chemistry Chemical Physics, 2017. **19**: p. 15856-1586363.
67. Delacourt C. , et al., *Design of an electrochemical cell making syngas ($CO+H_2$) from CO_2 and H_2O reduction at room temperature.* Journal of the Electrochemical Society, 2008. **155**(1): p. B42-B49.
68. Jones J.P. , Prakash P. , and Olah G. , *Electrochemical CO_2 reduction: Recent advances and current trends.* Israel Journal of Chemistry, 2014. **54**: p. 1451-1466.
69. Jhong M. , Ma S. , and Kenis P. , *Electrochemical conversion of CO_2 to useful chemicals: Current status, remaining challenges, and future opportunities.* Current Opinion in Chemical Engineering, 2013. **2**: p. 191-199.
70. Qiao J.L. , et al., *A review of catalysts for the electroreduction of carbon dioxide to produce low-carbon fuels.* Chemical Society Reviews, 2014. **43**: p. 631-675.
71. Olah G. , Prakash S. , and Geoppert A. , *Anthropogenic chemical carbon cycle for a sustainable future.* Journal of the American Chemical Society, 2011. **133**(33): p. 12881-98.
72. Hara K. , Kudo A. , and Sakata T. , *Electrochemical reduction of carbon dioxide under high pressure on various electrodes in an aqueous electrolyte.* Journal of Electroanalytical Chemistry, 1995. **391**: p. 141-147.
73. Todoroki M. , et al., *Electrochemical reduction of high pressure CO_2 at Pb, Hg and In electrodes in an aqueous $KHCO_3$ solution.* Journal of Electroanalytical Chemistry, 1995. **394**(1-2): p. 192-203.
74. Hara K. , Sonoyama N. , and Sakata T. , *Electrochemical reduction of CO_2 by using metal supported gas diffusion electrode under high pressure.* Studies in Surface Science and Catalysis, 1998. **114**: p. 577-580.
75. Hara K. , Kudo A. , and Sakata T. , *Electrochemical reduction of high pressure carbon dioxide on Fe electrodes at large current density.* Journal of Electroanalytical Chemistry, 1995. **386**(1-2): p. 257-60.
76. Hara K. , Kudo A. , and Sakata T. , *Electrochemical CO_2 reduction on a glassy carbon electrode under high pressure.* Journal of Electroanalytical Chemistry, 1997. **421**(1-2): p. 1-4.

77. Dufek E.J. , et al., *Operation of a pressurized system for continuous reduction of CO_2.* Journal of the Electrochemical Society, 2012. **159**(9): p. F514-F517.
78. Hara K. , et al., *Electrochemical reduction of CO_2 on a Cu electrode under high pressure.* Journal of the Electrochemical Society, 1994. **141**(8): p. 2097-2103.
79. Hara K. and Tadayoshi S. , *Large current density CO_2 reduction under high pressure using gas diffusion electrodes.* Bulletin of the chemical Society of Japan, 1997. **70**(3): p. 571-576.
80. Kaneco S. , et al., *Electrochemical reduction of CO_2 on Au in KOH+methanol at low temperature.* Journal of Electroanalytical Chemistry, 1998. **441**: p. 215-220.
81. Dufek E.J. and Mcllwain M.E. , *Bench-scale electrochemical system for generation of CO and syn-gas.* Journal of Applied Electrochemistry, 2011. **41**(6): p. 623-631.
82. Mikkelsen M. , Jorgensen M. , and Krebs F.C. , *The teraton challenge. A review of fixation and transformation of carbon dioxide.* Energy and Environmental Science, 2010. **3**: p. 43-81.
83. Mao X. and Hatton T.A. , *Recent advances in electrocatalytic reduction of carbon dioxide using metal-free catalysts.* Industrial & Engineering Chemistry Research, 2015. **54**(16): p. 4033-4042.
84. Dufek E.J. , Lister T.E. , and Mcllwain M.E. , *Influence of electrolytes and membranes on cell operation for syngas production.* Electrochemical and Solid-State Letters, 2012. **15**(4): p. B48-B50.
85. Rammal M. , *Electrochemical reduction of CO_2 to low-molecular-weight organic molecules,* in *Department of Chemical Engineering*. 2016, McGill University.
86. DeWulf D.W. , Jin T. , and Bard A.J. , *Electrochemical and surface studies of carbon dioxide reduction to methane and ethylene at copper electrodes in aqueous solutions.* Journal of the Electrochemical Society, 1989. **136**: p. 1686-1691.
87. Cook R.L. , MacDuff R.C. , and Sammells A.F. , *Electrochemical reduction of carbon dioxide to methane at high current densities.* Journal of the Electrochemical Society, 1987. **134**(7): p. 1873-1874.
88. Bandi A. , et al., *CO_2 recycling for hydrogen storage and transportation-Electrochemical CO_2 removal and fixation.* Energy Conversion and Management, 1995. **36**(6-9): p. 899-902.
89. Stucki S. , Schuler A. , and Constantinescu M. , *Coupled CO_2 recovery from the atmosphere and water electrolysis: Feasibility of a new process for hydrogen storage.* International Journal of Hydrogen Energy, 1995. **20**(8): p. 653-663.

90. Lackner K.S. , *Capture of carbon dioxide from ambient air.* The European Physical Journal Special Topics, 2009. **176**(1): p. 93-106.
91. Mizuno T. , et al., *Electrochemical reduction of carbon dioxide at Ti and hydrogen-storing Ti electrodes in KOH-methanol.* Electrochimia Acta, 1998. **43**(8): p. 899-907.
92. Xia J. , et al., *Solubility of CO_2 in (CH_3OH+H_2O).* Journal of chemical & engineering data, 2004. **49**(6): p. 1756-1759.
93. Snuffin L.L. , Whaley L.W. , and Yu L. , *Catalytic electrochemical reduction of CO_2 in ionic liquid $EMIMBF_3Cl$.* Journal of the Electrochemical Society, 2011. **158**(9): p. F155-F158.
94. Rosen B.A. , et al., *Ionic liquid-mediated selective conversion of CO_2 to CO at low overpotentials*. 2011, University of Illinois: Urbana. p. 643-4.
95. Hu B. , Guild C. , and Suib S.L. , *Thermal, electrochemical, and photochemical conversion of CO_2 to fuels and value-added products.* Journal of CO_2 Utilization, 2013. **1**: p. 18-27.
96. Asadi M. , et al., *Robust carbon dioxide reduction on molybdenum disulphide edges.* Nature Communications, 2014. **5**.
97. Zhou F. , et al., *High selective electrocatalytic reduction of carbon dioxide to carbon monoxide on silver electrode with aqueous ionic liquids.* Electrochemistry Communications, 2014. **46**: p. 103-106.
98. Li C.W. and Kanan M.W. , *CO_2 reduction at low overpotential on Cu electrodes resulting from the reduction of thick Cu_2O films.* Journal of the American Chemical Society, 2012. **134**(17): p. 7231-4.
99. Zhang S. , Kang P. , and Meyer T.J. , *Nanostructured tin catalysts for selective electrochemical reduction of carbon dioxide to formate.* Journal of the American Chemical Society, 2014. **136**: p. 1734-7.
100. Kumar B. , et al., *Photochemical and photoelectrochemical reduction of CO_2.* Annual Review of Physical Chemistry, 2012. **63**: p. 541-69.
101. Thorson M.R. , Siil K.I. , and Kenis P. , *Effect of cations on the electrochemical conversion of CO_2 to CO.* Journal of the Electrochemical Society, 2013. **160**(1): p. F69-F74.
102. Paik W. , Andersen T.N. , and Eyring H. , *Kinetic studies of the electrolytic reduction of carbon dioxide on the mercury electrode.* Electrochimia Acta, 1969. **14**(12): p. 1217-32.

103. Hori Y. and Suzuki S. , *Electrolytic reduction of carbon dioxide at mercury electrode in aqueous solution.* Bulletin of the chemical Society of Japan, 1982. **55**(3): p. 660-665.
104. Spichiger-Ulmann M. and Augustynski J. , *Specific cation effect upon the cathodic reduction of bicarbonate anions at palladium.* Nouveau Journal de chimie, 1986. **10**: p. 487-491.
105. Murata A. and Hori Y. , *Product selectivity affected by cationic species in electrochemical reduction of CO_2 and CO at a Cu electrode.* The Chemical Society of Japan, 1991. **64**: p. 123-127.
106. Kyriacou G. and Anagnostopoulos A. , *Influence of CO_2 partial pressure and the supporting electroyte cations on the product distriution in CO_2 electroreduction.* Journal of Applied Electrochemistry, 1993. **23**(5): p. 483-486.
107. Kaneco S. , et al., *Electrochemical reduction of carbon dioxide to ethylene at a copper electrode in methanol using potassium hydroxide and rubidium hydroxide supporting electrolytes.* Electrochimia Acta, 2006. **51**: p. 3316-3321.
108. Verma S. , et al., *The effect of electrolyte composition on the electroreduction of CO_2 to CO on Ag based gas diffusion electrodes.* Physical Chemistry Chemical Physics, 2016. **18**: p. 7075-7084.
109. Zhong H. , Fujii K. , and Nakano Y. , *Effect of $KHCO_3$ concentration on electrochemical reduction of CO_2 on copper electrode.* Journal of the Electrochemical Society, 2017. **164**(9): p. F923-F927.
110. Jitaru M. , et al., *Electrochemical reduction of carbon dioxide on flat metallic cathodes.* Journal of Applied Electrochemistry, 1997. **27**: p. 875-89.
111. Cave E.R. , Kuhl K.P. , and jaramillo T. , *Surface modification of gold for CO_2 electrochemical reduction.* Meeting Abstract, The Electrochemical Society, 2011: p. 1503.
112. Mariano R.G. , et al., *Selective increase in CO_2 electroreduction activity at grain-boundary surface terminations.* Science, 2017. **358**: p. 1187-1192.
113. Feng J. , et al., *Grani-boundary-dependant CO_2 electroreduction activity.* Journal of the American Chemical Society, 2015. **137**(14): p. 4606-4609.
114. Choi S. , et al., *A comprehensive study of formic acid oxidation on palladium nanocrystals with different types of facets and twin defects.* ChemCatChem Catalysis, 2015. **7**: p. 2077-2084.

115. Sun X. , et al., *Crystalline control of 111 bounded Pt_3Cu nanocrystals: Multiply-twinned Pt_3Cu icosahedra with enhanced electrocatalytic properties.* ACS Nano, 2015. **9**: p. 7634-7640.
116. Huang X. , et al., *High density catalytic hot spots in ultrafine wavy nanowires.* Nano Letters, 2014. **14**: p. 3887-3894.
117. Wang C. , et al., *Creation of controllable high-density defects in silver nanowires for enhanced catalytic property.* Nano Letters, 2016. **16**: p. 5669-5674.
118. Min X. , Chen Y. , and Kanan M.W. , *Alkaline O_2 reduction on oxide-derived Au: high activity and 4e$^-$ selectivity without (100) facets.* Physical Chemistry Chemical Physics, 2014. **16**(27).
119. Li C.W. , Ciston J. , and Kanan M.W. , *Electroreduction of carbon monoxide to liquid fuel on oxide-derived nanocrystalline copper.* Nature, 2014. **508**(7497): p. 504-507.
120. Gsell M. , Jakob P. , and Menzel D. , *Effect of substrate strain on adsorption.* Science, 1998. **280**: p. 717-720.
121. Mavrikakis M. , Hammer B. , and Norskov J.K. , *Effect of strain on the reactivity of metal surfaces.* Physical Review Letters, 1998. **81**: p. 2819-2822.
122. Barth J.V. , et al., *Scanning tunneling microscopy observations on the reconstructed Au(111) surface: Atomic structure, long-range superstructure, rotational domains, and surface defects.* Physical Review B, 1990. **42**: p. 9307-9318.
123. Hansen H.A. , et al., *Understanding trends in the electrocatalytic activity of metals and enzymes for CO_2 reduction to CO.* The Journal of Physical Chemistry Letters, 2013. **4**(3): p. 388-392.
124. Kas R. , et al., *Electrochemical CO_2 reduction on Cu_2O-derived copper nanoparticles controlling the catalytic selectivity of hydrocarbons.* Physical Chemistry Chemical Physics, 2014. **16**(24): p. 12194-201.
125. Reske R. , et al., *Particle size effects in the catalytic electroreduction of CO_2 on Cu nanoparticles.* Journal of the American Chemical Society, 2014. **136**(19): p. 6978-86.
126. Sen S. , Liu D. , and Palmore G.T. , *Electrochemical reduction of CO_2 at copper nanofoams.* ACS Catalysis, 2014. **4**(9): p. 3091-5.
127. Tang W. , et al., *The importance of surface morphology in controlling the selectivity of polycrystalline copper for CO_2 electroreduction.* Physical Chemistry Chemical Physics, 2012. **14**: p. 76-81.
128. Liu M. , et al., *Enhanced Electrocatalytic CO_2 reduction via field-induced reagent concentration.* Nature, 2016. **537**: p. 382-386.

129. Mohamed R.M. , McKinney D.L. , and Sigmund W.M. , *Enhanced nanocatalysts.* Material Science and Engineering, 2012. **73**: p. 1-13.
130. Nur Hossain M. , et al., *Enhanced catalytic activity of nanoporous Au for the efficient electrochemical reduction of carbon dioxide.* Applied Catalysis B: Environmental, 2018. **236**: p. 483-489.
131. Lu Qi. , et al., *A selective and efficient electrocatalyst for carbon dioxide reduction.* Nature Communications, 2014. **5**.
132. Rosen J. , et al., *Mechanistic insights into the electrochemical reduction of CO_2 to CO on nanostructured Ag surfaces.* ACS Catalysis, 2015. **5**: p. 4293-4299.
133. Ma M. , Trzesniewski B.J. , and Smith W.A. , *Selective and efficient reduction of carbon dioxide to carbon monoxide on oxide-derived nanostructured silver electrocatalysts.* Angewandte Chemie International Edition, 2016. **55**: p. 9748-52.
134. Delacourt C. , Ridgway P.L. , and Newman J. , *Mathematical modeling of CO_2 reduction to CO in aqueous electrolytes. II. Study of an electrolysis cell making syngas ($CO + H_2$) from CO_2 and H_2O reduction at room temperature.* Journal of the Electrochemical Society, 2010. **157**(12): p. 1911-1926.
135. Chen W. and Chen S. , *Oxygen electroreduction catalyzed by gold nanoclusters: Strong core size effects.* Angewandte Chemie International Edition, 2009. **48**(24): p. 4386-4389.
136. Lu Y. and Chen W. , *Size effect of silver nanoclusters on their catalytic activity for oxygen electro-reduction.* Journal of Power Sources, 2012. **197**: p. 107-110.
137. Kwak K. , et al., *A molecule-like $PtAu_{24}(SC_6H_{13})$ nanocluster as an electrocatalyst for hydrogen production.* Nature Communications, 2017. **8**.
138. Zhao S. , et al., *Atomically precise gold nanoclusters accelerate hydrogen evolution over MoS_2 nanosheets: The Dual interfacial effect.* Small, 2017. **13**(43): p. 1-7.
139. Nursanto E.B. , et al., *Gold catalyst reactivity for CO_2 electro-reduction: From nano particle to layer.* Catalysis Today, 2016. **260**: p. 107-111.
140. Liu C. , et al., *Computational studies of electrochemical CO_2 reduction on subnanometer transition metal clusters.* Physical Chemistry Chemical Physics, 2014. **16**(48): p. 26584-26599.
141. Yang Y. , et al., *Fundamental studies of methanol synthesis from CO(2) hydrogenation on Cu(111), Cu clusters, and Cu/ZnO(0001).* Physical Chemistry Chemical Physics, 2010. **12**(33): p. 9909-9917.

142. Alfonso D. and Kauffman D.R. , *Assessment of trends in the electrochemical CO_2 reduction and H_2 evolution reactions on metal nanoparticles.* MRS Communications, 2017. **7**(3): p. 601-606.
143. Mistry H. , et al., *Exceptional size-dependen activity enhancement in the electroreduction of CO_2 over Au nanoparticles.* Journal of American Chemical Society, 2014. **136**(47): p. 16473-6.
144. Yamada Y. , et al., *Nanocrystal bilayer for tandem catalysis.* Nature Chemistry, 2011. **3**: p. 372-376.
145. Rolison D.R. , et al., *Role of hydrous ruthenium oxide in Pt−Ru direct methanol fuel cell anode electrocatalysts: The importance of mixed electron/proton conductivity.* Langmuir, 1999. **15**(3): p. 774-779.
146. Green I.X. , et al., *Spectroscopic observation of dual catalytic sites during oxidation of CO on a Au/TiO_2 catalyst.* Science, 2011. **333**: p. 736-739.
147. Diao P. , et al., *Electrocatalytic activity of supported gold nanoparticles toward CO oxidation: The perimeter effect of gold–support interface.* Electrochemistry Communications, 2010. **12**(11): p. 1622-1625.
148. Wang J. , et al., *In situ growth of gold nanoparticles on SiO_2/lanthanide–polyoxometalates composite spheres: An efficient catalytic and luminescent system.* Journal of Alloys and Compounds, 2015. **632**: p. 87-93.
149. Ballarin B. , et al., *RF-sputtering preparation of gold-nanoparticle-modified ITO electrodes for electrocatalytic applications.* Nanotechnology, 2011. **22**.
150. Fujiwara H. , et al., *Effect of surface structures on photocatalytic CO_2 reduction using quantized CdS nanocrystallites.* Journal of Physical Chemistry B, 1997. **101**(41): p. 8270-8278.
151. Ikeda S. , Takagi T. , and Ito K. , *Selective formation of formic acid, oxalic acid, and carbon monoxide by electrochemical reduction of CO_2.* Bulletin of the chemical Society of Japan, 1987. **60**: p. 2517-22.
152. Teeter T.E. and Rysselberghe P.V. , *Reduction of carbon dioxide on mercury electrodes.* The Journal of Chemical Physics, 1954. **22**(4).
153. Chaplin R.P.S. and Wragg A.A. , *Effects of process conditions and electrode material on reaction pathways for carbon dioxide electroreduction with particular reference to formate formation.* Journal of Applied Electrochemistry, 2003. **33**: p. 1107-23.
154. Hori Y. and Suzuki S. , *Electrolytic reduction of carbon dioxide at mercury electrode in aqueous solution.* The Chemical Society of Japan, 1982. **55**: p. 660-5.

155. Jordan J. and Smith P.T. , *Free-radical intermediate in the electroreduction of carbon dioxide.* Proceedings of the Chemical Society, 1960: p. 246-247.
156. Yoo J.S. , et al., *Theoretical insight into the trends that guide the electrochemical reduction of carbon dioxide to formic acid.* ChemSusChem, 2015. **9**(4): p. 358-363.
157. Peterson A.A. and Norskov J.K. , *Activity descriptors for CO_2 electroduction to methane on transition metal catalysts.* The Journal of Physical Chemistry Letters, 2012. **3**(2): p. 251-258.
158. Kortlever R. , et al., *Catalysts and reaction pathways for the electrochemical reduction of carbon dioxide.* The Journal of Physical Chemistry Letters, 2015. **6**: p. 4073-82.
159. Gattrell M. and Gupta N. , *A review of the aqueous electrochemical reduction of CO_2 to hydrocarbons at copper.* Journal of Electroanalytical Chemistry, 2006. **594**: p. 1-19.
160. Cook R.L. , MacDuff R.C. , and Sammells A.F. , *Evidence for formaldehyde, formic acid, and acetaldehyde as possible intermediates during electrochemical carbon dioxide reduction at copper.* Journal of the Electrochemical Society, 1989. **136**(7): p. 1982-1984.
161. Feaster J.T. , et al., *Understanding selectivity for the electrochemical reduction of carbon dioxide to formic acid and carbon monoxide on metal electrodes.* ACS Catalysis, 2017. **7**: p. 4822-4827.
162. Konig M. , et al., *Solvents and supporting electrolytes in the electrocatalytic reduction of CO_2.* iScience, 2019. **19**: p. 135-160.
163. Pourbaix M. , *Atlas of electrochemical equilibria in aqueous solutions*. 1966, New York: Pergamon press.
164. Gupta N. , Gattrell M. , and Macdougall B. , *Calculation for the cathode surface concentrations in the electrochemical reduction of CO_2 in $KHCO_3$ solutions.* Journal of Applied Electrochemistry, 2006. **36**: p. 161-172.
165. Innocent B. , et al., *FTIR spectroscopy study of the reduction of carbon dioxide on lead electrode in aqueous medium.* Applied Catalysis B: Environmental, 2010. **94**(3-4): p. 219-224.
166. Singh M.R. , et al., *Hydrolysis of electrolyte cations enhances the electrochemical reduction of CO_2 over Ag and Cu.* Journal of the American Chemical Society, 2016. **138**: p. 13006-12.

167. Singh M.R. , Clark E.L. , and Bill A.T. , *Effects of electrolyte, catalyst and membrane composition and operating conditions on the performance of solar-driven electrochemical reduction of carbon dioxide.* Physical Chemistry Chemical Physics, 2015. **17**: p. 18924-36.

168. Schouten K.J.P. , Gallent E.P. , and Koper M. , *The influence of pH on the reduction of CO and CO_2 to hydrocarbons on copper electrodes.* Journal of Electroanalytical Chemistry, 2014. **716**: p. 53-7.

169. Ooka H. , Figueiredo M.C. , and Koper M. , *Competition between hydrogen evolution and carbon dioxide reduction on copper electrodes in mildly acidic media.* Langmuir, 2017. **33**: p. 9307-13.

170. Hori Y. , et al., *Electrochemical reduction of CO at a copper electrode.* The Journal of Physical Chemistry B, 1997. **101**: p. 7075-81.

171. Raciti, D., Mao M. , and Wang C. , *Mass transport modeling for the electroreduction of CO_2 on Cu nanowires.* Nanotechnology, 2018. **29**(4): p. 1-10.

172. Raciti D. , et al., *Local pH effect in the CO_2 reduction reaction on high surface area copper electrocatalysts.* Journal of the Electrochemical Society, 2018. **165**(10): p. F799-F804.

173. Billy J.T. and Co A.C. , *Experimental parameters influencing hydrocarbon selectivity during the electrochemical conversion of CO_2.* ACS Catalysis, 2017. **7**: p. 8467-79.

174. Lim C.F.C. , Harrington D.A. , and Marshall A.T. , *Effects of mass transfer on the electrocatalytic CO_2 reduction on Cu.* Electrochimia Acta, 2017. **238**: p. 56-63.

175. *CRC handbook of chemistry and physics*. 90th Edition ed. 2010, Boca Raton, FL: CRC Press/Taylor and Francis.

176. Lim C.F.C. , *Electrochemical reduction of carbon dioxide on copper electrodes*, in *Chemical and Process Engineering*. 2017, University of Canterbury.

177. Wigley T.M.L. and Plummer L.N. , *Mixing of carbonate waters.* Geochimica et Cosmochimica Acta, 1976. **40**: p. 989-995.

178. Weisenberger S. and Schumpe A. , *Estimation of gas solubilities in salt solutions at temperatures from 273 K to 363 K.* AlChE Journal, 1996. **42**: p. 298-300.

179. Schumpe A. , *The estimation of gas solubilities in salt solutions.* Chemical Engineering Science, 1993. **48**: p. 153-158.

180. Butler J.N. , *Carbon dioxide equilibria and their applications*. 1991: Taylor & Francis.

181. Lee J. and Tak Y. , *Electrocatalytic activity of Cu electrode in electroreduction of CO_2.* Electrochimia Acta, 2001. **46**(19): p. 3015-3022.

182. Kaneco S. , et al., *Electrochemical reduction of carbon dioxide to hydrocarbons with high faradaic efficiency in LiOH/Methanol.* Journal of Physical Chemistry B, 1999. **103**(35): p. 7456-7460.

183. Engelbrecht A. , et al., *On the electrochemical CO_2 reduction at copper sheet electrodes with enhanced long-term stability by pulsed electrolysis.* Journal of the Electrochemical Society, 2018. **165**(15): p. J3059-J3068.

184. Lim C.F.C. , Harrington D.A. , and Marshall A.T. , *Altering the selectivity of galvanostatic CO_2 reduction on Cu cathodes by periodic cyclic voltammetry and potentiostatic steps.* Electrochimia Acta, 2016. **222**: p. 133-40.

185. McCrory C.C.L. , et al., *Benchmarking hydrogen evolutin reaction and oxygen evolving reaction electrocatalysts for solar water splitting devices.* Journal of the American Chemical Society, 2015. **137**(13): p. 4347-4357.

186. Hori Y. , et al., *Silver-coated ion exchange membrane electrode applied to electrochemical reduction of carbon dioxide.* Electrochimia Acta, 2003. **48**(18): p. 2651-2657.

187. Li Y.C. , et al., *Electrocatalysis of CO_2 to syngas in bipolar membrane-based electrochemical cells.* ACS Energy Letters, 2016. **1**(6): p. 1149-1153.

188. Oloman C. and Li H. , *Electrochemical process of carbon dioxide.* ChemSusChem, 2008. **1**.

189. Albo J. , et al., *Towards the electrochemical conversion of carbon dioxide into methanol.* Green Chemistry, 2015. **17**: p. 2304-24.

190. Bevilacqua M. , et al., *Recent technological progress in CO_2 electroreduction to fuels and energy carriers in aqueous environments.* Energy Technology, 2015. **3**(3): p. 197-210.

191. Merino-Garcia I., et al., *Electrochemical membrane reactors for the utilization of carbon dioxide.* Chemical Engineering Journal, 2016. **305**: p. 104-120.

192. Kondratenko E.V. , et al., *Status and perspectives of CO_2 conversion into fuels and chemicals by catalytic, photocatalytic and electrocatalytic processes.* Energy and Environmental Science, 2013. **6**(11): p. 3112-35.

193. Whipple D.T. , Finke E.C. , and Kenis P. , *Microfluidic reactor for the electrochemical reduction of carbon dioxide: The effect of pH.* Electrochemical and Solid-State Letters, 2010. **13**(9): p. B109-B111.

194. Innocent B. , et al., *Electro-reduction of carbon dioxide to formate on lead electrode in aqueous medium.* Journal of Applied Electrochemistry, 2009. **39**: p. 227-32.

195. Shironita S. , et al., *MEthanol generation by CO_2 reduction at a Pt-Ru/C electrocatalyst using a membrane electrode assembly.* Journal of Power Sources, 2013. **240**: p. 404-410.
196. Wu J.J. , et al., *Electrochemical reduction of carbon dioxide II. Design, Assembly, and performance of low temperature full electrochemical cells.* Journal of the Electrochemical Society, 2013. **160**(9): p. F953-F957.
197. Mistry H. , et al., *Turning catalytic selectivity at the mesoscale via interparticle interactions.* ACS Catalysis, 2016. **6**: p. 1075-80.
198. Kas R. , et al., *Three-dimensional porous hollow fibre copper electrodes for efficient and high-rate electrochemical carbon dioxide reduction.* Nature Communications, 2016. **7**: p. 10748.
199. Weng L.C. , Bell A.T. , and Weber A.Z. , *Modeling gas-diffusion electrodes for CO_2 reduction.* Physical Chemistry Chemical Physics, 2018. **4**: p. 317-324.
200. Li H. and Oloman C. , *Development of a continous reactor for the electro-reduction of carbon dioxide to formate.* Journal of Applied Electrochemistry, 2007. **37**(10): p. 1107-1117.
201. Ma S. , et al., *Silver supported on titania as an active catalyst for electrochemical carbon dioxide reduction.* ChemSusChem, 2014. **7**(3): p. 866-874.
202. Costentin C. , Drouet S. , and Robert M. , *A local proton source enhances CO_2 electroreduction to CO by a molecular Fe catalyst.* Science, 2012. **338**: p. 90-94.
203. Kedzierzawski P. and Augustynski J. , *Poisoning and activation of the gold cathode during electroduction of CO_2.* Journal of the Electrochemical Society, 1994. **141**: p. L58-L60.
204. Jo K. , Kang H.Y. , and Yang H. , *Enhancement of the electrocatalytic activity of gold nanoparticles via anodic treatment and the decrease of the enhanced activity with aging.* Bulletin of the Korean Chemical Society, 2011. **32**(2): p. 728-730.
205. Kostecki R. and Augustynski J. , *Electrochemical reduction of CO_2 at an activated silver electrode.* Berichte der Bunsengeselleschaft fur physikalische Chemie, 1994. **98**(12): p. 1510-1515.
206. Yano H. , et al., *Electrochemical reduction of CO_2 at three-phase (gas|liquid|solid) and two-phase (liquid|solid) interfaces on Ag electrodes.* Journal of Electroanalytical Chemistry, 2002. **533**: p. 113-8.

207. Kyriacou G. and Anagnostopoulos A. , *Electroreduction of CO_2 on differently prepared copper electrodes: The influence of electrode treatment on the current efficiencies.* Journal of Electroanalytical Chemistry, 1992. **322**: p. 233-246.
208. Hara K. , et al., *High efficiency electrochemical reduction of carbon dioxide under high pressure on a gas diffusion electrode conaining Pt catalysts.* Journal of the Electrochemical Society, 1995. **142**(4): p. L57-L59.
209. Schouten K.J.P. , et al., *A new mechanism for the selectivity to C1 and C2 species in the electrochemical reduction of carbon dioxide on copper electrodes.* Chemical Science, 2011. **2**: p. 1902-9.
210. Hori Y. , et al., *Deactivation of copper electrode in electrochemical reduction of CO_2.* Electrochimia Acta, 2005. **50**: p. 5354-60.
211. Hori Y. , et al., *Production of methane and ethylene in electrochemical reduction of carbon dioxide at copper electrode in aqueous hydrogencarbonate solution.* Chemistry Letters, 1986: p. 897-898.
212. Damaskin B. , Petri O.A. , and Batrakov V.V. , *Adsorption of organic compounds on electrodes*. 1971, New York: Plenum Press.
213. Shiratsuchi R. , Aikoh Y. , and Nogami G. , *Pulsed electroreduction of CO_2 on copper electrodes.* Journal of the Electrochemical Society, 1993. **140**(12): p. 3479-82.
214. Yano H. , et al., *Efficient electrochemical conversion of CO_2 to CO, C_2H_4, and CH_4 at a three-phase interface on a Cu net electrode in acidic sloution.* Journal of Electroanalytical Chemistry, 2002. **519**(1-2): p. 93-100.
215. Xie J.F. , et al., *Efficient electrochemical CO_2 reduction on a unique chrysanthemum like Cu nanoflower electrode and direct observation of carbon deposition.* Electrochimia Acta, 2014. **139**: p. 137-144.
216. Cook R.L. , MacDuff R.C. , and Sammells A.F. , *On the electrochemical reduction of carbon dioxide at In Situ electrodeposited copper.* Journal of the Electrochemical Society, 1988. **135**(6): p. 1320-1326.
217. Zhang S. , et al., *Polyethylenimine-enhanced electrocatalytic reduction of CO_2 to dormat at nitrogen-doped carbon nanomaterials.* Journal of the American Chemical Society, 2014. **136**: p. 7845-7848.
218. Yang N. , Waldvoget S.R. , and Jiang X. , *Electrochemistry of carbon dioxide on carbon electrodes.* ACS Applied Materials & Interfaces, 2016. **8**(42): p. 28357-28371.
219. Wu J.J. , et al., *Achieving high efficient, selective, and stable CO_2 reduction on nitrogen-doped carbon nanotubes.* ACS Nano, 2015. **9**(5): p. 5364-5371.

220. Jermann B. and Augustynski J. , *Long-term activation of the copper cathode in the course of CO_2 reduction.* Electrochimia Acta, 1994. **39**: p. 1891-1896.
221. Batista E.A. and Temperini M.L. , *Spectroscopic evidences of the presence of hydrogenated species on the surface of copper during CO_2 electroreduction at low cathodic potentials.* Journal of Electroanalytical Chemistry, 2009. **629**: p. 158-163.
222. Wuttig A. and Surendranath Y. , *Impurity ion complexation enhances carbon dioxide reduction catalysis.* ACS Catalysis, 2015. **5**: p. 4479-84.
223. Shiratsuchi R. , Ishimaru S. , and Nogami G. , *Effects of surface structures of Au electrodes on the pulsed electroreduction of CO_2.* Denki Kagaku, 1997. **668-70**.
224. Friebe P. , et al., *A real-time mass spectroscopy study of the (electro)chemical factors affecting CO_2 reduction at copper.* Journal of Catalysis, 1997. **168**: p. 374-385.
225. Terunuma Y. , Saitoh A. , and Momose Y. , *Relationship between hydrocarbon production in the electrochemical reduction of CO_2 and the characteristics of the Cu electrodes.* Journal of Electroanalytical Chemistry, 1997. **434**: p. 69-75.
226. Kumar B. , et al., *Controlling the product syngas H_2:CO ratio through pulsed-bias electrochemical reduction of CO_2 on copper.* ACS Catalysis, 2016. **6**(7): p. 4739-4745.
227. Hoogvliet J.C. , et al., *Electrochemical pretreatment of polycrystalline gold electrodes to produce reproducible surface roughness for self-assembly.* Analytical Chemistry, 2000. **72**: p. 2016-2021.
228. Yano J. , et al., *Selective ethyene formation by pulse-mode electrochemical reduction of carbon dioxide using copper and copper-oxide electrodes.* Journal of Solid State Electrochemistry, 2006. **11**(4): p. 554-557.
229. Yano J. and Yamasaki S. , *Pulse-mode electrochemical reduction of carbon dioxide using copper and copper oxide electrodes for selective ethylene formation.* Journal of Applied Electrochemistry, 2008. **38**(12): p. 1721-1726.
230. Nogami G. , Itagaki H. , and Shiratsuchi R. , *Pulsed electroreduction of CO_2 on copper electrodes-II.* Journal of the Electrochemical Society, 1994. **141**(5): p. 1138-1142.
231. Shiratsuchi R. and Nogami G. , *Pulsed electroreduction of CO_2 on silver electrodes.* Journal of the Electrochemical Society, 1996. **143**(2): p. 582-586.
232. Pander J.E. , Ren D. , and Yeo B.S. , *Practices for the collection and reporting of electrocatalytic performance and mechanistic information for the CO_2 reduction reaction.* Catalysis Science & Technology, 2017.

233. Adams R.N. , *Electrochemistry at solid electrodes*. 1969, New York, USA: Marcel dekker INC.
234. Ranganathan S. , Kuo T.C. , and McCreery R.L. , *Facile preparation of active glassy carbon electrodes with activated carbon and organic solvents.* Analytical Chemistry, 1999. **71**(16): p. 3574-3580.
235. Zhong H. , et al., *effect of CO_2 bubbling into aqueous solutions used for electrochemical reduction of CO_2 for energy conversion and storage.* The Journal of Physical Chemistry, 2014. **119**: p. 55-61.
236. Lu Z. , et al., *State of water in perflurosulfonic ionomer (Nafion 117) proton exchange membrane.* Journal of the Electrochemical Society, 2008. **155**(2): p. B163-B171.
237. Ticianelli E.A. , et al., *Methods to advance technology of proton exchange membrane fuel cells.* Journal of the Electrochemical Society, 1988. **135**: p. 2209-14.
238. Amjadi M. , et al., *Preparation, characterization and cell performance of durable nafion/SiO_2 hybrid membrane for high-temperature polymeric fuel cells.* Journal of Power Sources, 2012. **210**: p. 350-7.
239. Kissinger P. and Heineman W.R. , *Laboratory techniques in electroanalytical chemistry*, ed. n. Edition. 1996: Marcel Dekker.
240. Janz G.J. and Taniguchi H. , *The silver-silver halide electrodes. Preparation, stability, and standard potentials in aqueous and non-aqueous media.* Chemical Reviews, 1953. **53**(3): p. 397-437.
241. Elgrishi N. , et al., *A practical beginner's guide to cyclic voltammetry.* Journal of Chemical Education, 2018. **95**: p. 197-206.
242. Kissinger P. and Heineman W.R. , *Cyclic voltammetry.* Journal of Chemical Education, 1983. **60**(9): p. 702-6.
243. Paulus U.A. , et al., *Oxygen reduction on a high surface area Pt/Vulcan carbon catalyst: a thin-film rotating ring-disk electrode study.* Journal of Electroanalytical Chemistry, 2001. **495**(2): p. 134-145.
244. Fernandez P.S. , et al., *Platinum nanoparticles produced by EG/PVP method: The effect of cleaning on the electro-oxidation of glycerol.* Electrochimia Acta, 2013. **98**: p. 25-31.
245. Hoare J.P. , *A cyclic voltammetric study of the gold-oxygen system.* Journal of the Electrochemical Society, 1984. **131**(8): p. 1808-1815.
246. Pozio A. , et al., *Comparison of high surface Pt/C catalyst by cyclic voltammetry.* Journal of Power Sources, 2002. **105**(1): p. 13-19.

247. Hayden B.E. , et al., *CO oxidation on gold in acidic environments: particle size and substrate effects.* The Journal of Physical Chemistry C, 2007. **111**(45): p. 17044-17051.
248. Wang J. , *Analytical electrochemistry*, ed. S. edition. 1948, New York: Wiley-VCH.
249. Cherevko S. , et al., *Gold dissolution: towards understanding of noble metal corrosion.* Journal of Royal Society of Chemistry, 2013. **3**: p. 16516-27.
250. Cherevko S. , et al., *A comparison study on gold and platinum dissolution in acidic and alkaline media.* Journal of the Electrochemical Society, 2014. **161**: p. H822-H830.
251. Rodriguez P. and Koper M. , *Electrolysis on gold.* Physical Chemistry Chemical Physics, 2014. **16**: p. 13583-94.
252. Bard A.J. and Faulkner L.R. , *Electrochemical methods: fundamentals and applications*. 2nd ed. ed. 2001, New Yourk: John Wiley.
253. Baldhoff T. , *Electrochemical micromachining of aluminium for microfluidic devices*, in *Chemical and Process Engineering Department*. 2018, University of Canterbury: Christchurch, New Zealand.
254. Rieger P.H. , *Electrochemistry*, ed. n. Eddition. 1994, Dordrecht: Springer.
255. Hong J. , et al., *Photocatalytic reduction of CO_2 : a brief review on product analysis and systematic methods.* Analytical Methods, 2013. **5**: p. 1086-1097.
256. Pavia D.L . *Introduction to organic laboratory techniques: a small-scale approach*, ed. n. Eddition. 2005: Thomson/Brooks/Cole.
257. Berezkin V.G. , Alishoyev V.R. , and Nemirovskaya I.B. , *Basic principles of gas chromatography.* Journal of Chromatography Library, 1977. **10**: p. 1-31.
258. Guiichon G. and Guillemin C.L. , *Methodology detectors for gas chromatography.* Journal of Chromatography Library, 1988. **42**: p. 393-480.
259. Clark E.L. , et al., *Differential electrochemical mass spectrometer cell design for online quantification of products produced during electrochemical reduction of CO_2.* Analytical Chemistry, 2015. **87**(15): p. 8013-8020.
260. Dong M.W. , *Modern HPLC for practicing scientists*. 2006: John Wiley & Sons.
261. Lam B. and Simpson A.J. , *Direct H NMR spectroscopy of dissolved organic matter in natural waters.* Analyst, 2008. **133**(2): p. 263-269.
262. Fulmer G.R. , et al., *NMR chemical shifts of trace impurities: Common laboratory solvents, organic, and gases in deuterated solvents relevant to the organometallic chemist.* Organometallics, 2010. **29**(9): p. 2176-2179.

263. Bertheussen E. , et al., *Acetaldehyde as an intermediate in the electroreduction of carbon monoxide to ethanol on oxide-derived copper*. Angewandte Chemie, 2015. **128**(4): p. 1472-1476.
264. Qiao J. , Liu Y. , and Zhang J. , *Electrochemical reduction of carbon dioxide: Fundametals and technologies*. Electrochemical Energy Storage and Conversion. 2016: CRC Press.
265. Marshall A.T. , et al., *Experimental consideration for electrocatalytic CO_2 reduction.* ECS Transactions, 2017. **80**(10): p. 1191-1201.
266. Jovanov Z.P. , *Towards synthetic fuels via electrolysis*, in *Department of Physics*. 2014, Technical University of Denmark.
267. Varela A.S. , *Catalysis of CO_2 electro-reduction and related processes*, in *Department of Physics*. 2013, Technical University of Denmark.
268. Rand D.A.J. and Woods R. , *A study of the dissolution of platinum, palladium, rhodium and gold electrodes in 1 M sulphuric acid by cyclic voltammetry.* Journal of Electroanalytical Chemistry and Interfacial Electrochemistry, 1972. **35**(1): p. 209-18.
269. Icenhower D.E. , Urbach H.B. , and Harrison J.H. , *Use of the potential-step method to measure surface oxides.* Journal of the Electrochemical Society, 1970. **117**(2): p. 1500-1506.
270. Bonewitz R.A. and Schmid G. , *Oxygen adsorption on gold and the Ce(III)/Ce(IV) reaction.* Journal of the Electrochemical Society, 1970. **172**(11): p. 1367-1372.
271. Rand D.A.J. and Woods R. , *The nature of adsorbed oxygen on rhodium, palladium and gold electrodes.* Journal of Electroanalytical Chemistry and Interfacial Electrochemistry, 1971. **31**(1): p. 29-38.
272. Capan A. and Parsons R. , *The effect of strong acid on the reactions of hydrogen and oxygen on the noble metals. A study of using cyclic voltammetry and a new teflon electrode holder*. Journal of Electroanalytical Chemistry and Interfacial Electrochemistry, 1972. **39**(2): p. 275-286.
273. Laitinen H.A. and Chao M.S. , *The anodic surface oxidation of gold.* Journal of the Electrochemical Society, 1961. **108**(8): p. 726-731.
274. Brummer S.B. and Makrides A.C. , *Surface oxidation of gold electrodes.* Journal of the Electrochemical Society, 1964. **111**: p. 1122-8.
275. Takamura T. , et al., *Specular reflection studies of gold electrodes in situ.* Journal of the Electrochemical Society, 1970. **117**(5): p. 626-630.

276. A.J., B., *Electroanalytical Chemistry: a Series of Advances*. Vol. 9. 1976, New York: Marcel Dekker.
277. Mac Arthur D.M. , *A study of gold reduction and oxidation in aqueous solutions.* Journal of the Electrochemical Society, 1972. **119**(6): p. 672-677.
278. Wang Y. , et al., *Activation effect of electrochemical cycling on gold nanoparticles toward the hydrogen evolution reaction in sulfuric acid.* Electrochimia Acta, 2016. **209**: p. 440-7.
279. Rand D.A.J. and Woods R. , *Electrosorption characteristics of thin layers of noble metals electrodeposited on different noble metal substrates.* Journal of Electroanalytical Chemistry and Interfacial Electrochemistry, 1973. **44**(1): p. 83-89.
280. Angerstein H. , Conway B.E. , and Stoicoviciu L. , *Elementary steps of electrochemical oxidation of single-crystal planes of Au-I. Chemical basis of processes involving geometry of anions and the electrode surfaces.* Electrochimia Acta, 1986. **31**(8): p. 1051-1061.
281. Chen Y. , et al., *Electrochemical impedimetric biosensor based on a nanostructured polycarbonate substrate.* International Journal of Nanomedicine, 2012. **7**: p. 133-140.
282. Burke L.D. and Nugent P.F. , *The electrochemistry of gold: The redox behaviour of the metal in aqueous media.* Gold Bulletin, 1997. **30**(2): p. 43-53.
283. Santos M.C. , Mascaro L.H. , and Machado S.A.S. , *Voltammetric and rotating ring-disk studies of underpotential deposition of Ag and Cu on polycrystalline Au electrodes in aqueous H_2SO_4.* Electrochimia Acta, 1998. **43**(16-17): p. 2263-2272.
284. Chen Z. , et al., *Electrochemical impedance spectroscopy detection of iysozyme based on electrodeposited gold nanoparticles.* Talanta, 2011. **83**(5): p. 1501-1506.
285. Bott-Neto J.L. , et al., *Au/C catalysts prepared by a green method towards C3 alcohol electrooxidation: A cyclic voltammetry and in situ FTIR spectroscopy study.* Journal of Electroanalytical Chemistry, 2014. **735**(57-62).
286. Padayachee D. , et al., *Influence of particle size on the electrocatalytic oxidation of glycerol over carbon-supported gold nanoparticles.* Electrochimia Acta, 2014. **120**: p. 398-407.
287. Chowdhury A.N. , et al., *Fabrication of Au(111) facet enriched electrode on glassy carbon.* Journal of Electroanalytical Chemistry, 2009. **634**(1): p. 35-41.
288. Yancey D.F. , Carino E.V. , and Crooks R.M. , *Electrochemical synthesis and electrocatalytic properties of Au@Pt dendrimer-encapsulated nanoparticles.* Journal of the American Chemical Society, 2010. **132**(32): p. 10988-10989.

289. Trasatti S. and Petri O.A. , *Real surface area measurements in electrochemistry* Pure & Applied Chemistry, 1991. **63**: p. 711-734.
290. Carvalhal R.F. , Freire R.S. , and Kubota L.T. , *Polycrystalline gold electrodes: A comparative study of pretreatment procedure used for cleaning and thiol self-assembly monolayer formation.* Electroanalysis Journal, 2005. **17**(14): p. 1251-1259.
291. Nagaraju D.H. and Lakshminarayanan V. , *Electrochemically grown mesoporous gold film as high surface area material for electro-oxidation of alcohol in alkaline medium.* The Journal of Physical Chemistry C, 2009. **113**(33): p. 14922-14926.
292. Oesch U. and Janata J. , *Electrochemical study of gold electrodes with anodic oxide films. Formation and reduction behaviour of anodic oxides on gold.* Electrochimia Acta, 1983. **28**(9): p. 1237-1246.
293. Finot M.O. , Braybrook G.D. , and McDermott M.T. , *Characterization of electrochemically deposited gold nanocrystals on glassy carbon electrodes.* Journal of Electroanalytical Chemistry, 1999. **466**(2): p. 234-241.
294. Kumar S. and Zou S. , *Electrooxidation of carbon monoxide on gold nanoparticles ensemble electrodes: effects of particle coverage.* The Journal of Physical Chemistry C, 2005. **109**(33): p. 15707-15713.
295. Kesavan S. and John S.A. , *Spontaneous grafting: A novel approach to graft diazonium cations on gold nanoparticles in aqueous medium and their self-assembly on electrodes.* Journal of Colloid and Interface Science, 2014. **428**: p. 84-94.
296. Park J.E. , Momma T. , and Osaka T. , *Spectroelectrochemical phenomena on surface plasmon resonance of Au nanoparticles immobilized on transparent electrode.* Electrochimia Acta, 2007. **52**(19): p. 5914-5923.
297. Sezgin S. , et al., *Scan rate effect of 1-4-methoxyphenyl-1H-Pyrrole electro-coated on Carbon fiber.* International Journal of Electrochemical Science, 2012. **7**: p. 1093-1106.
298. Liu T. , et al., *Newly reduced graphene oxide/gold oxide neural-chemical interface on multi-channel neural probes to enhance the electrochemical properties for biosensors.* RCS Advances, 2016. **6**(33): p. 27614-27622.
299. Saveant J.M. , *Elements of molecular and biomolecular electrochemistry: An electrochemical approach to electron transfer chemistry*. 2006, Hoboken, NJ: John & Wiley & Sons.

300. Valenti M. , et al., *Suppressing H_2 evolution and promoting selective CO_2 electroreduction to CO at low overpotentials by alloying Au with Pd.* ACS Catalysis, 2019. **9**: p. 3527-3536.
301. Kuhl K.P. , et al., *Electrocatalytic conversion of carbon dioxide to methane and methanol on transition metal surfaces.* Journal of the American Chemical Society, 2014. **136**(40): p. 14107-14113.
302. Kas R. , et al., *Manipulating the hydrocarbon selectivity of copper nanoparticles in CO_2 electroreduction by process conditions.* Chemelectrochem Communications, 2015. **2**: p. 354-358.
303. Ren D. , et al., *Selective electrochemical reduction of carbon dioxide to ethylene and ethanol on copper(I) oxide catalysts.* ACS Catalysis, 2015. **5**(5): p. 2814-2821.
304. Huang Y. , et al., *Electrochemical reduction of CO_2 using copper single-crystal surfaces: Effects of CO* coverage on the selective formation of ethylene.* ACS Catalysis, 2017. **7**(3): p. 1749-1756.
305. Ren D. , Ang B.S. , and Yeo B.S. , *Tuning the selectivity of carbon dioxide electroreduction toward ethanol on oxide-derived Cu_xZn catalysts.* ACS Catalysis, 2016. **6**(12): p. 8239-8247.
306. Pan H. , et al., *Semiconductor photocatalysis of bicarbonate to solar fuels: formate production from copper(I) oxide.* ACS Sustainable Chemistry and Engineering, 2018. **6**: p. 1872-1880.
307. Samjeske G. , et al., *Mechanistic study of electrocatalytic oxidation of formic acid at platinum in acidic solution by time-resolved surface-enhanced infrared absorption spectroscopy.* Journal of Physical Chemistry, 2006. **110**: p. 16559-16566.
308. Beden B. , Bewick A. , and Lamy C. , *A study by electrochemically modulated infrared reflectanc spectroscopy of the electrosorption of formic acid at a platinum electrode.* Journal of Electroanalytical Chemistry, 1983. **148**(1): p. 147-160.
309. Lovie J.D. , et al., *Formic acid oxidation at Platinum-Bismuth clusters.* Journal of the Electrochemical Society, 2014. **161**(9): p. H547-H554.
310. Perales-Rondon J.V. , et al., *Further insights into the formic acid oxidation mechanism on Platinum: pH and anion adsorption effects.* Electrochimia Acta, 2015. **180**: p. 479-485.
311. Benson E.E. , et al., *Electrocatalytic and homogeneous approaches to conversion of CO_2 to liquid fuels.* Chemical Society Reviews 2009. **38**(1): p. 89-99.

312. Dubois M.R. and Dubois D.L. , *Development of molecular electrocatalysts for CO_2 reduction and H_2 production/oxidation.* Accounts of Chemical Research, 2009. **42**(12): p. 1974-82.
313. Augustynski J. , Kedzierzawski P. , and Jermann B. , *Electrochemical reduction of CO_2 at metallic electrodes.* Studies in Surface Science and Catalysis, 1998. **114**: p. 107-116.
314. Dunwell M. , et al., *The central role of bicarbonate in the electrochemical reduction of carbon dioxide on gold.* Journal of the American Chemical Society, 2017. **139**(10): p. 3774-83.
315. Wasmus S. , Cattaneo E. , and Vielstich W. , *Reduction of carbon dioxide to methane and ethane- an online MS study with rotating electrodes.* Electrochimia Acta, 1990. **35**(4): p. 771-5.
316. Cherevko S. , et al., *Electrochemical dissolution of gold in acidic medium.* Electrochemistry Communications, 2013. **28**: p. 44-6.
317. Cruickshank A.C. and Downard A.J. , *Electrochemical stability of citrate-capped gold nanoparticles electrostatically assembled on amine-modified glassy carbon.* Electrochimia Acta, 2009. **54**: p. 5566-70.
318. Steven J.T. , et al., *Electrochemical stability of carbon-supported gold nanoparticles in acidic electrolyte during cyclic voltammetry*. Electrochimia Acta, 2016. **187**: p. 593-604.
319. Wang Y. , et al., *Surface oxidation of gold nanoparticles supported on a glassy carbon electrode in sulphuric acid ,edium: contrasts with the behaviour of macro gold.* Physical Chemistry Chemical Physics Communications, 2013. **15**.
320. Kodama K. , et al., *Electrochemical observation of high oxophilicity and its effect on oxygen reduction reaction activity of Au clusters Mass-Selectively deposited on glassy carbon.* Electrocatalysis, 2018: p. 1-9.
321. Noda H. , et al., *Kinetics of electrochemical reduction of carbon dioxide on a gold electrode in phosphate buffer solutions.* Bulletin of the chemical Society of Japan, 1995. **68**(7): p. 1889-95.
322. Wu J.J. , Sun sh. , and Zhou X.D. , *Origin of the performance degradation and implementation of stable tin electrodes for the conversion of CO_2 to fuels.* Nano Energy, 2016. **27**: p. 225-9.

323. Azuma, M., et al., *Electrochemical Reduction of Carbon-Dioxide on Various Metal-Electrodes in Low-Temperature Aqueous $KHCO_3$ Media.* Journal of the Electrochemical Society, 1990. **137**(6): p. 1772-1778.
324. Rodriguez P. , Koverga A. , and Koper M. , *Carbon monoxide as a promoter for its own oxidation on a gold electrode.* Angewandte Chemie International Edition, 2010. **49**: p. 1241-3.
325. Edens G.J. , Hamelin A. , and Weaver M.J. , *Mechanism of carbon monoxide electrooxidation on monocrystalline gold surfaces: Identification of a hydroxycarbonyl intermediate.* Journal of Physical Chemistry, 1996. **100**: p. 2322-2329.
326. Patel H.C. , et al., *Oxidation of H_2, CO and syngas mixtures on ceria and nickel pattern anodes.* Applied Energy, 2015. **154**: p. 912-20.
327. Taleshi Ahangari H. , Portail T. , and Marshall A.T. , *Comparing the electrocatalytic reduction of CO_2 to CO on gold cathodes in batch and continuous flow cells* Electrochemistry Communications, 2019. **101**: p. 78-81.
328. Centi G. , et al., *Electrocatalytic conversion of CO_2 to long carbon-chain hydrocarbons.* Green Chemistry, 2007. **9**(6): p. 671-8.
329. Ho Y. and Suzuki S. , *Electrolytic reduction of carbon dioxide at mercury electrode in aqueous solution.* The Chemical Society of Japan, 1982. **55**: p. 660-5.
330. Frese J.K.W. and Leach S. , *Electrochemical reduction of carbon dioxide to methane, methanol and CO on Ru electrodes.* Journal of the Electrochemical Society, 1985. **132**: p. 259-260.
331. Kumar R.S. , Kumar S.S. , and Kulandainathan M.A. , *Highly selective electrochemical reduction of carbon dioxide using Cu based metal organic framework as an electrocatalyst.* Electrochemistry Communications, 2012. **25**: p. 70-73.
332. Nguyen D.T. , et al., *Selective CO_2 reduction on zinc electrocatalyst: The effect of zinc oxidation state induced by pretreatment environment.* ACS Sustainable Chemistry and Engineering, 2017. **5**(12): p. 11377-11386.
333. Feng X. , et al., *Grain-Boundry-Dependent CO_2 electroreduction activity.* Journal of American Chemical Society, 2015. **137**(14): p. 4606-4609.
334. Wu J.J. , et al., *Electrochemical reduction of carbon dioxide: Effects of the electrolyte on the selectivity and activity with Sn electrode.* Journal of the Electrochemical Society, 2012. **159**(7): p. F-353-F359.

335. Summers D.P. and Frese J.K.W. , *Electrochemical reduction of carbon dioxide. Characterization of the formation of methane at ruthenium electrodes in carbon dioxide saturated aqueous solution.* Langmuir, 1988. **4**(1): p. 51-57.

336. Kim B. , et al., *Effects of composition of the micro porous layer and the substrate on performance in the electrochemical reduction of CO_2 to CO.* Journal of Power Sources, 2016. **312**: p. 192-198.

337. Woods R. , *Chemisorption at electrodes*, in *Electroanalytical chemistry: a series of advances*. 1976, Dekker: New York. p. 1-162.

338. Dutta A. , et al., *Morphology matters: Tuning the product distribution of CO_2 electroreduction on oxide-derived Cu foam catalysts.* ACS Catalysis, 2016. **6**: p. 3804-3814.

339. Arakawa H. , et al., *Catalysis Research of relevance to carbon management: Progress, challenges, and opportunities.* Chemical Reviews, 2001. **101**(4): p. 953-996.

340. Xiaoding X. and Moulijin J.A. , *Mitigation of CO_2 by chemical conversion: Plausible chemical reactions and promising products.* Energy and Fuels, 1996. **10**(2): p. 305-325.

341. Li K. , Peng B. , and Peng T. , *Recent advances in heterogenous photocatalytic CO_2 conversion to solar fuels.* ACS Catalysis, 2016. **6**(11): p. 7485-7527.

342. Rasul S. , et al., *A highly selective copper-indium bimetallic electrocatalyst for the electrochemical reduction of aqueous CO_2 to CO.* Angewandte Chemie international Edition 2014. **54**(7): p. 2146-2150.

343. Yang Y. , et al., *Efficient nanomaterials for harving clean fuels from electrochemical and photoelectrochemical CO_2 reduction.* Sustainable Energy and Fuels, 2018. **2**(3): p. 510-537.

344. Cave E.R. , et al., *Trends in the catalytic activity of hydrogen evolution during CO_2 electroreduction on transition Metals.* ACS Catalysis, 2018. **8**(4): p. 3035-3040.

345. Lu Qi. and Jiao F. , *Electrochemical CO_2 reduction: Electrocatalyst, reaction mechanism, and process engineering.* Nano Energy, 2016. **29**: p. 439-456.

346. Mistry H. , et al., *Exceptional size-dependent activity enhancement in the electroreduction of CO_2 over Au nanoparticles.* Journal of the American Chemical Society, 2014. **136**(47): p. 16473-16474.

347. Liu S. , et al., *Shape-dependent electrocatalytic reduction of CO_2 to CO on triangular silver nanoplates.* Journal of the American Chemical Society, 2017. **139**(6): p. 2160-2163.

348. Huang H. , et al., *Understanding of strain effects in the electrochemical reduction of CO_2: Using Pd nanostructures as an ideal platform.* Angewandte Chemie International Edition, 2017. **56**(13): p. 3594-3598.
349. Jin R. , et al., *Atomically precise colloidal metal nanoclusters and nanoparticles: Fundamentals and opportunities.* Chemical Reviews, 2016. **116**(18): p. 10346-10413.
350. Tyo E.C. and Vajda S. , *Catalysis by clusters with precise number of atoms.* Nature Nanotechnology, 2015. **10**(7): p. 577-588.
351. Liu C. , et al., *Carbon dioxide conversion to methanol over size-selected Cu_4 clusters at low pressures.* Journal of the American Chemical Society, 2015. **137**(27): p. 8676-8679.
352. Yang B. , et al., *Copper cluster size effect in methanol synthesis from CO_2.* The Journal of Physical Chemistry C, 2017. **121**(19): p. 10406-10412.
353. Xiao F.X. , et al., *Metal-cluster decorated TiO_2 nanotube arrays: A composite heterostructure toward versatile photocatalytic and photoelectrochemical applications.* Small, 2015. **11**(5): p. 554-567.
354. Alfonso D. , Kauffman D.R. , and Matranga C. , *Active sites of ligands-protected Au_{25} nanoparticle catalysts for CO_2 electroreduction to CO.* The Journal of Chemical Physics, 2016. **144**(18).
355. Austin N. , et al., *Elucifating the active sites for CO_2 electroreduction on ligand-protected Au_{25} nanoclusters.* Catalysis Science & Technology, 2018. **8**(15): p. 3795-3805.
356. Anderson D.P. , et al., *Chemically-synthesised, atomically-precise gold clusters deposited and activated on titania.* Physical Chemistry Chemical Physics, 2013. **15**(11): p. 3917-3929.
357. Asami K. , *A precisely consistent energy calibration method for X-ray photoelectron spectroscopy.* Journal of Electron Spectroscopy and Related Phenomena, 1976. **9**(5): p. 469-478.
358. Buttner M. and Oelhafen P. , *XPS study on the evaporation of gold submonolayers on carbon surfaces.* Surface Science, 2006. **600**(5): p. 1170-1177.
359. Kitsudo Y. , et al., *Final state effect for Au 4f line from gold-nano-particles grown on oxides and HOPG supports.* Surface Science, 2009. **603**(13): p. 2108-2114.
360. Turner S.M. , et al., *Selective oxidation with dioxygen by gold nanoparticle catalysts derived from 55-atom clusters.* Nature, 2008. **454**(7207): p. 981-983.

361. DiCenzo S.B. , Berry S.D. , and Hatford E.H. , *Photoelectron spectroscopy of single-size Au clusters collected on a substrate.* Physical Review B, 1988. **38**(12): p. 8465-8468.
362. Peters S. , et al., *Size-dependent XPS spectra of small supported Au-clusters.* Surface Science, 2013. **608**: p. 129-134.
363. Zhao S. , Jin R. , and Jin R. , *Opportunities and challenges in CO_2 reduction by gold- and silver-based electrocatalysts: From bulk metals to nanoparticles and atomically precise nanoclusters.* ACS Energy Letters, 2018. **3**: p. 452-462.
364. Conway B.E. , *Electrochemical oxide film formation at noble metals as a surfacechemical process.* Progress in Surface Sience, 1995. **49**(4): p. 331-452.
365. Lan Y. , et al., *Electrochemical reduction of carbon dioxide on Cu/CuO core/shell catalysts.* Chemelectrochem, 2014. **1**: p. 1577-1582.
366. Kauffman D.R. , et al., *Efficient electrochemical CO_2 conversion powered renewable energy.* ACS Applied Materials & Interfaces, 2015. **7**: p. 15626-15632.
367. kauffman D.R. , et al., *Probing active site chemistry with differently charged Au_{25} nanoclusters.* Chemical Science, 2014. **5**(8): p. 3151-3157.
368. Manthiram K. , Beberwyck B.J. , and Alivisatos A.P. , *Enhanced electrochemical methanation of carbon dioxide with a dispersible nanoscale copper catalyst.* Journal of the American Chemical Society, 2014. **136**(38): p. 13319-13325.
369. Currell G. and Dowman A. , *Essential mathematics and statistics for science*, ed. n. Eddition. 2009: Wiley-Blackwell.
370. Brauer G. , *Handbook of preparative inorganic chemistry*. 2nd eddition ed. Vol. 1. 1963.
371. Uson R. , et al., *Tetrahydrothiophene gold(I) or gold(III) complexes.* Inorganic Syntheses, 1989. **26**: p. 85-91.
372. Brandys M.C. , Jennings M. , and Puddephatt R.J. , *Luminescent gold(I) macrocycles with diphosphine and 4,4'-bipyridyl ligands.* Journal of the Chemical Society, Dalton Transactions, 2000. **2000**(24): p. 4601-4606.
373. Van der Velden J.W.A. , et al., *Gold clusters. Tetrakis[1,3-bis(diphenylphosphino)propane]hexagold dinitrate: preparation, x-ray analysis, and gold-197 Moessbauer and phosphorus-31{proton} NMR spectra.* Inorganic Chemistry, 1982. **21**(12): p. 4321-4324.

374. Shichibu Y. and Konishi K. , *HCl Induced nuclearity convergence in diphosphine protected ultrasmall gold clusters: A novel synthetic route to "Magic Number" Au_{13} clusters.* Small, 2010. **6**(11): p. 1216-1220.

375. Weare W.W. , et al., *Improved synthesis of small (dCORE ≈ 1.5 nm) phosphine-stabilized gold nanoparticles.* Journal of the American Chemical Society, 2000. **122**(51): p. 12890-12891.